P4/US/1/68

Proceedings of the
Symposium on

CORRELATION OF MATERIAL CHARACTERISTICS WITH SYSTEMS PERFORMANCE

held at

USAF CONFERENCE FACILITY
Orlando Air Force Base, Florida

May 10-12, 1967

Sponsored by

The Technical Cooperation Program

Arranged by

Air Force Materials Laboratory
Wright-Patterson Air Force Base, Ohio

VOLUME I

ACKNOWLEDGEMENT:

On behalf of the Working Group "Methods of Testing and Evaluation of Materials", the conference committee takes this opportunity to express its appreciation to the following:

The Air Force Materials Laboratory for arranging the use of the USAF Conference Facility at Orlando, Florida and for funding the support of the symposium.

Mr. W. J. Trapp, AFML, for organizing and conducting the symposium and for editing the proceedings.

The Research Institute of the University of Dayton for their assistance in conducting the symposium and printing of the proceedings.

The personnel of the USAF Conference Facility for their competent and thoughtful assistance at the conference site.

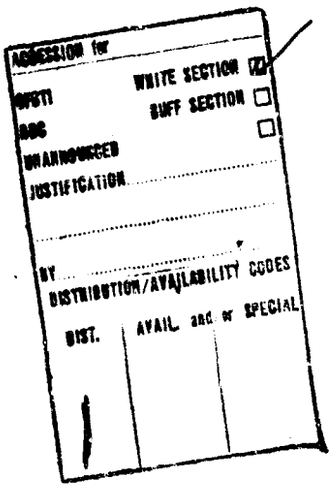

Symposium Committee

W. J. Trapp, Chairman
F. H. Edwards
J. A. Kies
Katharine Mather
P. J. Todkill

P4/US/1/68

Proceedings of the
Symposium on

CORRELATION OF MATERIAL CHARACTERISTICS WITH SYSTEMS PERFORMANCE

held at

USAF CONFERENCE FACILITY
Orlando Air Force Base, Florida

May 10-12, 1967

Sponsored by

The Technical Cooperation Program

Arranged by

Air Force Materials Laboratory
Wright-Patterson Air Force Base, Ohio

VOLUME 1

TABLE OF CONTENTS

APPENDIXES

AUTHOR INDEX

PREFACE

F. S. Williams and W. Trapp*

In 1957, the President of the United States and the Prime Minister of Great Britain made a "Declaration of Common Purpose". Subsequently the Canadian and Australian governments also subscribed to this document. The Declaration emphasized the principle of interdependence, based on the concept that the resources of the three countries, and in particular their skilled scientific and technical manpower, could be used to much greater advantage if closer collaboration could be achieved. Accordingly, provisions were made under this Declaration to exchange non-atomic information exchange considerations.

From this Declaration of Common Purpose there has emerged "The Technical Cooperation Program", the primary objectives of which is to eliminate wasteful duplication of Defense research and development effort. A sub-committee reviews the objectives, the resources employed, and the progress achieved in the four countries. It formulates proposals designed to obtain the maximum cooperation and optimum employment of the resources at hand. It also tries to insure complete and continuous interchange of information among the four countries in the specified fields of research and development.

As part of the organization of the TTCP, a Sub-Group on Materials was established which has within it the Working Panel on Methods of Test and Evaluation, the sponsor of the symposium described in these proceedings. The establishment of the Sub-Group on Materials derived from full recognition that advances in performance of weapon systems and supporting equipment were increasingly dependent upon the improvement in the knowledge of the properties and applications of materials and on the improvement of the materials themselves. The ability, however, to readily translate improvements in properties of materials into improvements in the performance of a system is dependent upon the validity of the method of characterizing or testing the material.

While there is an almost limitless variety of test methods in use for characterizing a material, there is very limited information available to show the significance of the test by relating variations in the material property to variations in the service performance of the component or system. Improvements in techniques of correlation would do much to stem the rising cost of test and evaluation.

*F. S. Williams, Chairman Working Panel on Methods of Test and Evaluation

W. Trapp, Chairman, Symposium Committee

The Panel came to the conclusion that it should solicit examples of efforts expended to relate material properties to systems performance as a means of establishing the "state-of-the-art, in this area and through this, to stimulate scientists and engineers in materials and materials application oriented organizations to seek more meaningful relationships, or correlations between laboratory tests and service performance.

With the foregoing as a background, the symposium was planned with a view to presenting papers on testing and evaluation, as applied to a broad spectrum of materials - metallic, non-metallic, and composite. The essential unifying theme or common denomination was the "correlation of material characteristics with system performance".

The Working Panel on Methods of Test and Evaluation desire to express its appreciation to all the participants of the symposium for their important contributions.

SELECTION/DEVELOPMENT OF NONDESTRUCTIVE TESTS FOR QUANTITATIVE PREDICTION OF MATERIALS PERFORMANCE

C. H. Hastings

Avco Corporation, Space Systems Division

Lowell, Massachusetts

Introduction

Although there is ample experimental evidence to support the philosophy of concurrent studies of nondestructive tests with materials and product development, it is surprising how many opportunities to realize the economic and technical advantages are being missed. An inadequate supply of professional NDT manpower, properly guided as to viewpoints and approach, continues to be a pacing item in intelligent use of NDT technology.

Thus, although correlations are being developed between NDT results and service-significant design properties, the application of these advances lags.

At a TTCP meeting held in Concord, California, in May 1965, progress in the development of NDT techniques for evaluating density, modulus, and ultimate tensile strength of bulk graphite at room temperature was reported.[1] In this report, NDT prediction capability for these properties was stated to be better than ±1% for density, $\pm 0.03 \times 10^6$ psi for modulus, and within ±300 psi for tensile strength. These correlations were shown to be valid for several different grades of bulk graphite and for both "with-the-grain" and "against-the grain" directions. Density variability was clearly identified as the correlation-dependent material variable. The combined use of a nondestructive gamma-ray gage and ultrasonic velocity results led to these correlations with properties significant to hardware design and service behavior.

Since the May 1965 report, efforts have been successfully devoted to other grades of graphite covering a wider range of these same properties. The same calibration curves have been found valid even though the modulus range has been tripled and the tensile strength range has been almost doubled.[2] Effort to promote the application of these advances at graphite vendor and user facilities has met with understanding but has been bogged down by equipment and personnel availability problems at those locations. Persistence in effort is expected to succeed in solving these latter problems, however.

Simultaneously, work has been extended to development of an NDT capability to predict thermal properties[2] such as conductivity, diffusivity, and emissivity under the continuing Air Force Materials Laboratory sponsorship.

Development of Infrared NDT for Thermal Properties Measurement

Reference (2) contains a theoretical justification for an infrared, transient heating, comparative technique for determining thermal conductivity. When thermal conductivity is combined with knowledge of modulus, tensile strength, and expansion coefficient, the relative ability of graphite to withstand thermal cracking may be empirically determined. Thermal conductivity is also a basic design property required for many calculations leading to satisfactory service behavior for hardware. Although considerable work remains to demonstrate the validity and practicability of the IR technique, results to date[3] are encouraging and suggest broad applicability to both high and low conductivity materials or practical hardware configurations.

The experimental arrangement is simply described by reference to Figure 1. The specimen is heated locally on one of its surfaces by focussed projection lamps which provide a constant radiant heat flux. The temperature history of the center of the heated area is simultaneously monitored using an infrared radiometer as the sensor. Analysis of the geometry of the recorded time-temperature trace, a comparison of it with the record from a "standard" material, and knowledge of the unknown's density and specific heat, permits the determination of both conductivity and thermal diffusivity. The local density determinations can be made by nondestructive radiation gaging techniques and the specific heat can be obtained from handbooks. For graphites, the specific heat values can be considered constant for chemically similar grades. It is not important that the heat flux incident on the specimen be known and the temperature rise of the specimen is only a few degrees above ambient so that the technique is indeed nondestructive. However, certain boundary conditions must be maintained for successful measurements. The required adherence to these conditions is presently being evaluated. Important boundary considerations are:

a. The heat flux input should be constant with time and uniform over the heating area,

b. The specimen dimensions should appear semi-infinite to heat flow during the time period of heating and observation. Unidirectional heat flow into the specimen is assumed,

c. The emissivity must be uniform over the area being heated for any one observation and its value relative to the reference material must be known.

The equations relating heat flux, time of heating, thermal properties of the specimen and surface temperature combine into the form $y = (x)^{1/2}$, suggesting a parabolic response curve. Figure 2a, taken from one channel of a dual channel recorder, shows the total radiometer response to specimen irradiation. It includes the reflected infrared radiation from the specimen surface (21 divisions) plus the self emitted radiation due to specimen temperature rise over a 3 second heating cycle (2 divisions). The first step in the measurement process is to determine the reflectance from Figure 2a. Emissivity is then defined as one minus the reflectance for opaque materials. In Figure 2b, which is an expansion of the top of the 2a trace, one sees only the self emitted radiation due to specimen heating. The reflected radiation has been eliminated by adjusting the recorder voltage offset. From this Figure 2b trace, the change in voltage, ΔV, over a selected time interval, say between one and two seconds after heating initiation, is determined. The entire trace is about four seconds long.

Figure 3 shows a superposition of expanded traces for lead, steel, graphite, aluminum, and copper. The different ΔV's are immediately apparent. By calculation relating an unknown material specimen (a) to a known, say copper (b), over the same heating interval, the unknown's thermal conductivity and diffusivity can be determined. The equations are of the form:

$$\frac{K_a}{K_b} = \left(\frac{\epsilon_{\lambda a}}{\epsilon_{\lambda b}}\right)^4 \frac{\left(\rho C_p\right)_b}{\left(\rho C_p\right)_a} \left(\frac{\Delta V_b}{\Delta V_a}\right)^2$$

$$\frac{a_a}{a_b} = \left(\frac{\epsilon_{\lambda a}}{\epsilon_{\lambda b}}\right)^4 \frac{\left(\rho C_p\right)_b^2}{\left(\rho C_p\right)_a^2} \left(\frac{\Delta V_b}{\Delta V_a}\right)^2$$

where:
- K = thermal conductivity
- a = thermal diffusivity
- ϵ_λ = emissivity at IR wavelengths
- ρ = density
- C_p = specific heat
- ΔV = voltage change over a time interval, from radiometer trace

At present, the capability of split-bar static techniques is about ±10% accuracy, at best, for graphite. Measurement of room temperature thermal conductivity usually requires extrapolation from several points measured for elevated temperature, say 100, 150, and 200° F. Typical time for one specimen may be one to several days. Diffusivity is determined by separate additional measurements.

The IR NDT technique is presently being evaluated quantitatively for accuracy. It appears to have a strong potential for further improvement by optimizing boundary conditions, heating sources and calibration. Thermal conductivity and diffusivity are both determined in a matter of minutes for a given area on a specimen. Since determinations are made on areas only 1/16 inch across, opportunity to detect variability within practical fabrications exists. The conventional static technique yields an average K value assuming uniformity within a one inch diameter specimen which must be machined from the material or part.

If one realizes that much unexplained "random" failure of hardware in service is attributed to unrecognized material variability, this IR NDT technique shows promise of minimizing the need to assume material homogeneity on the basis of small sample size, destructive measurements, with respect to thermal properties.

NDT/Mechanical Properties Correlations for Reinforced Plastics

The use of reinforced plastics as primary structural load-bearing members is attractive because of their high specific strength. Designers tend to approach application problems with caution or trepidation, however, because of their relatively poor characterization (relative to common engineering metal alloys) and their high coefficients of mechanical property variability. Nondestructive tests are being developed to assist the fabricator in uniform processing and the inspector in qualifying hardware to design property specifications.

Effort has been directed to glass reinforced resins of epoxy, phenolic, polybenzimidazole, silicone, and polyester systems. The problem is approached by attempts to define the material variables exerting strongest control on significant design properties and quantitative NDT for evaluating these material variables.

There is a long list of material and process variables which have been suggested by various investigators as influential on mechanical properties of glass laminates. However, their relative significance is not clear.

Figure 4 is typical of an abortive attempt to find a simple relationship between tensile modulus and density in a certain specific glass laminate system. The pattern of points is fairly hopeless from the point of view of statistically valid correlation. One might attempt to draw lines for the specific systems, as has been done in this figure for the PBI and polyester laminates. Effort to generalize broadly for all laminates seems futile.

For our initial studies, we chose to hold as constant as possible the following:

1. Glass fabric - 181 weave, E glass

2. Coupling agent (fabric finish), appropriate to each resin system and constant for a given system
3. Degree of cure, optimized
4. Moisture content, held to minimum
5. Laminate thickness, nominally 3/8 inch or about 40 plies

The following parameters were controlled as variables for study:

1. Resin content
2. Void/porosity content

Other parameters were considered uncontrolled and randomized. Twenty-five laminate panels, 12" x 12" in area, were prepared.

Initial NDT screening to detect macro defects and map panel variability involved radiometric gaging, radiography, ultrasonic velocity measurements, low frequency (1 KHz) dielectric and microwave (35 Ghz) dielectric tests. These checks were made on 2" x 2" grid squares layed out on each panel to assure meaningful location of mechanical test specimens by:

a. excluding macro flaws
b. including extremes and intermediate values of material variability

In this way, material variability significance could be studied as it related to NDT in "flaw free" material.

Details of the NDT techniques employed are described in reference (4) and are rather conventional.

Destructive characterization included:

a. Density (gravimetric)
b. Resin content
c. Void volume
d. Dielectric constant and dissipation factor
e. Tensile properties (modulus of elasticity, strength, proportional limit, total strain-to-failure)
f. Flexure properties (modulus of elasticity, modulus of rupture, total deflection)

Although the long range goal of data analysis is to seek quantitative correlations between NDT and design/service critical properties, work to date has succeeded in revealing trends in relationships rather than precise correlations. The NDT data is plotted empirically against mechanical test data. Chemical characterization is applied to keep track of resin/glass ratio, degree of cure, and porosity.

In reality, none of the destructive tests for reinforced plastics against which the NDT results are plotted are reliable or well understood. Under these circumstances, tight correlations are not to be expected. The trends which have been found represent a glimmer of hope in untangling an indescribable tangle of variables interacting in complex ways. A few of the trends uncovered are described.

Figure 5 shows a clear, general trend between gravimetric density measured on 3/4" diameter cores and ultrasonic velocity measured on the same cores for five glass-resin laminate systems. Scatter can be explained by the presence of other parametric variables, i.e. size and location of porosity, degree of cure, resin content, etc. Figure 6 covering the epoxy system alone reveals a fairly tight relationship for the non-porous specimens as a function of resin content. The dark points represent specimens containing unknown amounts of closed porosity as well as resin content variability. This suggests a relationship as expressed in Figure 7 where void content and resin or glass content are parameters relating density to ultrasonic velocity.

The equation for ultrasonic longitudinal wave velocity:

$$V_L = \left[\frac{E}{\rho} \frac{(1-6)}{(1+\sigma)(1-2\sigma)} \right]^{1/2}$$

where: E = Young's modulus
ρ = density
σ = Poisson's ratio

is written for an isotropic material. Although plastic laminates are notably anisotropic and are composites of widely different materials, the inter-relationship of modulus, density, Poisson's ratio and velocity is worth investigating experimentally. For five glass-resin laminate systems, as previously listed, Figures 8 and 9 show crossplots of tensile and flexure modulus against $V_L^2 \rho$ (density normalized ultrasonic velocity factor). Ultrasonic velocity is measured parallel to the ply direction and density can be obtained by gamma ray gaging at the same measurement positions on the material. Velocity measurements in the parallel-to-fabric direction responds primarily to reinforcement elastic properties and to the resin/microporosity within the cloth layers. It is this "wetting out" of plies which exerts a major influence on tensile and flexure modulus and yields the same regression line slope for both modulii. The difference in scatter between the two plots is attributable to the more sophisticated accounting for shear deflections in the flexure test. No accounting is currently made in tensile tests for load distribution anomalies related to specimen/reinforcement geometry. Studies of micromechanics of reinforced plastics now in progress

should lead to reductions in data scatter and improved interpretation of destructive test results.

It is interesting to note that ultrasonic velocities measured perpendicular to fabric plies respond with exaggerated sensitivity to macroporosity located between plies, which does not appear to have equally large influence on tensile and flexure modulus. Hence, correlations are not as clear cut. However, the perpendicular velocity measurements permit identification of porosity between plies and suggests the presence of process variability which, if carried too far, would certainly degrade mechanical properties.

Without going into detail, other NDT correlations are being found[4, 5] which are expected to yield practical tools to untangle the many variables influencing mechanical properties of reinforced plastics. Low frequency dielectric constant measurements respond to tensile modulus as influenced by degree of cure while loss tangent responds to Shore D hardness values as affected by cure state.

NDT Measures Service Life for Diffusion Coatings on Refractory Metals

Columbium, molybdenum, tantalum, and tungsten alloys are of interest for hypersonic aircraft, glide reentry and other vehicles requiring radiation cooled structural members. The almost complete lack of oxidation resistance of these alloys above 1000° F requires protective coatings impervious to oxygen to permit their use above 2500° F. Except for sensitivity to rapid oxidation, these refractory metals have excellent strength in the operating temperature range.

Diffusion-formed silicide coatings have been developed which provide the required protection. However, they have not been reliably produced and numerous idiopathic failures observed have not been explained. Prior requests for NDT quality tests have been frustrated by lack of information on what failure controlling characteristics should be measured. Coating thickness was suggested as important and numerous "edge failures" suggested edge contour as significant. Little quantitative failure data were available to support these ideas.

A combined failure mechanism/NDT development study was undertaken[6, 7] for the Air Force Materials Laboratory, in which the coated refractory was regarded as a complex materials system, the variables in each component of which must be characterized if failure factors were to be defined. Three base metal coating combinations were studied as described in Table I. For each case, critical variables NDT screening techniques

shown in Table II were applies to the significant zones of the system. Nominally, the substrates are 20 mils thick and the coatings 2-5 mils thick on each side of the substrate. All variables were presumably scooped-up by NDT screening of uncoated substrate prior to service evaluation of the coated specimens. Substrate variables detected by NDT were positioned within 2 x 2 inch specimens subsequently coated by commercial coating vendors employing their "standard" procedures.

Following complete NDT characterization, the specimens, some with and some without NDT detected variability, were subjected to 2600° F, air atmosphere, furnace exposure cycles of 1-4 hours. Periodic NDT was applied between exposure cycles to note base line departures and failure progress. Low pressure tests (0.5 mm of Hg) were also conducted at 3000° F and Mach 3 velocity in an arc plasma environment to simulate heating at 100,000 foot altitude.

Edge failures were found to be due primarily to chemical interaction between coated specimens and Vycor furnace support blocks. Changing to an inert support virtually eliminated edge failures due to edge contour.

As might be expected, failure mechanisms differed for each coating-substrate system. Findings can be summarized as follows:

a.) TZM/W-3: -- The laminar grain structure of TZM alloy exhibited a strong tendency to delamination. Propagation of delamination defects initiated from points of stress concentration (identification edge notches). Edge delaminations were easily detected before and after specimen coating by dye penetrant and low power (40X) microscopy. Progress of failures due to delamination could be monitored by radiography between furnace cycles. Oxygen entering unsealed delaminations eats away the substrate, leaving a hollow shell of coating material. Failures due to coating life were related to starting coating thickness and time in furnace, temperature, and pressure/velocity for the arc exposures. Eddy current coating thickness measurements correlated well with actual thickness measurements before and at intervals during exposure. Figures 10-15 show these correlations. Of course, the eddy current measurement can be made from one side only, accessibility to both sides is not a requirement, as is the case for micrometer measurements.

Figure 16 shows metallographic results as a function of furnace exposure. Although micrometer readings showed only a 0.001 inch increase after 70 hours of exposure, Figure 14 suggests larger increase in coating thickness. Actually, the coating is growing at the expense of the substrate, also evident from weight loss observations. From this observation, the validity of eddy current readings and the misleading nature of micrometer readings during service is quite clear.

b.) Cb 752/Cr-Ti-Si: -- Unlike the TZM/W-3 system, this coating showed weight and thickness increase with furnace exposure time. Eddy current data, Figure 17 also showed an increase. In this case, the coating is gaining thickness by a process of oxidation, without corresponding loss of substrate. The primary mode of failure of Cb 752/Cr-Ti-Si was by pin hole burn-through. Dye penetrant and backscatter radiography showed "low-density" areas before furnace exposure which correlated faithfully with burn-through. Electron microprobe analysis of typical spots showed a chromium barrier layer deficiency, permitting substrate columbium to diffuse outward and coating silicon to diffuse inward. The $Cb\,Si_2$ and $Cb_3\,Si_2$ compounds so formed have relatively poor oxidation resistance, leading to elevated temperature burn-through in these local areas. NDT can readily detect this deficiency in the coating process.

c.) B-66/PFR-30: -- This system performed so poorly, due to erratic variability of coating quality, that it was dropped from further study. Catastrophic failures associated with cracks, spalls, chipping, and porosity were observed prematurely during furnace exposure. Many of these conditions were visually obvious prior to furnace testing.

Table III summarizes the failure modes and mechanisms observed, defines failure controlling material variables, and recommends the NDT methods found effective.

Not only was NDT found effective for quality evaluation (failure prediction) prior to simulated service exposure, the periodic eddy current thickness monitoring during life is suggested as an effective tool for predicting remaining life during service.

Conclusions

By carefully planned and searching applications of NDT principles, quantitative calibration of these techniques can be developed for innumerable problem areas. The essential ingredients for success are proven relationships between service required materials properties (design criteria), property controlling material variables, and useful material-energy interactions.

Understanding failure mechanisms is necessary to defining a tractable NDT problem.

Our work has shown that NDT can quantitatively predict mechanical and thermal properties of graphite and other materials -- a task usually thought to require statistical sampling and destructive tests. The evaluation of reinforced plastics

is complicated by their composite nature and a lack of understanding of relative significance of process/material variables. NDT is offered as a powerful tool, not only for quality assessment but also for understanding these little understood materials. For oxidation resistant, diffusion coatings, several NDT techniques in combination can predict failures in new hardware and show strong potential for measuring remaining life during service.

Acknowledgements

Obviously, the work of many people has been covered in this paper. The engineers and scientists principally concerned include Messrs. George Lockyer, Arnold Schultz, John Zurbrick, Russell Stinebring and Thomas Sturiale of the Avco Space Systems Division. Their essential contributions are gratefully acknowledged, in addition to the support of many other individuals.

Work discussed was sponsored by the Air Force Materials Laboratory, Dayton, Ohio, under the following contracts:

Subject	Contract	Monitor
Graphite	AF33(615)-1601 and -3942	W. L. Shelton
Diffusion Coatings	AF33(615)-2855 and -3377	W. L. Shelton
Plastics	AF33(615)-1705	H. A. Kamm

References

1. Investigation of Nondestructive Methods for the Evaluation of Graphite Materials, Lockyer, G. E., Technical Report AFML-TR-65-113, May, 1965.

2. Same titled, Lockyer, G. E., Lenoe. E. M., and Schultz, A. W., Technical Report AFML-TR-66-101, May, 1966.

3. A Unique Infrared Comparative Method for Determining the Thermal Conductivity and Diffusivity of Solids, Schultz, A. W., Paper presented at the Seventh Annual Symposium on Physics of NDT, Chicago, Illinois, September, 1966 (Sponsored by AFML, Research and Technology Div., Wright-Patterson Air Force Base, Ohio).

4. Development of Nondestructive Methods for the Quantitative Evaluation of Glass Reinforced Plastics, Zurbrick, J. R., Technical Report AFML-TR-66-269, June, 1966.

5. The Mystery of Plastics Variability: Nondestructive Testing Holds the Key, Zurbrick, J. R., Presented at the Silver Anniversary Technical Conference, Society of Plastics Engineers, May, 1967.

6. Development of Nondestructive Methods for Evaluating Diffusion-Formed Coatings on Metallic Substrates, Stinebring, R. C. and Sturiale, T., AFML-TR-66-221, September, 1966.

7. Understanding Failure Required for Meaningful Test Selection, Stinebring, R. C., Proceedings of 1967 Annual Symposium on Reliability, January, 1967, paper 7B1.

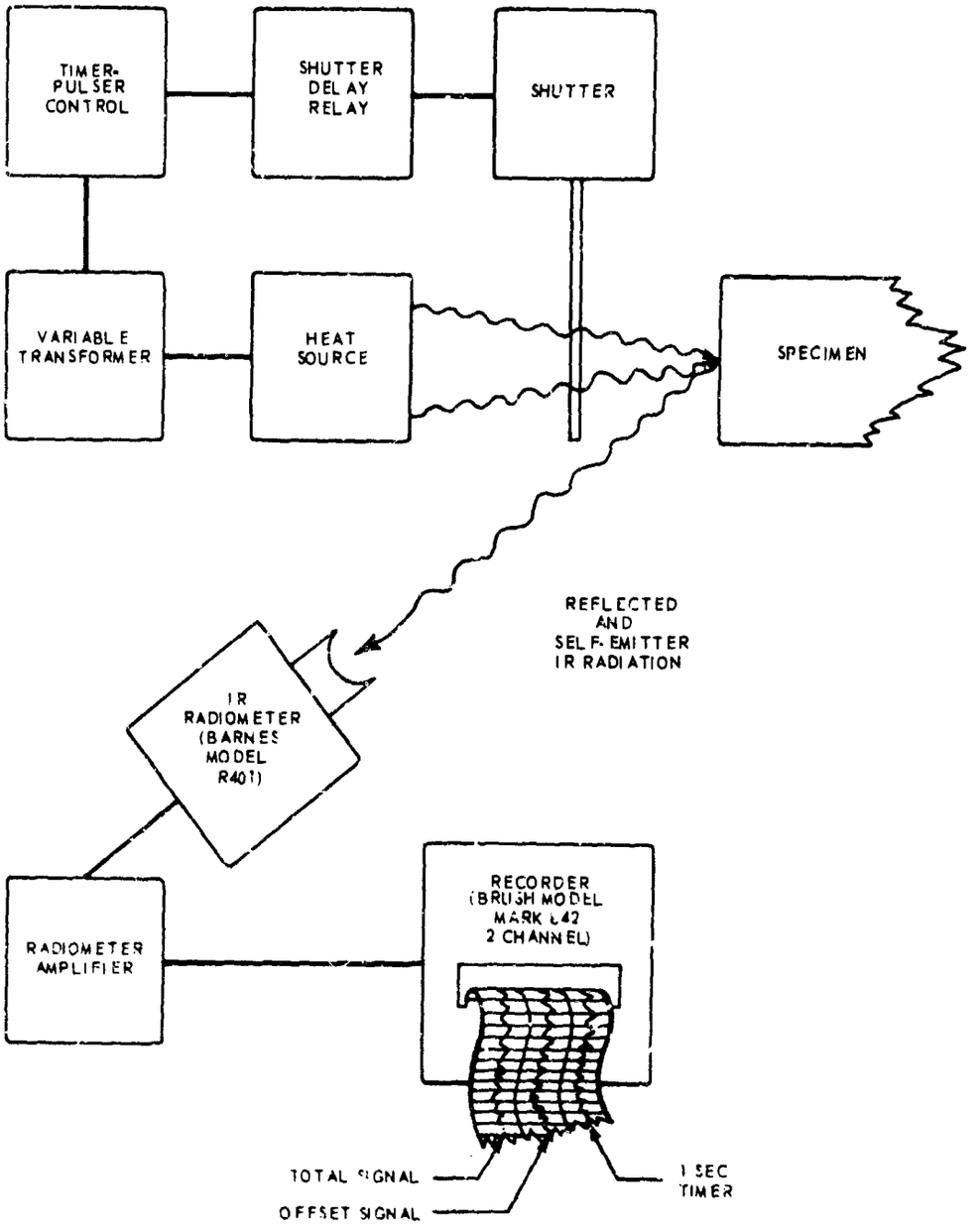

Figure 1. SCHEMATIC DIAGRAM OF THE EXPERIMENTAL ARRANGEMENT USED TO MEASURE THERMAL CONDUCTIVITY/DIFFUSIVITY

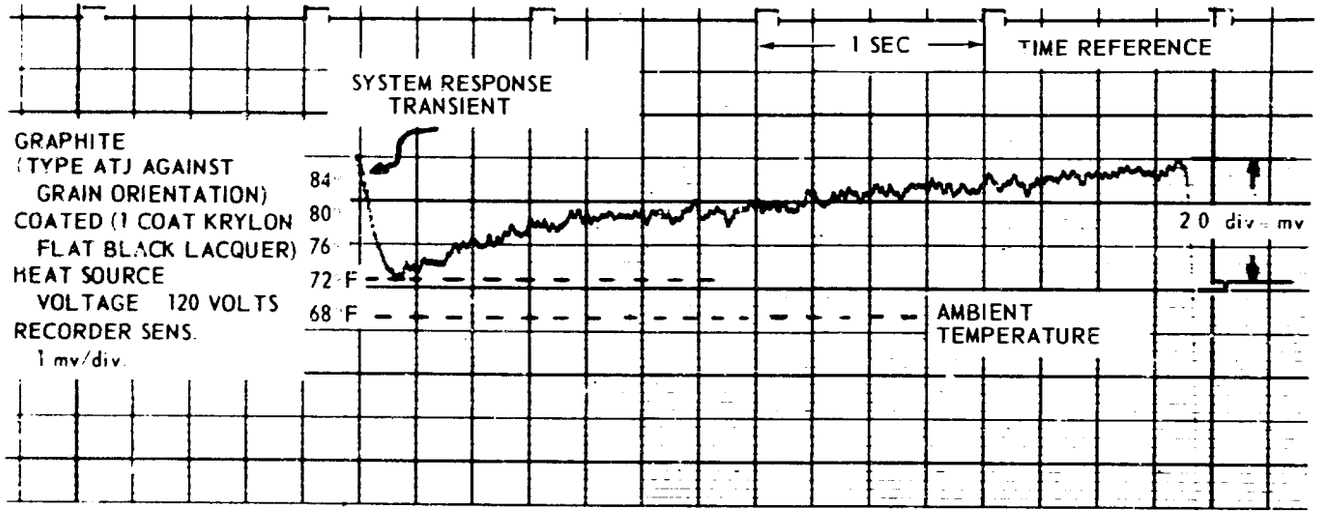

Figure 2b. SELF-EMITTED RADIATION HISTORY (VOLTAGE AMPLIFICATION OF IR RISE IN FIGURE 2a)

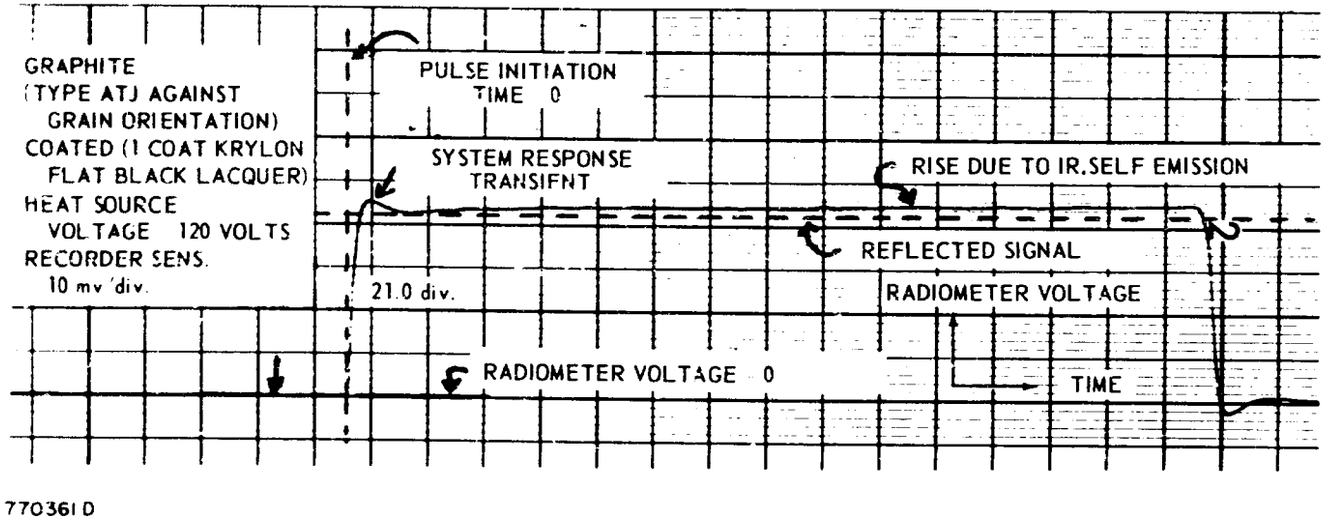

770361 D

Figure 2a. TOTAL INFRARED RADIANT SIGNAL RECEIVED BY RADIOMETER (REFLECTED PLUS SELF-EMITTED COMPONENTS)

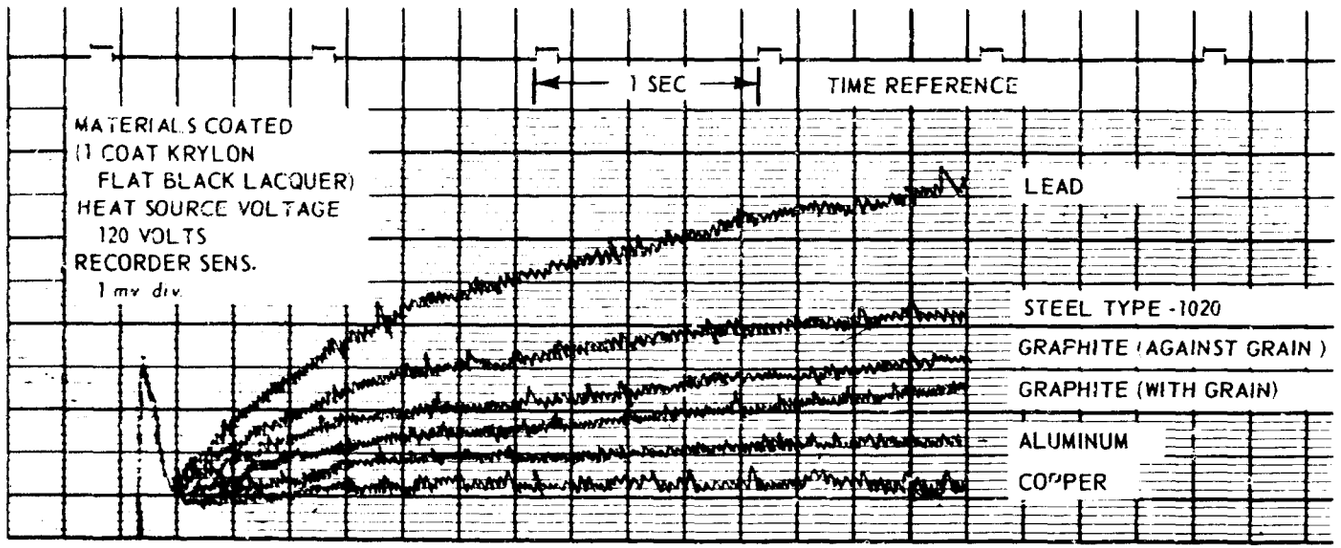

Figure 3. SUPERPOSITION OF SELF-EMITTED RADIATION HISTORIES OF COPPER, ALUMINUM, GRAPHITE (TYPE ATJ WITH AND AGAINST THE GRAIN ORIENTATION), STEEL (TYPE 1020), AND LEAD

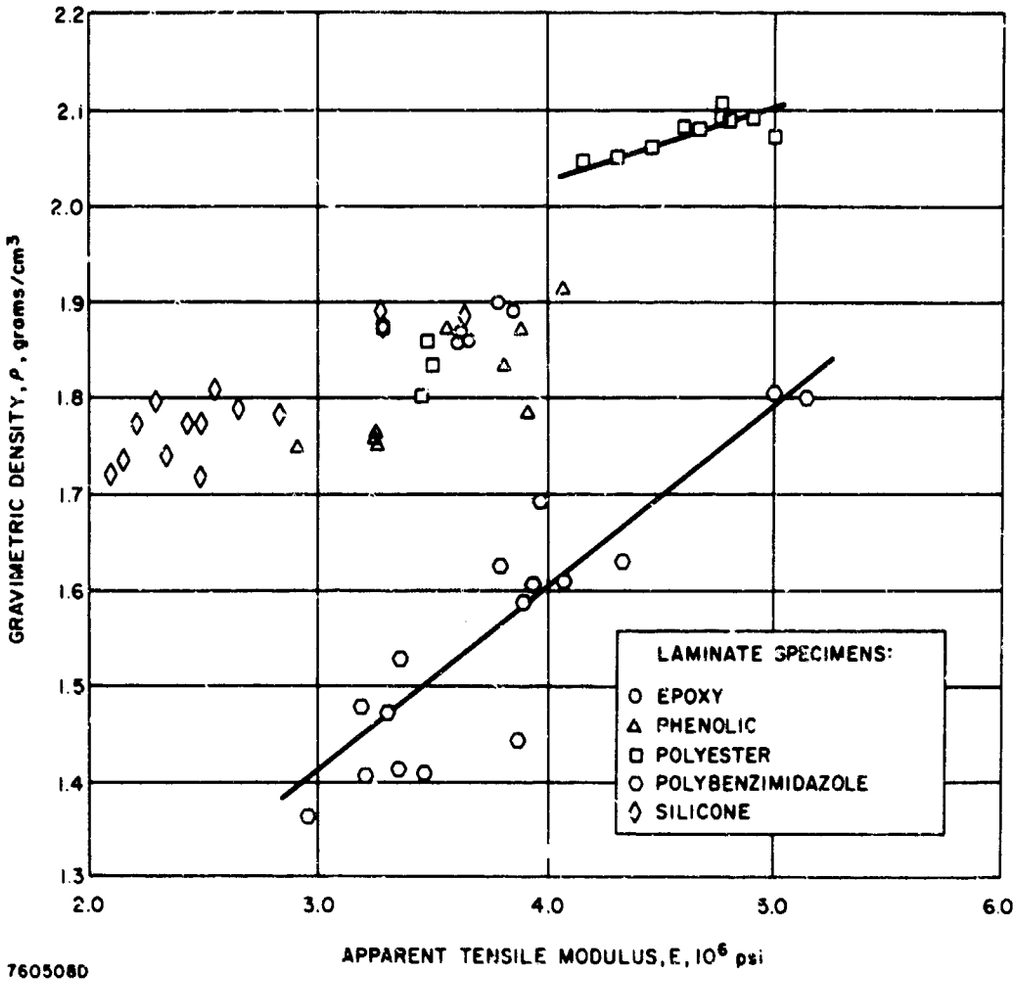

Figure 4 RELATIONSHIP BETWEEN DENSITY AND APPARENT TENSILE MODULUS FOR FIVE RESIN SYSTEMS

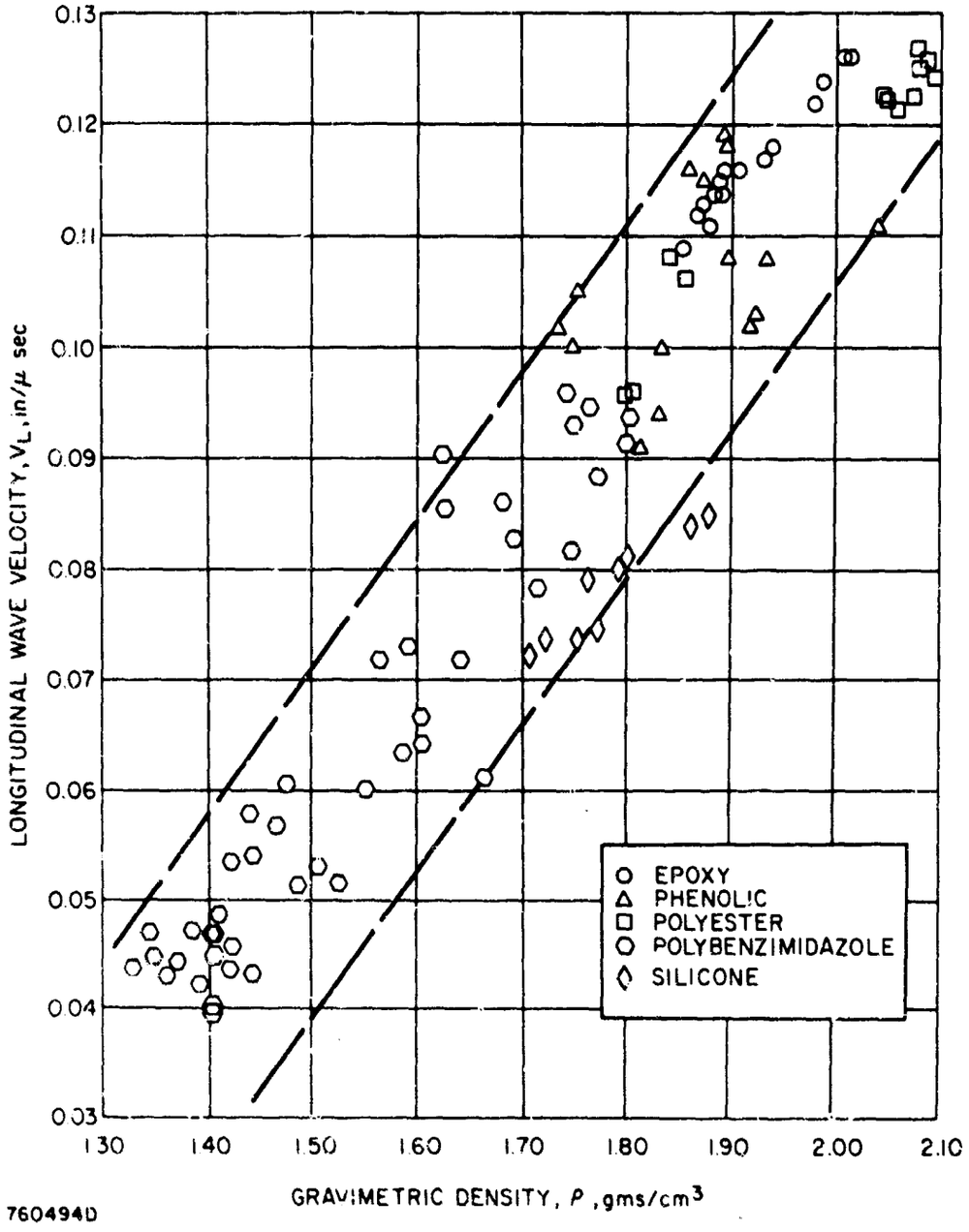

Figure 5 TREND BETWEEN ULTRASONIC VELOCITY AND DENSITY FOR 5 RESIN SYSTEMS IN 181 GLASS FABRIC REINFORCED LAMINATES

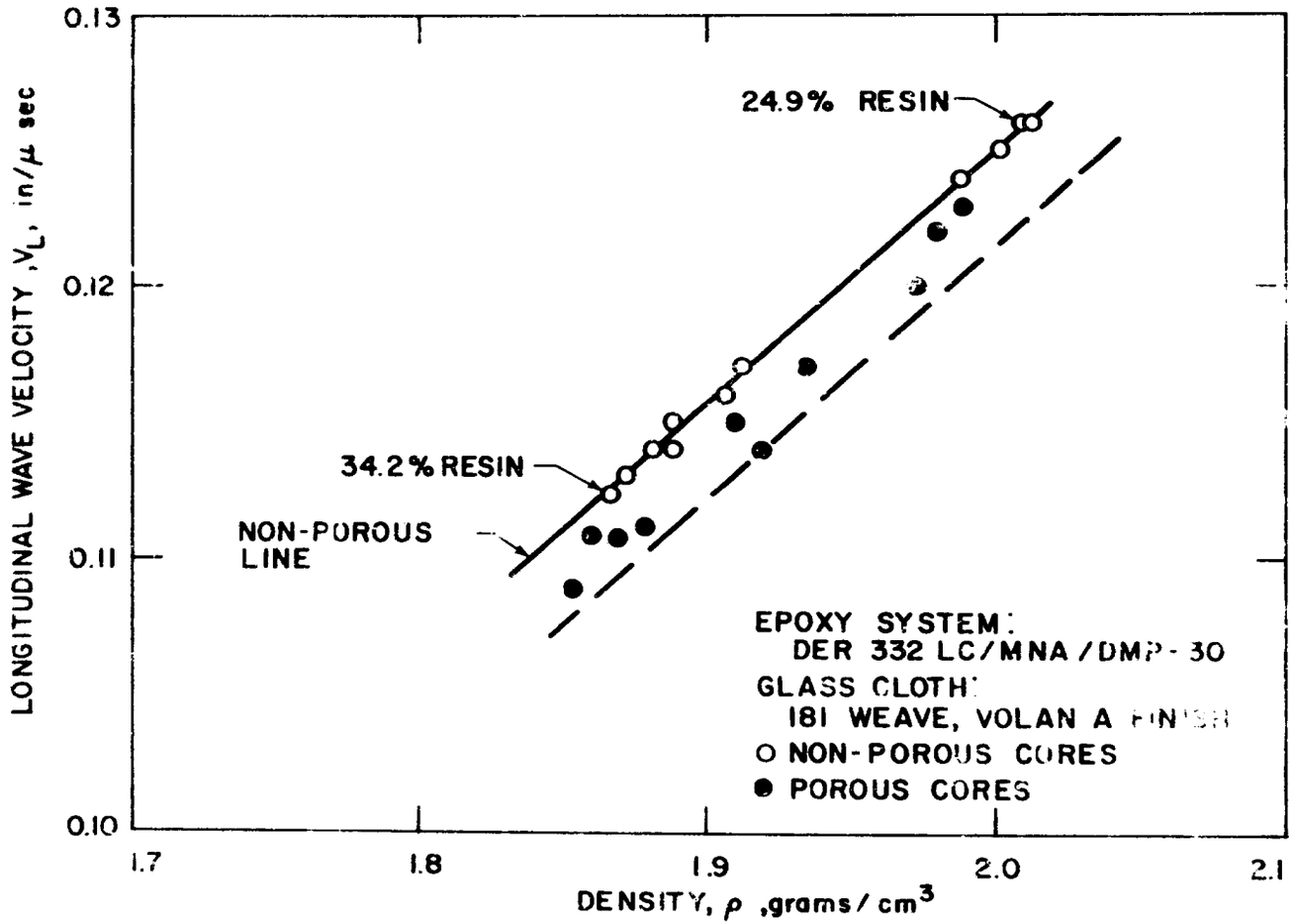

Figure 6. EFFECT OF UNDETERMINED SMALL PERCENTAGES OF POROSITY ON ULTRASONIC VELOCITY AT 1 MHz FOR THE EPOXY SYSTEM

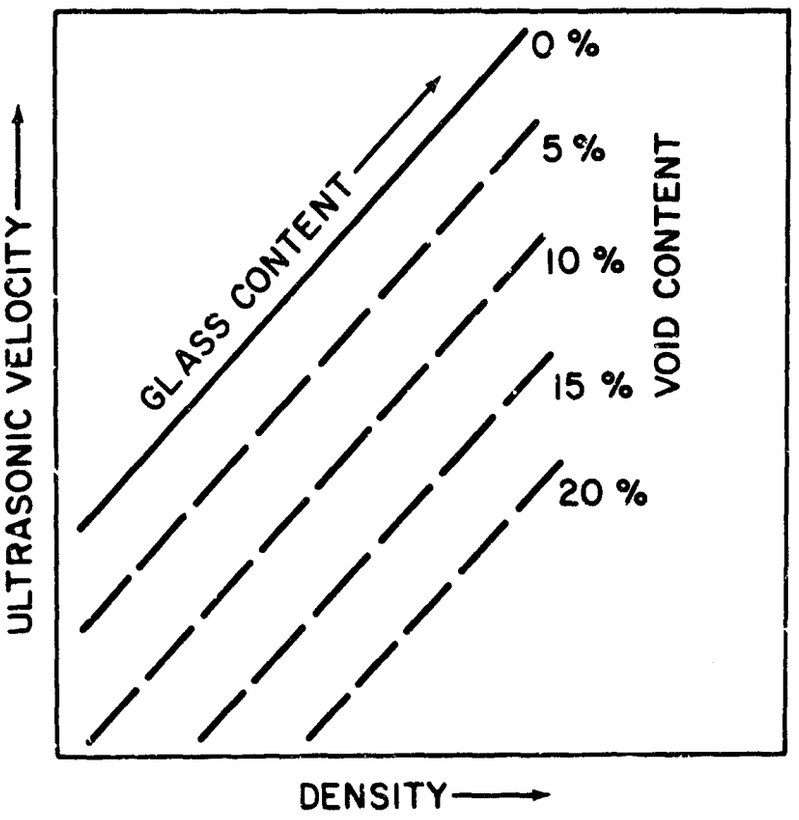

Figure 7. GENERAL PARAMETRIC RELATIONSHIP WHICH MAY EXIST IN THREE-COMPONENT LAMINATE SYSTEMS

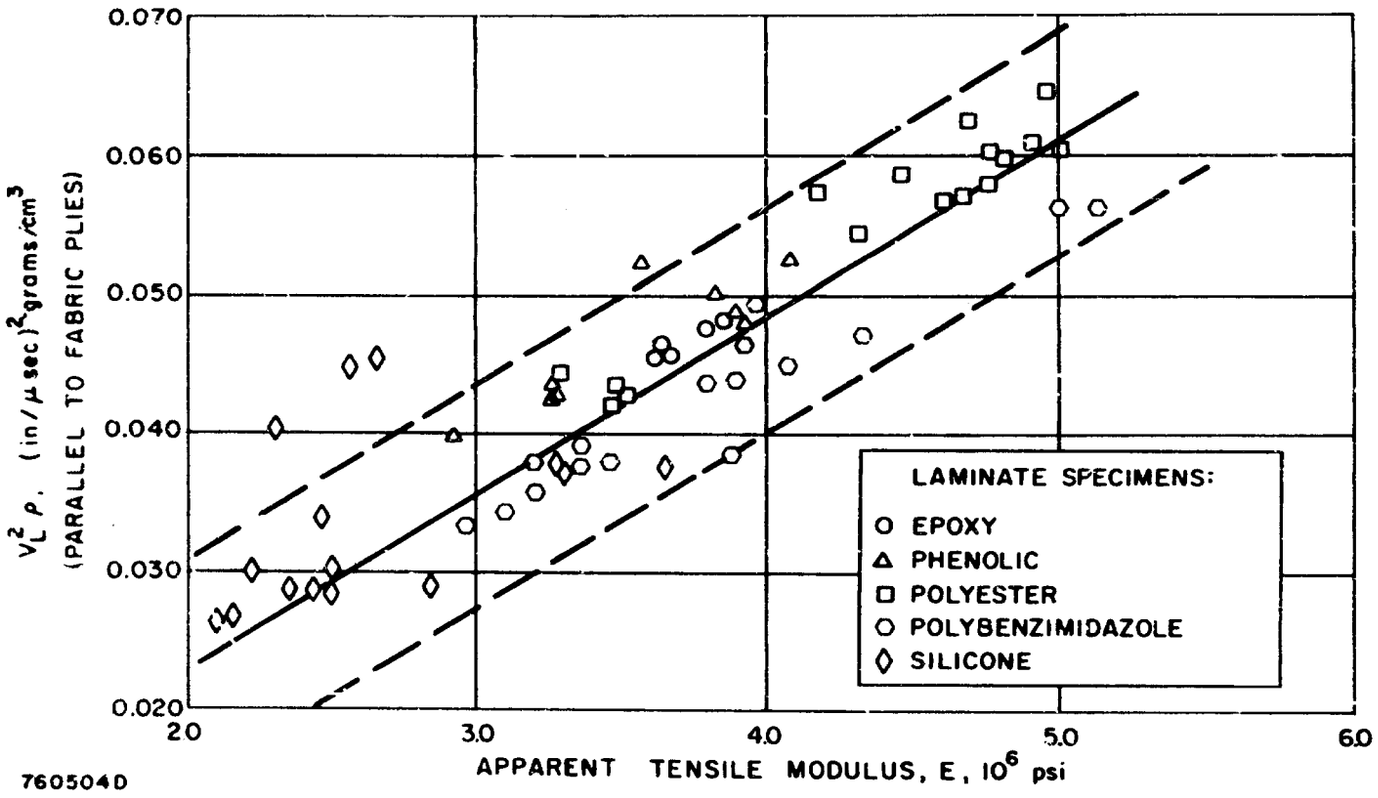

Figure 8. CORRELATION BETWEEN $V_L^2 \rho$ AND APPARENT TENSILE MODULUS FOR FIVE RESIN SYSTEMS (V_L MEASURED PARALLEL TO FABRIC PLIES)

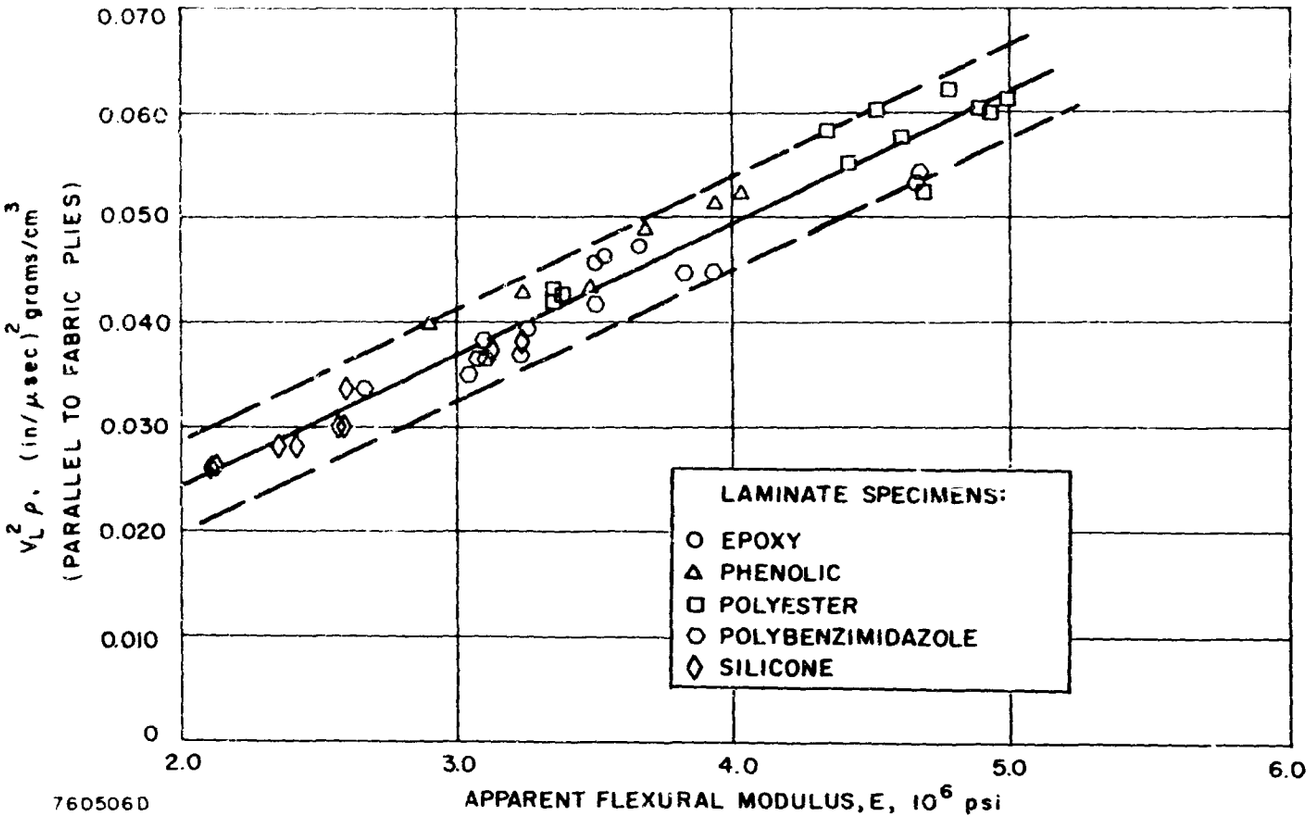

Figure 9. CORRELATION BETWEEN $V_L^2 \rho$ AND APPARENT FLEXURAL MODULUS FOR FIVE RESIN SYSTEMS (V_L MEASURED PARALLEL TO FABRIC PLIES)

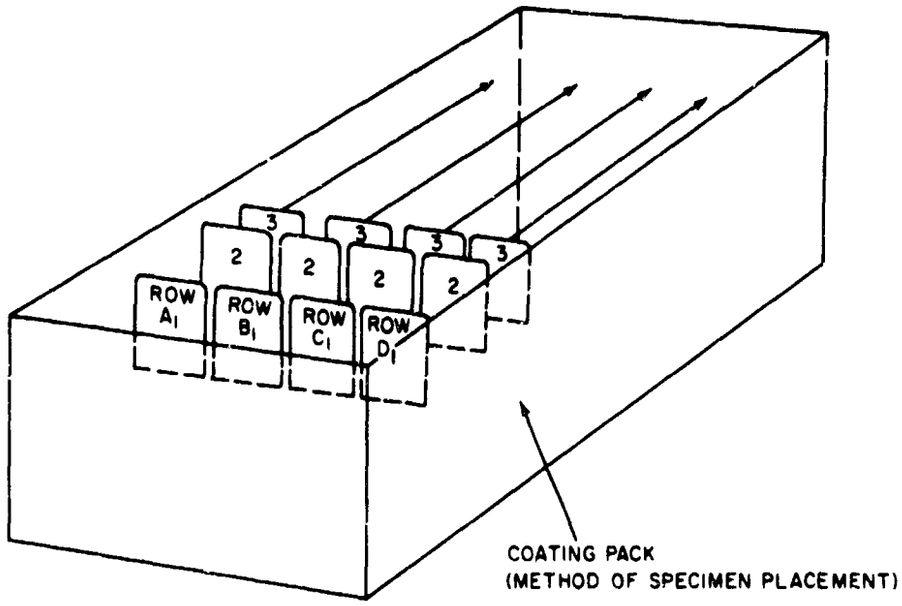

Figure 10. PLACEMENT OF SPECIMENS IN CHROMALLOY CORP COATING PACK

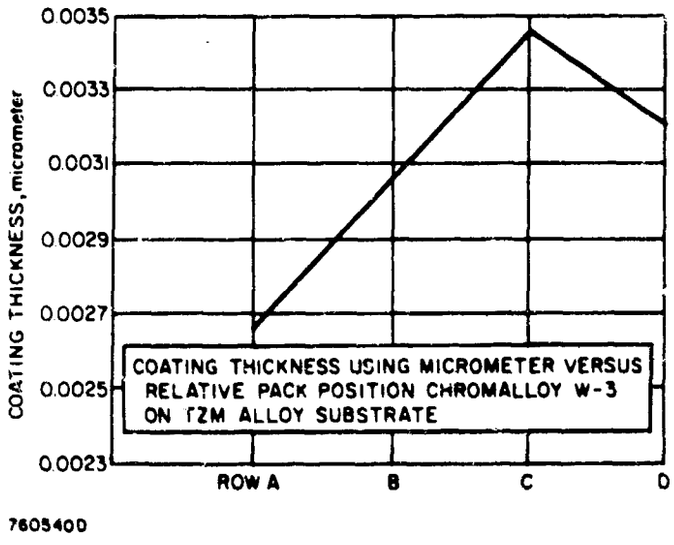

Figure 11. RELATION OF COATING THICKNESS TO PACK POSITION

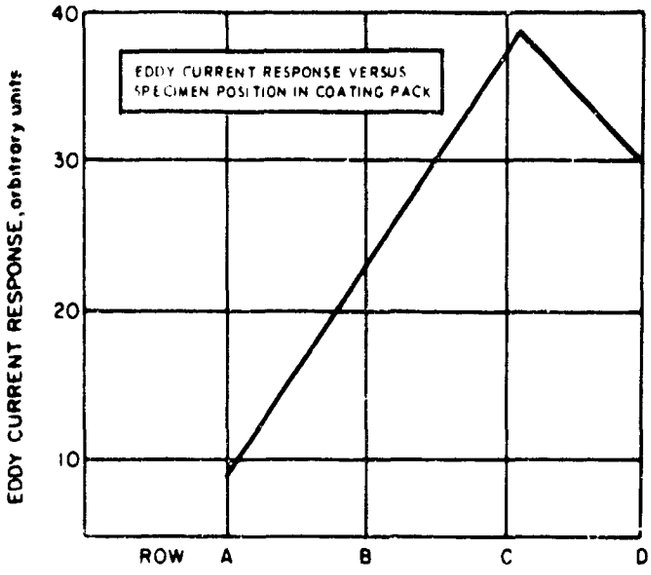

Figure 12. RELATION OF EDDY CURRENT READING AND PACK POSITION

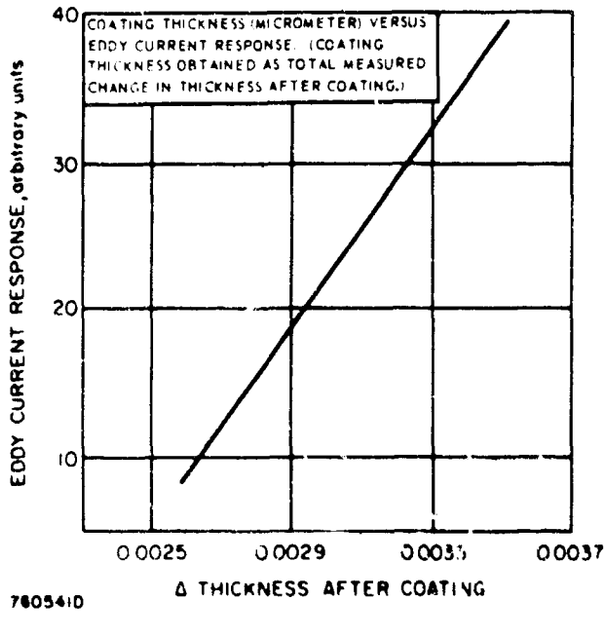

Figure 13. MICROMETER THICKNESS READING VERSUS EDDY CURRENT

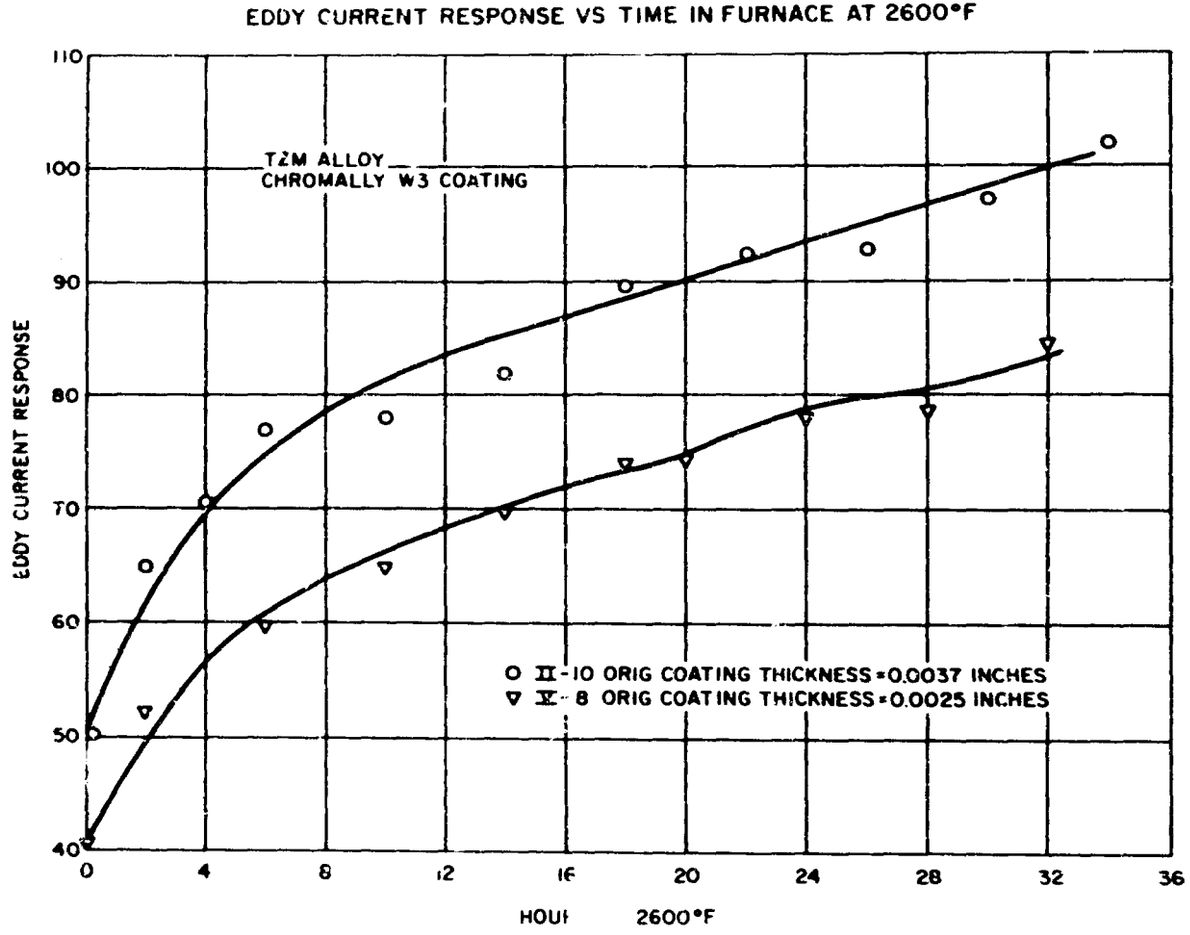

Figure 14. EDDY CURRENT RESPONSE VERSUS TIME IN FURNACE AT 2600 F -- TZM - W-3

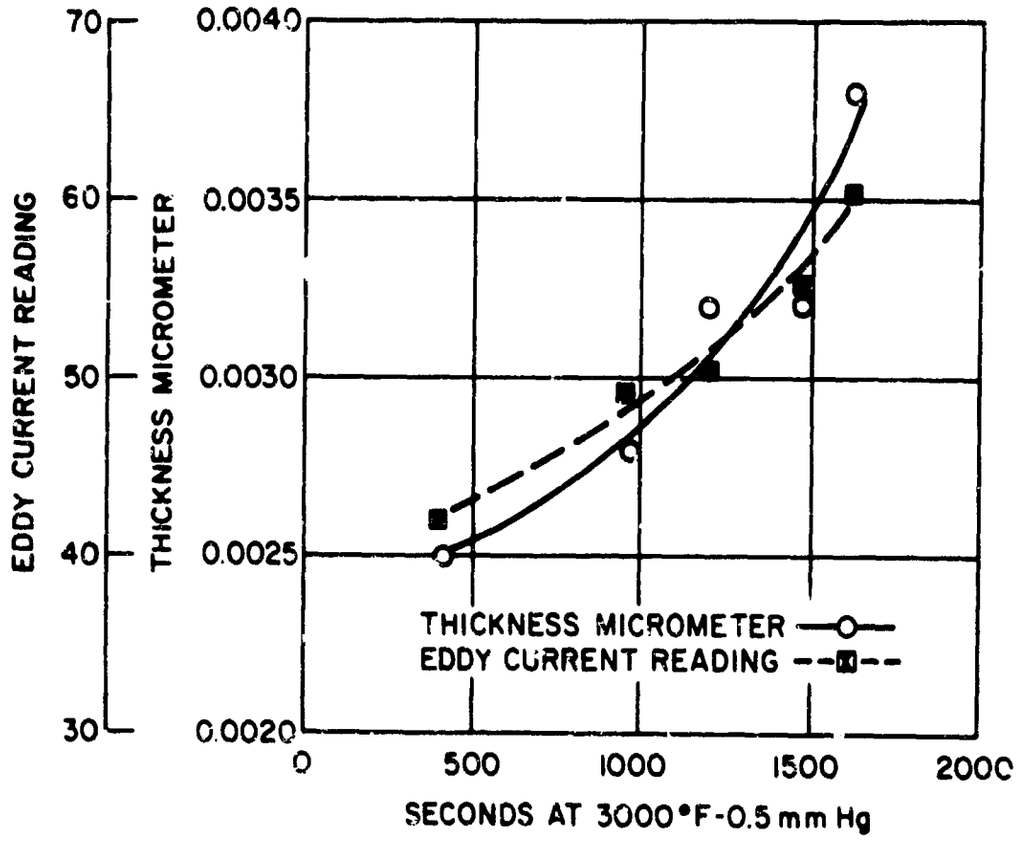

Figure 15. OVERSARC TEST ON TZM – W-3 SPECIMEN COATING THICKNESS AND EDDY CURRENT VERSUS ACTUAL LIFETIME AT 3000 °F, 0.05 mm Hg

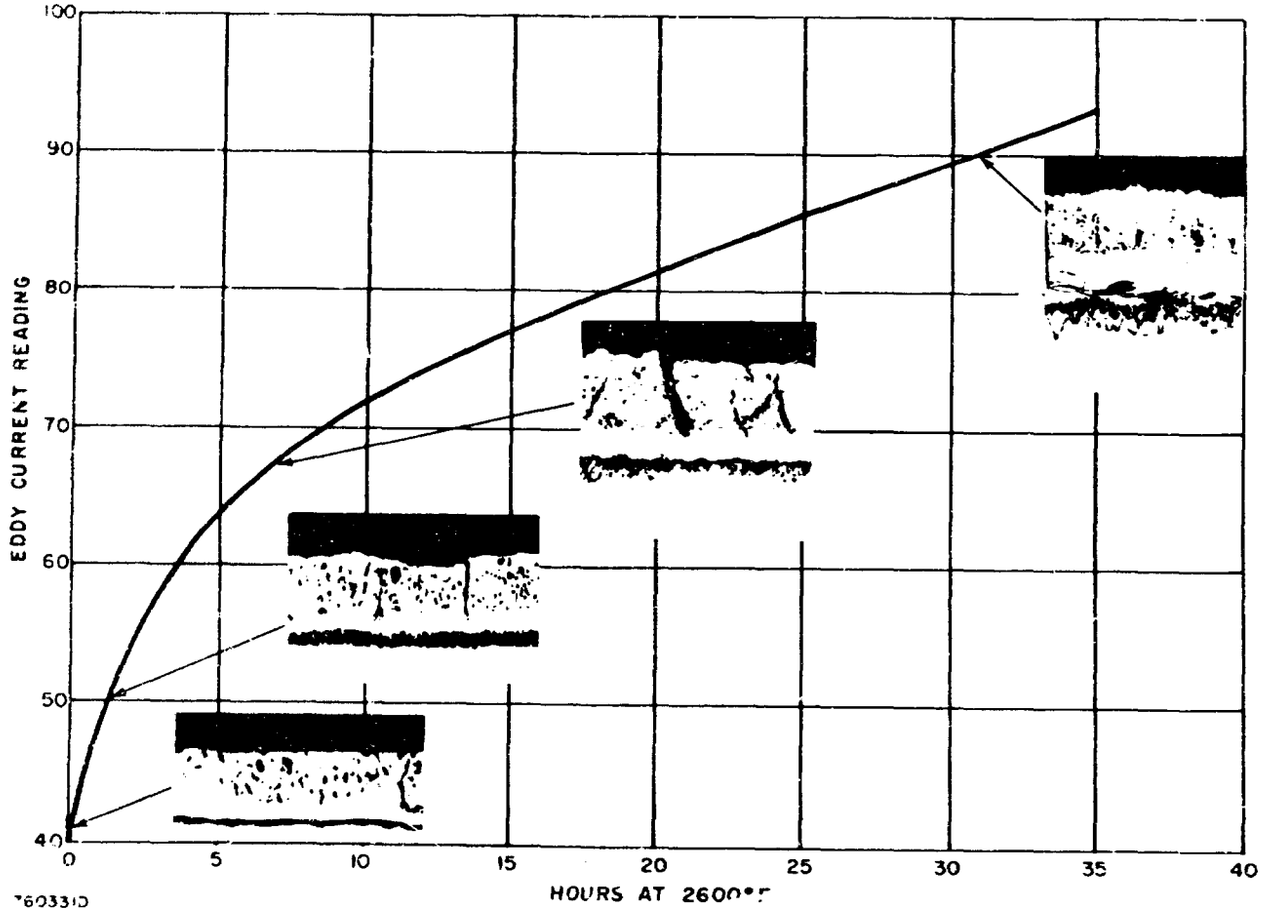

Figure 16. TZM ALLOY CHROMALLOY - W-3 COATING, METALLOGRAPHY AND EDDY CURRENT VERSUS TIME IN FURNACE AT 2600 °F

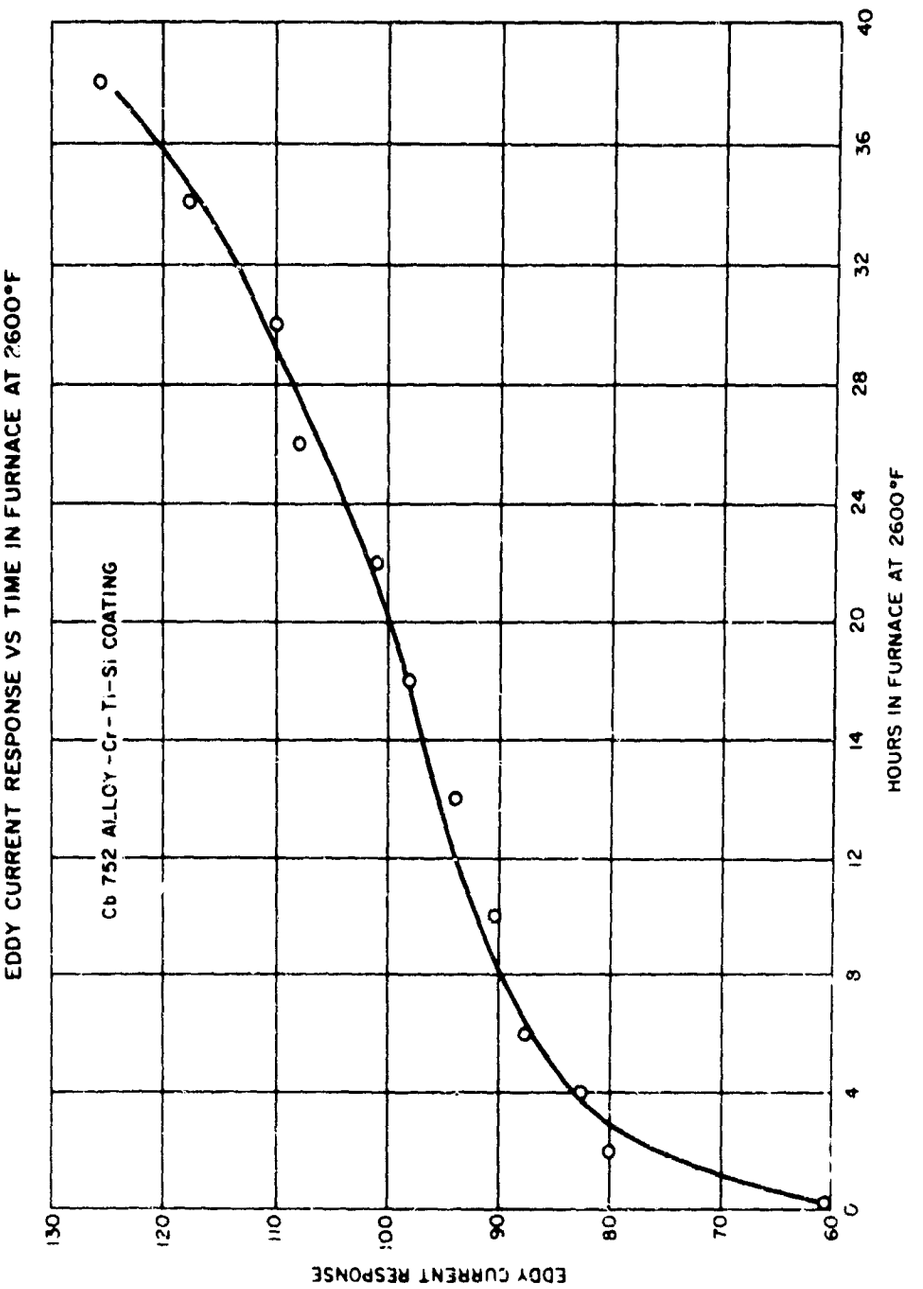

Figure 17. EDDY CURRENT RESPONSE VERSUS TIME IN FURNACE AT 2600 F (Cb 752 Cr-Ti-Si)

TABLE I

SELECTED SUBSTRATE-COATING COMBINATIONS

Substrate	Supplier	Coating to be applied	Coating Vendor
TZM (Mo-0.05Ti-0.1Zr)	Universal Cyclops	W-3	Chromalloy Corporation
Cb 752 (Cb-10W-2.5Zr)	Union Carbide (Stellite)	Cr-Ti-Si	TRW Inc
B-66 (Cb-5V-5Mo-0.1Zr)	Fansteel	PFR-30	Pfaudler Corp

TABLE II

NONDESTRUCTIVE TECHNIQUES SUGGESTED BY MATERIAL-ENERGY INTERACTIONS

Zone	Variable	Tests Available
Coating surface zone	Texture, continuity	Reflectometric methods Microscopic and optical methods
	Emissivity	Infrared analysis, optical reflectance
Coating subsurface zone	Density, porosity, thickness uniformity, purity	Ultrasonic velocity, x-ray scatter, electrical resistivity, eddy current tests, infrared
	Elastic modulus, ductility, strength	Ultrasonic and sonic techniques
Interfacial zone	Bond integrity, brittle layers, laminar flaws	Ultrasonic attenuation, infrared transmission
	Thickness of diffusion zone	Resistivity, eddy current tests, backscatter techniques
Substrate zone	Compatibility, cleanliness (before diffusion coating)	Eddy current, optical reflectivity, visual and microscopic
	Impurities and inhomogeneity	Ultrasonic velocity, radiography
	Surface condition	Surface roughness gaging, reflectometry, visual and microscopic

TABLE III

FAILURE MODES, MECHANISMS, VARIABLES AND EFFECTIVE NDT

Substrate	Coating	Observed Failure Mode	Proposed Failure Mechanism	Significant Variable or Deficiency	Effective NDT Methods
Cb 752 Stellite Div of Union Carbide	Cr-Ti-Si TRW Inc	local burnthrough in furnace at 2600, 2800, and in plasma arc at 3000 °F	accelerated diffusion of substrate and increased oxidation susceptibility	local areas of the coating associated with these failures had differing density, structure and composition. Areas are Cr poor and Cb rich	radiography (std and backscatter) dye penetrant, thermo-electric electron beam probe
		general failure of coating in many areas 2600 °F (prolonged exposure)	long term diffusion of oxygen inward and substrate outward	degradation as a result of long exposure to oxidizing environment	eddy current (8 MHz)
TZM Universal Cyclops Corp	W-3 Chromalloy Corp	rapid oxidation of substrate with burnthrough in plasma arc at 3000°F 0.5mm Hg	vaporization of coating in reduced pressure environment with exposure of substrate to oxid environ	initial coating thickness	eddy current (8 MHz)micrometer
		loss of substrate at local areas in the identification notches: 2600°, 2800°F	delams in the substrate opened or propagated during furnace test. Notches are areas of high stress concentration.	highly laminar orientation of grain structure. Tendency to delaminate when stressed	dye penetrant, microscope, radiography
Ti-6Al Fansteel Corp	PFR-30 Pfaudler Corp	rapid oxid in lg areas: 2600 °F	rapid diff of oxygen into substrate due to open networks	cracks in coating	dye penetrant, microscope (40X)
		rapid oxid in lg areas: 2600°F	same as above	porous, grossly non-uniform coating areas	dye penetrant, visual, microscope (40X)
		oxid in local areas: 2600°F	spalling of coating at elevated temp in the local areas	poorly adhering coating	visual, microscope (40X)

STRESS WAVE AND FRACTURE OF HIGH-STRENGTH METALS

G. S. Baker and A. T. Green

Aerojet General Corporation

Sacramento, California

1. INTRODUCTION

The emission of stress waves (acoustic emission) from deforming materials, both metallic and non-metallic, has been known for many years.[1] Listening by ear or by a stethoscope, many investigators have used this "noise" to recognize the nearness to fracture in tensile tests on high-strength metals. In latter years, attempts using microphones,[2] piezoelectric transducers,[3] and accelerometers[4,5,6] have been made to use these stress-wave emissions to detect the presence of growing defects in high-strength metals undergoing cracking.

The Aerojet-General Corporation has developed a system utilizing a Stress-Wave Analysis Technique (SWAT) to detect, locate, and monitor the growth of flaws in a structure under load. Energy released during incremental extensions of the flaw is detected as stress-waves in the material. These elastic-waves travel at velocities which are characteristic of the particular material. Each sensor attached to the test specimen detects the wave front at a different time depending on the flaw's distance from the sensor. The time differentials in the arrival of the waves at the sensors are used to define the origin of the waves and thus locate the flaw.

The reduction to practice of the SWAT concept and system development has been accomplished during the past five years on various Aerojet programs. The applications to metallics followed the significant development that had been made on a glass laminated material. In the development of glass-filament-wound rocket motor cases, it was noted that noises were emitted by the cases during pressurization. A research program determined that a significant relationship existed between these noises and the structural integrity of the motor case. Ultimately, a stress-wave detection and analysis technique was developed that predicted the burst strength on the second cycle of pressurization based on the "Stress-Wave Signature" of that case obtained during the proof hydrotest. Reference (7) provides a description of the results of the technique on earlier programs. This relationship between the noises emitted and the structural integrity of the case has been explained in terms of a "failures per unit area" concept.

The "failures per unit area" concept is based on a premise that equal cross-sectional areas of the same material can withstand an equal number of discrete failures. This premise is applied, basically, by measuring the energy released during a series of replicate specimen tests and relating this value to the strength of the specimen. Series of tests provide a statistical basis for the establishment of the relationship which can then be projected, by simple ratio, to other test specimens of the same material.

Although the situation is conceptively somewhat different in the case of metal chambers (single flaw as a failure source instead of a statistical distribution of weak areas) the application of SWAT techniques to metal structures should be as fruitful as for the filament wound chambers.

The application of SWAT to titanium and maraged steel motor cases showed that incremental crack growth preceded failure. This was verified in laboratory tests using tensile specimens made of various materials containing inflicted flaws. The failure in all specimens preceded by distinct stress-wave emissions as the flaws increased towards a critical size. However, since the distribution of stress-wave emissions preceding failure will vary with varying material properties and with the nature of the flaw resulting in failure, application of the SWAT techniques to metal chambers needs an understanding of the basic mechanisms of stress-wave emissions.

The present paper is composed of two parts: 1) a report on a laboratory investigation of stress-wave emission in small stressed steel samples, and 2) a review of the practical application of SWAT (acoustic monitoring techniques) to the detection and location of flaws and failure origins in high-strength metal chambers.

II. LABORATORY INVESTIGATIONS

A. EXPERIMENT PROCEDURES

The loading system employed in bend tests on small laboratory specimens is shown schematically in Figure 1. The use of this arrangement results in nearly pure bending with the bending moment constant over the entire test length of the specimen. The low axial load (i.e., 50 lbs to produce a maximum fiber stress of 100,000 psi) results in nearly all the stored elastic energy for fracture propagation is in the specimen rather than in the testing machine (i.e., the specimen is soft whereas the machine is hard). For tests with precracks, a small hole was drilled in the center of the sample and a fatigue crack initiated in cantilever bending. The sample size is approximately 3" x 3/4" x 1/8". Thus, the samples were subscale from the fracture mechanics viewpoint.

The placement of the accelerometer in these laboratory tests apparently is not critical. Tests using impacts of small tungsten pellets ($\sim 10^{-3}$ gm) show little difference in amplitudes as a function of accelerometer placement.

The output of the accelerometer is amplified and fed to an oscilloscope for direct viewing during the test and recorded on tape for later playback at reduced speed and oscillograph recording.

Table I shows yield stress, ultimate stress, % elongation, and W/A for the major materials used in the program. The fracture toughness (W/A) was evaluated using precrack Charpy impact specimens. In addition to these tests, tests were made on a 4340 steel tempered from 100°F to 1130°F. These samples were 1/16" thick.

B. MICROCRACK FORMATION

The initial tests were designed to determine if sources other than cracks were giving detectable stress-wave emissions and to establish the crack size necessary to produce detectable stress-wave emissions at the 0.01g level. This level of sensitivity was chosen as the highest useable in a practical chamber test due to background noises. The testing of unflawed samples were interrupted before a detectable stress-wave emission, or after one or several stress-wave emissions. The sample was then examined metallographically to determine the deformation processes not resulting in a stress-wave emission and the size limits between cracks resulting in stress-wave emission and those which did not result in detectable emission at the sensitivity level used (0.01g). These tests showed that gross plastic deformation; fracture of inclusions, small fractures corresponding to a grain dimension in length, and the small amount of crack growth accompanying the formation of the plastic zone at the crack tip of a fatigue precrack do not result in stress-wave emissions at the 0.01g level.

Figure 2 represents typical cracks which did not result in detectable stress-wave emission. Figure 2a shows a microcrack nucleated in a 300 grade maraging steel sample by an intermetallic inclusion. The crack has terminated with only minor growth in the metal and it would be expected to be relatively stable upon further unidirectional stressing. The estimated crack area in less than 10^{-6} in.^{2}.

Figure 2b is a microcrack (300 grade 18% Nickel maraging steel) of essentially one grain size. Again, the crack is expected to be stable against further stressing and no stress wave emission was detected.

Figure 2d is a somewhat larger stable microcrack (D6aC-600°F temper) of unknown origin (presumably nucleated by an inclusion). Again, no stress-wave emission was detected due to this crack. Crack area is estimated at 10^{-6}in.^{2}. Figure 2c (D6aC-600°F temper) is another crack nucleated by an inclusion (the thin horizontal line in the figure). The crack is estimated to be slightly less than 10^{-5} in.^{2}. No stress-wave emission was detected due to this crack.

In all four cases shown, the crack area is estimated to be below 10^{-5} in.^{2}, and the cracks are stable and would not result in failure of a structure. Thus, with a level of sensitivity of 0.01g, one does not detect the many small microcracks due to fracture of single grains or inclusions cracking or tearing away from the metal matrix.

Somewhat larger cracks, approaching those of dangerous dimensions, do give detectable stress-wave emissions. Figure 3 shows cracks in D6aC samples (600°F temper) which have resulted in detected stress-wave emissions. Figure 3a shows a side view of a crack nucleated by a thin tape-like inclusion like that in Figure 2d. The initial cracking produced a pulse of greater than

0.1g and subsequent growth under continued stressing produced several pulses greater than 0.01g. The area of the initial crack was approximately 4×10^{-5} in.^{2}. Figure 3b shows a crack of area between 10^{-5} in.^{2} and 10^{-4} in.^{2} which resulted in stress-wave emission. In both cases, the surface of the sample (tension) is on the left.

In general, in these materials the formation of a crack with area greater than 10^{-5} in.^{2} resulted in stress-wave emissions; formation of a crack with area less thar 10^{-5} in.^{2} did not result in detectable stress-wave emission (0.01g sensitivity). The material type or heat treatment appears to have effect on the type of microcracking which occurs, but no major effect on the size of crack necessary for detectable stress-wave emission.

C. EXTENSION OF MACROSCOPIC CRACKS

Tests were carried out to determine the amount of extension of pre-existing crack necessary for the appearance of detectable stress-wave emission. Samples were fatigue precracked and then stressed till the detection of one or several stress-wave emissions. The samples were then either sectioned and the crack examined metallographically or refatigued to complete failure.

Figure 4 shows fracture surface of two samples (D6aC-1075°F temper) fatigue pre-cracked, tested till the detection of stress-wave emissions and then refatigued. The area of crack extension during the unidirectional stressing shows up as a light area in Figure 4 and is too small to distinguish in Figure 4a. During the testing of the sample in Figure 4a, 4 pulses less than 0.02g were detected. In the test of sample Figure 4b, 11 emissions between 0.01g and 0.02g and three emissions over 0.1g were detected. The corresponding areas are less than 5×10^{-5} in.^{2} and approximately 4×10^{-4} in.^{2}.

Figure 5 shows, by sectioning, crack extensions in samples (300 grade 18% Nickel maraging steels) tested to: Figure 5a, no stress-wave emission; Figure 5b, one stress-wave emission; and Figure 5c, several stress-wave emissions. In these materials, the fatigue precracks widen with no extension upon initial loading and then narrow cracks nucleate and grow at the corners. Stress-wave emission is invariably associated with significant growth of these cracks.

The behavior of D6aC samples is similar to that of the maraging steels. Results on other programs, however, have shown that for metals with ductility significantly higher than the 200 grade maraging steel, macroscopic subcritical crack growth can occur without stress-wave emission detectable at the 0.01g level.

D. STRESS-WAVE EMISSION FROM SAMPLES TESTED TO COMPLETE FRACTURE

In addition to investigations of the source of the initial stress-wave pulse or pulses from a sample, the stress-wave emission from subcritical crack growth in samples tested to complete fracture was investigated. Figure 6 shows the load-time (cross head travel) curve for a fatigue precracked sample (D6aC-600°F temper) tested to fracture at room temperature. The initial stress-wave emission occurred at point A during the tests. Figure 7 shows typical oscilloscope traces of the stress-wave emissions at points B, C, D, and E along the curve of Figure 6. Each trace represents one second of test. The recording system saturated at 0.3g so the largest pulses on oscilloscope traces represent this amplitude or higher pulses. Undoubtedly pulses over 1g were present.

Figure 8 shows the curves of the total number of stress-wave pulses which have occurred as a function of test time for several levels of amplitude for the same test as shown in Figure 6. It is seen that as the crack grows, not only the total number of stress-wave pulses increases, but their rate of occurrence and their amplitudes also increase, particularly as the crack approaches critical size. This will be shown again more strikingly in the applications portion of the paper.

The behavior of the D6A1-1075°F temper and the maraging steels is similar, although number and amplitudes of stress-wave emissions depends strongly on material condition. This was shown strikingly by a series of tests on 4340 steel samples tempered between 100°F and 1100°F. Figure 9 gives the total number of pulses of amplitude greater than 0.1g before fracture as a function of temper temperature. Figure 10 shows the spread in load, (stress) between the initial pulse and the fracture load. For low temper temperatures (brittle samples) little or no subcritical crack growth occurs and none or only a few stress-waves are emitted. The generation of a stress-wave requires crack growth. At intermediate temper temperatures (in ranges where the material is normally used) significant subcritical crack growth occurs at stresses well below the failure load and many stress-waves are emitted. At higher temper temperatures, the subcritical crack growth still occurs but at a lower stress and apparently in smaller steps. The amplitude of the stress-waves emitted decreases drastically and the number somewhat more slowly.

Several tests on the D6A steels were run with the load recording system set for extremely high sensitivity in an attempt to correlate load drops (crack growth steps) with specific acoustic emissions. Figure 11 shows the load-time-crack extension curve and schematically the acoustic emission for a short interval near the maximum load of such a test. Although one can correlate some of the large stress-wave emissions with load drops, not all large stress-wave pulses correlate with load drops. From this, one can calculate an upper limit for the area of crack growth responsible for a specific stress-wave pulse.

The load sensitivity is such that a crack growth step of 2×10^{-6} in.^{2}, would be detected as a load drop. This means that those acoustic pulses, some as large as 1g, not correlated with a detectable load drop are caused by crack growth steps less than 2×10^{-6} in.^{2} in area. Comparing this value with the minimum crack area or crack extension area (approximately 10^{-5} in.^{2}) necessary to produce a detectable (0.01g, stress-wave pulse and the average area per pulse in large scale subcritical crack growth (also 10^{-5} in.^{2}) one sees that the majority of crack growth occurs in steps too small or too slow to produce detectable (0.01g) stress-wave emission. Presumably heterogeneities and the statistical nature of their distribution apparently ensure the presence of one in a crack surface area of the order of 10^{-5} in.^{2}.

III. APPLICATIONS

A. NASA -- FEASIBILITY PROGRAM

Based on the successful use of SWAT on the glass-filament wound cases and the demonstration of stress-wave emission from flawed metal samples, NASA sponsored a program for the investigation of the applicability of SWAT towards preventing failures during hydrotests of the 260-inch diameter motor cases[5]. In conducting this program, stress-wave data recordings were obtained during the manufacturing proof tests of various rocket motor cases and also from laboratory tests of tensile specimens with pre-induced flaws.

1. Tensile Specimen Tests

Tensile specimen tests on 200 grade 18% Nickel maraged steel demonstrated the significance of SWAT. Specimens, designed in accordance to ASTM requirements for valid fracture toughness measurements, with precrack surface flaws (Figure 12), were tested under a constantly rising uniaxial load to a point near failure and then unloaded when critical stress-wave emissions were observed. Figure 13 "Stress-Wave Emissions vs. Load, Interrupted Test of Specimen 217", shows a typical stress-wave emission pattern versus time from the first loading cycle of the specimen, and the second loading cycle carried to failure. This specimen failed on the second cycle, at a lower load, than that sustained during the first cycle. This data was obtained by recording stress-wave emissions with an accelerometer-tape recorder system and then playing the data back through a level-recorder to display each wave as a single peak on the strip chart.

Figure 14 shows the cross-section view through the flaw in a tensile specimen tested to a load release point in one cycle. After the test, the specimen was baked to heat-tint the gross cracked area, then saw-cut part through the broken in bending while conditioned and exposed at -320°F -- liquid nitrogen temperature -- in order to preserve the marking of the stable crack growth that had occurred during the initial tensile loading cycle. The flaw grew through approximately 90% of the thickness of this specimen.

Similar specimens which varied only in the size of the initial pre-crack flaw produced stress-wave results as displayed in Figure 15. Here, each stress-wave is represented by a vertical line. Observation of crack growth area and comparison of the number of stress-waves, gave a basis for the "failures per unit area" concept in the homogeneous materials. Specimens of identical material with smaller cross-sectional areas have fewer stress-waves before failure. In fact, relationships between stress-wave emissions and incremental crack growth are being defined in various research programs at this time. References 8 through 11 present the published results of some of the work to date.

2. Motor Case Tests

Figures 16 and 17 show the instrumentation locations, and a detailed drawing of the weld seam and defects that initiated the failure of a 260-inch diameter chamber. This chamber failed in hydrotest due to undetected defects. The failure report (Reference 12) notes that "During the post failure inspection of welds, eleven defect areas were found that had not been evident, or not rejectable, by the applicable standards prior to hydrotest." The investigating committee's report also stated "all applicable NDT inspection techniques must be utilized since no single one is infallible, --"and "it appears possible to have submerged defects within welds that are not detectable by NDT methods now available." The material used in this chamber was 250 grade 18% nickel maraged steel fabricated by the submerged arc welding technique. Note that prior to failure, two stress-waves had originated in the general area of fracture initiation.

During this program, SWAT was applied in a series of pressurization tests on rocket motor cases of AMS 255 steel which had been rejected by their manufacturers as unsalvagable due to gross-porosity in the weld seams. The chambers were SWAT tested in order to obtain stress-wave data from growth of natural manufacturing defects such as weld porosity. These rejected cases [illegible] the design strength levels very satisfactorily and were finally burst at pressures very close to design ultimate. Between repeated pressurization tests, to increasing pressure levels, radiographs taken of areas of maximum stress-wave activity barely showed the interactions between the pores as minor cracking.

Stress-waves were recorded in each of these tests with the SWAT accelerometer-tape recorder system. Minimum signal resolution was, in most cases, .1g-units. The AMS 255 chambers tested, with gross porosity, had more stress-wave activity from the failure source, prior to failure, than any other chambers tested.

B. SUMMARY OF CHAMBERS TESTED

Table II presents a listing of a number of pressure vessels which have been proof or burst pressure tested with SWAT applied. Table III shows the SWAT established location of failure for a series of chambers as compared to the origin defined metallurgically. The SWAT technique was first applied on 6Al-4V titanium motor cases as a means of locating the primary origin of failure. Successful results, together with the observation that stress-wave emissions preceded failure, led to application of the technique on other programs.

One program, on 4130 steel chambers, was conducted to establish whether the technique might be applied as a real-time process control during structural testing. A series of tests were automatically terminated, after crack growth had initiated but prior to complete specimen failure, by utilizing the stress-wave data as the control input.

In all chambers which were tested and failed, stress-wave emission, from the failure source, was detected prior to complete destruction of the specimen.

Through the use of the triangulation capability, the stress-waves preceding failure and at failure were used to define the primary failure origin. The distance from the stress-wave located origin to the metallurgically defined origin of failure is listed in Table III. The largest vehicle which failed during a test with SWAT applied was the 250 grade 18% Nickel, maraged steel 260-inch diameter large solid rocket motor case. Stress-wave sensors were located approximately 192 inches apart during this test. The stress-wave defined origin of failure was 12 inches from the metallurgically defined origin.

C. NASA - ALUMINUM ALLOY

The type of stress-wave activity detected during flaw growth in crack induced tensile specimens of 2014-T6 aluminum alloy is shown in Figure 18. A view of the fracture surface of two aluminum tensile specimens is shown in Figures 19 and 20. These specimens were loaded in constantly rising uniaxial load and after large amounts of stress-wave emission, or crack opening displacement, was observed, the load application was interrupted and the specimen cycled in high-frequency fatigue. This was done to extend the present boundary and thus provide a surface marking relating the amount of slow crack to that particular amount of stress-wave activity (Reference 13).

D. NON-DESTRUCTIVE TEST ADJUNCT

The fact that flaws, of any size, can remain undetected during NDT inspection procedures is the justification for the use of SWAT. The area located by stress-wave emission data can be intensively scanned with a greater degree of probable success than previously available. The fact that SWAT is basically a passive NDT process, in that the defect must grow in order to propagate a stress-wave, is a distinct advantage in its application to long-term tests or in-service use on various vehicles.

We know, and refer you to, Part I of this paper, that stress-wave emissions can and do occur from growth of flaws that are considerably smaller than the size that can be detected by the best and most discerning NDT inspection techniques heretofore available. This means that incremental flaw growth can be sensed at levels considerably smaller than the "critical sizes." If the original defect is already sufficiently large as to be detectable, NDT inspection should readily detect it. If it cannot be located, the specimen may still be structurally sound; however, that particular portion of the specimen should be more closely observed during future use. In all tests to date, on engineering materials, we have never witnessed flaw growth proceeding directly to specimen failure without stress-wave emission during the defect extension process.

E. SWAT SUMMARY

Figure 10 diagrammatically represents the applied SWAT system. The research or laboratory system comprises sensors, amplifiers, tape recorder and display items. Specific pieces of instrumentation are selected in order to satisfy various objectives or needs. For use in manufacturing areas, the SWAT system is comprised of sensors, amplifiers, data acquisition sub-systems, stress-wave analyzers, and display items. The stress-wave analyzer operates on the stress-wave data inputs and provides as output the location of the defect either printed or as geometric display in real-test-time.

We are currently using SWAT systems and techniques in two areas of prime concern. The first is as an adjunct to non-destructive test inspection techniques employed after manufacturing processes. In this application, SWAT provides complementary information regarding the structural integrity of a manufactured article. The total absence of stress-wave emissions, during a proof pressure test, for instance, provides the highest degree of confidence in the structural reliability of the part.

Stress-wave indications during these tests do not necessarily mean rejection. Through the capability to triangulate to the stress-wave origin, NDT inspections are greatly assisted. The inability of the NDT inspection to locate the flaw means that it is still smaller than the limiting sensitivity of the system. If a large flaw is found, however, it may mean the difference between success or failure of the part.

The second use of SWAT is through techniques associated with materials research programs described in Part I of this paper and in References 9 through 11. We are hopeful that relationships developed during these material research studies will enable us to assess the degree of structural degradation to a manufactured item prior to, or during, its useful life.

ACKNOWLEDGEMENTS

The investigations reported under Part II "Laboratory Investigations" were conducted under the sponsorship of the U. S. Air Force Materials Laboratory, Research and Technology Division Contract AF 33(615)-5027.

REFERENCES

1. Acoustic Emission from Metals. Its Detection, Characteristics and Source: B. H. Schofield, Proceedings of the Symposium on Physics and Nondestructive Testing, p. 63 (Southwest Research Inst. 1963)

2. Determination of the Driving Force for Crack Initiation from Acoustic Records of G_c Tests on High Strength Metals for Rocket Motor Castings; H. E. Romine, NWL Report 1770; U. S. Naval Weapons Lab., 4 October, 1961.

3. Crack Initiation in Metallic Materials, Q. Rept. 1 June to 30 Nov. 1965; V. Weiss, G. Krause, C. Chave, Jr., G. Marchetto. Q. Rept. 1 Dec. 1965 thru 28 Feb. 1966, V. Weiss, G. Krause, G. Marchetto; NOw-65-0355-d, Report #3.

4. Christensen, R. H., Cracking and Fracture in Metals and Structures, Proceedings of the Crack Propagation Symposium, Vol. II, p. 326, Cranfield, Eng. 1961.

5. Green, A. T., Lockman, C. S., Brown, S. J., and Steele, R. K., Feasibility Study of Acoustic Depressurization System, NASA CR-55472 March 1966.

6. Crimmins, P. P., Hartbower, C. E., and Gerberich, W. W., Characterization of Fatigue-Crack Growth by Stress-Wave Emission, Final Report, NASA-Langley Research Center, June 1966.

7. Steel, R. K., Green, A. T., and Lockman, C. S., "Acoustic Verification of Structural Integrity of POLARIS Chambers", Society of Plastic Engineers 20th Annual Meeting, Atlantic City, New Jersey, 27-30 January 1964.

8. Gerberich, W. W., Hartbower, C. E., Feasibility Study for Measuring Fatigue-Crack Growth Rate in Welded HY-80 Steel Using Stress-Wave Emission, UAN-N000(167)-64934(X) (FBM) July 1966.

9. Hartbower, C. E., Gerberich, W. W., Mechanism of Slow Crack Growth in High Strength Steel, AF 33(615)-2788, February 1966.

10. Aerojet-General Corporation Special Report 1-4081-01-5.4-001 Downey Plant, Stress-Wave Analysis of Lunar Excursion Module (LEM) Tanks During Proof and Burst Tests, 13 December 1966.

11. Steele, R. K., Green, A. T., and Lockman, C. S., Acoustic Monitoring of Hydrotests, Weld Imperfections Symposium, Lockheed, Palo Alto, California, 27 September 1966.

References (cont.)

12. Srawley, J. E., and Esgar, J. B., "Investigation of Hydrotest Failure of Thiokol Chemical Corporation 260-inch Diameter SL-1 Motor Case", NASA TMX-1194, January 1966.

13. Green, A. T., et al, Stress-Wave Detection, Saturn S-II, NASA CR-61161, December 1966.

TABLE I

MATERIALS CHARACTERIZATION

ALLOY	HEAT TREATMENT	ULTIMATE STRENGTH (ksi)	YIELD STRENGTH (ksi)	ELONGATION %	W/A
18% Maraging					
CR-20	900°F 4 Hrs	240	230	11	1299
CR-300	925°F 3 Hrs	279	270	8.7	781
D6aC	600°F 2 Hrs	272	228	11.5	334
	1075°F 2 Hrs	225	205	16	1035

TABLE II

STRESS-WAVE ANALYSIS TECHNIQUE

APPLIED TO

PRESSURE VESSELS

PROGRAM	NUMBER OF VESSELS	MATERIAL	PURPOSE OF TEST	SPONSORING AGENCY
Minuteman	27	6Al-4V Titanium	8 Burst 19 Proof	Air Force
Large Solid Rocket	7 4 - 36" dia. 2 - 260" dia. 1 - 156" dia.	18% Nickel 200 grade maraged steel	4 Burst	NASA
Large Solid Rocket	1	18% Nickel 250 grade maraged steel	1 Proof (Vessel failed in test)	NASA
Experimental	2	AMS-355 Steel	2 Burst	NASA
Saturn	1	2014-T6 Aluminum	1 Proof	NASA
M-1	1	341 Stainless Steel	1 Proof	NASA
NERVA	1	6063-T6 Aluminum	1 Proof	AEC-NASA
Apollo	8	6Al-4V Titanium	1 Burst 7 Proof	Grumman (NASA)
Aerojet	5	4130 Steel	5 Burst	AGC
TOTAL	53		20 Burst 33 Proof	

TABLE III

SWAT LOCATION OF FAILURES

CHAMBER	MATERIAL	DIAMETER	LENGTH	NUMBER OF STRESS-WAVE SENSORS	DISTANCE FROM STRESS-WAVE ORIGIN TO METALLURGICALLY DEFINED ORIGIN OF FAILURE
Large Solid Rocket	18% Nickel, 250 grade maraged steel	260"	690"	24	12"
Minuteman	6Al-4V Titanium	52"	110"	5	2.5"
Large Solid Rocket (Subscale)	18% Nickel, 200 grade maraged steel	36"	100"	7	2.0"
Experimental	AMS-355 Steel	26"	156"	10	0
Experimental	AMS-355 Steel	26"	156"	10	0.5"
Minuteman	6Al-4V Titanium	52"	110"	5	2.5"
Large Solid Rocket (Subscale)	18% Nickel, 200 grade maraged steel	36"	100"	7	1.75"

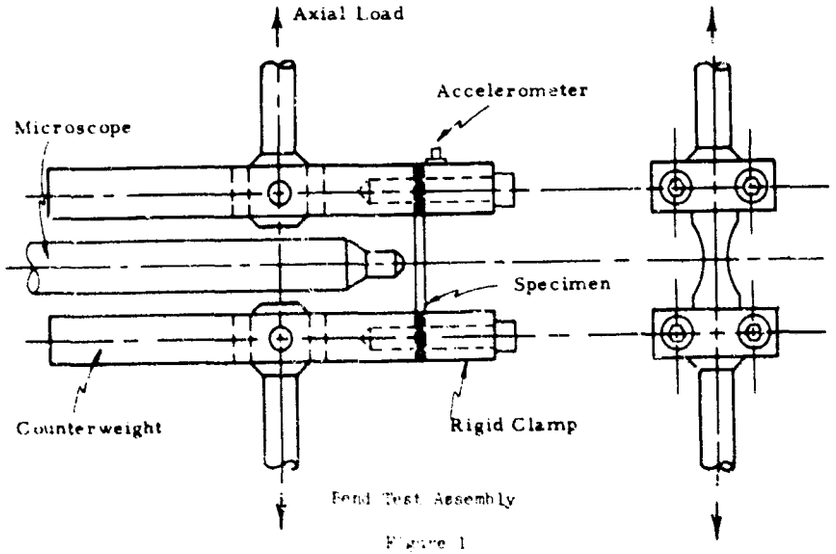

Figure 1

(1900X)

a. 300 grade 18% N_i Maraging Steel

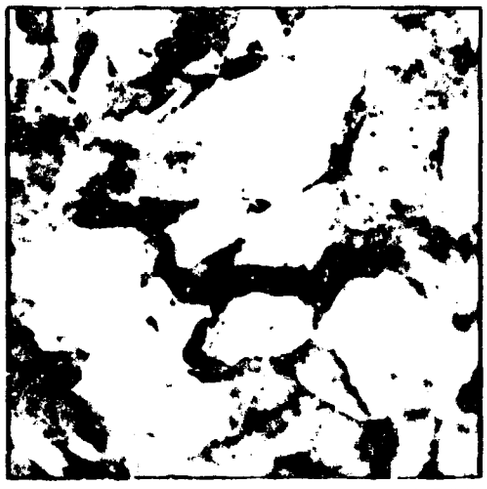

(2500X)

b. 300 grade 18% N_i Maraging Steel

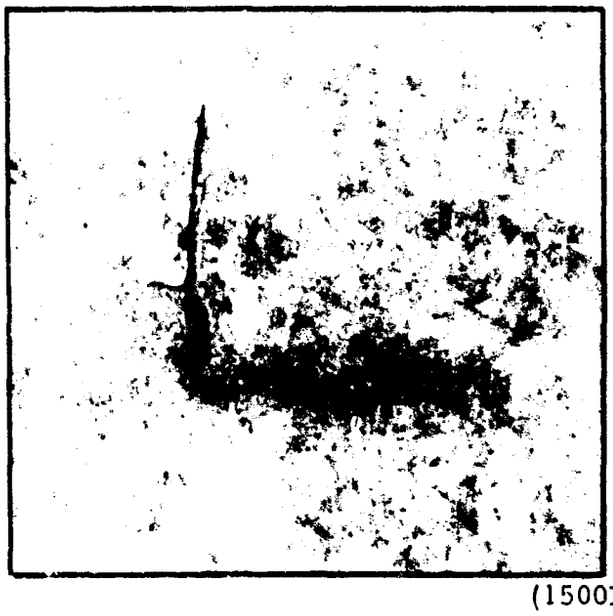

(1500X)

c. D6aC-600°F Temper

(1000X)

d. D6aC-600°F Temper

Figure 2. Cracks not resulting in stress wave emission

a. D6aC-600°F Temper (375X)

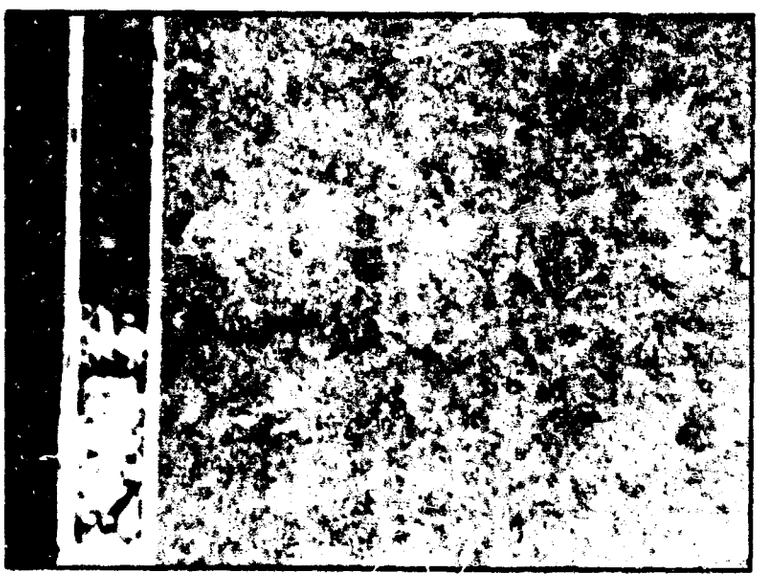

b. D6aC-600°F Temper (375X)

Figure 3. Cracks resulting in stress wave emission

a. D6aC-1075°F Temper (63X)

b. D6aC-1075°F Temper (63X)

Figure 4. Crack extensions resulting in stress wave emission

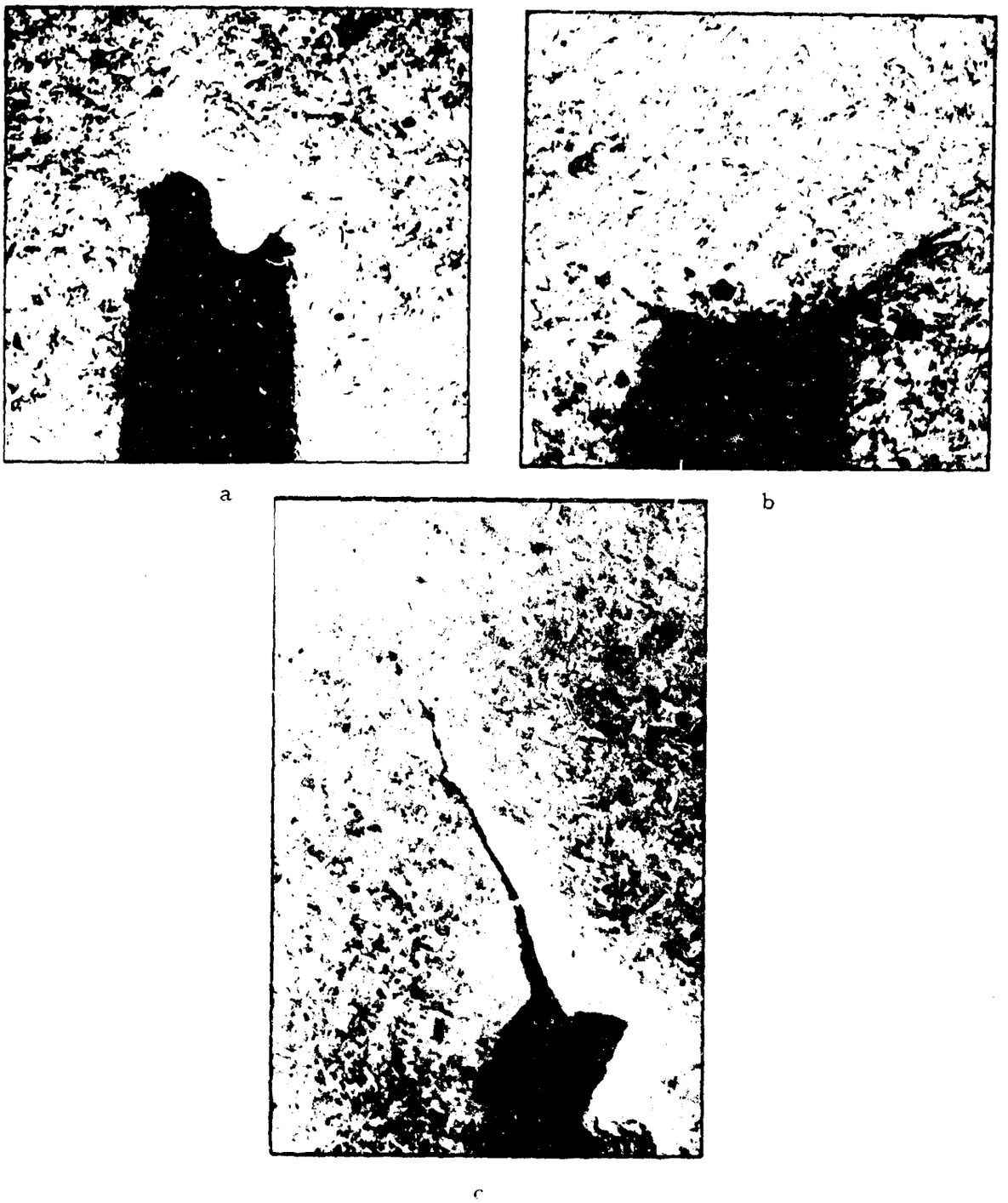

Figure 5. Crack growth from the tip of a fatigue precrack after: a, no stress wave emission (240X); b, one stress wave emission (240X); and c, several stress wave emissions (160X) (300 grade maraging steel)

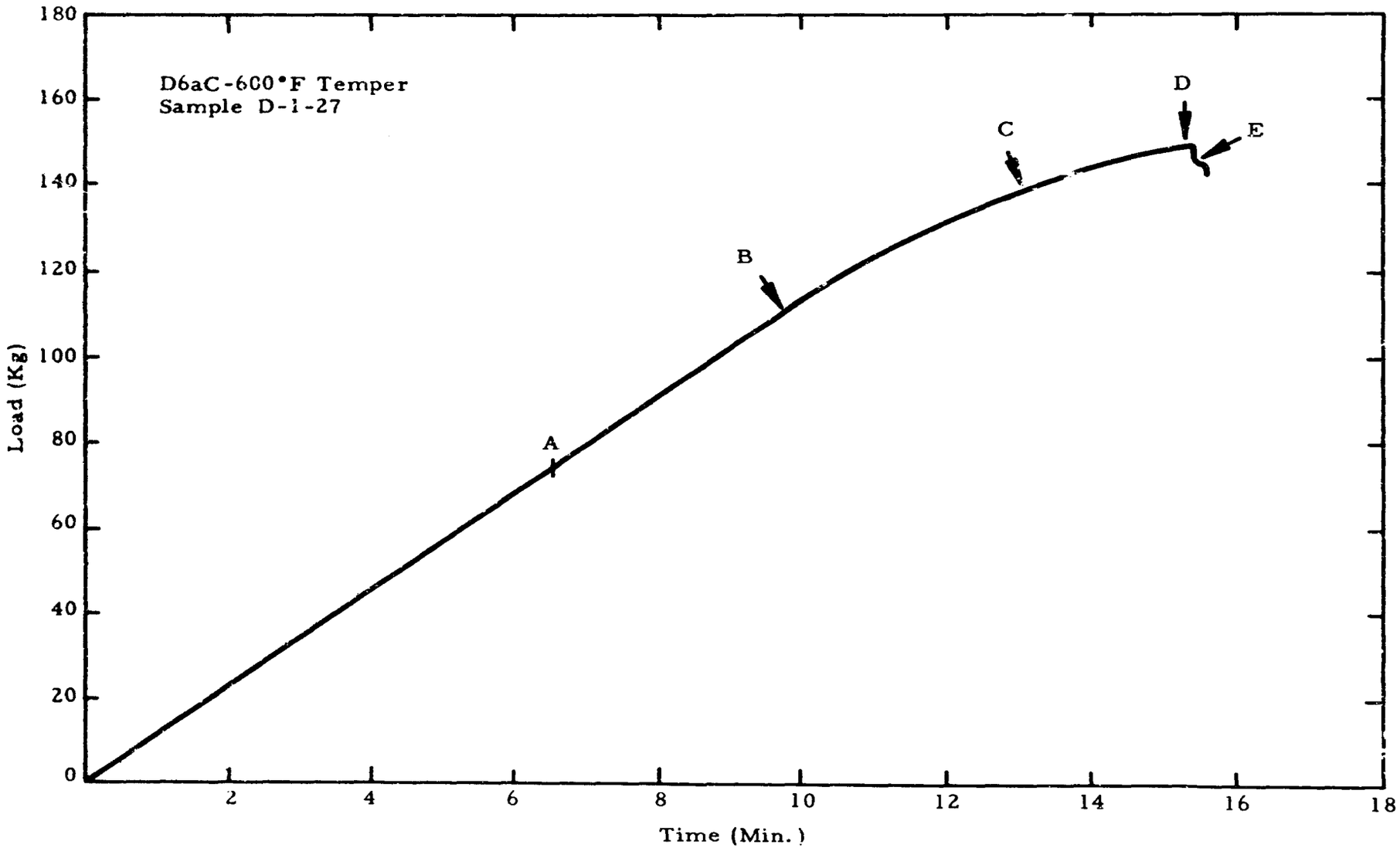

Figure 6. Load-time curve for D6aC-600°F sample. Initial stress wave at point A.

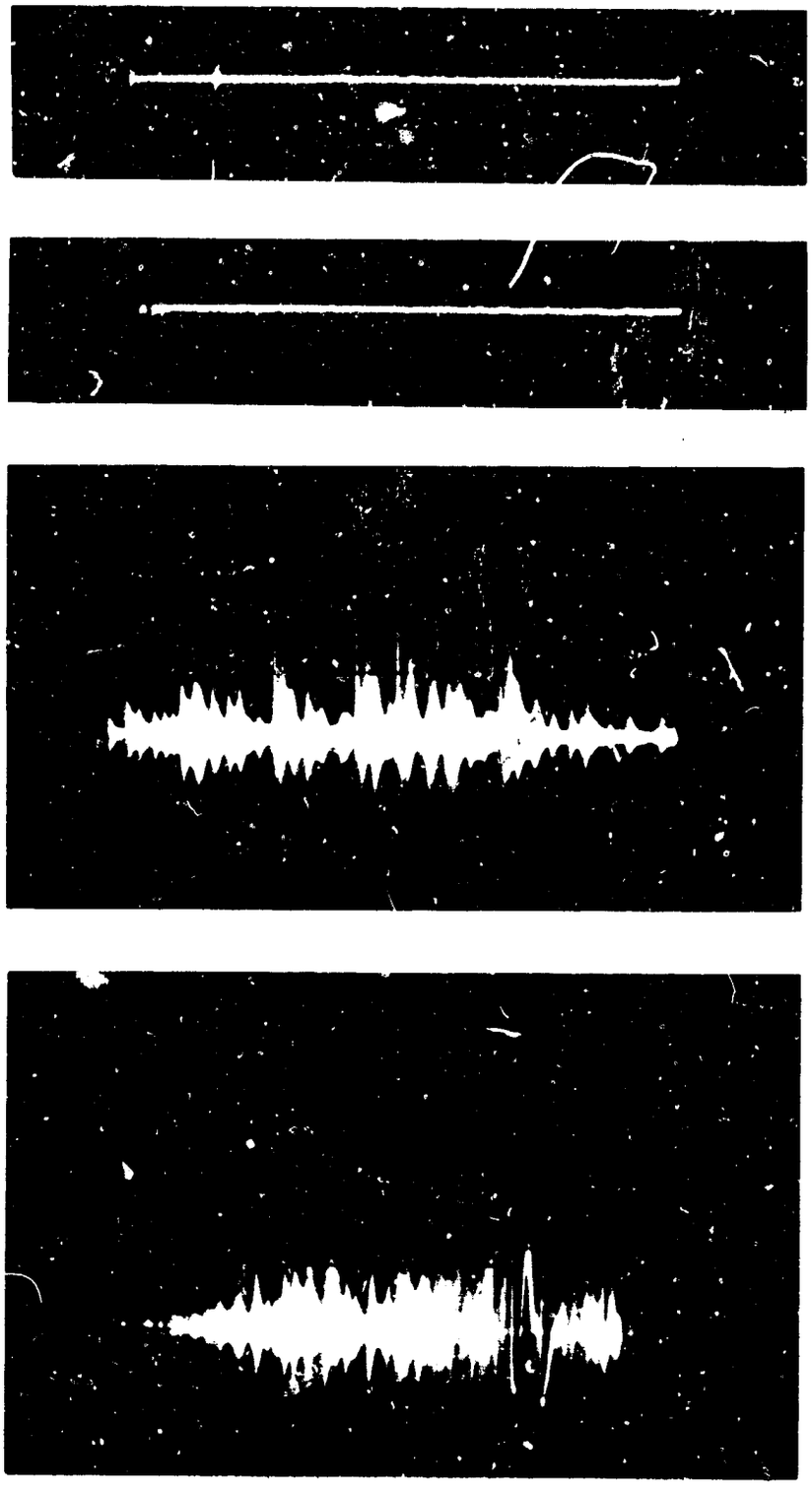

Figure 7. Oscilloscope traces from Points A, B, C, and D on the load-time curve of Figure 6

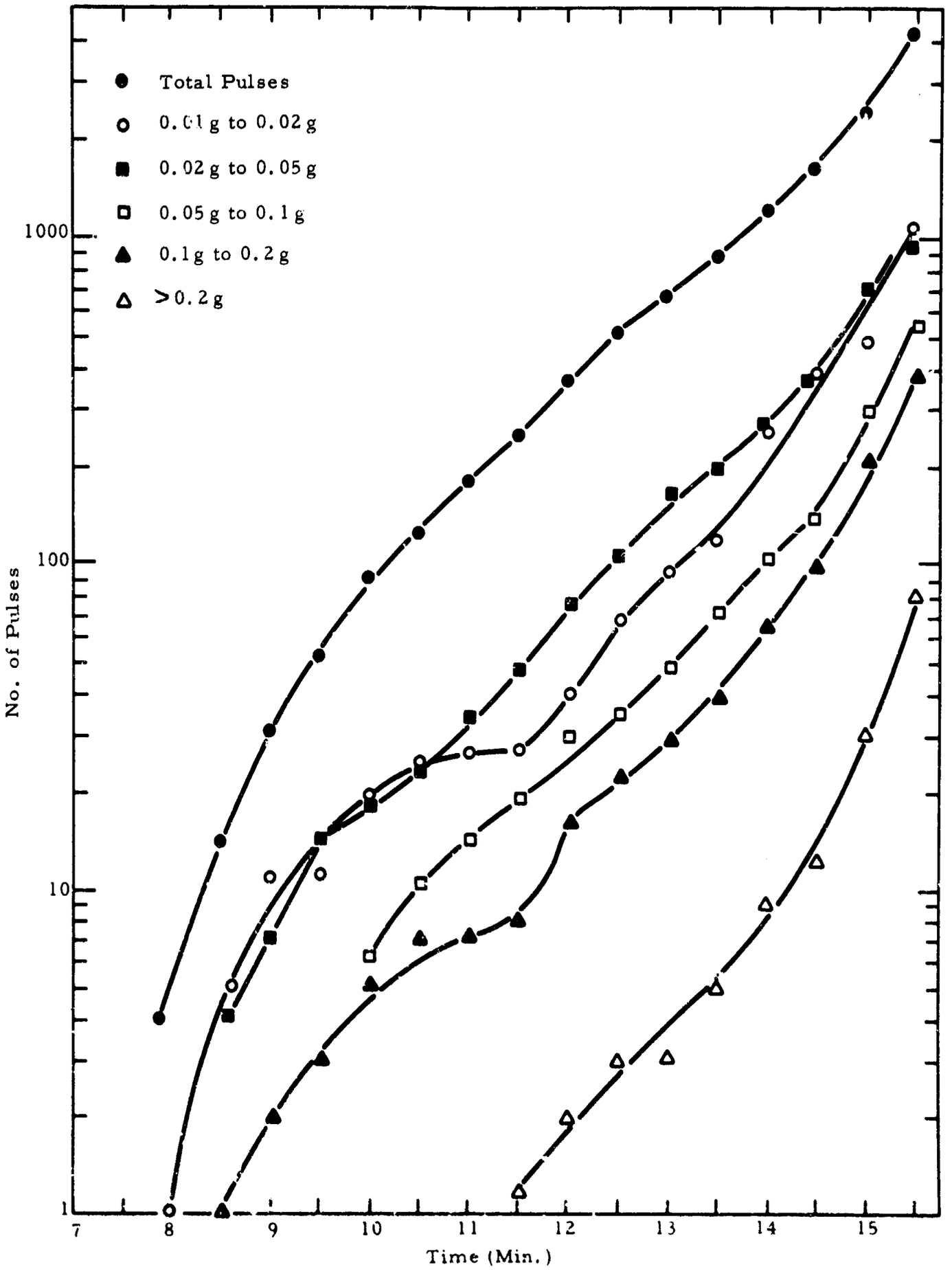

Figure 8. Number of stress wave pulses as a function of time for sample of Figure 6

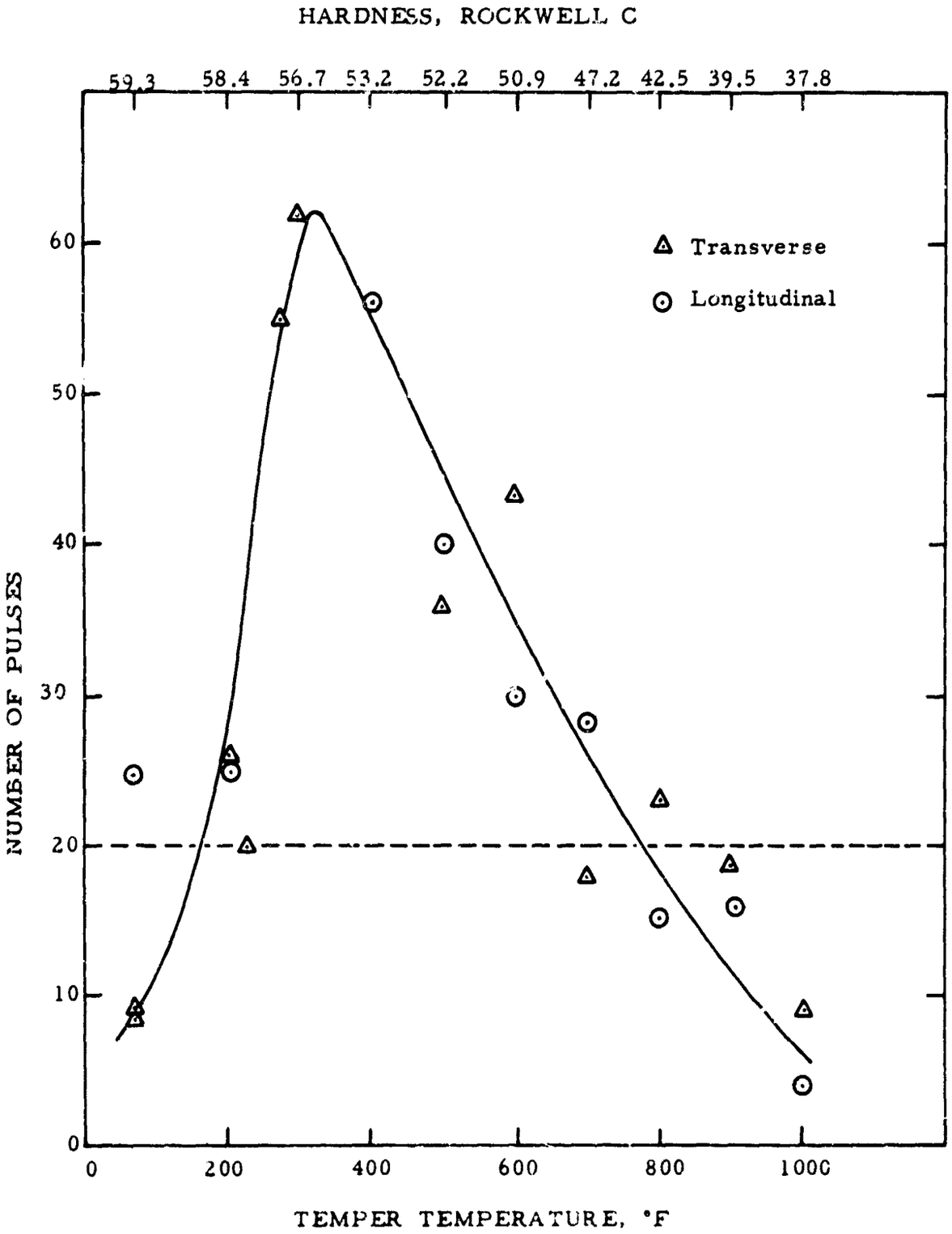

Figure 9 Number of Pulses Preceding Fracture as a Function of Tempering Temperature for Precracked 4340 Samples

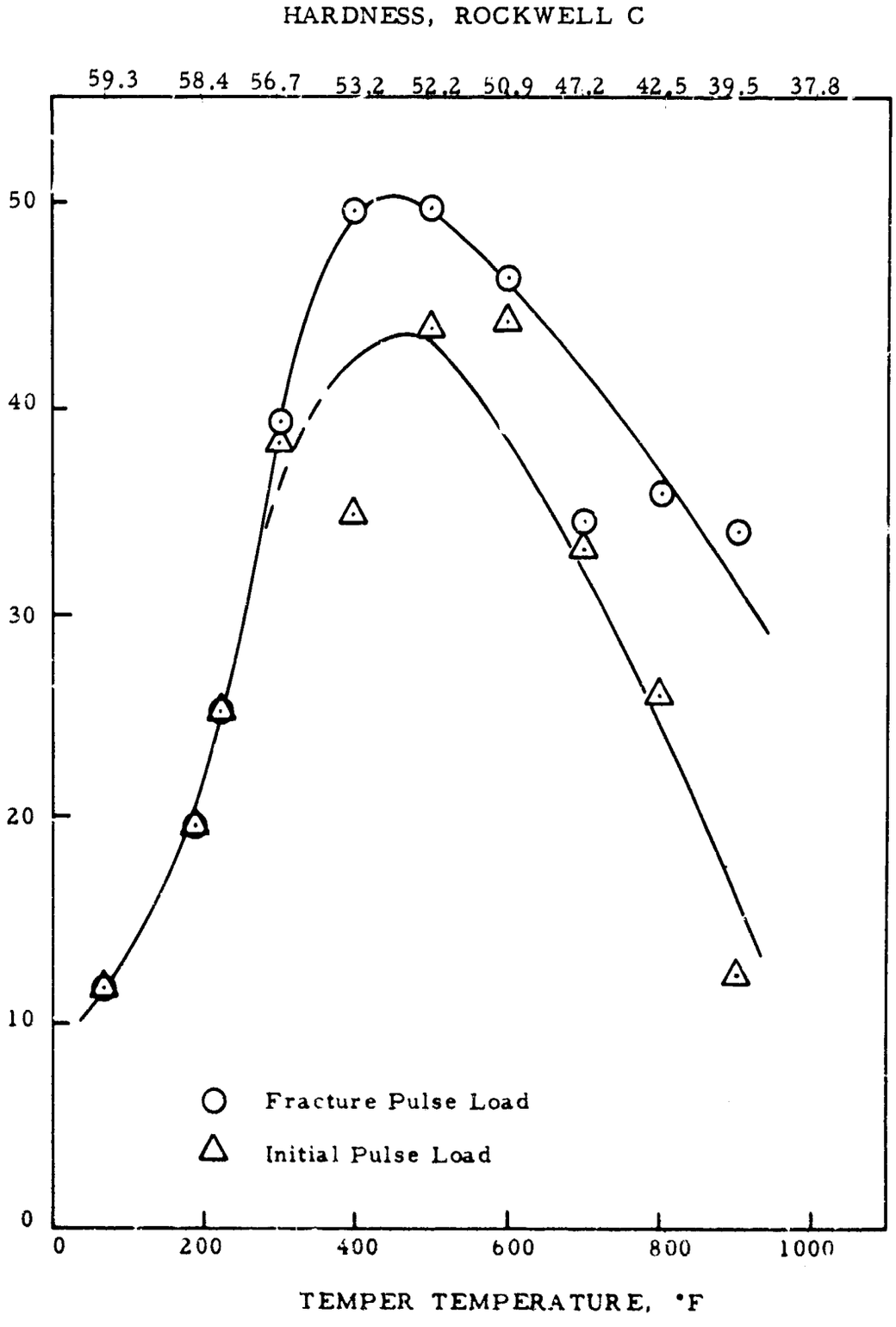

Figure 10 Load at Initial Pulse and Failure Load for Same Set of Samples as Figure 9

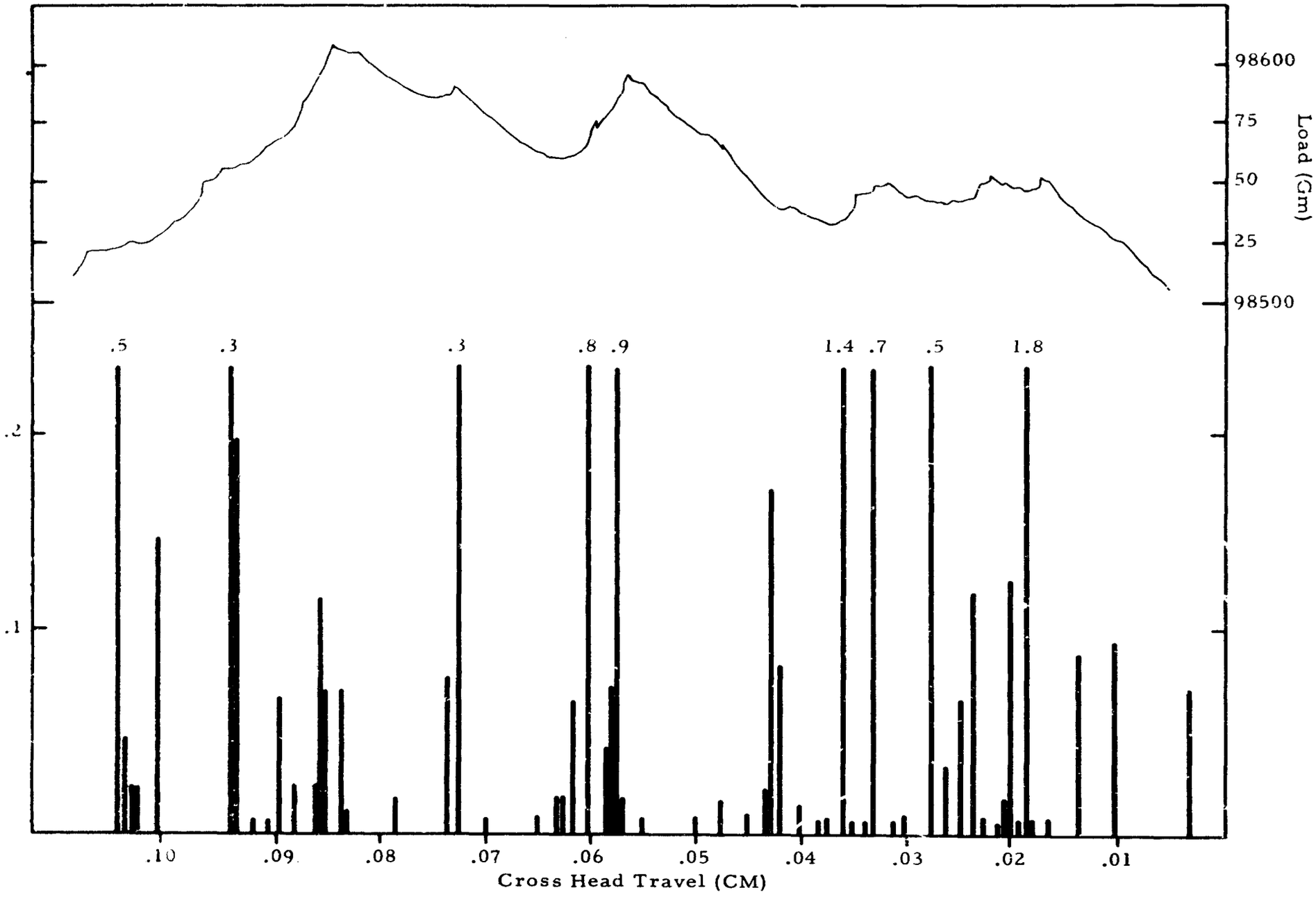

Figure 11. Load-cross head extension curve and stress wave emission near maximum load for a D6aC-600°F sample

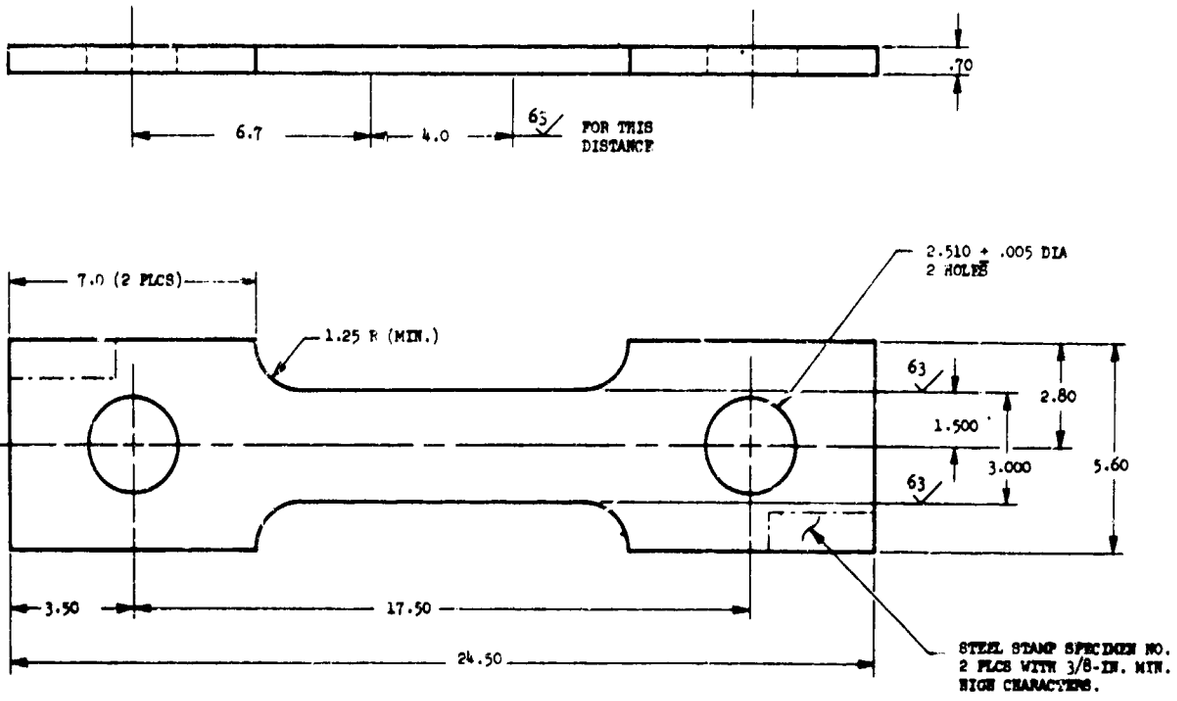

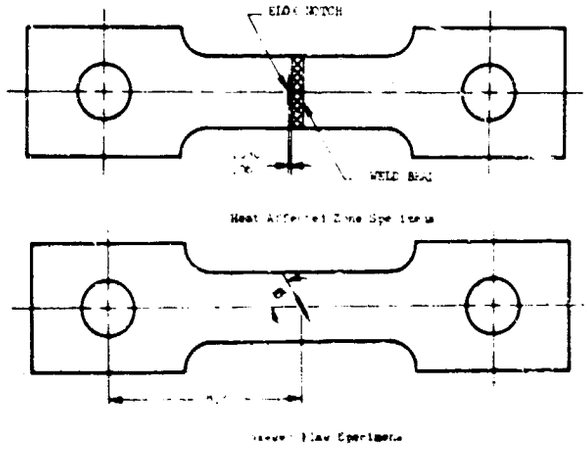

18% Nickel, 200 grade, Maraged Steel

Tensile Test Specimen

Figure 12

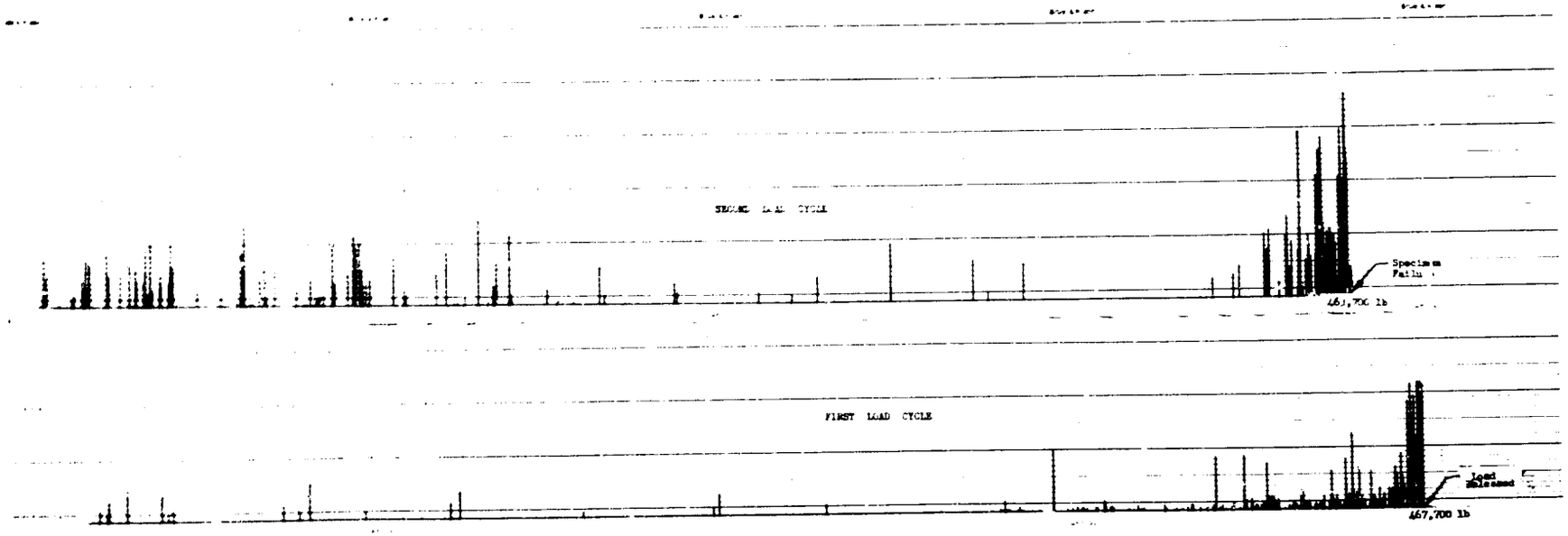

Stress-Wave Emissions vs Load, Interrupted Test of Specimen 217

Figure 13

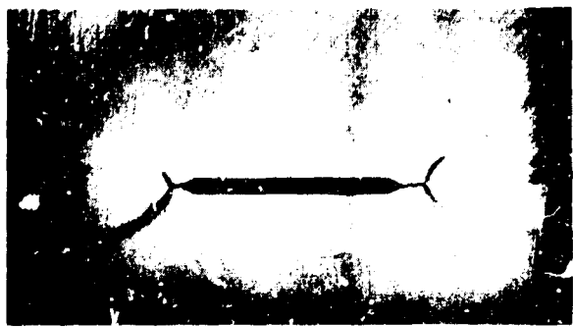

Stable Crack Extension

Figure 14

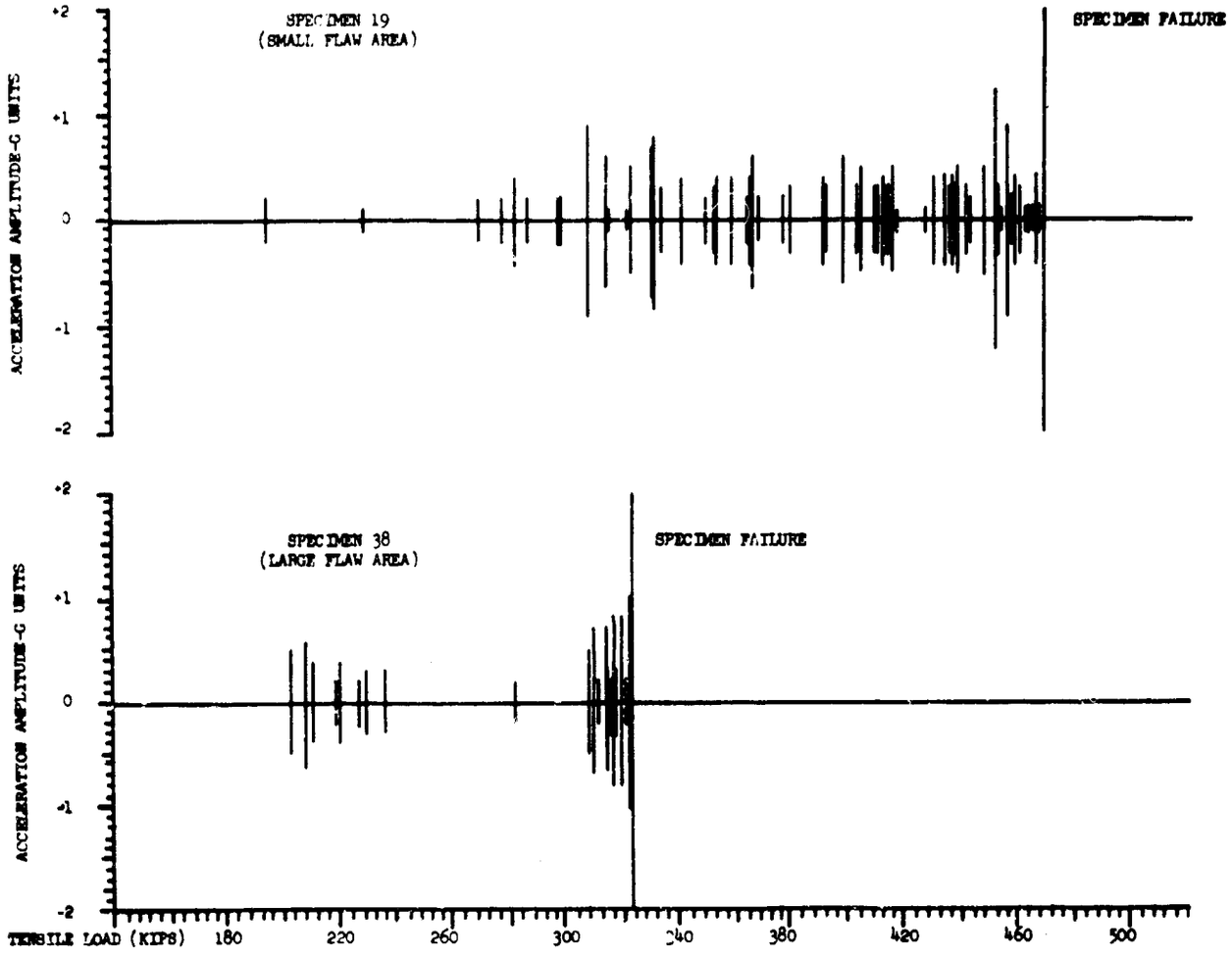

Stress-Wave vs Load, Parent Metal (Flaw Size Comparison)

Figure 15

● Accelerometer

○ 518.5 Circle of uncertainty and pressure (psi) at stress wave initiation

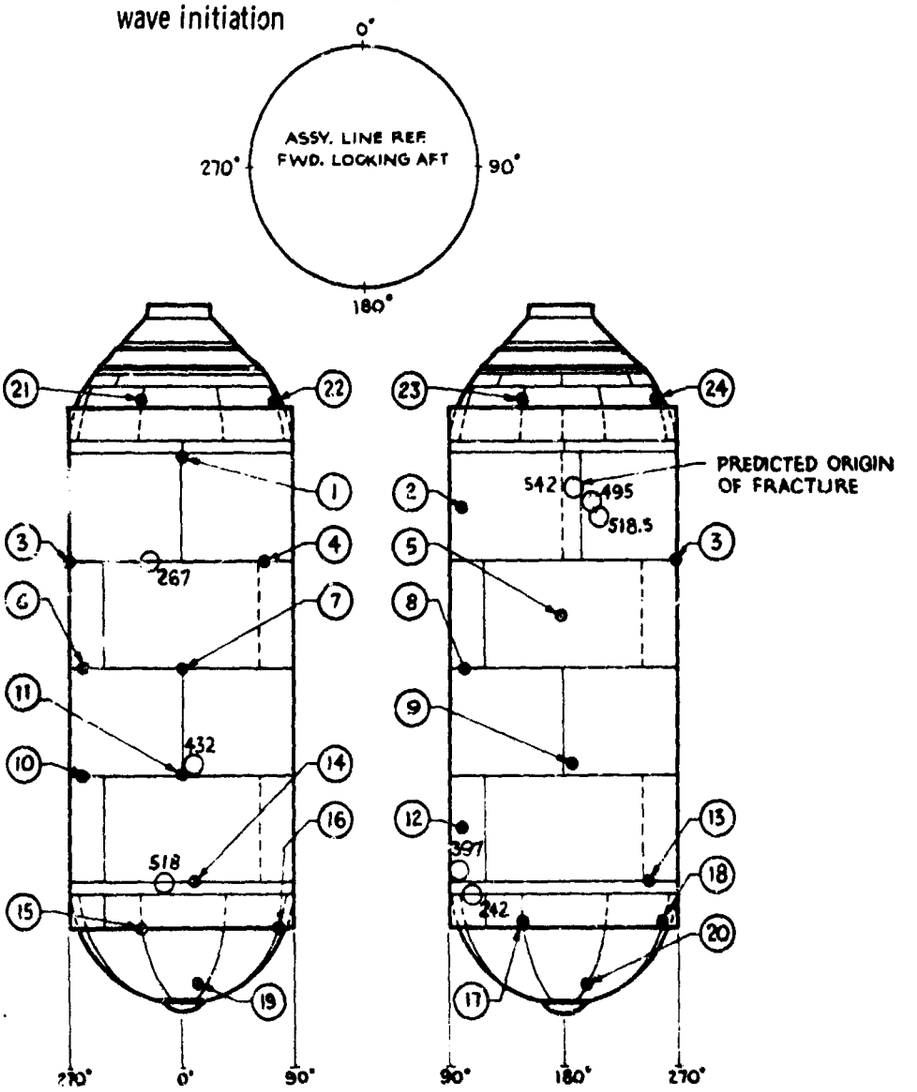

Locations of accelerometers and stress wave origins on 260 inch diameter SL-1 motor case.

Figure 16

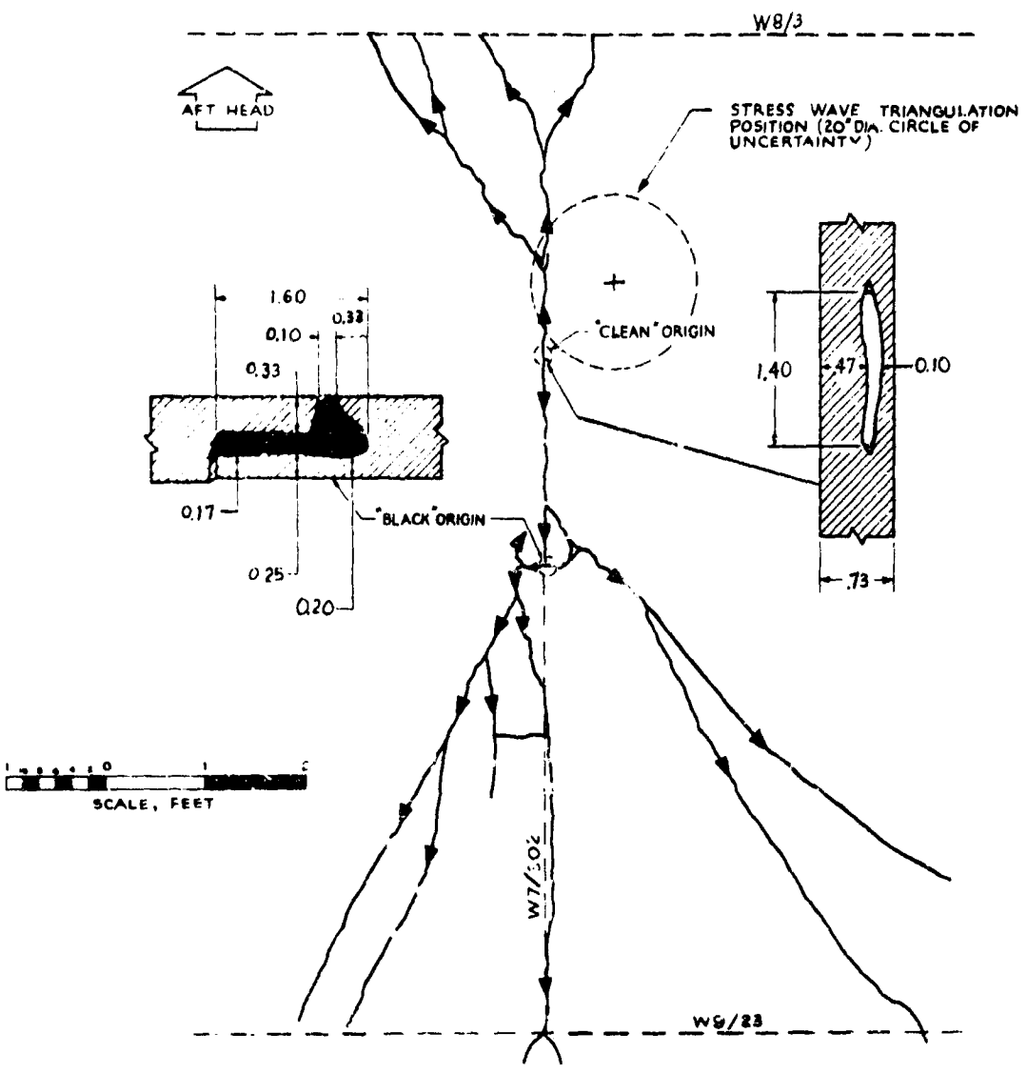

(b) Detail in the immediate vicinity of the primary and secondary origins. Inset sketches show shapes and dimensions of the two origins.

Map of fracture paths as viewed when looking at inside surface developed onto plane obtained by unrolling cylinder. Arrowheads indicate directions of fracture propagation.

Figure 17

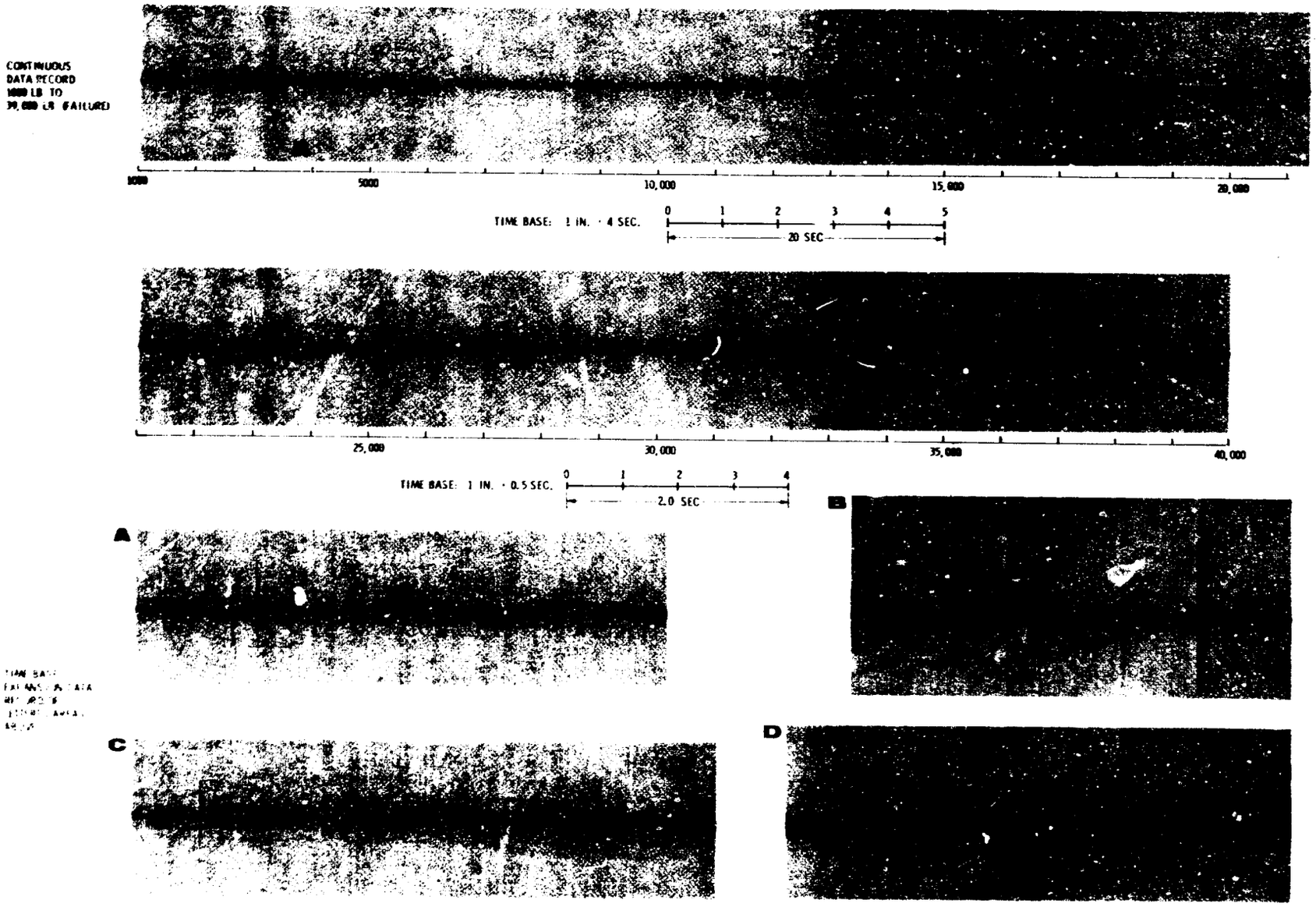

Stress-Wave Data vs Specimen Load for 0.375-in. Material

Figure 18

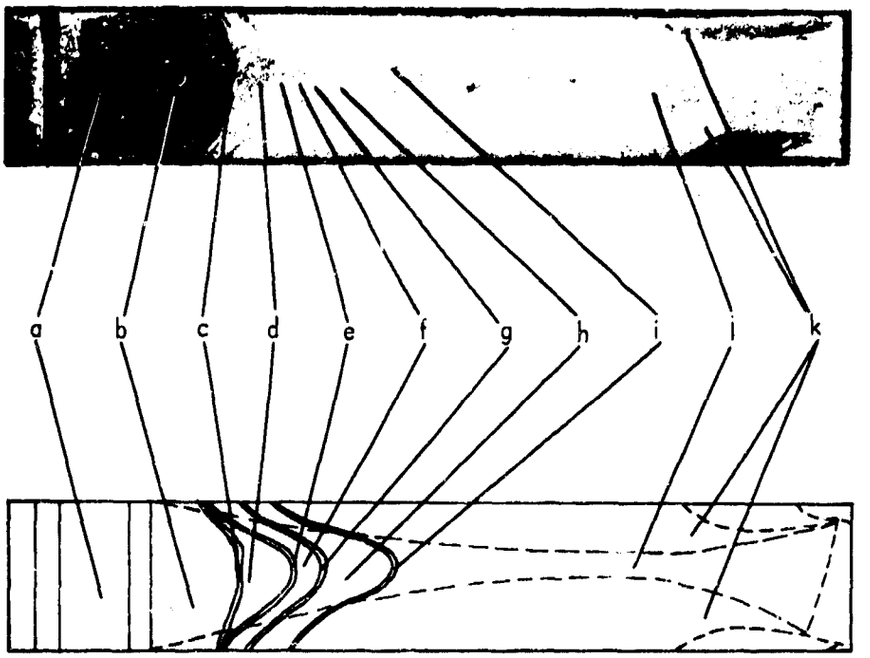

Legend:

a - Machined edge notch
b - Tension-tension fatigue pre-crack
c - Single cycle tensile crack extension
d - Tension-tension fatigue crack extension (1000 cycles)
e - Single cycle tensile crack extension
f - Tension-tension fatigue crack extension (1000 cycles)
g - Tensile crack extension (15 cycles)
h - Tension-tension fatigue crack extension (1000 cycles)
i - Tensile crack extension (5 cycles)--failure occurred on fifth cycle
j - Plane-strain fracture area
k - Shear lips

Fracture Surface of Single Edge Notch Specimen No. 7

Figure 19

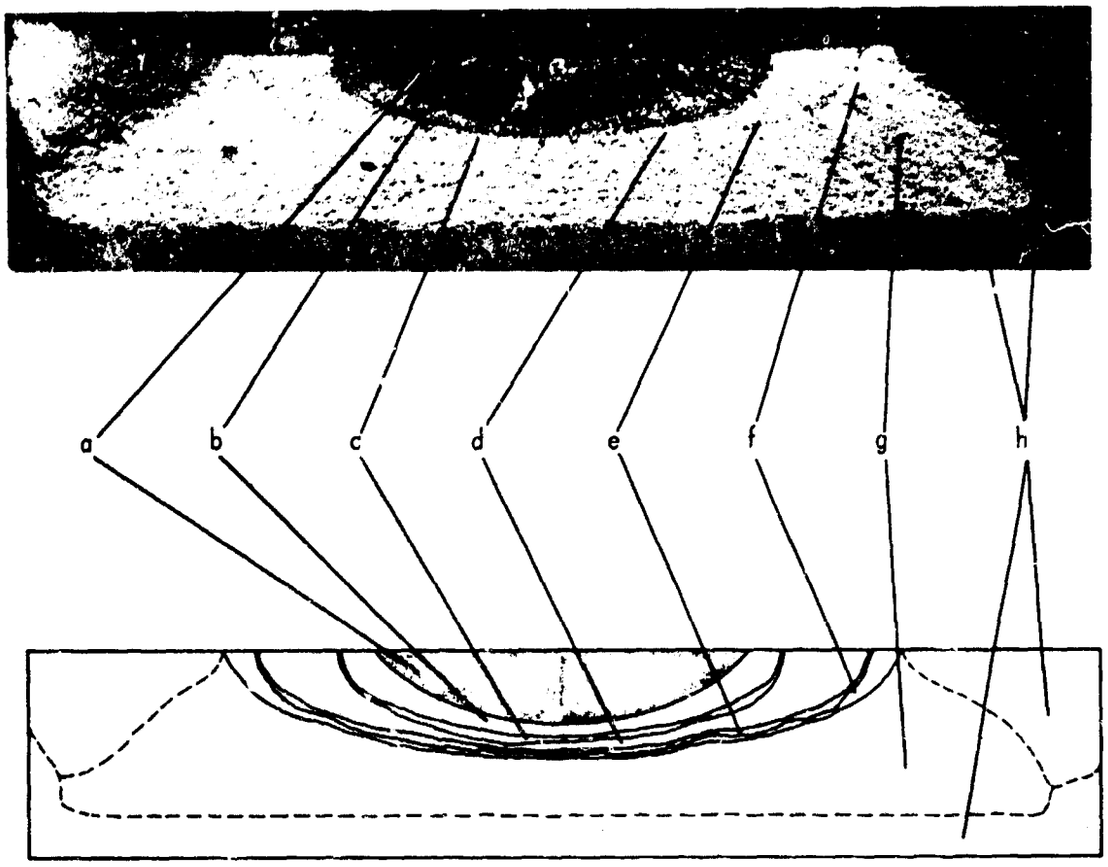

Legend:

a - Electrical Discharge Machining Notch
b - Bending fatigue precrack
c - Single cycle tensile crack extension
d - Bending fatigue crack extension
e - Single cycle tensile crack extension
f - Bending fatigue crack extension
g - Plane-strain fracture area
h - Shear lips

Fracture Surface of Part-Thru Crack Specimen No. 16

Figure 20

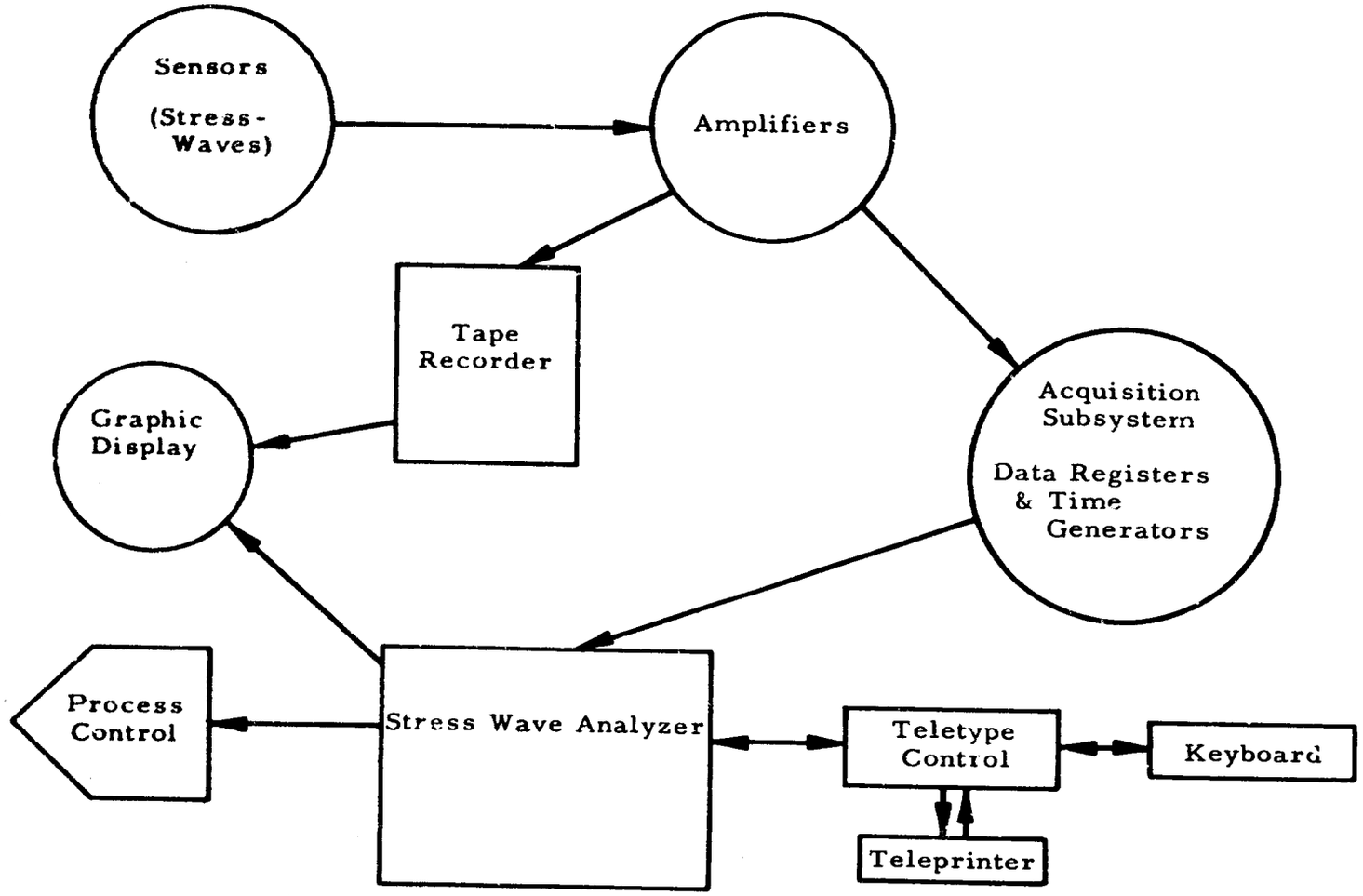

Figure 21. Schematic representation of the SWAT system

CORRELATION OF TESTING WITH SERVICE BEHAVIOR

W. C. Wake

Rubber and Plastics Research Association

of Great Britain

SHAWBURY SHREWSBURY

Shropshire, U. K.

1 - Introduction

This communication surveys aspects of work on testing and ageing actively pursued in the RAPRA laboratories. It may also be regarded as an interim report on a planned 20 year storage and test programme which is now in its ninth year. This programme is concerned with the rate of deterioration of rubber components which are not stressed, except for one case of permanent compression, but stored unstressed in three climatically differing locations. The conventional accelerated tests by oven ageing at various temperatures and high as well as normal oven humidity, were carried out at the commencement of the programme and it is now possible to compare actual performance over 7½ years (the latest date for which results are available) with the predictions of accelerated ageing.

The known disadvantages of heat oven ageing, even when carried out in a multi-cell type oven, have led to attempts to introduce stress relaxation measurements to replace or supplement conventional tensile measurements before and after accelerated ageing. Commercial apparatus for this purpose capable of insertion in the cells of a multi-cell oven became available after the 20 year ageing programme had started. Replicate compounds were, therefore, made and their stress relaxation behaviour followed. An attempt was made to investigate the relationship between structure and strength for natural rubber vulcanisates and hence to probe more deeply into the relationship between stress relaxation and strength changes for these materials. This work has immediate bearing on the interpretation of accelerated tests generally and justifies reference to it.

The fourth section of the paper, before the brief concluding section, considers the possibility of predicting the life of a rubber component, not from ageing tests on unstressed test pieces, but from the time to break of a test piece on which a load is hung. Acceleration is attained either by exaggerating the load or elevating the temperature, preferably both, and considering whether the required life will come within a reasonable fraction of an indicated life extrapolated to the estimated temperatures and loads, if extrapolation is necessary. This work is speculative and the results so far obtained are fragmentary.

2 - Stress Relaxation as a Test Method

Stress relaxation measurements as a means of obtaining insight into the changes which occur in the network of a vulcanizate were first described in 1944 by Tobolsky, Prettyman and Dillon[1]. Briefly, measurements of the continuous relaxation of stress give a quantitative measure of the degradative reactions occurring by oxidative, hydrolytic or thermal mechanisms, and intermittent stress relaxation an indication of total changes. RAPRA work has extended the finer theoretical interpretations[2-6] and, for the use of the services, considered in detail the interpretation and use of the method to displace or supplement other accelerated ageing procedures[7]. As most academic work on stress relaxation has been concerned with gum vulcanizates it is necessary to recall that the effect of structure-building fillers, such as carbon black and silica do not interfere with most stress relaxation measurements[5].

Effect of Fillers: Measurements were made with black-filled natural rubber and SBR peroxide cured vulcanizates in vacuo and in air, both at 120°C. 50 pphr of HAF black caused little or no increase in relaxation in vacuo when compared with the natural rubber gum stock but markedly decreased the relaxation apparent in an SBR gum stock. For intermittent relaxation, which in the apparatus used[8] is measured at the end of a 20 second period of extension following the 2 seconds during which extension occurs, experiments were made with a recorder having a 10 seconds' response time to full deflection. After this period no decay of stress was observable showing that any relaxation due to the black occurred within the 10 seconds' response time of the apparatus and that the presence of black does not make intermittent measurements impossible though their interpretation is less clear.

It is well-known that the tensile set can be calculated from measurements of intermittent and continuous relaxation by means of the two network theory. Such calculations have been made for black loaded natural rubber vulcanizates and confirm that loading with fillers has only a small effect on the stress relaxation.

Silica loaded rubber was found free of any complicating physical relaxation process but did interfere to some extent with intermittent but not continuous relaxation. A possible explanation is that a limited number of active sites exist on the particle surface to which cut chains can chemisorb.

Correlation with Conventional Oven Ageing: Figures 1 and 2 show the correlation obtained by plotting the loss of stress after 20 hours continuous relaxation at 100°C against the loss in tensile strength after 14 days oven ageing at 70°C (Figure 1) and 3 days at 100°C (Figure 2) for natural rubber vulcanizates. The data define fairly satisfactorily pairs of correlation curves, one for the gum and one for the filled vulcanizates. A number of comments are appropriate. Tensile strength measurements on aged stocks can show considerable scatter and examination of the data leaves no doubt that many of the deviations arise from poor strength measurements. For example, 1 in both figures refers to a low sulphur thiuram cure and 2 to a sulphurless black-filled compound. Both should be good heat-ageing materials as correctly indicated by the stress relaxation measurements but not by the tensile strength. Additionally, it is not clear why the filled vulcanizates should lie on a different correlation curve from the gum vulcanizates nor why vulcanizates loaded with HAF black and precipitated calcium carbonate should lie on the same curve.

In discussing these correlations it has been argued[7] that only continuous stress relaxation should be considered and that the principal use for concomitant measurements of intermittent stress relaxation is the detection of undercured vulcanizates.

3 - Interim Results from the 20 Year Ageing Programme

Outline of Programme[3]: During 1956 compounds from a range of rubbers were prepared, packed into specially manufactured copper-free aluminium containers arranged to allow free circulation of air, similarly packed in crates and replicate packages were (i) held in a temperature controlled laboratory at Shawbury, (ii) dispatched to a hot, wet location at Cairns in Western Australia, (iii) dispatched to a hot, dry location at Cloncurry also in Western Australia. The containers were so packed and arranged that a complete set of test pieces could be withdrawn by withdrawing a single crate. Figure 3 shows the layout of each box containing test pieces, carefully spaced on aluminium wires with ceramic separators, for a range of tensile, set, resilience and other tests. The sole stressed test piece was a 1.129" dia. ring ½" thick with a ⅜" dia. hole and compressed 25% by nut, bolt and washers.

It is proposed in this paper to discuss the behaviour of the following rubbers chosen from the rubbers stored.

Table 1 Details of Compounds

Designation	Polymer	Brief Description
A	Natural Rubber	HAF black and CBS/S cure
B		HAF black and TMT/MBT cure
E	SBR	HAF black and CBS/S cure
F		HAF black and TMT/MBTS cure
J	General purpose butyl	FEF black and MBT/TMT/S cure
K	Low unsaturation butyl	HAF black and MBTS/p. quinone dioxime cure
P	ABR (25% acrylonitrile)	SRF black and MBTS/S cure
R	ABR (35% acrylonitrile)	SRF black and TMT/CBS/TMHQ cure
X	Silicone	2.4 dichlorobenzoyl peroxide cure

Correlation between Storage and Accelerated Ageing

Natural Rubber: The standard tyre tread compound A drops in tensile strength somewhat over the 7½ years, though erratically. The erratic shape obtained when strength is plotted against time bears no relation to figures obtained by accelerated ageing at 70°C. Accelerated ageing at 70°C with 100% RH is more severe than the dry ageing whereas the shelf ageing at Cairns differs little from that elsewhere. The good ageing compound B shows constant tensile results up to 56 days at 70°C and up to the 7½ years at all three sites. The accelerated ageing at 100% RH gives very irregular results and does cause a fall to about 80% of the original strength. It is obvious from this short recital that apart from showing that B is superior in ageing to A, the accelerated ageing tensile tests have yielded little information from which the extended behaviour could be predicted. Hardness measurements show compound A to harden gradually to a small extent over the 7½ years but accelerated ageing gives constant readings for 7, 14 and 28 days at 70°C, and shows a steady fall with 100% RH. There is, therefore, no relation between extended behaviour and accelerated ageing.

Similarly for the good ageing compound B, the small, erratic changes in the measured hardness over the 7¼ years contrast with the steady rise in accelerated ageing at 70° and 82°C and at 70°C with 100% RH.

The simpler and more rapidly obtained assessment by continuous stress relaxation contrasts A with B by showing that the latter requires 10 times as many hours at 100°C to lose 50% of stress. Since the decay of stress is approximately proportional to log (time) a better figure of comparative merit is probably the ratio of the logs, namely, 2.25.

Compression Set (CS) and Extended Time Set (ETS): Of particular interest is the comparison between the compression set (24 hours at 70°C, lubricated plates, 30 minutes recovery) and the compression found after storage over the years with 25% compression. This situation corresponds to a gasket stored in situ or an oil or liquid seal held in position in store without movement. Three points are of interest; the nature of the systematic changes which occur and the extent to which the initial compression set can predict either the compression set after ageing or select those rubbers which will show greatest recovery from extended time compression. The latter two points are easily disposed of. There is no correlation to be found in the present series of experiments either for a single rubber or over a range of rubbers as can be realised from Table 2 which gives results obtained initially and at the conclusion of the first year's exposure[10]. The figures quoted are for 10 minutes recovery before measurement. (Standard practice changed in 1963 and 30 minutes is now accepted as recovery time. Fortunately initial compression set figures had 10, 30 and 60 minutes recovery noted.)

Table 2 Comparison of Initial and 1 Year Compression Set

Compound	Initial	Site of Storage					
		Shawbury		Cairns		Cloncurry	
		CS	ETS	CS	ETS	CS	ETS
A, NR, Tyre tread	9	9	43	10	67	10	58
B, NR, Good ageing	20	19	65	19	76	18	71
D, NR, High chalk	14	12	74	11	87	11	94
E, SBR, General purpose	10	12	42	9	56	9	55
F, SBR, Good ageing	10	13	23	12	28	12	34
J, Butyl, General purpose	9	10	28	10	42	9	40
P, AcR, General purpose	11	9	41	7	53	8	54
X, Silicone	2	2	47	1	50	2	46

The systematic changes which occur in the compression set of compound A are shown in Figure 4. The consistency of the pattern gives confidence that the changes are real and it is particularly noteworthy that the accelerated ageing shows the same general pattern, exaggerated when the humidity is high. The least severe ageing condition also reproduces the final rise shown by the more moderate storage place. The curing system employed, CBS/S, is not an exceptionally efficient system and at the conclusion of the normal time of vulcanization it is probable that there are still polysulphic crosslinks which react further with rubber hydrocarbon during the earlier period of ageing quite apart from any oxidation phenomena. This would account for the initial rise in compression set. When this intramolecular rearrangement slows down or ceases, compression set then falls and subsequent changes reflect oxidative behaviour. Compound A may, in fact, be slightly undercured.

The extended time set is irregular, possibly slight variations in actual compression exaggerate variation due to other causes but the general trend is that of a set of about 55% after 1 year increasing to 85% after $7\frac{1}{2}$ years in the warmer climate but remaining steady in the controlled atmosphere at Shawbury.

The behaviour of the good ageing compound B shows patterns not quite so consistent, as is apparent from Figure 5. However, with the exception of storage at Cairns, the effect of both storage or oven ageing is ultimately to reduce the rather large compression set substantially and this can only be due to a combination of cross-link lability and oxidative crosslinking. This receives support from the reduction in swelling shown by the vulcanizate in benzene, one of the many properties checked in this programme. Swelling is reduced to 50% of the unaged value by ageing 56 days at 70°C and 100% RH or 60% at 82°C whilst storage produces less marked reductions. The oxidative contribution will be more marked in storage whereas thermal lability of (poly)sulphide links will influence the oven ageing more. The drop is greater on prolonged storage and is therefore oxidative. The generally good ageing properties seem therefore to stem as much from the ability of the vulcanizate to form further crosslinks as well as from the slower rate of chain scission shown by stress relaxation.

This increased formation of crosslinks on ageing adversely affects the performance of the vulcanizate under continuing compression. The extended time compression set, although irregular, increases generally in all three storage sites to values of 70% at Shawbury and 92% at Cloncurry. This behaviour of a compound chosen for good heat ageing should be carefully noted; it is characteristic of the curing system used.

Styrene Butadiene Rubber: The general purpose compound E shows constant tensile strength at Shawbury and Cloncurry and in accelerated ageing at 82°C. At Cairns the tensile strength drops by 11%. In oven ageing at 100°C the strength falls 37% in 28 days. The elongation at break drops in all three storage places and in all accelerated procedures. The hardness rises in all places in the $7\frac{1}{2}$ years about the same amount and roughly equivalent to 14 days at 100°C or 50 days at 82°C.

The good ageing compound F keeps its tensile in all three locations and ageing at 82° or 100°C produces negligible change. The accelerated tests reduce the elongation at break; for example, at 100°C only 44% of the original elongation remains after 56 days. The hardness similarly increases more in over the 56 days of the accelerated ageing than during the $7\frac{1}{2}$ years of storage. Nevertheless, the changes are both uniform and in the same direction and could be scaled.

Continuous stress relaxation measurements show the greater rate of chain (or crosslink) scission of the general purpose compound and, as with the natural rubber compounds, the ratio of the log (time) for loss of 50% stress gives a figure for the relative merits of the two compounds. It is 1.6. For these compounds intermittent stress relaxation measurements were made for the first 10 hours and these figures suggest that there is little to choose between the added crosslinking of the two compounds which occurs on ageing. The superior properties of the good ageing compound arise therefore from the slower rate of scission which, since the polymers are the same, suggests that it is the sulphur crosslinks which are the points of scission. Further work would be required to remove these remarks from the realms of mere speculation.

It is reasonable to summarise the situation by stating that changes in tensile properties found by accelerated ageing are paralleled by the storage over the period examined.

Compression Set and Extended Time Set: Changes in compression set with time seem erratic whilst the oven ageing leaves it virtually unaltered except where 100% RH is employed. This causes an immediate increase from 7.7 to 12.5 with compound E and from 8.3 to 17.6 followed by a fall with compound F. The accelerated ageing tests give, therefore, no information relevant to the behaviour of the rubbers when stored in the three locations. The extended time set also shows erratic changes which are not correlated with the change in compression set measured at the same time on a rubber stored without stress. The ETS generally increases to 60-70% over the $7\frac{1}{2}$ years for compound E and rather less for compound F.

Butyl Rubber: Two compounds, J and K were designed for general purpose and good ageing respectively. J was formulated with a rubber of relatively high unsaturation (Butyl 301) and compounded with FEF black and cured with MBT/TMT/S.

K was formulated with a rubber of relatively low unsaturation (Butyl 100) with HAF black and a curing system involving MBTS/S and p-quinone dioxime. This was, of course, before the introduction of the resin curing system which would certainly have been preferred had it been available.

The tensile strength of the general purpose rubber increases slowly in all three locations by 12½% over the 7½ years whilst accelerated ageing strength remains constant up to 14 days after which the 70°C, 100% RH test pieces increase by 12½% whilst the 100°C, dry test pieces move erratically ending in 56 days with a 16% decrease. The elongation at break remains remarkably steady.

By contrast, the good ageing compound, after a period of steady behaviour for 3½ years falls 10% in the two more severe locations. This behaviour is paralleled in the accelerated tests, the fall being 10% at 70°C, 100% RH but much more severe at 100°C in which there is no steady period before the fall and, after 56 days, one-third of the strength has been lost. The "good ageing" rubber therefore behaves worse than the general purpose rubber in accelerated ageing and loses 10% strength in 7½ years storage compared with the gain of 12½% by the general purpose rubber. It is natural to enquire the reason for this behaviour.

In the first place, a very efficient crosslinking system was used for compound J. Both sulphur itself and a sulphur donor (TMT) were available for reaction with the accelerator and with adequate isoprene residues in the polymer. Swelling of this vulcanizate in benzene showed an increase of 111% and samples stored over the 7½ years did not change from this figure. No antioxidant was added to the compound, although there is, of course, some in the polymer before mixing. The ageing behaviour would be expected to follow the pattern of a polyisoprene sulphur cured rubber though more slowly because of the much lower solubility of oxygen.

The good ageing compound used a curing system, the mechanism of which is unknown but presumably acts in two ways. The MBTS/S crosslinks the relatively fewer unsaturated centres and the PQD links the isobutene part through methyl groups in the same way as a peroxide system works. In the first place, the MBTS/S is a less efficient system than the MBT/TMT/S system used for the general purpose rubber. It can, therefore, be expected that the average sulphur content of the crosslinks formed will be higher, the bonds therefore more thermally mobile and possibly more susceptible to oxidation. Recent work[11] has shown that the isoprene residue is far more reactive toward oxidative attack than its relatively low concentration would suggest.

The swelling of K in benzene was slightly greater than that of J (131% instead of 111%) showing a lower crosslink density.

Accelerated ageing at 82°C reduced this, suggesting a redistribution of sulphur with some new crosslinks formed. The initial period of ageing at 100°C produced a similar reduction in swelling but between 28 and 56 days oxidation had increased the swelling to its initial value. The higher swelling of K in benzene compared with J is in line with initial compression set which for K is 14% and J, 8%. K undoubtedly is less well crosslinked than J in that there are fewer crosslinks and some of these probably polysulphidic.

The extended time compression set similarly shows the general purpose J to advantage compared with K, the latter showing about 10% greater set in all three locations. Lastly, stress relaxation measurements, shown in Figure 6, show the rate of change, presumably due to oxidation, very closely the same whilst initial, mainly bond rearrangement, changes in the first hour (not shown on the log plot) operate to the detriment of the "good ageing" compound.

To sum up. The curing system used for the rubber of lower unsaturation has negatived any advantage which the lower unsaturation might have shown. On the whole the accelerated ageing tests predict this behaviour.

Butadiene-Acrylonitrile Rubbers: Compounds P and R comprised two acrylonitrile rubbers of 25% and 35% acrylonitrile content respectively. They also differed in that the general purpose compound P was cured with the relatively inefficient MBTS/S system and compound R, the "good ageing" compound with a CBS/TMT system. The two compounds were of the same hardness and modulus (300%) but R was stronger than P and more extensible. Unfortunately, owing to the different polymers it is not possible to estimate the relative crosslinking from the relative swelling in benzene.

The general picture of property changes with ageing for both rubbers is one of general hardening, an increase in crosslinking. The strength of compound P rises on accelerated ageing but remains constant in storage. The strength of R falls on accelerated ageing but rises slightly in storage. Compression set is reduced for both rubbers by accelerated ageing at 82°C and 100°C, the greatest reduction being during the first 7 days. The change during storage is much less marked and the good ageing rubber actually increases its compression set during storage at Cairns, the hot, wet site, a change which is not shown by accelerated ageing at 70°C and 100% RH. The extended time set is less for the good ageing rubber than for the general purpose rubber, at least up to 5½ years.

Continuous stress relaxation (Figure 7) shows R to relax at a very much slower rate indeed than P. Since this test eliminates the effect of added oxidative or other crosslinking, this implies that chain scission is very much less. The ageing changes shown by R must, therefore, be caused almost entirely by additional crosslinking and since modulus and hardness increase less than P, its susceptibility to oxidative changes is much less.

This is not brought out clearly in the accelerated ageing tests with physical property changes because these are relatively insensitive where hardening takes place. There is no real indication in the usual tensile and hardness tests that compound R will resist oxidation so very much better than P but the stress relaxation results offer proof that this is so.

Silicone Rubber: This compound was based on a slightly unsaturated dimethylsilicone gum filled with silica, coloured with ferric oxide and cured with 2,4 dichlorobenzoyl peroxide. Accelerated ageing at 82°C gives a 10% increase in strength during the first 7 days which is retained thereafter. At 100°C irregular behaviour disguises a slight rise. Swelling in benzene indicates that there is, in fact, very little change in crosslinking. At all three storage sites there is an increase in strength of 25% during the first year and a slow climb to an overall increase of 37% over $7\frac{1}{2}$ years. It should be noted that this change is not accompanied by change of swelling in benzene and cannot arise from post curing by residual peroxide. The hardness too shows little change but the elongation at break drops during accelerated ageing but not during storage. The general picture suggested by these changes is that the network does not change in density during storage but is a slightly different one to that formed initially. Accelerated ageing adds to the peroxide formed crosslinks some formed by post curing or reaction with unsaturated centres. In storage these additional links may also be formed but these only compensate some chain scission which continuous stress relaxation shows to occur linearly with log (time).

Compression Set and Extended Time Set: The curing system provides direct carbon-to-carbon crosslinks and these are not labile bonds. The compression set is, therefore, very low, about 1% and is only increased by the longer periods of ageing. Storage does not change it, an expected result from the discussion above. Extended time set, as usual, increases over the $7\frac{1}{2}$ years, though erratically, to about 55%.

It is apparent that the relatively small changes which take place on prolonged storage are incorrectly predicted by the usual tensile tests except where, as for hardness, no change occurs.

4 - Time-to-Failure Studies

Conventional ageing studies are made on unstressed test pieces; in continuous stress relaxation, the test piece is stressed throughout the test, the strain being held constant and the stress falling. The third alternative is to maintain the stress constant throughout the ageing period.

A convenient approximation to this condition is to keep the load constant and record the time to break. Such a test can be regarded as an accelerated test of, for example, an O-ring which is fitted with a small strain or some load bearing device in which stress cannot decay. Acceleration is obtained in two ways; by increasing the load and by increasing the temperature.

It is difficult to understand why this third alternative has not received more attention. Values associated with catastrophic events are usually more widely scattered than other parameters; tensile strength is more variable than modulus and impact strengths of rigid materials are well-known to be widely distributed. Recent advances in statistical method associated with E. J. Gumbel[12] suggested to the writer that these extreme events might be more handlable by using doubly exponential distributions. It was this possibility which led to the initiation of this programme of work although, in the event, the only failure times for which replicates have been obtained are closer to a normal or to a square distribution than they are to the double exponential.

However, the logs of means of groups of results obtained with a resin-cured butyl rubber are plotted in Figure 8 against the reciprocal of the absolute temperature of the test. As is seen, reasonably straight lines are obtained but longer term experiments will be necessary before extrapolation to lower temperatures is feasible. The lines are, very roughly, parallel but those at lower extensions must curve towards the temperature axis with temperature fall as it is difficult to believe that butyl rubber will last 20,000 years under zero load at room temperature! Estimation of life at a moderate load giving, say, 200% extension does seem feasible and if more is known about the distribution of failure times it should be possible to quote a $\frac{1}{2}$ life with a given probability that a fixed proportion of test pieces will survive this time. For the load corresponding to 200% initial extension, this seems to be about 16 hours for the compound used. An alternative use for data of this sort is to specify a maximum load which the component is to sustain for a given time.

5 - Conclusions

The prediction of the properties after long term storage in tropical and other locations is particularly important in service applications. If the initial properties are a reasonable basis for judgment that a rubber is capable of doing a certain job then the properties after storage are an equally good guide to see if it is still serviceable.

How long the rubber will last actually doing the job depends on its deformation. This may require actual simulation to determine or it may be possible to assume the effect of deformation trivial compared with the effect of the environment.

During the brief survey which has been given of the 20 year ageing programme, the nature of the curing system has repeatedly come forward in explanations of the changes in properties. Knowledge of the curing system is essential if even an attempt is to be made to predict long term properties from initial tensile properties and the same properties after ageing. The following conclusions seem to come from this work:

(1) Unless there is interest in analysing the reasons for given changes, there seems little point in determining intermittent as well as continuous stress relaxation. If a single figure of merit is wanted for a compound's ability to resist ageing it is the time (or log time, to lose 50% stress. This figure is far less subject to uncertainties than, for example, tensile strength after ageing. The whole series of tensile properties determined for the natural rubber compounds do very little other than show that compound B is better than compound A.

(2) Tensile properties which change considerably during accelerated ageing cannot be used to predict changes during storage.

(3) Compression set changes in accelerated ageing of natural rubber follow the same pattern as those which occur during storage but as the magnitude differs, prediction is not possible.

(4) Compression set as normally measured bears no relation at all to the set shown on compression throughout the storage period. This Extended Time Set is large even after only 1 year even with rubbers, such as silicone rubber, which show very small normal compression set. It also increases with time and many rubbers in the 20 year programme are expected to show 100% compression set after 10 years. It may be that 100% set will be approached but never attained and that the sealing of gaskets, etc. is satisfactory provided that some recovery power exists. It seems more probable, however, that low set over a long period of time is not a necessary property of gaskets.

Acknowledgments

Much of the work reported here was carried out under Government Contracts for Departments which are now parts of the Ministry of Technology. The author wishes to thank the Ministry for permission to use this work and to quote from reports prepared for them. In addition to work acknowledged by quoting references, several of the author's colleagues have helped with unpublished work and comments. Stress relaxations in connection with the 20 year ageing programme were made available in advance of reporting by Messrs Hall and Meardon.

References

1. A. V. Tobolsky, I. B. Prettyman and J. H. Dillon, J. appl. Phys., 1944, 15, 380.

2. J. Scanlan, J. polym. Sci., 1960, 43, 501.

3. J. Scanlan, Trans. farad. Soc., 1961, 57, 839.

4. L. J. Maisey and J. Scanlan, J. appl. polym. Sci., 1961, 5, 818.

5. L. J. Maisey and J. Scanlan, Proc. 4th Rubb. Technol. Conf., 1962, 631.

6. L. J. Maisey and J. Scanlan, J. appl. polym. Sci., 1963, 7, 1147.

7. J. Scanlan, Final Report to Ministry of Aviation on Work on Stress Relaxation carried out under Contract PD/23/023, dated April 1964.

8. H. W. Wallace & Co. Ltd., "The Wallace-Shawbury Self Recording Agetester", Croydon, 1964.

9. R. C. Moakes and colleagues, Unpublished work.

10. R. C. Moakes, RAPRA Bulletin, 1962, (3), 79.

11. L. D. Loan, J. polym. Sci., 1964, A, 2, 2127.

12. "Contributions to Order Statistics", Ed. A. E. Sarham & B. G. Greenberg, John Wiley, New York, 1962.

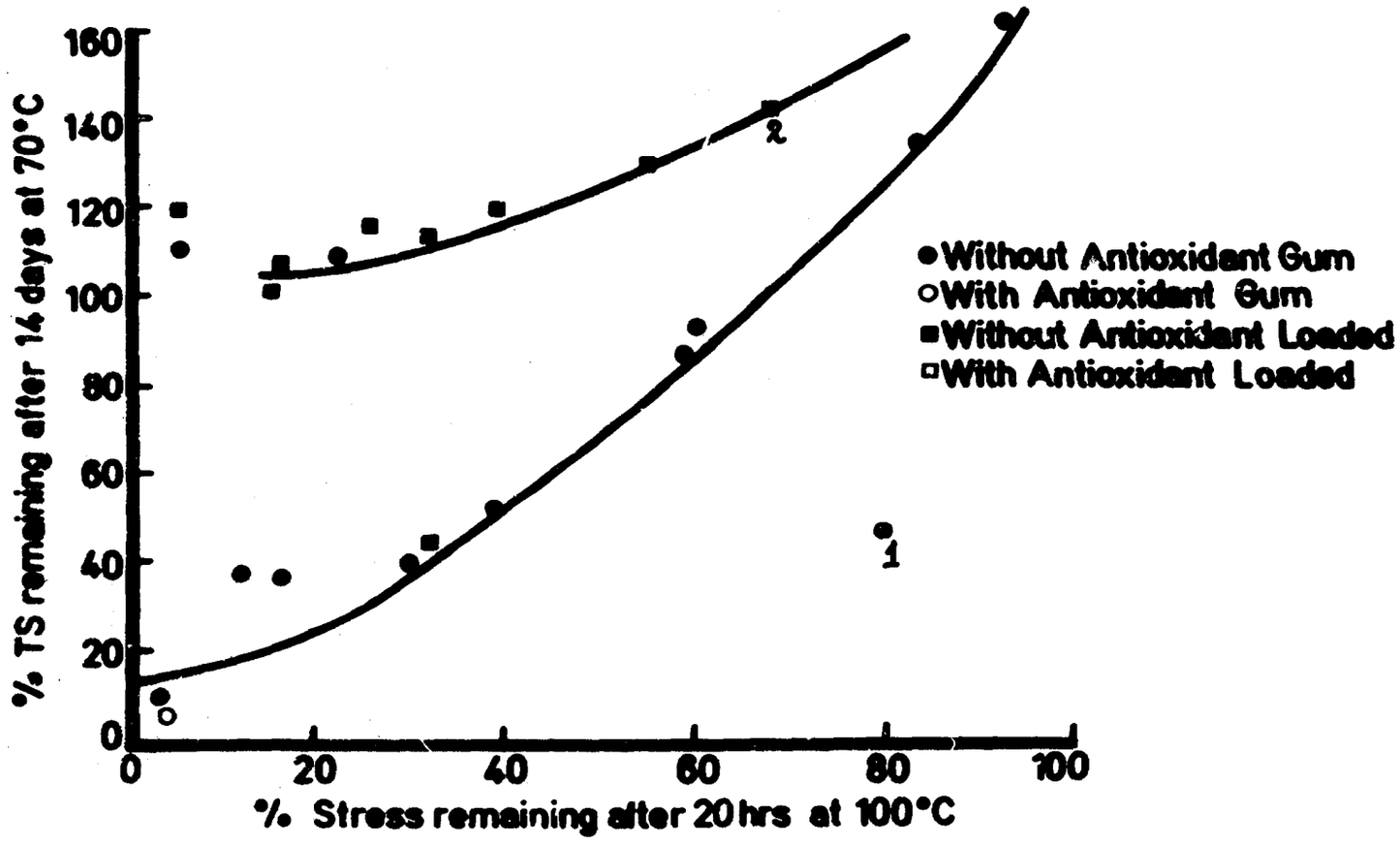

Fig. 1 Correlation of Tensile Strength With Stress Relaxation After 14 Days at 70°C.

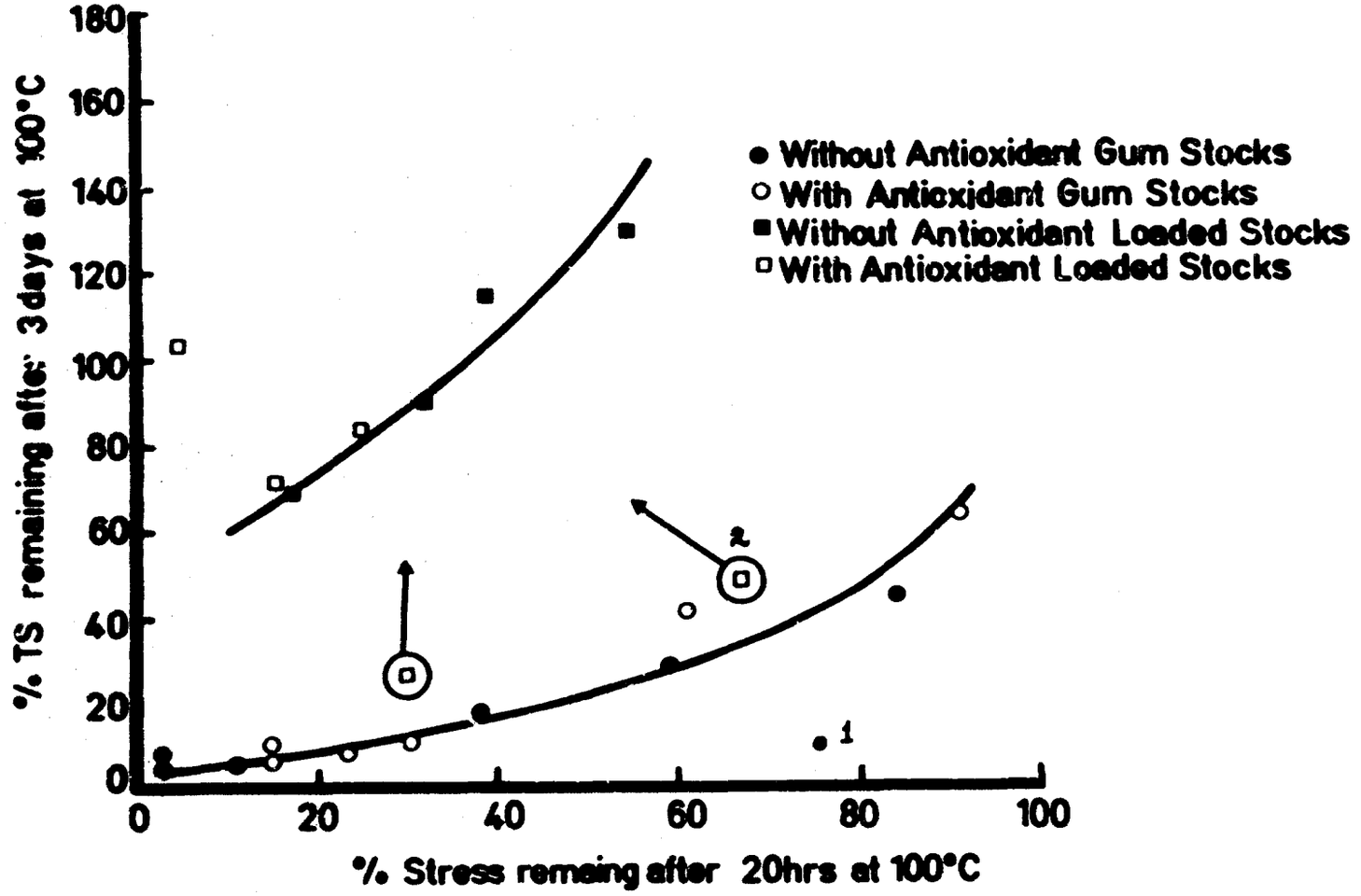

Fig. 2 Correlation of Tensile Strength With Stress Relaxation After 3 Days at 100°C.

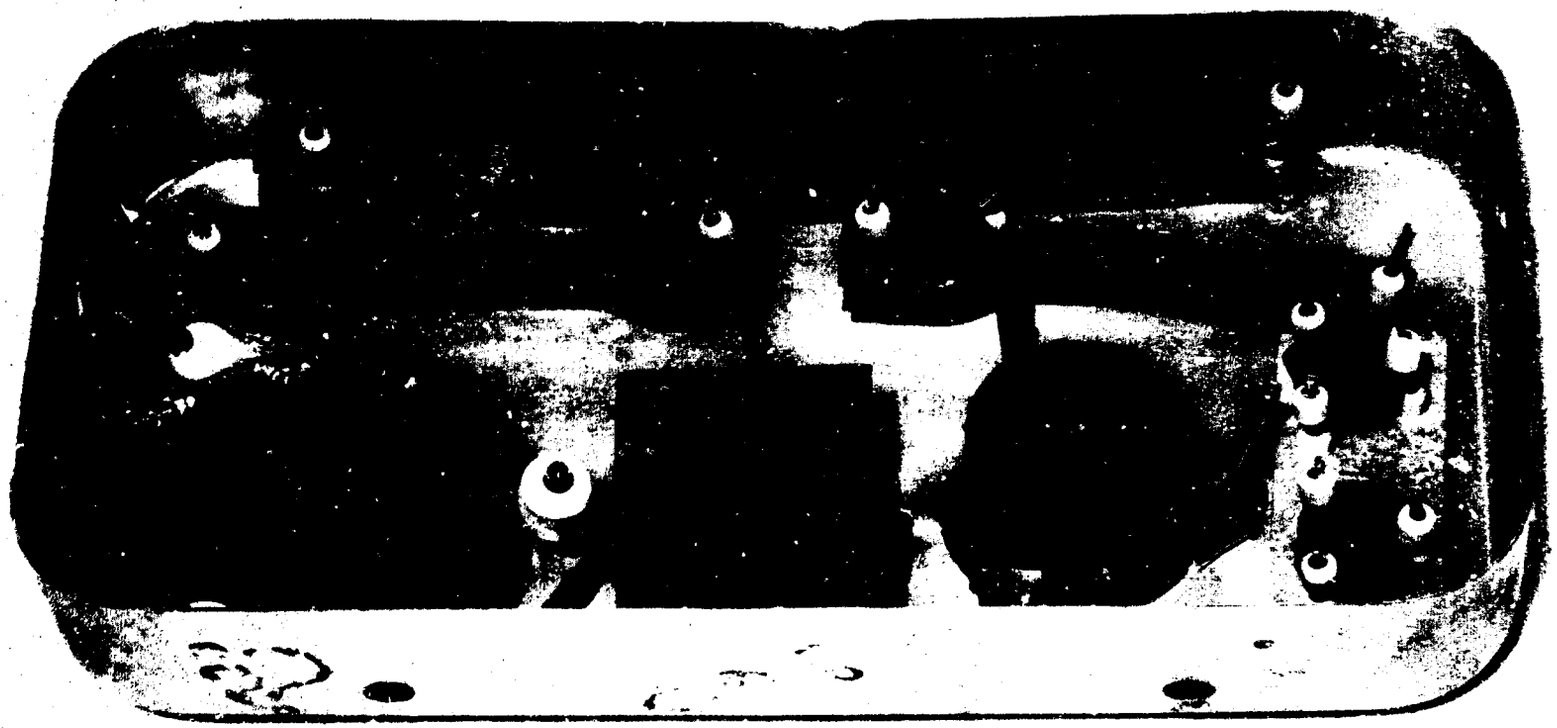

Fig. 3 Container With Test Pieces.

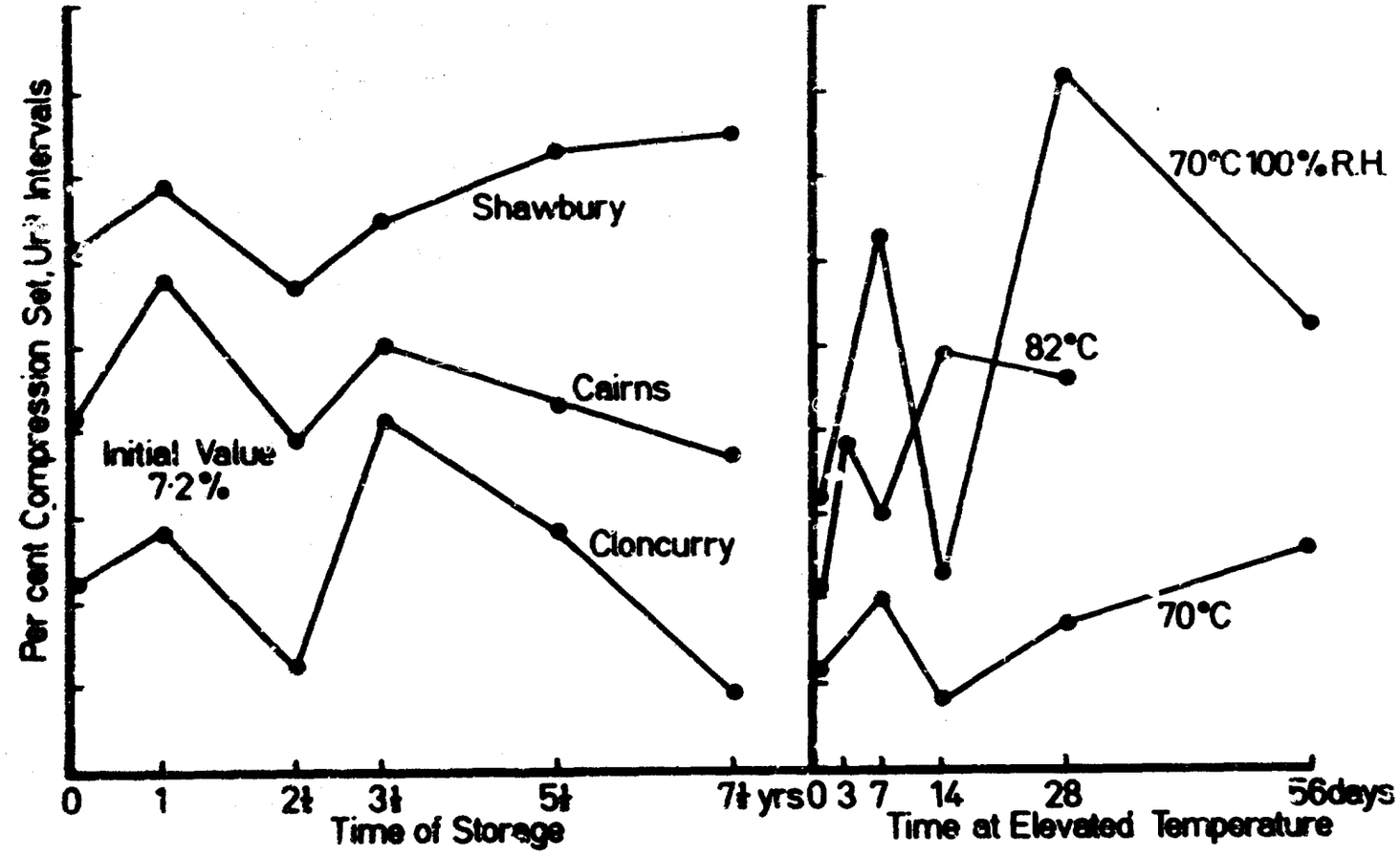

Fig. 4 Test Results of Compound A.

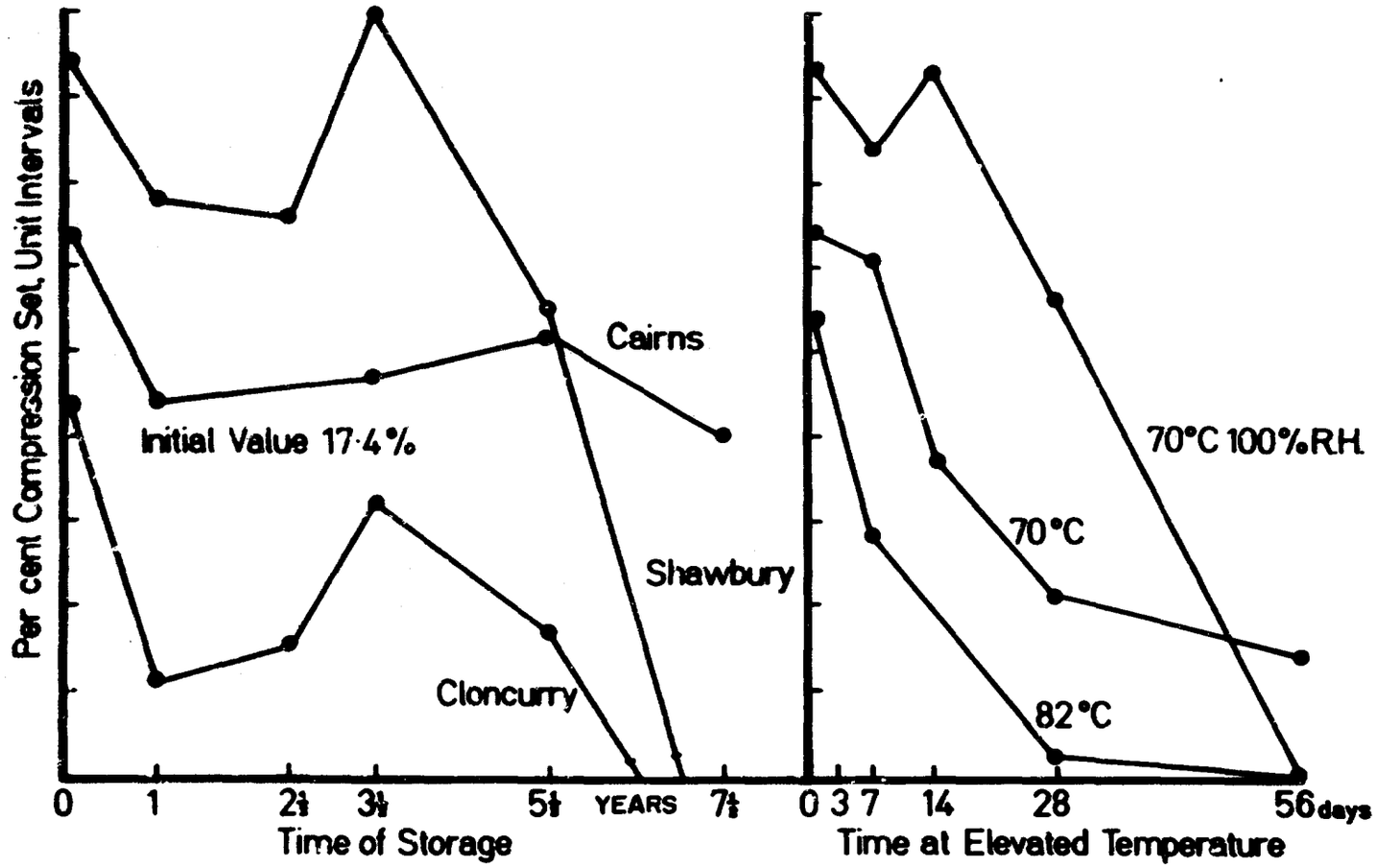

Fig. 5 Test Results of Compound B.

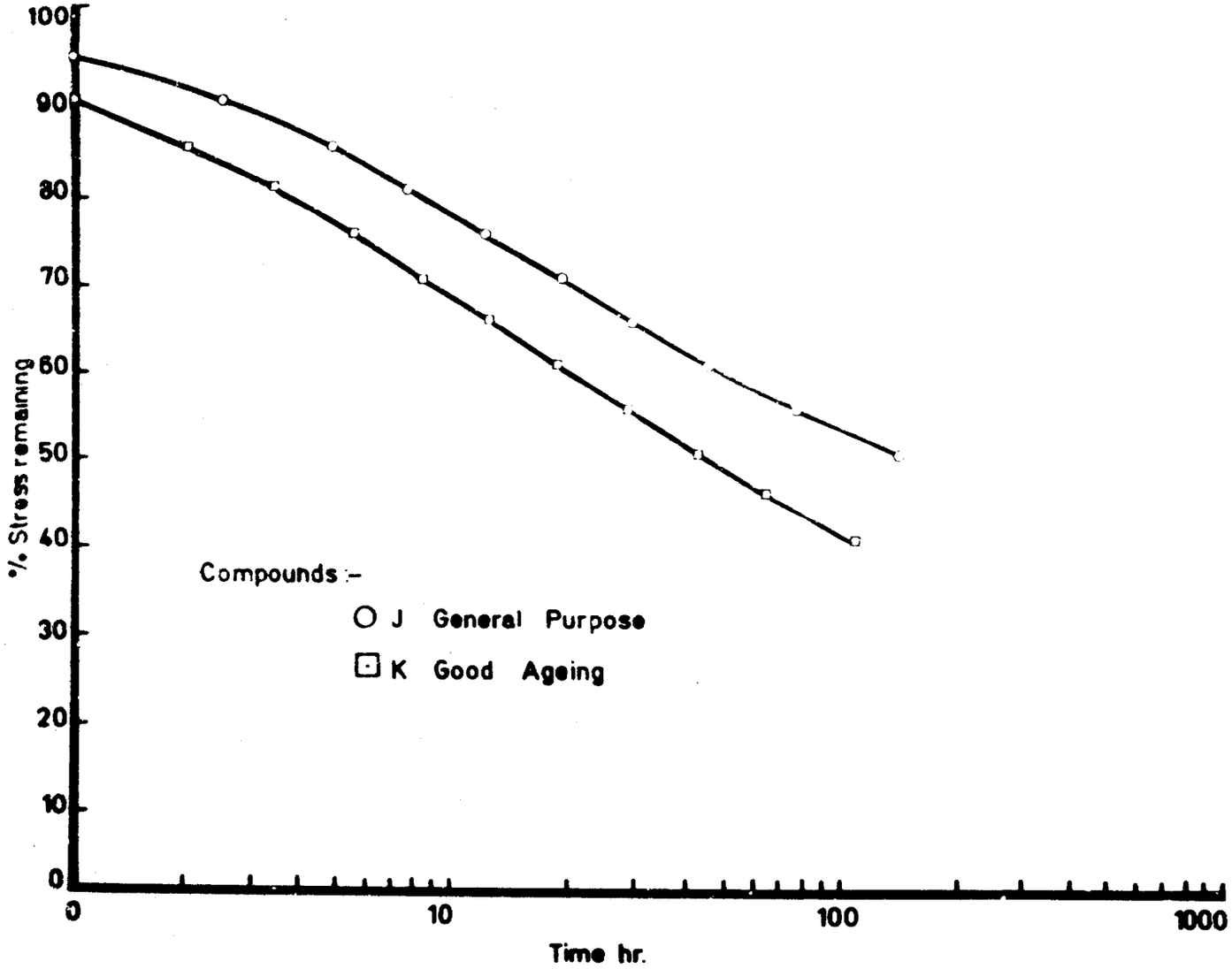

Fig. 6 Stress Relaxation of Butyl Rubber Compounds.

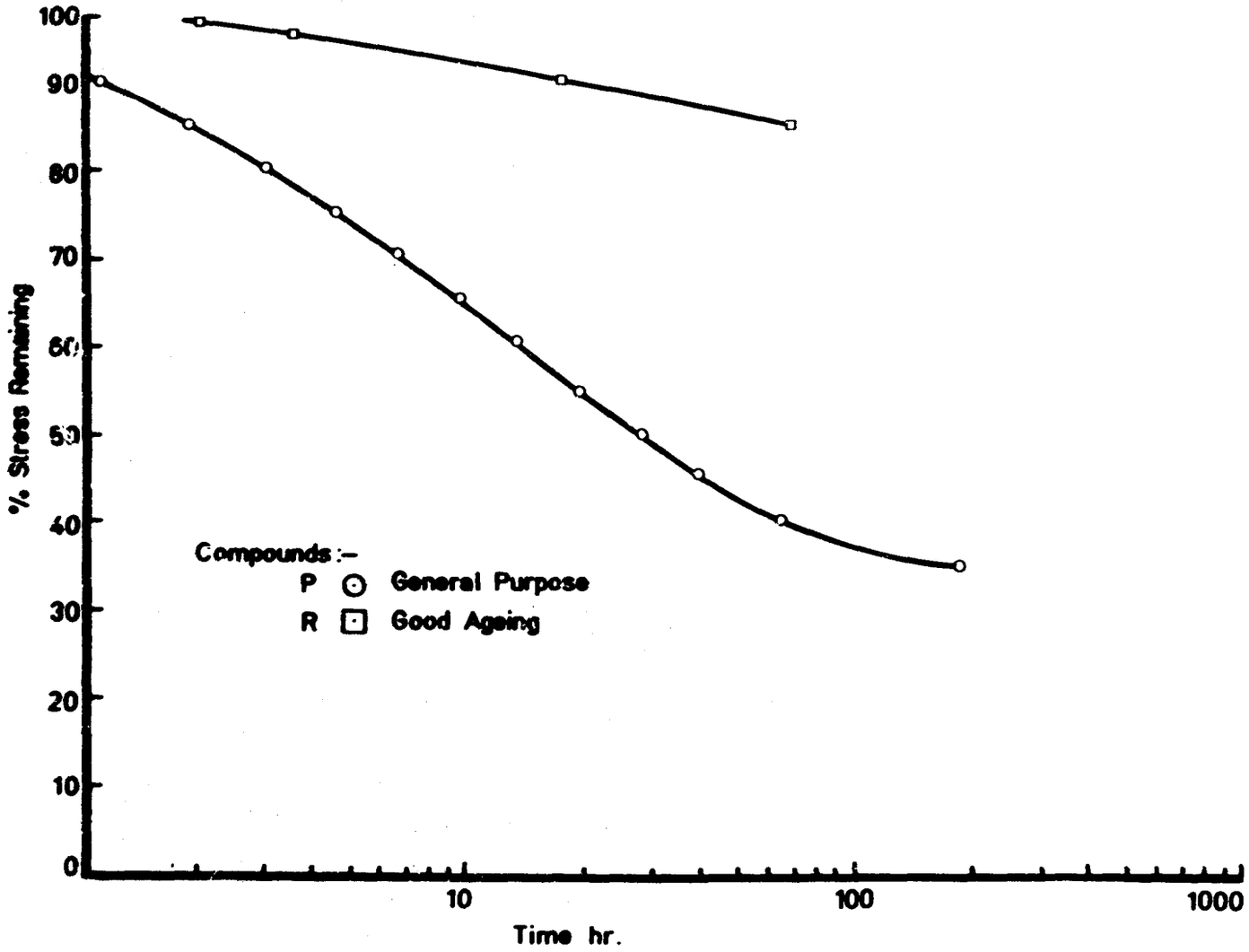

Fig. 7 Stress Relaxation of Nitrile Rubbers.

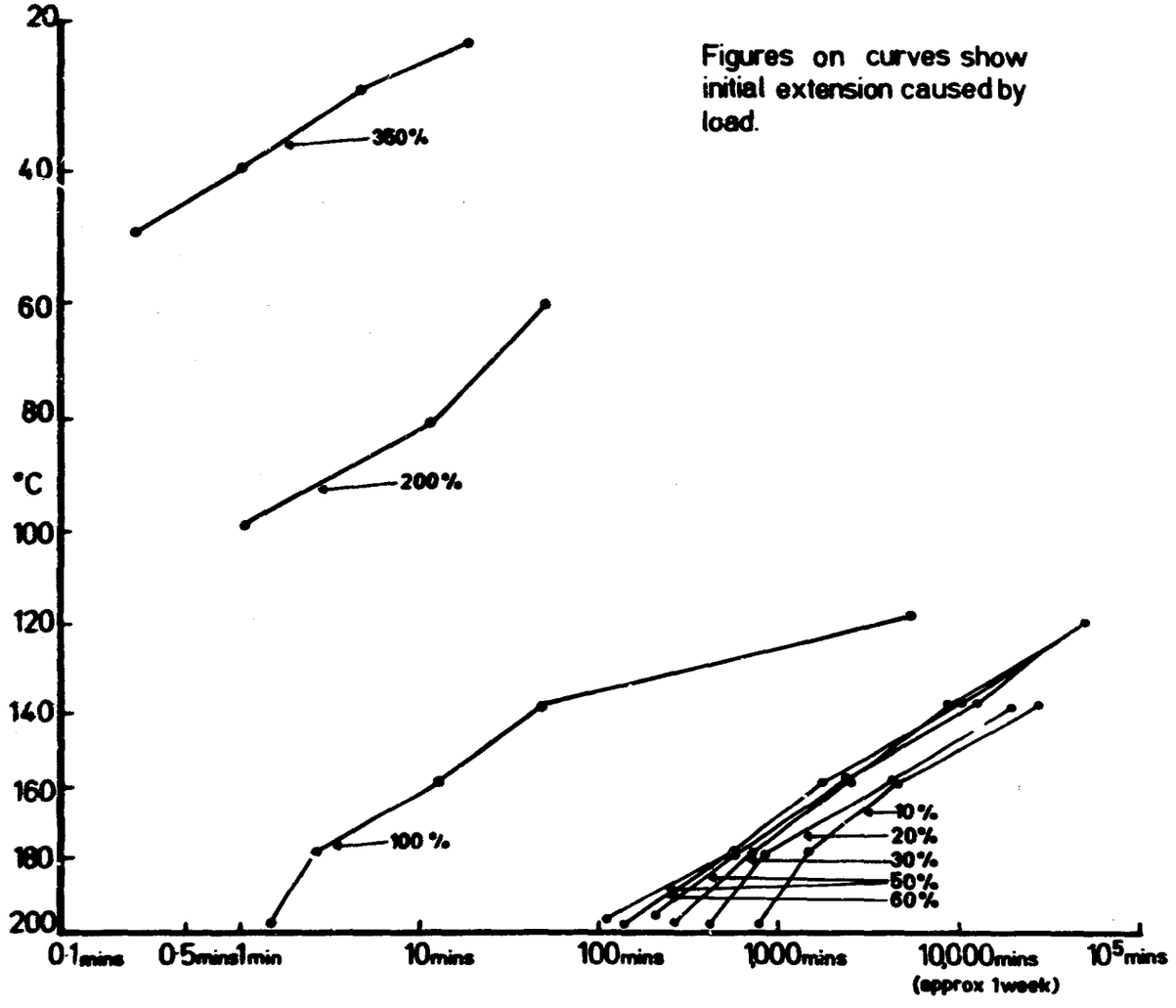

Fig. 8 Groups of Stress Relaxation Test Results of Resin-Cured Butyl Rubber.

NONDESTRUCTIVE TECHNIQUES FOR SEGREGATING 20MM MACHINE GUN BARRELS HAVING LOW IMPACT PROPERTIES

E. H. Rodgers

U. S. Army Materials Research Agency

Watertown, Massachusetts

INTRODUCTION

A study of the results of examinations conducted on fractured 20mm machine gun barrels that had failed in field service and while undergoing cold room tests led to the following conclusions:

1. The failed barrels had low impact properties.
2. The sharpness of the radii at the root of the locking threads was a contributing factor to these brittle type failures.
3. A nondestructive means of segregating inferior or slack-quenched barrels from the many in use and in storage required immediate development.

Our laboratories undertook to develop such a nondestructive test. This study covers the work performed by the various laboratories during the feasibility investigation and the metallurgical studies conducted during the development and adaptation type tests for the examination of these barrels, as well as work performed in field segregation tests. Studies were conducted to determine the uniformity of chemical composition, mechanical properties and heat treatment throughout the entire length of several representative barrels and similar data obtained in the failure area of the remaining weapons were tabulated for evaluation with the results of magnetic and ultrasonic attenuation tests.

Materials

The correlation study which I will discuss with you today involves a large quantity of 20mm machine gun barrels. Numerous failures in field service and also during cold room tests prompted a complete evaluation by our laboratories into the mechanical and metallurgical properties of these barrels.

Visual Examination

Visual examination of the fractured surfaces and bore sections of the barrels was conducted to determine the mode of failure, type of fracture, and the effect of service upon the progressive stress damage in the origin of rifling area. These studies confirmed the observations that the origin of failure was located in the sharp radii at the root of the barrel-locking lugs as clearly shown in Figure 1. Further examination of these barrels revealed no evidence of progressive stress damage, and the appearance of the fractures was typical of those found in other brittle steels. Hence it was tentatively concluded that the failures were classic fractures initiated by a sharp notch at the locking-lug root radii. Figure 2 shows a typical fatigue crack originating at the undersized root radius of the locking lug.

Microstructure Examination

A microstructure examination was conducted by utilizing an electrolytically polished spot on the outside surface of the barrel and comparing the results obtained with results of studies conducted at radial locations on a transverse plane in the same barrel area. This study was conducted to determine if such a nondestructive surface microexamination would indicate the microstructure throughout the wall of the tube. From this data it was determined that a surface microexamination would not be indicative of the properties at any other location within a slack-quenched barrel.

Chemical Analysis

Chemical analyses showed that representative results varied only slightly and was considered satisfactory and should have been capable of producing the desired properties and microstructure with proper heat treatment.

Mechanical Properties

Transverse and longitudinal mechanical properties of the barrels were determined by taking specimens from the breech, midsection, and muzzle end of several barrels. The geometry of the barrel required the use of subsize transverse specimens in most instances, but it was possible to obtain standard V notch charpy impact specimens at the breech end of each barrel. Although all property values varied from one end of the barrel to the other, the most conspicuous difference was found in the transverse impact values. Tensile and impact values were determined in the area of the barrel where fracture was most likely to occur. Results of barrel toughness will be discussed later in this talk.

Metallographic Examination

Metallographic examination revealed that many of the barrels were slack-quenched, resulting in undesirable tempered nonmartensitic products in the microstructure. This study also proved that the microstructure at the surface of the barrels was not representative of the microstructure found near the bore. Figure 3b shows the satisfactory microstructure containing tempered martensite with a small amount of tempered low-temperature bainite and Figure 3a the unsatisfactory microstructure containing ferrite and tempered high temperature bainite. This second condition not only occurred near the bore of many barrels but also in some cases near the surface. Figure 4 illustrates the relation of impact strength and microstructure as found in this particular examination.

Nondestructive Testing

Having determined the metallurgical and mechanical properties of the barrels, it was now necessary to provide, if possible, a nondestructive method for segregation of unacceptable barrels from those of acceptable quality. A magnetic test which provided a rapid means of detecting variations in the magnetic and electrical properties of ferromagnetic materials caused by differences in their physical and metallurgical characteristics, was chosen for the initial screening operation. The reason for this selection was because of the known sensitivity of the magnetic response to the surface layer of material being tested, and the fact that in the fractured barrels examined the origin of the failure was located at the surface.

The Magnetic Test

Utilizing a magnetic comparator type of instrumentation, with two test coils, the unit was balanced at the desired current settings with the coils empty. The presentation on the screen displayed only a straight line showing that the unit was in balance. Two standards of good quality were placed respectively in the test coils. Any slight difference in the two barrels used for standards was compensated for by the balancing knobs on the instrument proper. Now many variables will effect the electrical imbalance of the unit; chemical variations, hardness, geometry, surface conditions, discontinuities and heat-treat conditions all tend to effect the sensitivity. Fortunately, for the purpose of the problem at hand, most of these variables were eliminated. The chemical analyses were very close, and the hardness varied only a few points. Geometric conditions, as well as surface finish were pretty exact, and these conditions simplified the sorting problem considerably. One standard barrel is left in its appropriate coil and the screening may then commence. Any difference in the electrical and magnetic properties of the two barrels under test caused an electrical imbalance between the coils, and a resultant signal was observed on the screen. Figure 5 shows indications of the signal from a relatively tough barrel and of a brittle barrel respectively. In our screening, only the signal amplitude was taken into consideration. The proper rejection level was obtained from previous laboratory studies of over one hundred barrels. The magnetic test values of these barrels had been correlated and plotted against charpy V notch impact values obtained at 40°C. Examination of this plot revealed that of all the barrels examined which showed magnetic test values of less than 10 on the screen scale used, only one tube had an impact value of less than the required five foot-pounds. Only three barrels exceeding the rejection level of 10 on the

magnetic scale had impact values slightly greater than five foot-pounds. On the basis of this data, it was decided to reject any barrel showing a magnetic reading of 10 or above. Upon evaluating these results with microstructure studies, it was decided that any barrel rejected by the magnetic test would also be rejectable by microstructure. The determination was also made that due to the surface nature of the magnetic test, and the extreme variance in the microstructure throughout the barrel wall, it would be advisable to subject the magnetically accepted barrels to further tests more penetrating in nature in order to insure rejection of possible border-line cases. It should be noted that since the magnetic test is only sensitive to the surface layer of metal (shallow penetration), a correlation between the magnetic readings and the surface microstructure should be expected. This correlation was found to exist. Barrels having martensitic structures in the outside surface area gave very low magnetic readings while those with ferritic structures on the outside surface gave very high magnetic readings. Those with bainite gave readings of intermediate value. Since the barrel fracture initiated at the outer barrel surface, it was essential that a martensitic microstructure exist in this area if crack initiation was to be minimized. The magnetic comparator has been demonstrated to be capable of detecting microstructural differences in steel, but only with relatively shallow penetration from the outer surface. The instrumentation had been adjusted, with the appropriate standards, so that only barrels which contained approximately 90% martensite and low temperature bainite near the outer surface would be accepted; all others would be rejected. Since the percentage of martensite diminishes from the outer surface to the bore, this procedure is valid. Barrels rejected by this test were placed in category C and were given no subsequent testing. However, of the barrels accepted by the magnetic test, some would have little resistance to crack propogation because of upper bainitic and ferritic microstructures in the inner two-thirds of the barrel. Hence, these barrels were tested with an ultrasonic attenuation test.

The Ultrasonic Attenuation Test

The mechanism of ultrasonic absorption or attenuation in steel is an involved function of many factors; however, as the frequency rises to the high megacycle range, the predominating factor may become one of scattering, particularly if the microstructure presents a nonhomogenous pattern of martensite with ferrite and high temperature bainite as was the case of the slack-quenched barrels. The measurement of the high frequency transmission characteristics thus provide a valuable tool for the nondestructive determination of microstructure as affected by heat treatment. Attenuation measurements made over a wide range of frequencies show that the ultrasonic absorption factor increases with frequency at a rate which is determined by the incidence of scatterers, e.g. microstructure, all other factors being equal. Research work in this area has shown a correlation in this particular case, between high frequency transmission characteristics and impact tests, particularly where a homogenous microstructure exists. In this particular study we were extremely fortunate (or even lucky). Other attempts at correlation have been attempted between impact properties versus microstructure that have not matched; particularly where extremely dirty grain boundaries exist. For heterogenous microstructures resulting from inadequate heat treatment, the correlation is excellent between the attenuation and the quality of the steel as determined by microscopic studies.

An example of the first application of this principle to the mass inspection of manufactured steel items is the program of segregation of 20mm machine gun barrels. Attenuation measurements were carried out at a frequency of fifty megacycles and the barrels were sorted in accordance with the ultrasonic transmission characteristics of the steel. A standard 10 megacycle crystal, operated at its fifth harmonic, was used as the transducer to transfer the energy through a liquid couplant into the cylindrical surface of the barrel. The somewhat unusual geometry of the test piece involved some special considerations. The results obtained from ultrasonic attenuation versus microstructure is shown in Figure 6. A comparison of the results of this test, with the microstructure of each individual barrel examined, revealed that barrels considered border-line cases were occasionally acceptable or not acceptable by the ultrasonic test. It was found, however, that when the ultrasonic test was used in conjunction with the magnetic test, many of the so-called border-line cases were rejected magnetically and that due to the sensitivity of both tests, it was more likely that a normally acceptable barrel would be rejected than a rejectable barrel accepted.

Field Screening of the Barrels

The actual field screening of the machine gun barrels was accomplished at various collection points in the States. Each barrel, after being unpacked and removed from its protective tube, was placed on a conveyor line and transported to the first inspection station where they were segregated by the electromagnetic comparator into acceptable and rejectable categories. All barrels accepted at this station were passed on to the second inspection station. During transit between stations, the heavy section near the breech end was washed with alcohol and painted with glycerine. As each barrel reached the inspector, the crystal transducer was applied to the glycerine-wetted surface and manipulated to give the best possible echo indication on the screen of the ultrasonic attenuation comparator. The first echo just touching the preset exponential line. The acceptability of the barrel depended upon whether the succeeding echo peaks were above or below the preset limit of acceptable attenuation. The inspection process as outlined, was reduced to a very simple and rapid procedure. All barrels having a magnetic value of 0 to 10 on the scope scale were believed to have an impact value of 5 foot-pounds or more and were considered acceptable subject to further inspection by the attenuation method. Any magnetic reading greater than 10 would reject that particular barrel as having impact values of less than 5 foot-pounds. Average daily outputs of 1000 were screened although as many as 1500 were screened in a single day's operation. Of the total quantities field screened during an eleven month period, 74 percent were acceptable, and 6 percent were rejected as being unusable, and the balance of 20 percent was limited to ground firing. A selected quantity of both acceptable and rejected barrels were subjected to cold room tests. No failures resulted from the accepted barrels while those in the rejectable category failed after repeated firings at low temperature. Further substantiation of the effectiveness of these complementary tests is given by the fact that there have been no failures in the acceptable barrels released for high altitude cold temperature use.

Problems Encountered in the Field Testing

Several problems were encountered in carrying out the field segregation and are noted for record:

(1) All magnetic and electronic equipment, jigs, spare parts and miscellaneous supplies, were shipped by air from Watertown, Massachusetts to the collection points, and even with extreme precautions, such as careful packing and handling, the ultrasonic units had to be overhauled before they could be used after each shipment.

(2) Regardless of the number of spare parts shipped with the equipment, breakdowns occurred on other components, such as transformers, etc, which created delays in operation.

(3) Lack of sufficient material-handling personnel did, at times, curtail production rates.

(4) Difficulties occurred in obtaining inspection personnel available for prolonged periods of time.

(5) Interservice communications between command channels required special attention to assure proper coverage of regulations and procedures.

In spite of these apparent difficulties, production inspection rates were far in excess of those anticipated at the start of the project.

CONCLUSIONS

On the basis of the results of the investigation, it was concluded:

(1) That because of the extreme variance in the microstructure throughout the wall thickness and length of the slack-quenched barrels, any surface microexamination or muzzle-end and mechanical test would not be indicative of the conditions existing at any other location within the barrel; therefore, such a test was not feasible for the segregation of slack-quenched barrels.

(2) That the magnetic comparison test was correlative with the microstructure near the surface of the barrels at the location of the highly susceptible locking lug area.

(3) That where extreme variations in microstructure occurred, the ultrasonic attenuation measurements correlated with average microstructure.

(4) That if barrels acceptable by magnetic tests were also subjected to an ultrasonic attenuation test, the chances of accepting a border-line case was practically eliminated.

(5) That due to the sensitivity of these tests when used in conjunction with each other, an acceptable barrel could be rejected but a rejectable barrel could not be accepted.

MUZZLE END

BREECH END

2X

Fig. 1 Fractured Faces of Barrel No. 3.
(Arrows indicate points of failure origin)

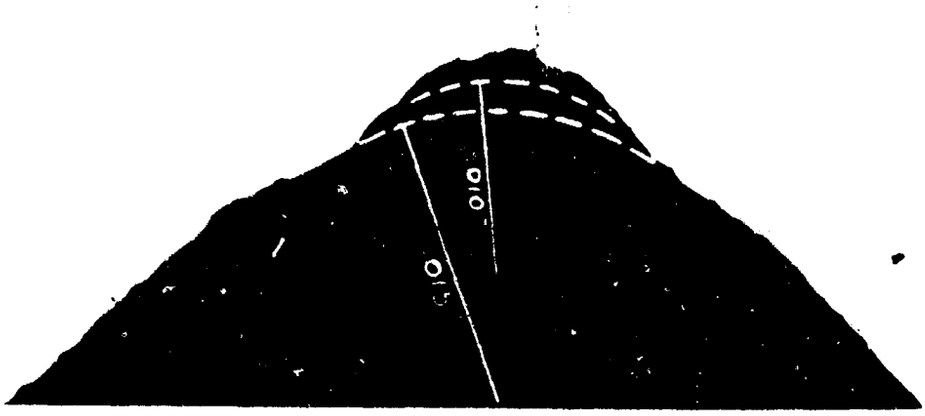

100X

Fig. 2 Typical Fatigue Cracking Originating at Undersize Root Radius of Locking Lug.

Fig. 3a Bore at Breech of Barrel No. 235105
Unsatisfactory Microstructure.

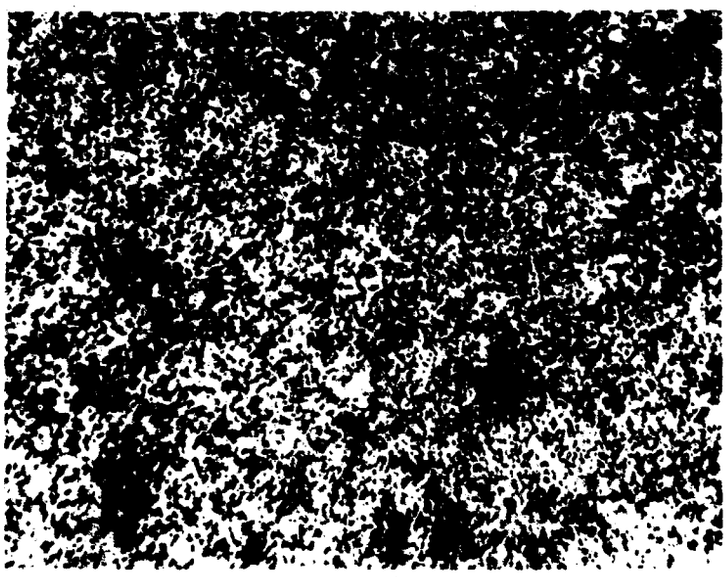

Fig. 3b Surface of Breech of Barrel No. 234223
Satisfactory Microstructure.

Barrel	Impact* Strength	Microstructure			
		Tempered Martensite	H. T. B.	L.T. B.	Ferrite
A	15.5	100%	—	—	—
B	8.6	70%	15%	15%	—
C	2.5	10%	70%	—	20%

*V-Notch Charpy at -40°F

Fig. 4 Relations of Impact Strength and Microstructure of Machine Gun Barrels.

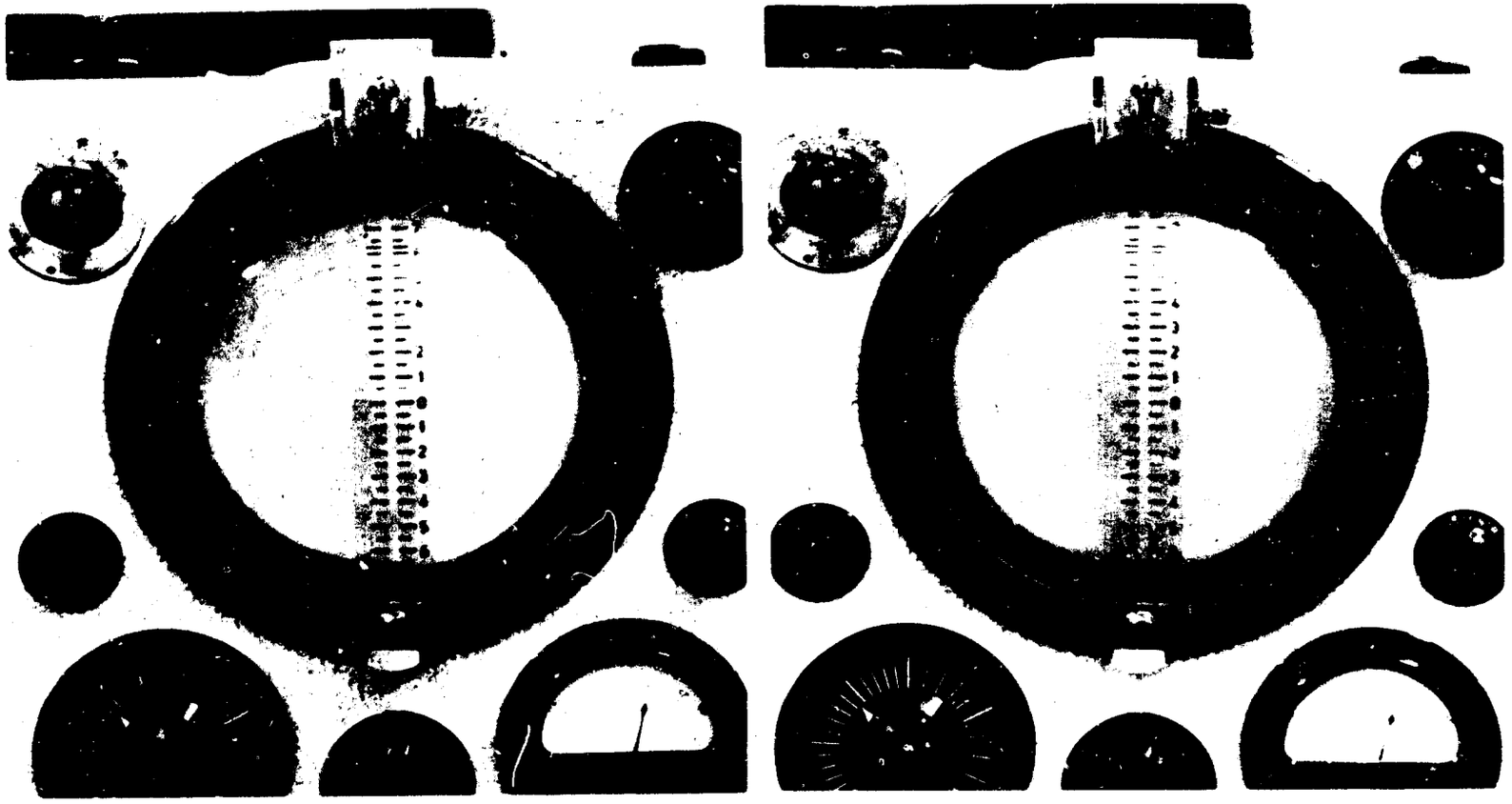

a. Tough Barrel

b. Brittle Barrel

Fig. 5 Electromagnetic Indications of Gun Barrels

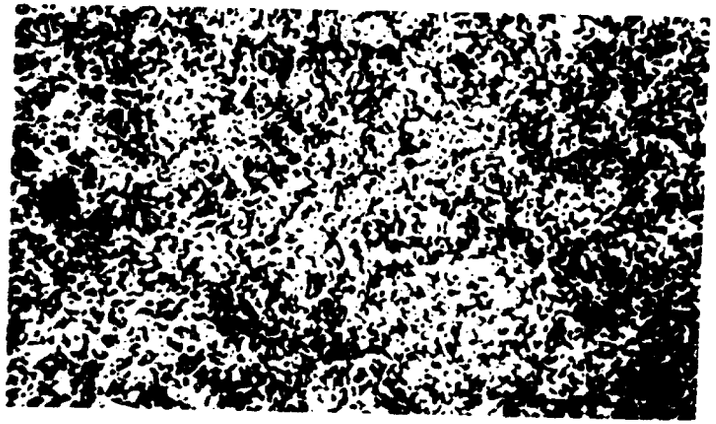

100% TEMPERED MARTENSITE X1000

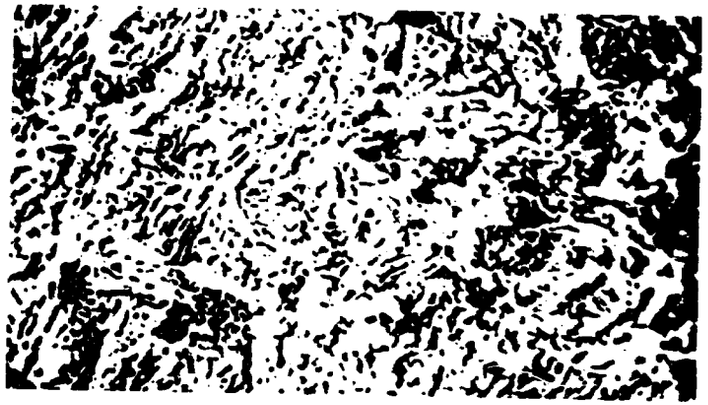

10% TEMPERED MARTENSITE X1000

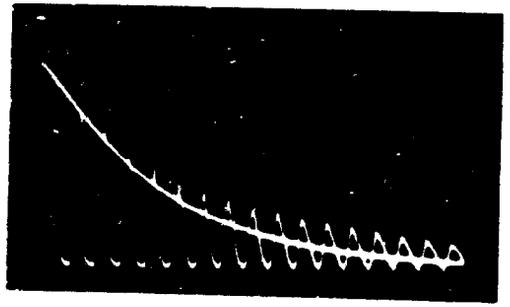

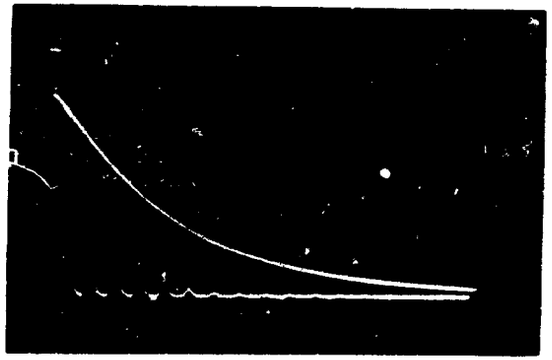

Fig. 6 Microstructures Versus Ultrasonic Attenuation Patterns

ANISOTROPY MEASUREMENTS AND THEIR RELATIONSHIP TO THE DEEP DRAWING OF THE HAWK MISSILE OIL ACCUMULATOR HOUSING

R. M. Colton and J. D. Colgate

U. S. Army Research Agency

Watertown, Massachusetts

INTRODUCTION

Definition of Problem

This study was initiated as a result of a formability problem experienced during the "hydroforming" or deep-drawing of H11 sheet steel into the Hawk Missile oil accumulator dome. The problem was manifested as a tearing or fracturing of the dome at its base during or directly following forming. The forming blank or disk and a successfully drawn dome are shown in Figure 1. Four distinct types of failures were experienced and are shown in Figures 2a to 2d. The failures were caused by excessive anisotropy in the blank or disk stock and inadequate annealing techniques performed on the stock prior to forming of the dome. The inadequate annealing affected the ductility and yield strength properties of the stock and materially influenced the drawability of the dome.

To determine the nature and magnitude of the specific parameters which caused the limited drawability and cracking, a review was made of previous history in drawing of the component. It was determined that the component had been successfully drawn, with an overall acceptance rate of 95 percent for a previous period of about a year, and that the problem first occurred when a completely new heat of the H11 steel sheet stock was hydroformed. The hydroforming technique was not modified between the last acceptable heat and the forming of the new questionable heat. The chemical composition of the new heat was as specified. Therefore, the cause of limited drawability was tentatively attributed to the effects of processing the new heat prior to forming. This included both rolling and heat treatment techniques. It was noted that most failures were accompanied by a large degree of "earing" or scalloping in the flange of the drawn dome and that failure initiated at the junction of two of the ears. A crack then was initiated at this point whose fracture path extended from the juncture vertically to a point within several inches of the hemispherical portion (top) of the dome. It was quite obvious that a marked degree of planar anisotropy was causing the large ears, thus producing the sharp juncture point. In addition, the rapid work hardening of the material during forming resulted in increased notch sensitivity and raised the brittle-ductile transition temperature of the material from room temperature to a region well above the forming temperature of the workpiece. These occurrences were responsible for crack initiation and propagation at the region of high stress concentration, the earing juncture point.

Relation between Anisotropy and Drawability

Anisotropy of both the normal and planar manifestation has been recognized for more than 15 years as one of the prime factors in determining the drawability of sheet metals and alloys. The literature is replete with theories explaining the relationship between anisotropy and crystallographic texturing and structures,[2-4] earing during drawing,[5-7] strain rate,[8] drawability,[6-9-12] deformation processing,[13] strength and plasticity of metals,[14-15] texture origin,[2-16-18] grain orientation,[19-20] and sheet rolling techniques[6] for various metals.[7-21-24] For example, Larson[23] has indicated that marked increases in strength of sheet material, under biaxial as compared with uniaxial tension, can be achieved in textured α and $\alpha + \beta$ type titanium alloys, thus extending the useful qualities associated with anisotropy.

Anisotropy in a material is influenced by variations in its mechanical and/or physical properties as a function of the directions in which the specific property is measured. As indicated by previous investigations in deep drawing of sheet material, the degree of mechanical anisotropy found in a material greatly affects its drawability as defined by D/d (where D is the diameter of the forming blank and d is the diameter of the drawn cup).

Mechanical anisotropy is manifested by the presence of various combinations of three phenomena: (1) internal stress-induced directionality, commonly referred to as the Bauschinger Effect;[3] (2) mechanical fibering, commonly evidenced by nonmetallic inclusion stringers or directionally oriented second phases; and (3) crystallographic texturing, evidenced by preferred orientation of crystallographic planes. The mode of crystallographic texturing is influenced, among other things, by material composition and processing heat treatment history.

Whiteley and Wise[6] have made an extensive study in interrelating crystallographic texturing, hot- and cold-rolling techniques and other aspects of mill practice, drawability, heat treatment, and earing for low-carbon (0.03C to 0.08C) killed and rimmed steels. Whiteley[25] and Whitelev and Wise[6] have shown that the average width-to-thickness plastic strain ratio defined as normal anisotropy and expressed as

$$\bar{P} = 1/4 \, (R_0 + 2R_{45} + R_{90}) \qquad (1)$$

is a practical way to measure the drawability of low-carbon steel as $\bar{R}$ increases. In Equation 1, R_θ refers to the width-to-thickness plastic strain ratio determined from flat tensile specimens oriented at an angle with respect to the principal rolling direction of the sheet.

R_θ is mathematically expressed

$$R_\theta = \frac{\epsilon_w}{\epsilon_t} = \frac{\ln W_o/W}{\ln t_o/t}$$

where W_o = initial width

W = final width

t_o = initial thickness

t = final thickness.

They have also shown that ΔR, which represents variations in R_θ and is defined as a measure of planar anisotropy, can be expressed as follows:

$$\Delta R = 1/2 \, (R_o - 2R_{45} + R_{90}).$$

The degree of earing in a deep drawn shape can be determined by the absolute value of R (Reference 6). That is, as ΔR increases, severity of earing increases. Consequently, $\bar{R}$, as a measure of normal anisotropy, is indicative of the resistance to thinning in a sheet material and ΔR, a measure of planar anisotropy, is indicative of the tendency of the sheet to deform at different rates as a function of angular orientation within the major plane of the sheet. In the deep drawing of sheet material, the degree of $\bar{R}$ and ΔR are affected by composition; mechanical properties; strain-hardening exponent; hot-rolling finishing temperature; degree of cross rolling and reduction; and microstructure.

Hydroforming or Deep Drawing of H11 Sheet

Hydroforming is a hydraulic form of deep drawing, and has been adequately described in the literature.[26-27] However, little information is available on deep drawing of H11 steel. Unterwesser[28] presents information on conventional deep drawing (as opposed to hydroforming) of H11 steel into 28-inch-diameter and up to 52-inch-long cup shapes. Unterwesser recommends that the H11 material should be 90 to 100 percent spheroidized and should not exceed 90 Rockwell B in hardness and 95,000 psi in tensile strength. The fact that these requirements were similar to those ultimately specified for hydroforming the 9-inch-diameter by 8-inch-high dome, Figure 1, is indicative of the equivalence in severity of forming for the two processes.

Hydroforming is quite similar to conventional deep drawing except that the solid female die associated with deep drawing is replaced by a rubber diaphragm hydraulically supported under pressure so that the diaphragm conforms to the shape of the male die, thus completely surrounding the formed piece. At all times, prior to, during, and after forming, the entire outside surface of the blank is under high hydrostatic compressive forces in addition to the tensile forces normally encountered in conventional deep drawing. The internal surface is subject to the normal deep-drawing forces influenced by the shape of the male punch or die. Figure 4 shows the sequence of operations involved in hydroforming a dome-shaped component and indicates the magnitude of the hydraulic pressures involved.

In the actual hydroforming or deep drawing of the hot-rolled H11 sheet into dome-shaped configurations, the following factors affect its drawability: hold-down force; internal pressure; lubrication; workpiece temperature; D/d ratio; workpiece thickness; workpiece flatness; anisotropy (including the effect of the anisotropy variables noted previously); yield strength and ductility.

MATERIAL

Several heats of H11 steel in the form of 1/8-inch-thick disks were utilized on this study. The heats used and the corresponding studies are listed below:

Heat	Study
34382, 33762, 34529, 34633	General Mechanical Properties
34382, 34529, 34633	Microstructures
34382, 34529	X-Ray Diffraction
34382, 33762, 34529, 34633	Anisotropy

All material used was in accordance with specification AMS 6439.

PROCEDURE

General Mechanical Properties

Yield strength, tensile strength, elongation, and reduction of area values were obtained from standard flat tensile specimens, Figure 5, using a strain rate of 0.005 in/in/min until a 0.2 percent offset was obtained, followed by a strain rate of 0.02 in/min until failure. The specimens were oriented as shown in Figure 6. Brittle-ductile transition determinations made from specimens shown in Figure 7 were obtained from the annealed and formed material. All specimens were oriented with the length dimension parallel to the major rolling direction of the disk.

Microstructure

Microstructural determinations were made on specimens obtained from sheet material having high and low values of $\bar{R}$ and exhibiting complete (Figure 8a) and incomplete (Figure 8b) spheroidization. The rolling direction was determined using metallographic techniques (Figure 9).

X-Ray Diffraction Studies

Studies were conducted on the sheet material representative of random and highly textured structures. Tracings were made using an X-ray diffractometer with an iron target. The specimens were held in a commercial reflection-type pole figure device and intensities recorded on a strip chart.

Anisotropy Measurements

Values for R_θ were determined using two methods. In the first method standard flat tensile specimens were equipped with 90-degree strain gages (Type FABX-12-12) which record strains in both the longitudinal and transverse directions (in the plane of the specimen). Both elastic and plastic strains were recorded up to a total strain of approximately 1.5 percent. Accurate readings beyond this point could not be obtained. The flat test specimens were machined from the disks parallel with the rolling direction and at increments of 30 degrees up to 150 degrees as shown in Figure 6. The $\bar{R}$ and ΔR values were calculated in accordance with the procedure outlined in Reference 15. A strain rate of 0.005 in/in/min was used until strain gage measurements were discontinued, then 0.02 in/min was used until specimen failure.

In the second method, strains were measured with an extensometer. The strain rate used was 0.005 in/in/min until a 0.2 percent yield strength offset was obtained followed by 0.02 in/min until fracture. The failed specimens were measured directly for plastic strain with micrometers in the width and thickness directions. Three micrometer readings were taken for each specimen at the location shown in Figure 10. Each individual reading had to be within 0.002 inch of the average value of three readings for each specimen orientation. Specimens were oriented at 0, 45, and 90 degrees to the original rolling direction of the sheet (Figure 6). The $\bar{R}$, R_θ, and ΔR values were calculated from Equations 1, 2, and 3.

RESULTS

General Mechanical Properties

Although significant variations in mechanical properties were observed from heat to heat (possibly resulting from varying hot-rolling finishing temperatures and degree of spheroidization), relatively slight variations were observed as a function of test specimen orientation within a particular heat, that is, 0, 45, 90, and 135 degrees to rolling direction, Figure 11. These results are in direct opposition to those variations observed for R_θ values (Figure 12), where relatively large variations of R_θ are observed within a particular heat. This phenomenon is probably indicative of predominantly crystallographic texturing of the material, with little or no mechanical fibering or internal stresses being present. These factors are normally influential in causing directionality in mechanical properties.

Brittle-Ductile Transition Temperature Studies

The brittle-ductile transition curves based upon energy absorption and fracture fibrosity are shown in Figure 3. Heats 34633(P), 33762(C), 34382(P), which were tested in the annealed condition prior to hydroforming, showed transition temperatures (50 percent fibrosity) at or below room temperature. Heat 34382(C), which represented the hydroformed material,

showed a shift in the transition temperature from room temperature to almost 100 C. This shift is most likely a result of strain hardening induced by the plastic deformation caused by the hydroforming process.

Anisotropy Studies - R_θ, $\bar{R}$, and ΔR Determinations

In all cases observed, see Figure 12, including strain gage and micrometer strain ratio determinations, $R_0 < R_{45}$ and $R_{90} < R_{135}$, and in most cases, $R_0 < R_{90}$ and $R_{45} < R_{135}$. These results produce negative ΔR values which are indicative of 45 degrees earing,[6] typically observed in hot-rolled sheet material. Again, in all cases the R_θ values obtained from 0 to 180 degrees in strain gage measurements are lower than the respective values obtained in micrometer measurements. Concurrently, the $/\bar{R}/$ and ΔR values are greater for the micrometer than for the strain gage measurements. Since the strain ratios obtained using micrometer measurements represent relatively large amounts (15 percent) of strain, it is assumed that $\bar{R}$ and ΔR are not constant, and probably increase in absolute value as total strain increases, as is actually shown in Figure 13. There is a variation in both $\bar{R}$ and ΔR from heat to heat as shown in Figure 14. However, the absolute value of ΔR changes at twice the rate as $\bar{R}$, as shown in Figure 15, where the slope of the ΔR versus $\bar{R}$ curve is approximately 2.

Microstructural Determinations

In all heats observed, the material exhibited various degrees of spheroidization; Figure 8 shows the two extremes observed. There appears to be no specific correlation between degree of spheroidization and $\bar{R}$, ΔR, or yield strength. However, some correlation exists between degree of spheroidization, elongation, and tensile strength values. In addition, the degree of grain boundary carbide precipitation appears to be related to ductility and tensile strength. A typical microstructure showing rolling direction is shown in Figure 9.

X-Ray Diffraction Determinations

In all cases the X-ray diffraction studies, conducted as a function of sheet orientation, substantiate the results obtained from the strain ratio determinations. For example, in the case of low ΔR values ($</0.25/$), random orientation of the (110) (no observable intensity peaks) were observed as shown in Figure 16. However, where ΔR was high ($>/0.25/$), a high concentration of (110) observable intensity peaks), oriented between 60 and 90 degrees to the plane of the sheet, was observed. The highest concentrations occurred in the principal rolling (three peaks) and transverse (one main peak) directions of the sheet (Figure 17).

$\bar{R}$ was approximately 0.9 to 1.2 in all cases of random orientation of the (110), as is expected since this range is indicative of an isotropic material ($\bar{R} \sim 1$).[6] As Whiteley and Wise[6] have shown to be the case in an anisotropic bcc material, heats exhibiting $\bar{R} > 1.2$ result in preferred orientation of the (110) at 60 to 90 degrees relative to the principal rolling direction.

DISCUSSION

Throughout this section, reference will be made to "good" and "poor" heats of material. A good heat is defined as one which produced 90 percent or more of acceptable hydroformed domes, as shown in Figure 1 (heat 34529). A poor heat is one which produced less than 75 percent acceptable hydroformed domes (heat 34633).

General

In the deep drawing of H11 steel, anisotropy caused by internal stresses has shown some effect as evidenced by the tendency of the blank disks to exhibit an "out of flatness" condition. Mechanical fibering has only a slight effect since the inclusion rating of the material is quite low and under proper annealing conditions complete and random spheroidization of the carbide phase is obtained. However, the third phenomena, crystallographic texturing, plays a dominant role in the drawability of the sheet material.

It was found that marked planar anisotropy $\Delta R > 0.25$ was present in the poor stock (heat 34382) and little planar anisotropy $\Delta R < 0.25$ was present in the good stock (heat 33762). Concurrently, the normal anisotropy ($\bar{R}$) was considerably higher for heat 34382 than for heat 33762, as shown in Figure 14. In addition, it was noted that in most cases, incomplete spheroidization (Figure 8b), low ductility, and high yield and tensile strengths (Figure 11), were observed with the poor material; and good spheroidization (Figure 8a), higher values of ductility, and lower values of yield and tensile strengths were observed with the good material.

In reviewing Figures 11 and 14, it was found that the disks exhibiting elongation values in excess of 25 percent, yield strength values below 55,000 psi, and a minimum of planar anisotropy $\Delta R < 0.25$ produced acceptably drawn domes. When these conditions were not obtained, a high percentage of failures of the four types shown in Figure 2 were observed.

The first type of failure, Figure 2a, where a high ΔR caused extensive earing resulting in high stress concentration, has been previously mentioned. The second type of failure, Figure 2b, wherein brittle fracture occurred around the circumference of the dome, at a point between the flange and top of the dome, was attributable to incomplete spheroidization which resulted in material with low ductility and high yield and tensile strength values. The third type of failure, Figure 2c, which fractured at the midpoint of extremities of the circumference of the ears, was caused by a combination of incomplete spheroidization (lack of ductility) and moderately high values of planar anisotropy (ΔR). The fourth type of failure, Figure 2d, which was ductile in nature, occurred shortly after initiation of deep drawing. Such a failure results when the blank hold-down force is excessive, thus causing the drawing tensile force to exceed the yield and tensile strengths of the material. This phenomena causes localized circumferential yielding and necking and ultimate rupture.

Determination of R_θ, $\bar{R}$, and ΔR Values

The R_θ can be determined experimentally by several methods. Since R_θ is defined as $\delta\epsilon_w/\delta\epsilon_t$, as measured on a conventional sheet tensile specimen, both width and thickness strain readings can be recorded at any time during the actual tensile test. However, if the test load is applied at the time of measurement, allowance must be made for elastic strain and this value subtracted from the total strain to produce the actual plastic strain.[23]

Strain measurements can be made by means of strain gages[23] or a special mechanical extensometer which is electronically connected to automatic recording devices. However, the extensometer is only useful during initial plastic straining, since the possibility of experiencing a premature failure of the specimen, which would damage the expensive mechanical device, is quite high and certainly not worth the chance. Consequently, the use of strain gages is normally recommended, but only during initial plastic deformation. Strain gages cannot be used to measure thickness strain as they are not normally small enough to be attached to the thickness dimension of a sheet specimen. Consequently only longitudinal (length) and transverse (width) strain gages can be applied to the specimen. Longitudinal and transverse strains are recorded and the ϵ_t is calculated from the relationship

$$\epsilon_t + \epsilon_w + \epsilon_l = 0 \qquad (4)$$

Both the strain gages and the extensometer have the drawback of not being able to determine R_θ at high plastic strains (>1 percent). Since most deep-drawing operations usually result in a plastic strain of 2 to 10 percent one does not truly evaluate the anisotropic behavior of the material in the crucial deformation range using the above techniques. Consequently, width and thickness strain measurements of failed sheet specimens, where elongations of 4 to 30 percent (tensile elongations measured after maximum load) have been obtained can provide important strain ratio or R_θ value data.

In this study both strain gages and failed specimen measurement techniques were used. Both measurements indicated similar cyclical strain ratio variations as specimen orientation went from the rolling direction (0 degrees) to the transverse direction (90 degrees) as shown in Figure 12. The normal anisotropy ($\bar{R}$) values obtained at small plastic strains, indicated by the strain gage measurements, were not as great as those obtained at the higher plastic strains, measured by the failed specimen techniques.

The $/\Delta R/$ was also much less for the small strain reading than for the higher measurements. This would indicate that ϵ_w/ϵ_t is a function of total plastic strain, as shown in Figure 13, and not constant as is actually observed in ϵ_w/ϵ_t strain gage plots for small plastic strain, as shown in Figure 18.

Correlation of Factors Affecting Drawability

The factors considered to be most important in influencing drawability of H11 annealed sheet are R_θ, $\bar{R}$, ΔR, yield strength, ductility, and brittle-ductile transition temperatures. In general, the values of $\bar{R} \sim 1$ for all heats represent a fair degree of drawability.[6] However, large variations in R_θ, producing high ΔR values, lower the effective degree of drawability by increasing susceptibility to earing. As mentioned previously, extensive earing can cause regions of stress concentration leading to component failure, or produce a shape which is dimensionally deficient. The ΔR and $\bar{R}$ are generally[29] interrelated phenomena as supported in Figure 15. However, ΔR is more greatly affected by processing variables than $\bar{R}$. As illustrated in Figure 15, ΔR and $\bar{R}$ show a linear relationship with the slope $\Delta R/\bar{R} = -2$. Any change in $\bar{R}$ will cause twice as great a change in ΔR. Plots of R_{45} versus ΔR and R_{45} versus $\bar{R}$, Figure 19, are also linear relationships. A measurement of R_{45} automatically establishes $\bar{R}$ and ΔR for a particular material.[29] There appears to be no direct relationship between R and drawability but when $\bar{R}$ is used in conjunction with ΔR, ductility, and yield strength, such a relationship is established.

The variation in both $\bar{R}$ and ΔR from heat to heat is probably indicative of varying hot-rolling finishing temperatures[6] as shown in Figure 14, with $|\Delta R|$ increasing as hot-rolling temperature decreases while $\bar{R}$ increases a lesser amount at hot-rolling finish temperature decreases.[6]

It is well known that the brittle-ductile transition temperature is a function of heat-treatment cycle, processing procedure, and degree of plastic deformation, with brittle-ductile transition temperature normally increasing with increased work hardening or plastic strain.

Thus, forming of the H11 steel sheet into the desired shape at temperatures in excess of the observed brittle-ductile transition temperature with approximately 10 percent plastic strain, but below the blue brittleness range would greatly decrease the tendency to fracture during forming. Drawability would also be enhanced by decreasing the effective yield strength of the material and increasing its ductility (percent elongation) and normal anisotropy ($\bar{R}$). Heat 34529, which had a brittle-ductile transition temperature greater than room temperature, was considered a good heat while those with brittle-ductile transition temperature less than room temperature could not be evaluated on this criterion alone.

Texturing, as evidenced by $\bar{R}$ values in excess of 1 with corresponding high ΔR values, Figures 12 and 14, has been substantiated by X-ray diffraction studies, Figure 17.

The hydroforming of domes of a quality equal to or better than the component shown in Figure 1 has been shown to be mainly a function of ΔR, ductility, yield strength, and brittle-ductile transition temperature. In turn, parameters are influenced by microstructure (annealing treatment), provided hot-rolling finishing temperature and composition are kept constant.

CONCLUSIONS

1. The primary causes for poor drawability of the H11 sheet material were excessively high values of planar anisotropy (ΔR), most likely caused by low hot-rolling finishing temperatures, and incomplete spheroidization resulting in low ductility and high strength values, caused by incomplete annealing.

2. To prevent acceptance of the H11 sheet material which exhibits these detrimental qualities, the following specifications were recommended. Material exhibiting minimum elongation values of 25 percent, maximum yield strength values of 55,000 psi, and a maximum R value of 0.25 would be considered acceptable. If all of the above criteria were not met, rejection would be recommended. Heat 34529, which was considered a good heat, met these criteria and heats 34633 and 34382, which were considered poor heats, failed to meet all these criteria.

3. All heats of the H11 sheet evaluated, with the exception of heat 34382 ($\bar{R}$ = 1.04, 1.09, 1.27, 1.52), exhibited $\bar{R}$ values from 0.90 to 0.99. This range, at best, indicates only fair drawability. Consequently, even with drawing variables kept at optimum levels, the severity of hydroforming the accumulator dome would cause a base level failure rate during drawing of approximately 2 to 9 percent. Only when $R>1.0$ could one expect the base level failure rate to be less than 2 to 3 percent.

4. Since $\bar{R}$ decreases linearly as ΔR, and since improved drawability is desired, we must settle for an increase in the tendency toward earing for the H11 sheet material evaluated. Therefore, a point must be established where the severity of earing (ΔR) is more detrimental than the improvement in drawability ($\bar{R}$) is beneficial.

5. The ΔR, R_{45}, and $\bar{R}$ are mutually dependent upon each other and are linearly related for the H11 steel evaluated.

6. For the H11 steel evaluated, $\bar{R}$, a measure of normal anisotropy (drawability), is not affected by processing changes as greatly as ΔR, a measure of planar anisotropy, since $\Delta R/\bar{R} = 2$.

7. The strain ratio, $d\epsilon_w/d\epsilon_t = R_\theta$, shows a tendency to increase as total strain increases for the H11 steel evaluated. This was indicated by lower R_θ values for strain gage measurements at low strains as compared with the broken tensile bar measurements at higher strains.

LITERATURE CITED

1. SOCIETY OF AUTOMOTIVE ENGINEERS, INC. Aeronautical Materials Specification, AMS 6437, November 1, 1959.

2. BURKE, J. E. "The Origin of Recrystallization Textures." U. S. Atomic Energy Commission, AECU-1610, 25 July 1951.

3. BURNS, R. S., and MEYER, R. M. Sheet Metal Ind., v. 35, 1958, p. 261.

4. MUELLER, M. H., CHERNOCK, W. P., and BECK, P. A. Comments on Inverse Pole Figure Methods, Transactions AIME, v. 212, 1958, p. 39.

5. McEVILY, A. J., Jr. "Analysis of Ear Formation in Deep Drawing." NASA Technical Note 3439, May 1955.

6. WHITELEY, R. L., and WISE, D. E. "Relation Among Texture, Hot Mill Practice and the Deep Drawability of Sheet Steel." Flat Rolled Products III, Metallurgical Society Conferences (AIME), v. 16, 1962, p. 47-61.

7. BALDWIN, W. M., Jr., HOWARD, T. S., and ROSS, A. W. "Relative Triaxial Deformation Rates." Transactions AIME, v. 166, 1946, p. 86.

8. DIETER, G. E., Jr. "Strain Rate Effects in Deformation Processing." Fundamentals of Deformation Processing, Syracuse University Press, Chapter VII, 1964.

9. WHITELLY, R. L. "The Importance of Directionality in Drawing Quality Sheet Steel." ASM Transactions, v. 52, 1960, p. 154.

10. LANKFORD, W. T., SNYDER, S. C., and BAUSCHER, J. A. "New Criteria for Predicting the Press Performance of Deep Drawing Sheets." ASM Transactions, v. 42, 1950, p. 1197.

11. WHITELEY, R. L., WISE, D. E., and BLICKWEDE, D. J. Sheet Metal Ind., v. 38, 1961, p. 349.

12. GILLES, R. "How Do You Test A Deep Drawing Steel?" Metals Progress, v. 85, no. 5, May 1964.

13. HOSFORD, W. S., Jr., and Backofen, W. A. "Strength and Plasticity of Textured Metals." Fundamentals of Deformation Processing, Syracuse University Press, Chapter X, 1964.

14. HILL, R. "A Theory of the Yielding and Plastic Flow of Anisotropic Metals," Proc. Royal Soc., Ser. A, v. 193, 1948, p. 281.

15. HILL, R. "On Discontinuous Plastic States with Special Reference to Localized Necking in Thin Sheets." Journal of the Mechanics and Physics of Solids, v. 1, 1952, p. 19.

16. BACKOFEN, W. A., HOSFORD, W. F., Jr., and BURKE, J. J. "Texture Hardening." ASM Transactions, v. 55, March 1962, p. 264.

17. BECKER, Joseph. "Oriented Growth in Primary Recrystallization." Transactions AIME, v. 191, 1951, p. 115.

18. BOWLES, J. S., and BOAS, W. Journal Institute of Metals, v. 74, 1948, p. 501.

19. BURKE, J. E. "The Migration of Grain Boundaries." ASM Seminar on Atom Movements, ASM, 1951.

20. BECK, Paul A. "Theory of Annealing Textures." Jwurnal of Metals, v. 3, 1951, p. 475.

21. LANKFORD, W. T., LAW, J. P., and CENSAMER, M. "The Plastic Flow of Aluminum Alloy Sheet Under Combined Loads." Transactions AIME, v. 171, 1947, p. 574.

22. HU, L. W. "Studies on Plastic Flow of Anisotropic Metals." ASME, v. 23, September 1956, p. 444.

23. LARSON, F. R. "Anisotropy in Relation to Sheet Processing." Fundamentals of Deformation Processing, Syracuse University Press, Chapter VII, 1964.

24. BALDWIN, W. M., Jr. "Effect of Rolling and Annealing Upon Copper Strip." Transactions AIME, v. 166, 1946, p. 591.

25. WHITELEY, R. L. "Anisotropy in Relation to Sheet Processing." Fundamentals of Deformation Processing, Syracuse University Press, Chapter VIII, 1964.

26. ZIMMERMAN, J. R. "Hydroforming." Machining Design, 27 June 1957.

27. EDLUND, H. E. "Deep Drawing for Simple and Intricate Shapes." Industry, March 1953, vol. XVIII, no. 8.

28. UNTERWESSER, P. M. "Tool Steel Bows to Deep Drawing." The Iron Age, 18 September 1958.

29. COLTON, R. M., and ENYEDY, G. T. "Interrelationship Between Anisotropy and Crystallographic Structure." U. S. Army Materials Research Agency, AMRA TR 65-15, July 1965.

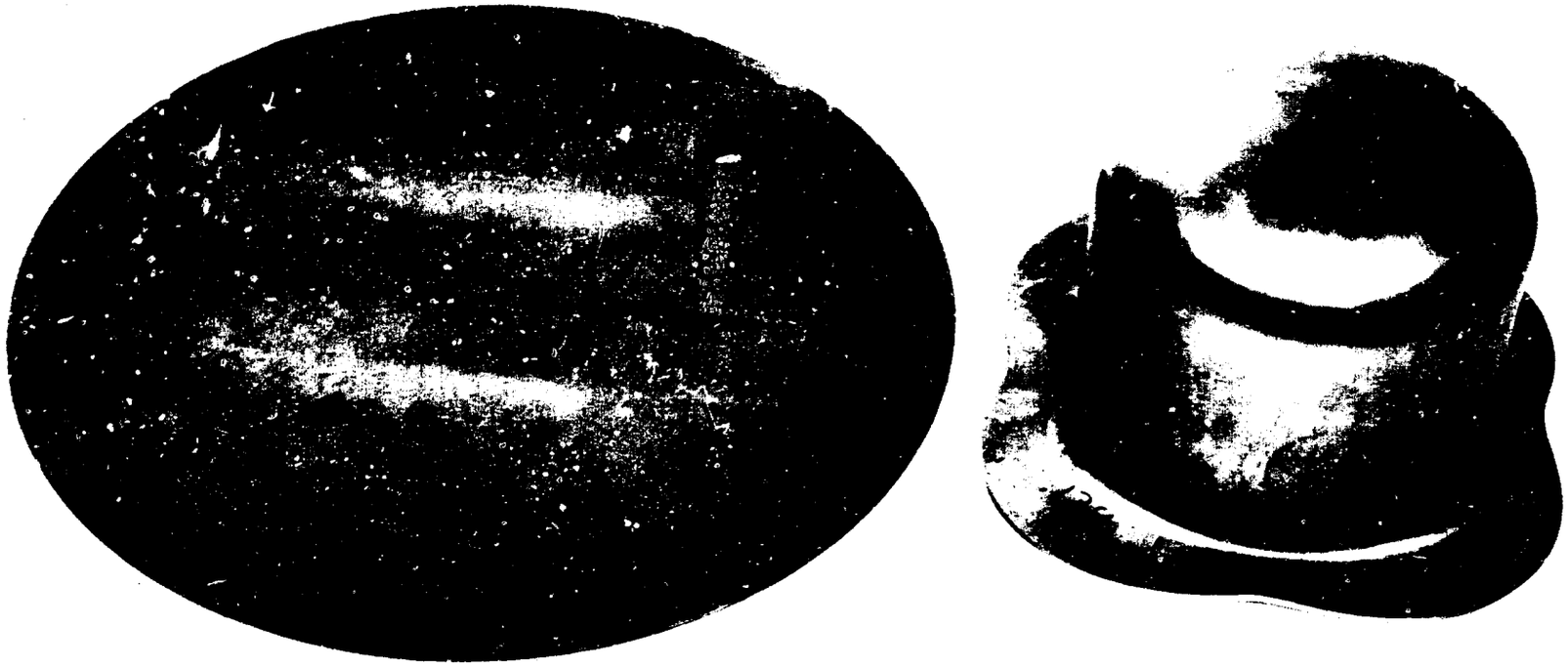

Figure 5. HYDROFORMED DOME AND DISK

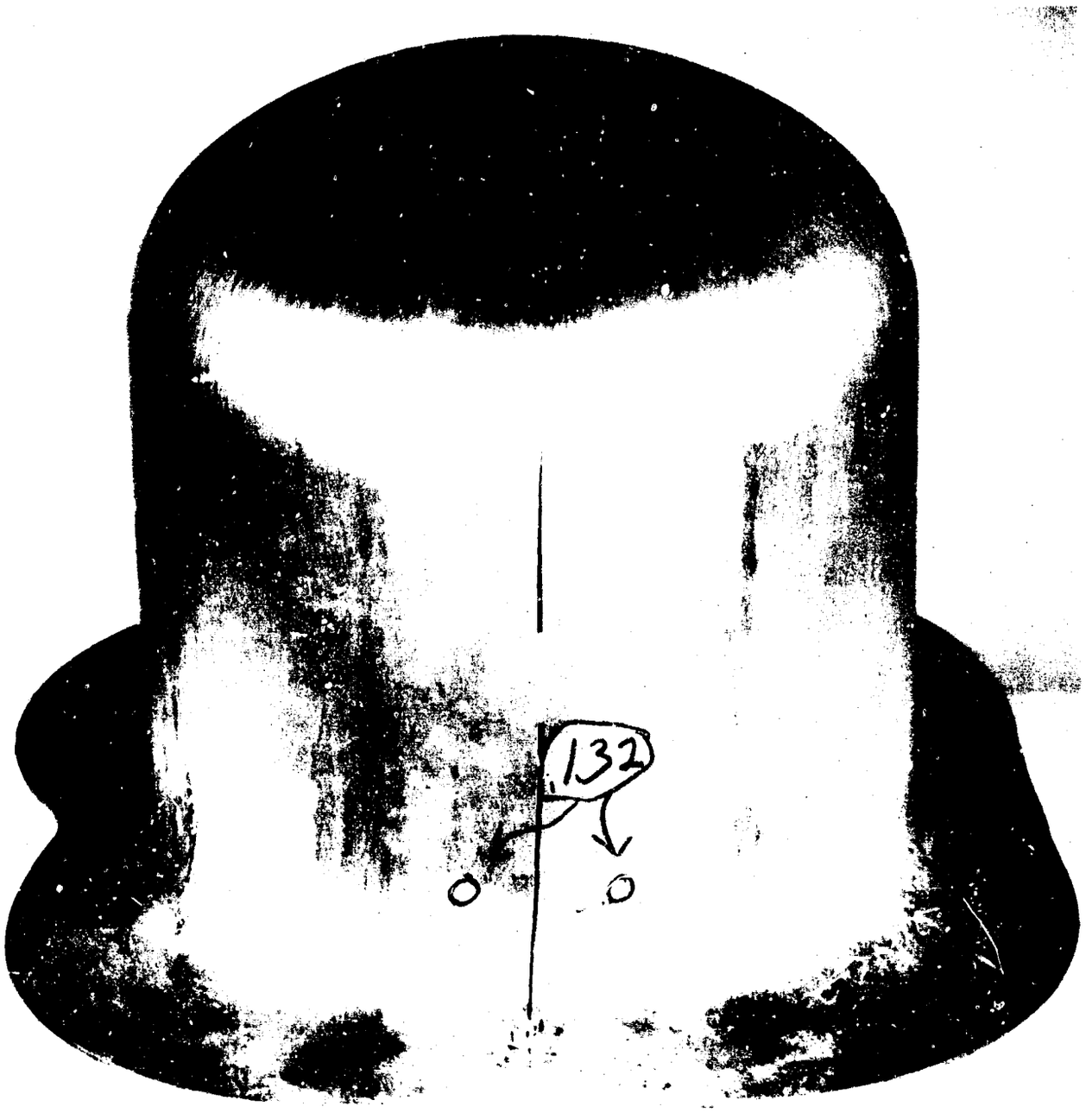

Figure 2a. FAILURE WHERE A HIGH ΔR CAUSED EXTENSIVE EARING, THUS RESULTING IN HIGH STRESS CONCENTRATION

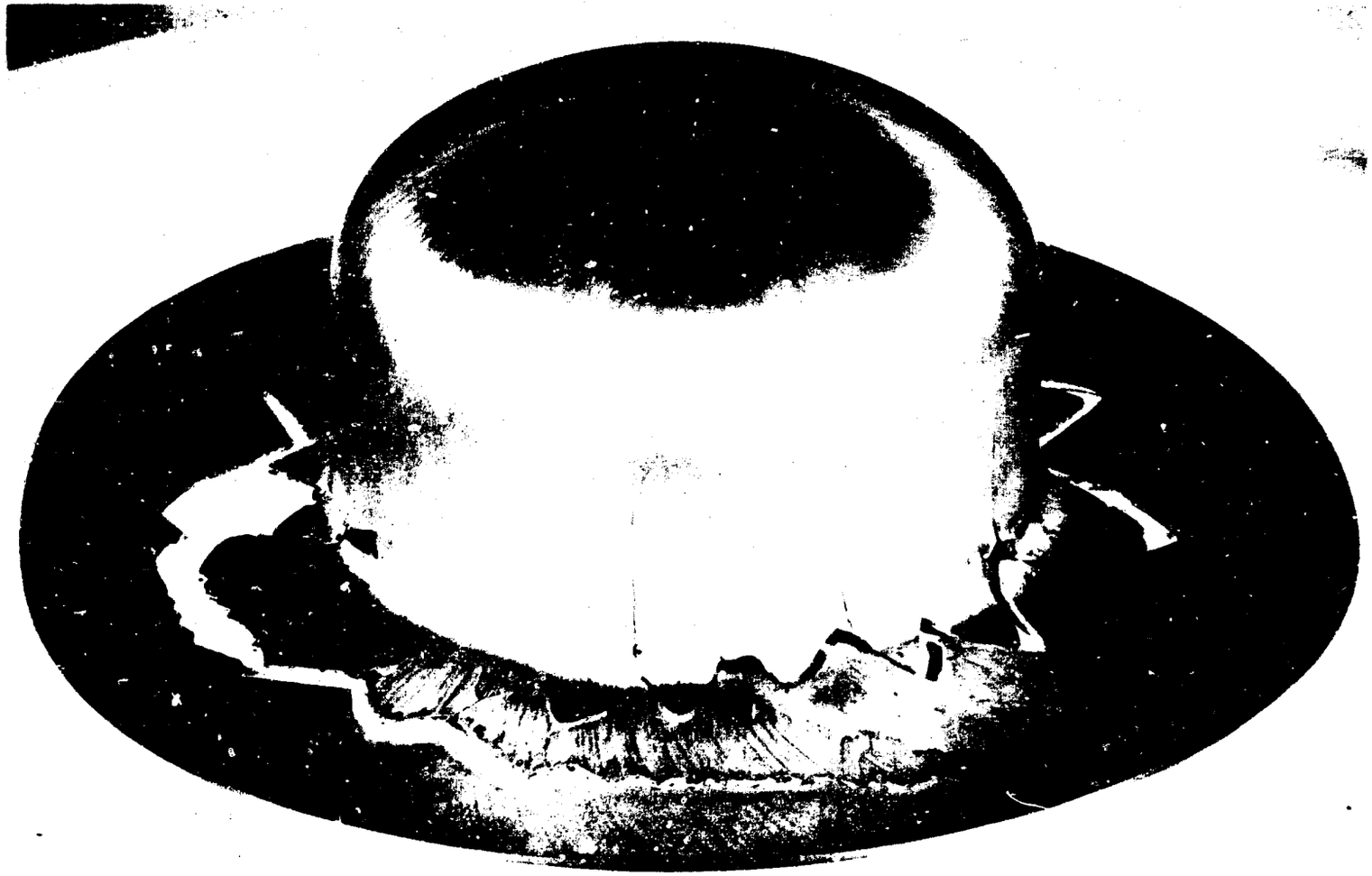

Figure 2b. FAILURE CAUSED BY INCOMPLETE SPHEROIDIZATION

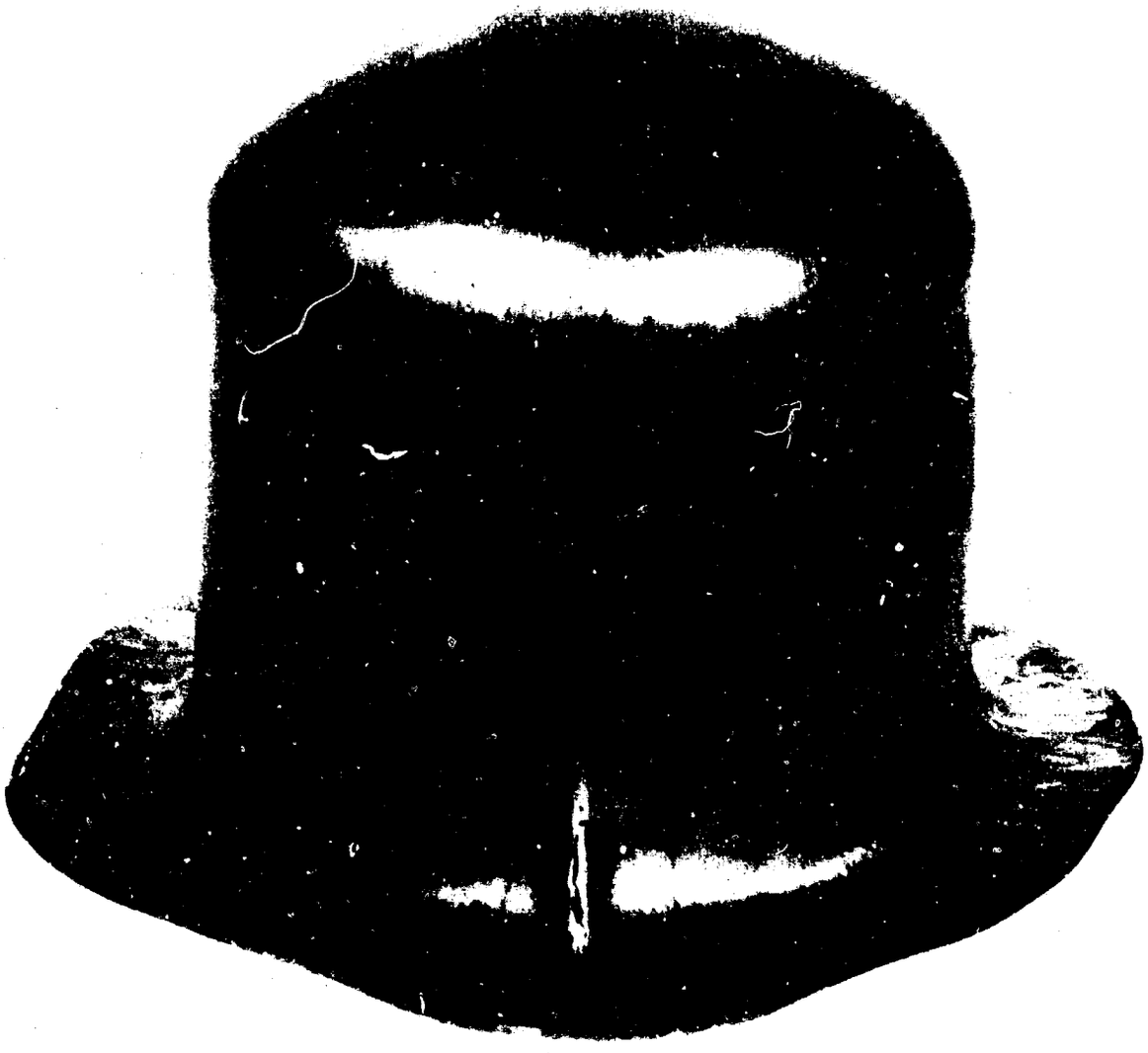

Figure 2c. FAILURE CAUSED BY A COMBINATION OF INCOMPLETE SPHEROIDIZATION AND MODERATELY HIGH VALUES OF PLANAR ANISOTROPY (ΔR)

Figure 2d. FAILURE CAUSED BY EXCESSIVE BLANK HOLD-DOWN FORCE

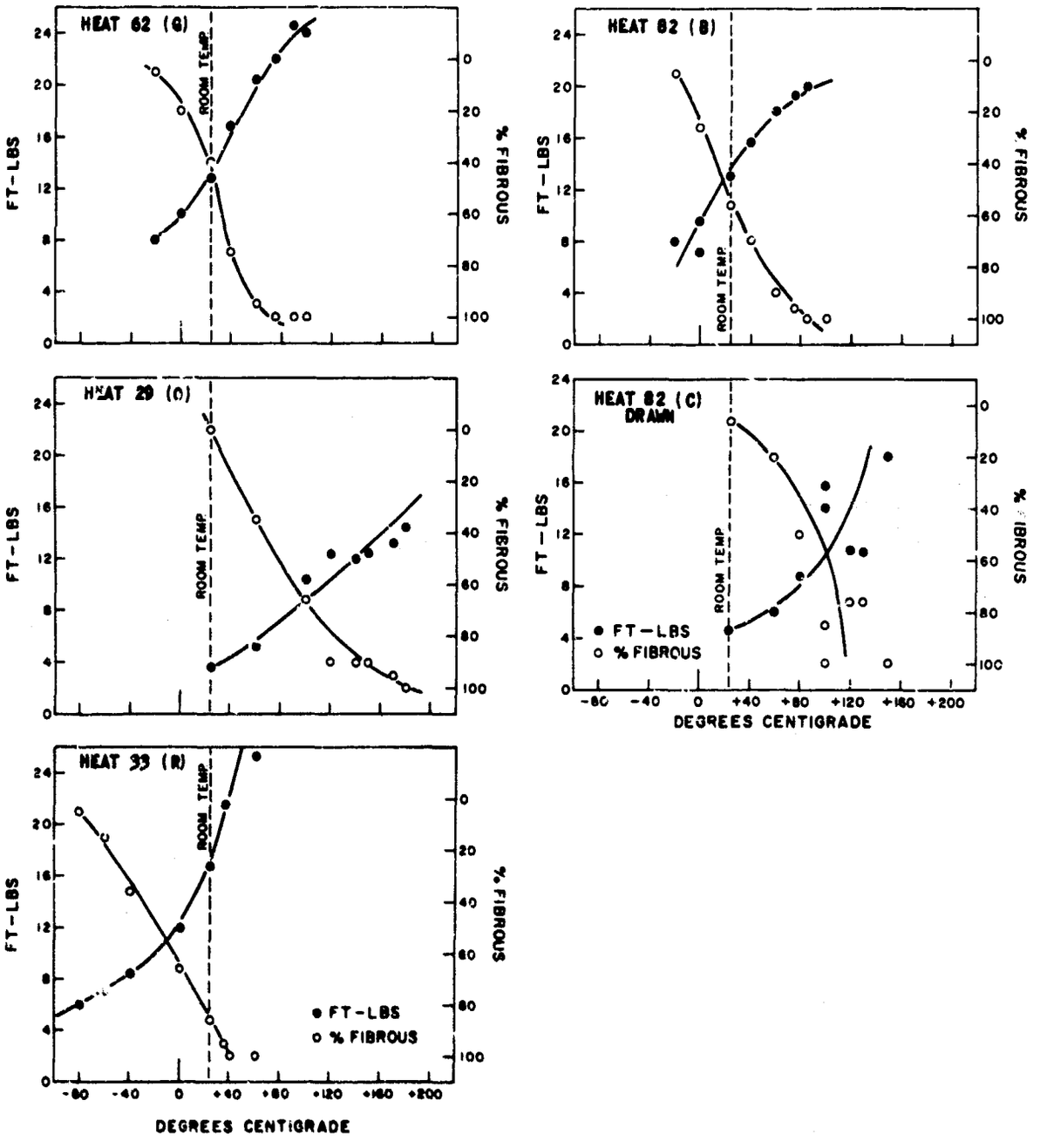

Figure 3. DUCTILE TO BRITTLE TRANSITION

The six steps in the Hydroform operating cycle:

1. Blank is placed on the draw ring.

2. Dome is lowered, clamping blank to holder.

3. Starting pressure is applied to force blank against punch.

4. Punch moves upward increasing pressure and forming part.

5. Pressure is released and dome is raised.

6. Work is stripped from the punch.

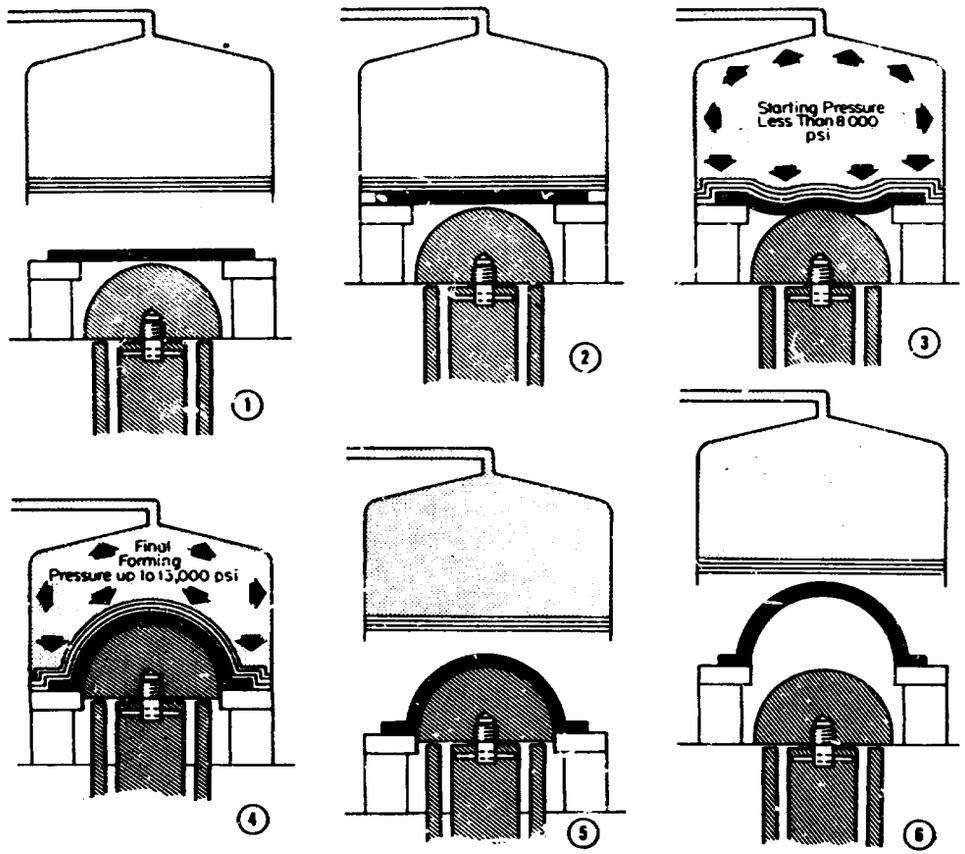

Courtesy of Steel Magazine

Figure 4. SEQUENCE OF OPERATION IN HYDROFORMING

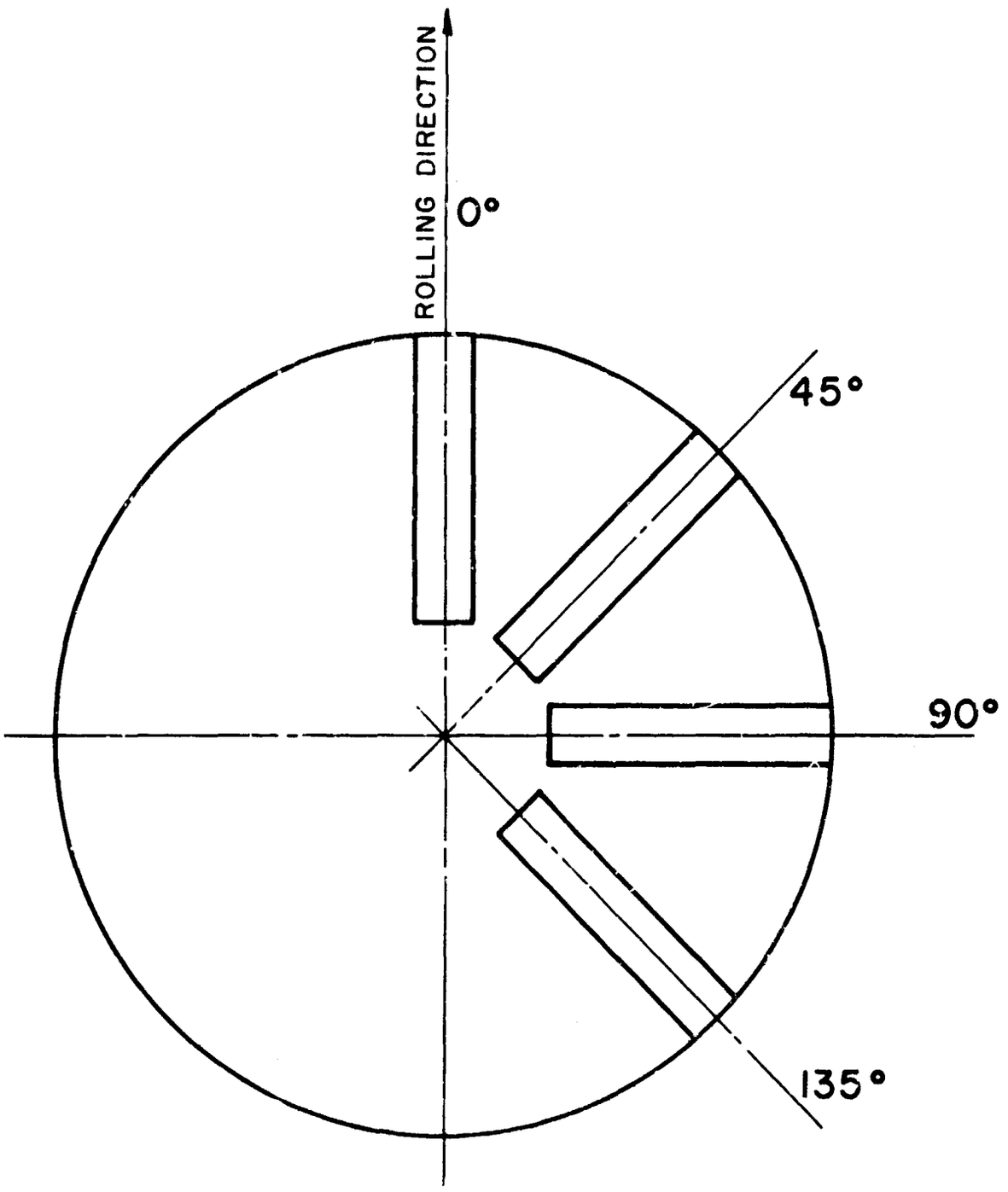

Figure 6. LOCATION OF TENSILE SPECIMENS FOR HEATS 29, 33, AND 82

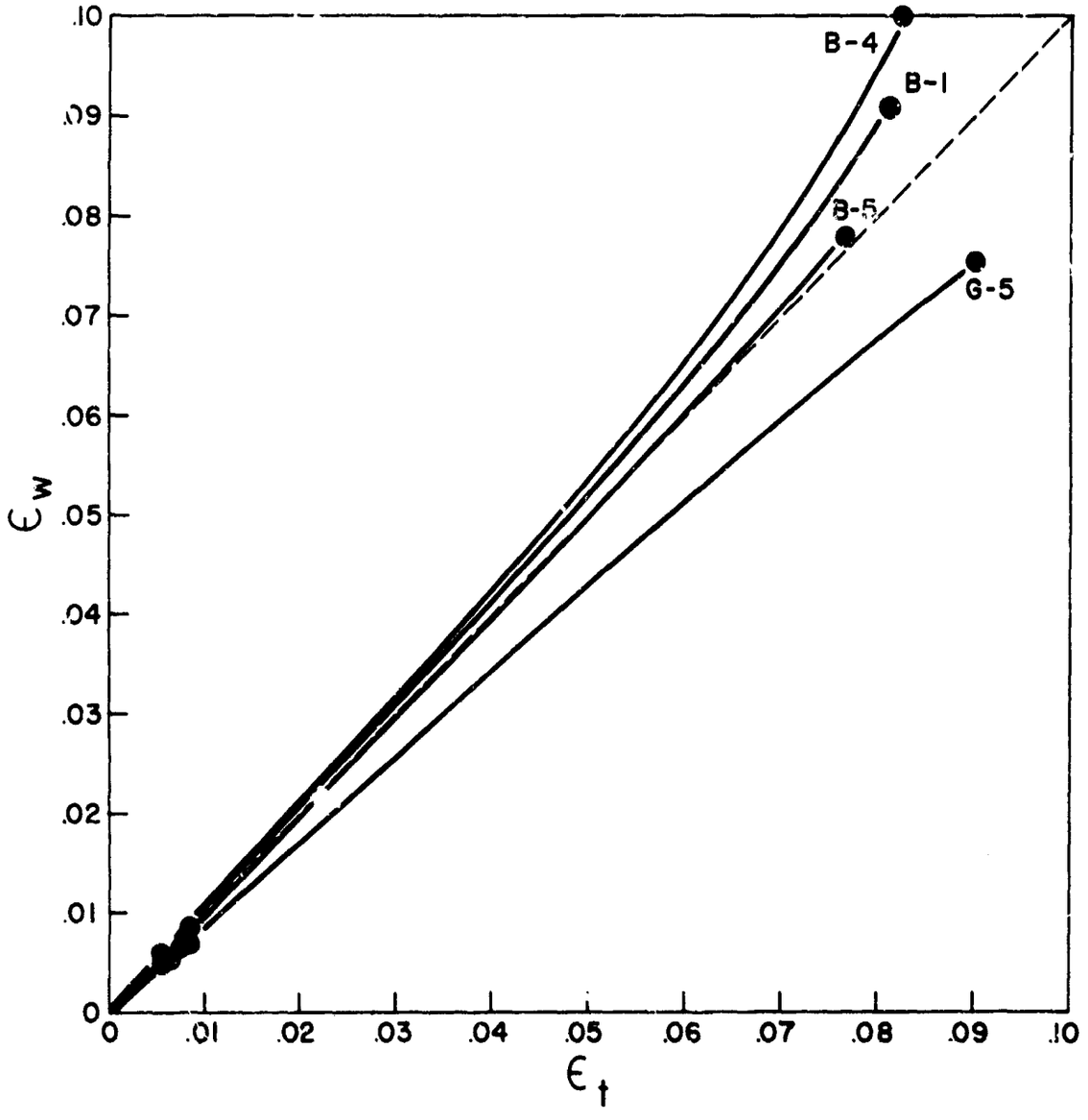

Figure 13. ϵ_w VERSUS ϵ_t

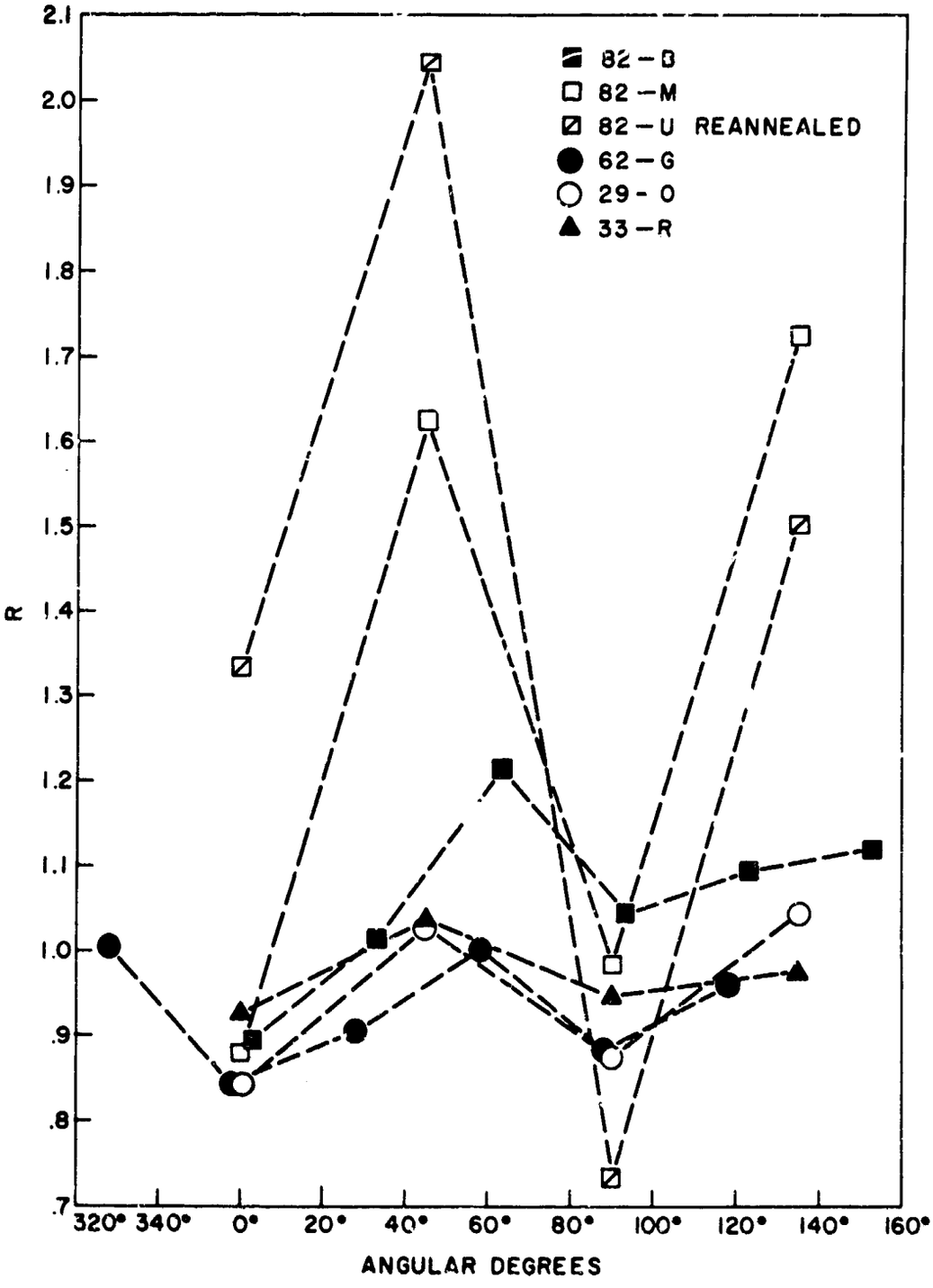

Figure 12. $\bar{R}$ VERSUS SPECIMEN ORIENTATION FOR MICROMETER STRAIN MEASUREMENTS IN ANGULAR DEGREES FROM ROLLING DIRECTION

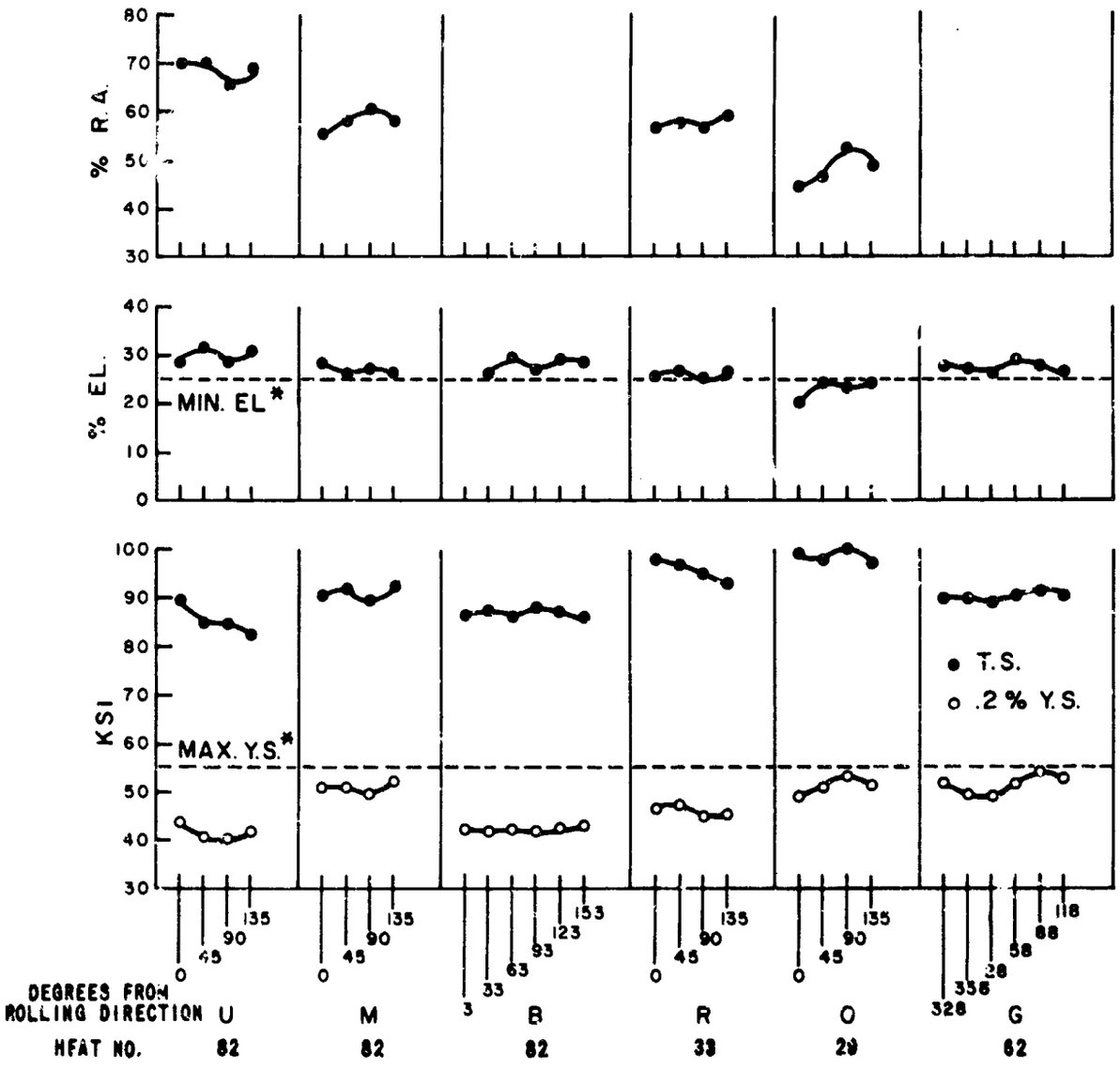

*See Conclusions Page 9

Figure 11. MECHANICAL PROPERTIES VERSUS SPECIMEN ORIENTATION

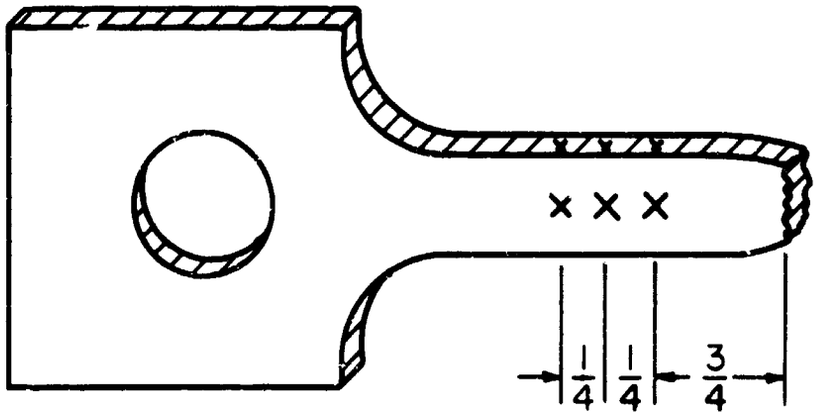

Figure 10. LOCATION OF MICROMETER STRAIN MEASUREMENTS

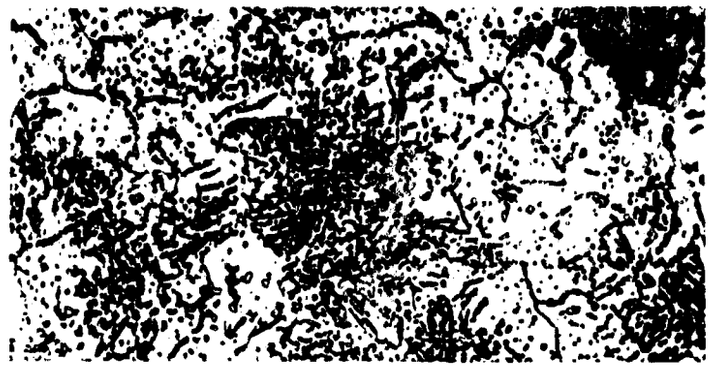

1000X

Figure 8b. MICROSTRUCTURE SHOWING INCOMPLETE SPHEROIDIZATION
Etchant 1 g $CuCl_2$, 50 cc HCl, 25 cc HNO_3, 150 cc H_2O

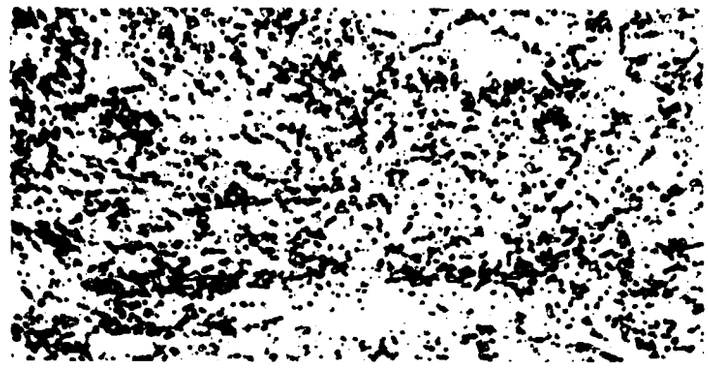

1000X

Figure 8a. MICROSTRUCTURE SHOWING COMPLETE SPHEROIDIZATION
Etchant 1 g $CuCl_2$, 50 cc HCl, 25 cc HNO_3, 150 cc H_2O

100X

Figure 9. TYPICAL MICROSTRUCTURE SHOWING ROLLING DIRECTION
Etchant 1 g $CuCl_2$, 50 cc HCl, 25 cc HNO_3, 150 cc H_2O

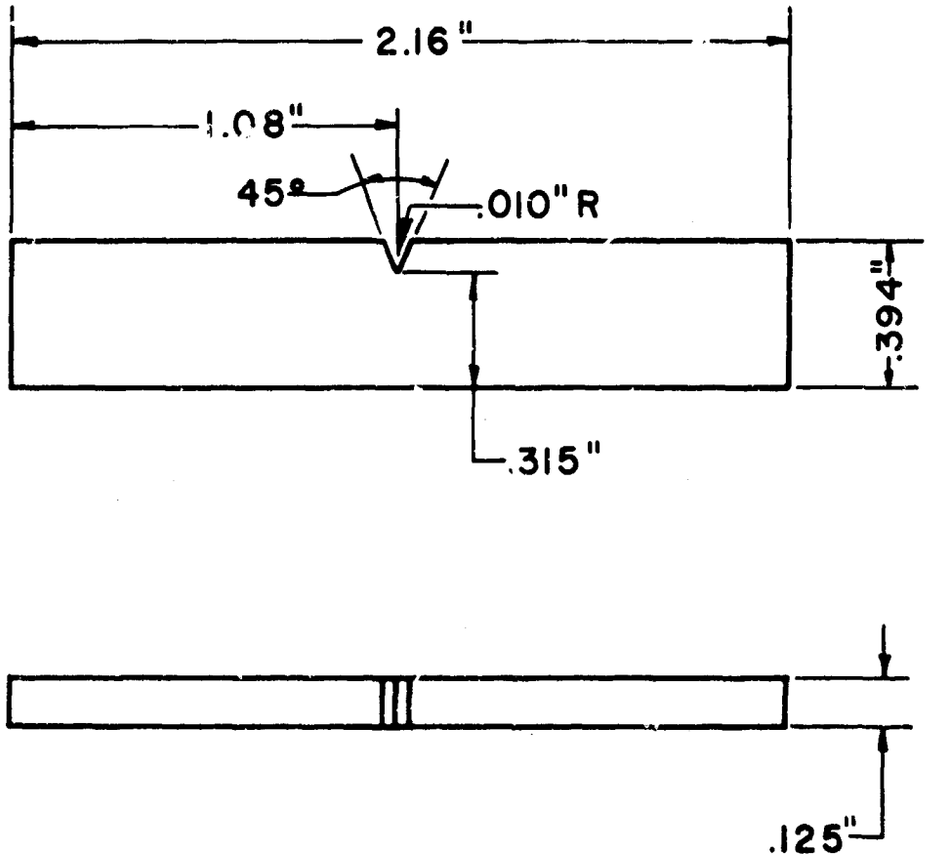

Figure 7. BRITTLE DUCTILE TRANSITION SPECIMEN

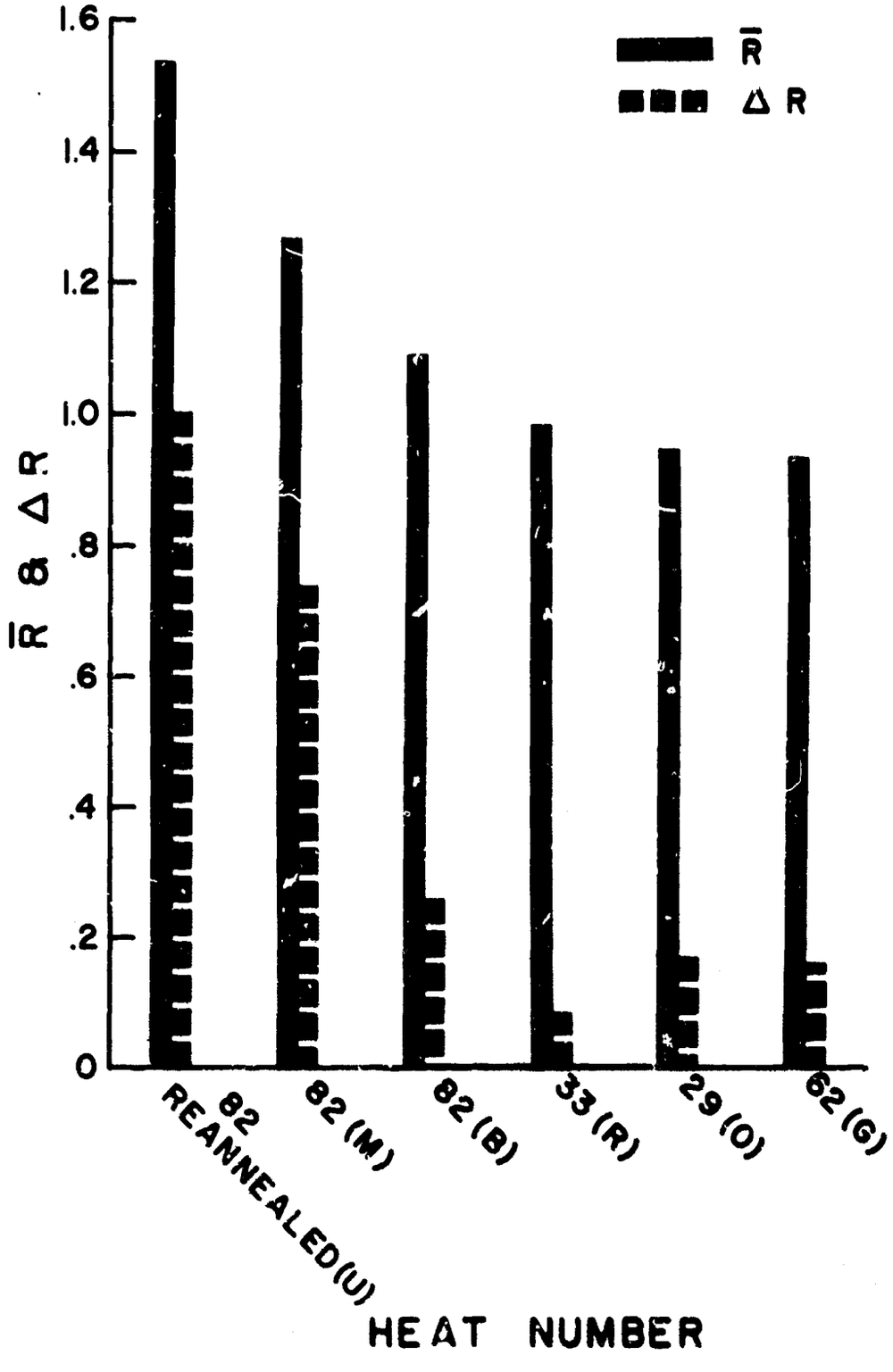

Figure 14. $\bar{R}$ AND ΔR VERSUS HEAT NUMBER

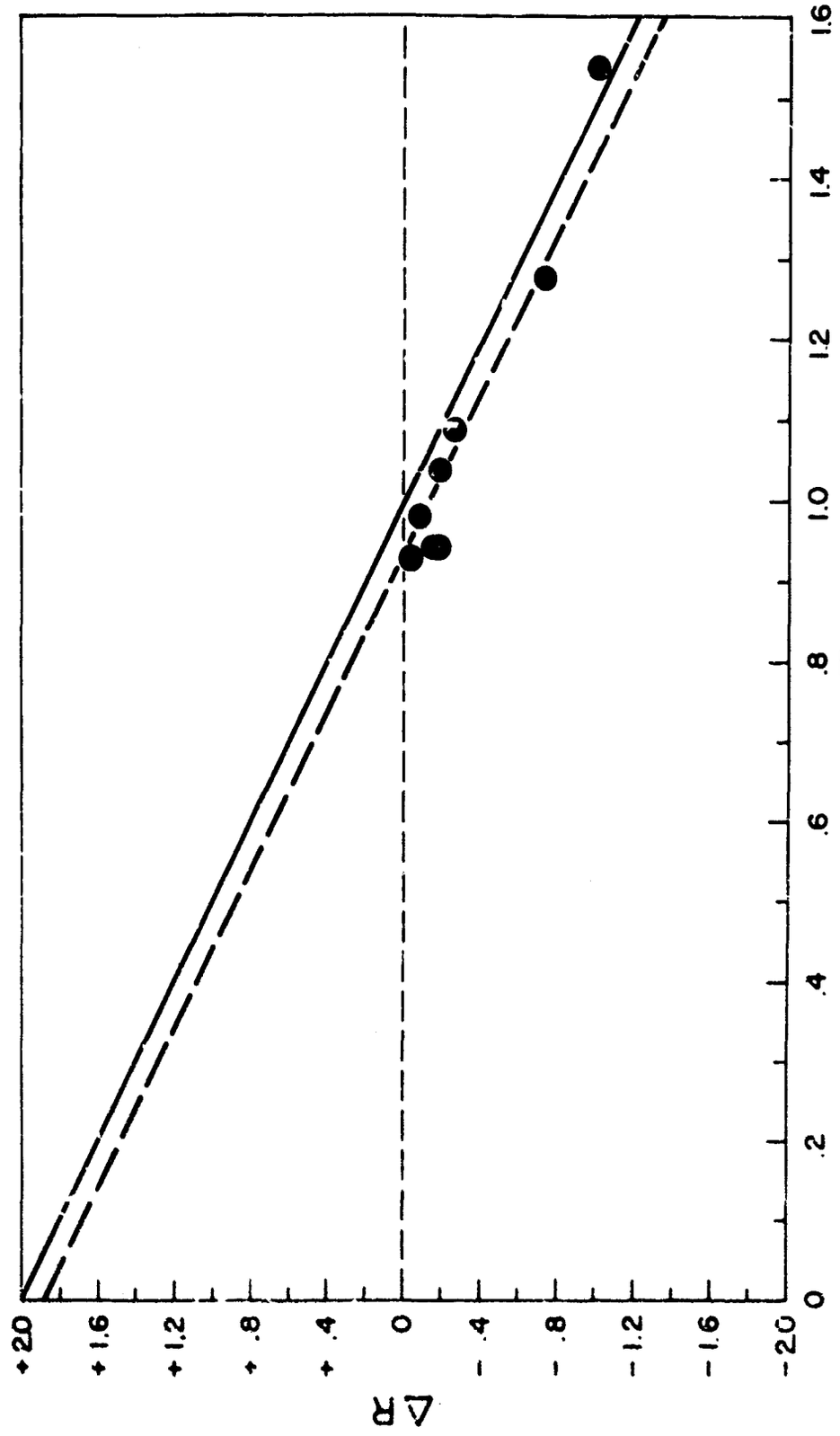

Figure 15. ΔR VERSUS R̄

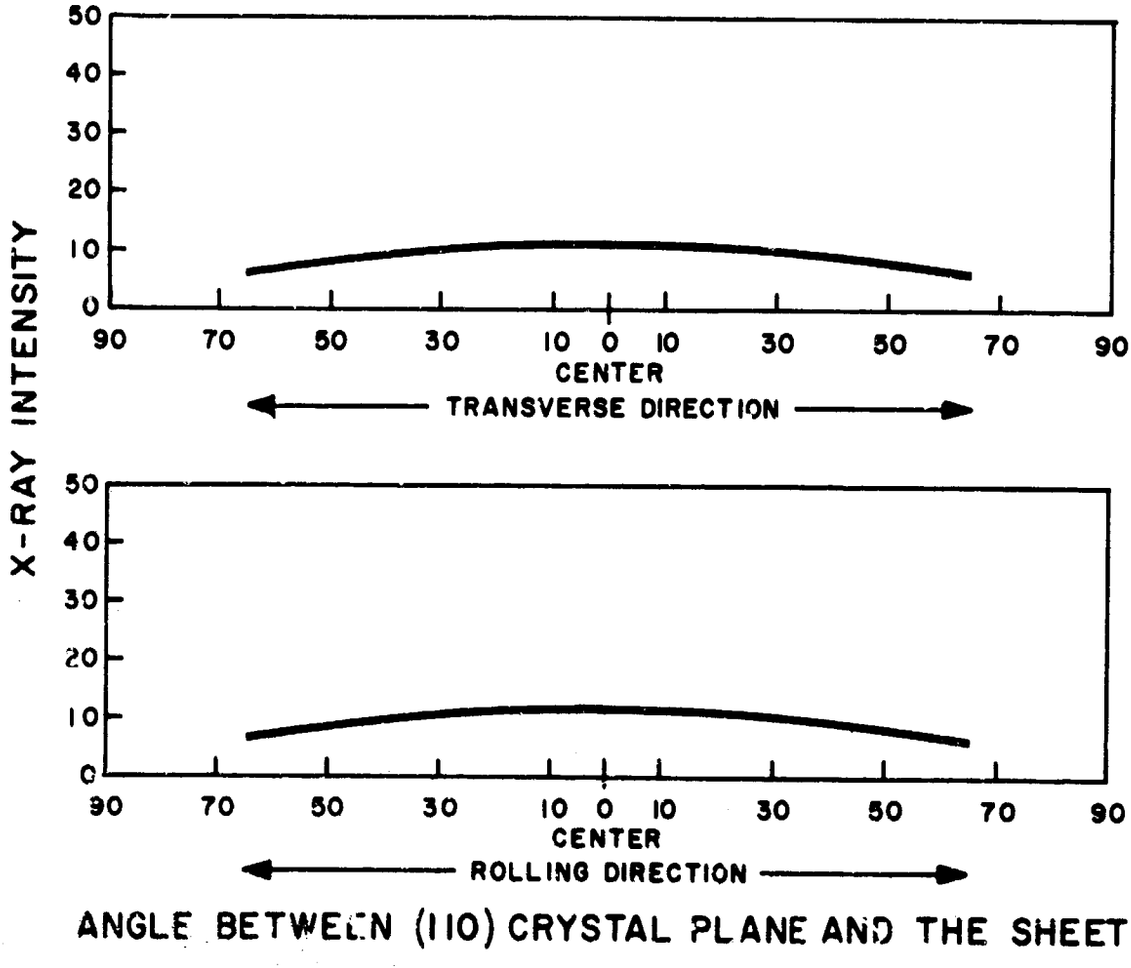

Figure 16. TYPICAL X-RAY RANDOM PATTERN

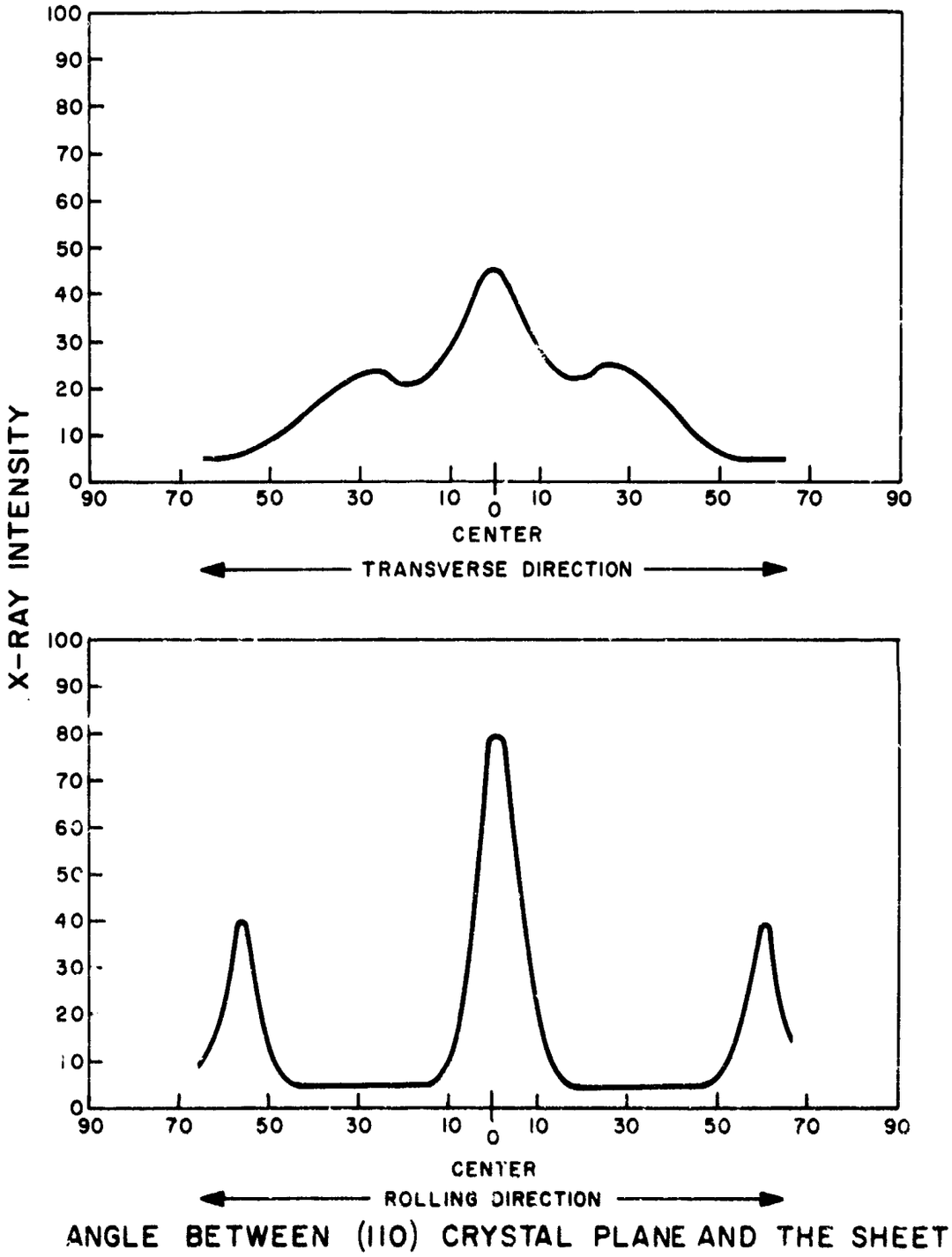

Figure 17. TYPICAL X-RAY PREFERRED PATTERN

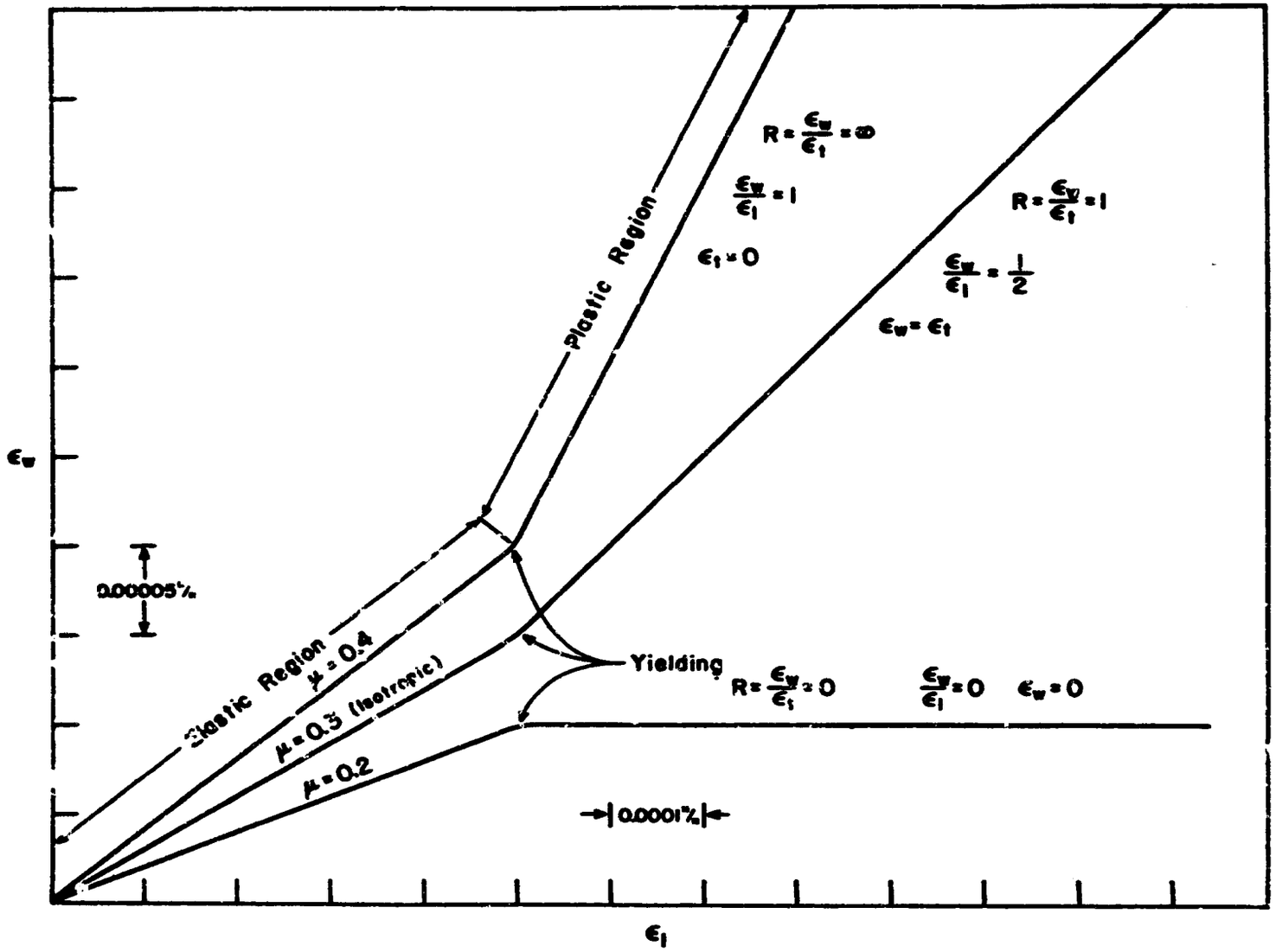

Figure 18. SCHEMATIC REPRESENTATION OF THE LIMITS OF LONGITUDINAL VERSUS WIDTH STRAIN RATIOS

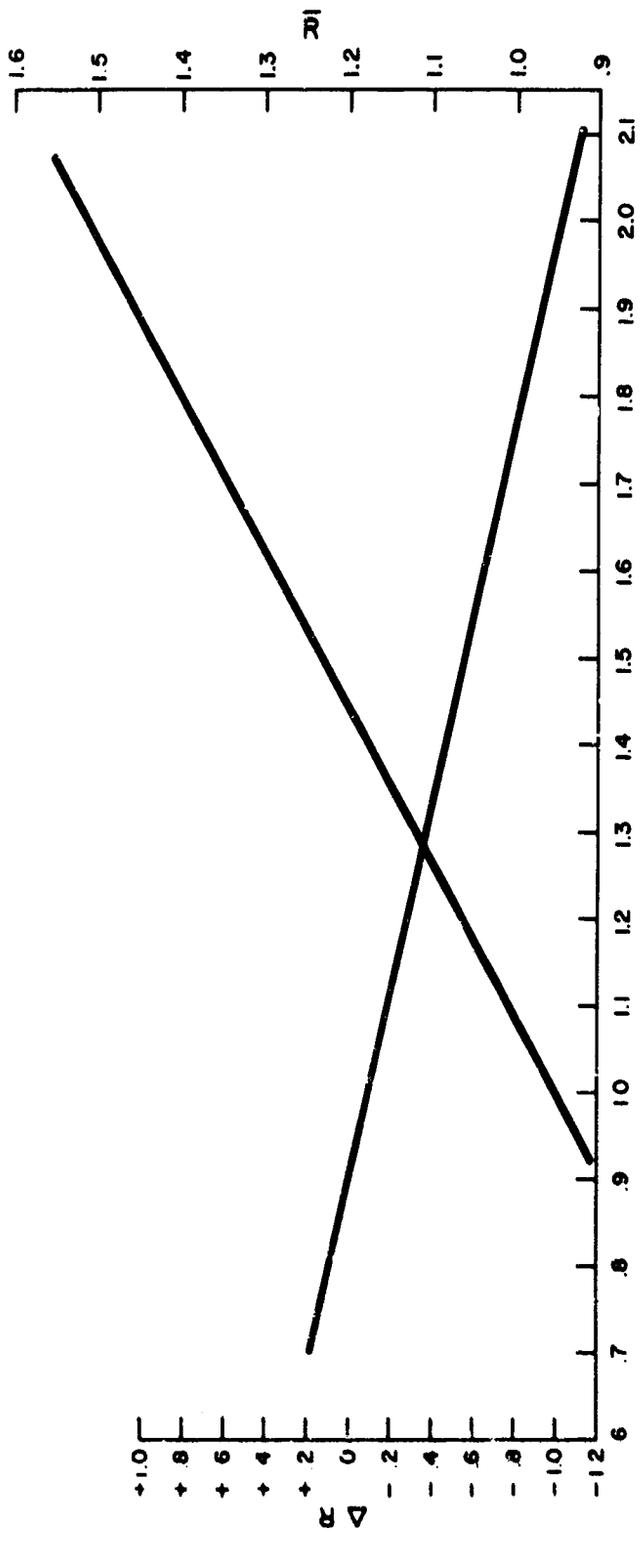

Figure 19. ΔR AND $\bar{R}$ VERSUS R45

STRESS CORROSION AND CORROSION FATIGUE BEHAVIOR OF 250 KPSI MARAGING STEEL IN SEA WATER

R. D. Barer

Pacific Naval Laboratory, H.M.C. Dockyard

Esquimalt, B. C. Canada

PNL has been involved in a co-operative program with de Havilland, Mines Department and Hydrofoil Materials Steering Committee to evaluate behaviour of maraging steel subjected to stress in fresh sea water.

Initial stress-corrosion exposures at PNL were made with ring-type specimen holders. After some time, it became evident that a more accurate method of loading was needed. Specifically, it was decided the need could be met with a unit applying a static load through a lever system and having provision for careful alignment of specimens. Such a unit was designed by LCDR K.W. Moore and G.N. Dennison at PNL. Twelve of these units were subsequently built in Dockyard to very close tolerances. A photograph of the units is in Figure 1.

The specimens for the PNL stress corrosion unit have a 3/16" diameter and a gauge length of 1 1/2". Specimen is also shown in Figure 1.

The specimens were machined from round stock purchased from Vanadium Alloys. In view of comments in the literature that there appeared to be metal which was relatively crack resistant whereas metal from other heats was not*, we thought it would be useful to keep track of specimens from each length of steel, in case some were from different heats. Specimens machined from one length were labelled A1, A2, etc. and those from a second length B1, B2, etc.

Following machining, the specimens were to be heat treated for 3 hours at 900°F to a nominal strength level of 250,000 psi. It was intended to stress the initial non-welded specimens to 80% of ultimate so that results could be obtained in a reasonable time and still provide useful indications of an engineering nature. Later it was intended to stress at lower levels, as time permitted, to get more data at levels closer to actual operating conditions. After getting some useful knowledge from the relatively uncomplicated non-welded material it was intended to then expose the welded specimens which de Havilland was to prepare.

* Dr. G.J. Biefer, "Hydrogen and Stress-Corrosion Cracking of 18% kpsi Maraging Steel", PM-1-65-3, 1 February 1965.

An important part of the program was to establish (a) whether or not cathodic protection is beneficial to maraging steel, and (b) what level of cathodic protection is practical.

It needs to be borne in mind that the aluminum alloy hull requires 0.9 v minimum and that the maraging steel requires approximately 0.75 v protection. It should also be borne in mind that a practical engineering design must have something of the order of 0.2 v driving potential difference. A final point to remember is that the maraging steel near the aluminum must also be polarized to slightly above the 0.9 v potential in order to prevent the aluminum hull acting as an anode (which could be serious at breaks in a painted aluminum hull). All these factors, in practical terms, necessitate driving potentials of one volt and preferably higher.

Results

It appeared that we were on to a major discovery when 5 specimens of bar A failed after 25 to 48 hours exposure, whereas another 5 specimens from the same bar and exposed under identical conditions had a first failure after 76 days (the final one lasted 118 days). A careful check was made of all factors which might have been involved, including an electron microscope study* and spectrographic analysis of metal from several lengths. These were the same composition within every close tolerances. It was concluded that inadequate control in heat treating resulted in under-strength material and, consequently, the stressing was at 94% for those which failed rapidly, rather than approximately 83% for those which lasted 76-118 days.

Subsequent specimens showed that at levels from approximately 83% to 95% (based on hardness levels) duration was generally in the 10 to 16 day range, with a few failing at 2 to 3 days. These were all non-welded and not cathodically protected. Similar specimens (see Table 1) when cathodically protected at one volt lasted from 35 to 180 days.

In an attempt to determine whether a higher level (1.2 v) of cathodic protection could be tolerated, but at lower stress levels, series of triplicate specimens from bar F were run at 85%, 80%, 75% and 70% of ultimate and at 1.2 v cathodic protection. These specimens were carefully cleaned of cathodic deposit several times daily to avoid any shielding effects. While there appeared to be some tendency for increased life at lower stress levels, these results need to be confirmed at 65%, 60% and lower levels.

* Dr D. Tromans, "Metallography of Three Maraged Steel Specimens", UBC Department of Metallurgy, July 1966.

All the above specimens were non-welded plate. Having now some background with plate, the welded specimens from de Havilland (machined from the material actually used on FHE 400) were exposed at 50% of ultimate, with and without cathodic protection at 1 v. While an occasional specimen lasted much longer, failures at 3 to 4 days, irrespective of cathodic protection, were rather jolting.

As a first approach to improve performance, it was decided to see whether heat treating could be beneficial. Three specimens were re-heat-treated at 1500°F for one hour and then aged for three hours at 900°F. These were exposed at 50% and with 1 v cathodic protection, and have lasted over 216 days to date (November 30, 1966).

Naturally, it was realized that to re-heat-treat the foils themselves would be a rather major and difficult project - one to be avoided if possible. This experiment did however, if all else failed, provide a means of improving the stress corrosion behaviour of the welded maraging steel.

To assess a potentially more feasible means of improving the durability of the foils, samples of welded maraging were carefully shot peened at Mines Department (to a depth of .012" compression layer). These three specimens were exposed at 50% and 1 v and have lasted for 102 and 109 days, and one is still on at 197 days (November 30, 1966).

It was also established, through discussion with de Havilland representatives that 50% was a high level, and that 40% or lower were more realistic approaches to extreme and momentary stress exposures of the foil material. Consequently specimens (welded) were exposed at 40% and 1 v. There was a marked improvement with one failing at 50 days, the remaining two are still on at 109 days (November 30, 1966).

The next phase of the investigation was to establish the corrosion fatigue behaviour of both unwelded and welded material (see Table II)

Flat plate specimens (Figure 2) for the Tatnall-Krouse Fatigue Testing machine were prepared, initially of 0.10" thickness. These were exposed to fatigue while vibrating within a cell through which flowed fresh sea water at 210 c.c./minute. Stress amplitude was 48,000 psi about a mean stress of approximately 50,000 psi, peaking at 98,000 psi.

Results from a group of 6 specimens with no C. P. was uniformly 106,000 cycles to 124,000 cycles. The next group of 3 specimens with C. P. of just over 1 v gave results, incomplete because each was removed before failure because of a leaking seal, of 303,600, 340,700 and 5,658,000 cycles (the latter almost 4 days at a cycling rate of over 900 cpm). Another group of two specimens exposed to C. P. of 1.2 volts went 439,300 (stopped with leaky seal) and 8,139,800 which broke outside the sea water cell!

Another two groups were exposed at 62,000 psi mean stress and 62,000 psi stress amplitude (peaking 125,000 psi). The unprotected group survived for 50,600, 56,300 and 60,500 cycles. With 1.2 v C. P. the other group of three went 120,500 and 207,400 (with failure outside the cell in each of these cases) and one went 1,247,600 cycles. An air test of the 62,000 psi level gave failure at 88,800 and 213,200.

Two additional specimens of interest in the 62,000 psi mean stress group are:

(a) One exposed unstressed at 1.2 v for almost 1 week prior to cycling, lasted 1.4 million cycles.

(b) One exposed unstressed to "poisoned" H_2SO_4 electrolyte for almost 4 hours, then run in sea water cell. Failed in 27,500 cycles.

The first preliminary exposures of welded flat specimens gave failures at 56,100, 90,100, and 11,100 cycles for the 48,000 psi mean stress tests and no cathodic protection. A second series, also at 48,000 psi mean stress, gave the following results:

No cathodic protection	86,600, 75,100, 114,200 and 97,100 cycles.
With one volt C. P.	191,400, 246,000, 325,800, 3,925,600 and 182,000 cycles.

Much additional work is planned both with and without cathodic protection.

Discussion of Results

(a) Stress Corrosion

While there is a great deal of scatter in the results and, ideally, many more samples need to be exposed, I believe we can make some tentative observations:

1. It is still not clear why one group of specimens was able to survive to 76-118 days (with no C.P.) while the general duration of others was more in the 10-16 day range.

2. The latter group gave what we believe to be an important increase in range of 35 to over 180 days with C.P. at 1 volt.

3. We did not determine the lower stress level at which 1.2 v might prove to be beneficial. We suspect such a level exists at 50% or slightly lower stress level.

4. Metallurgical studies have not been undertaken to any extent to show nature of cracked surfaces, i.e. hydrogen effects.

5. Specimens exposed at over 80% stress level without C.P. have in general failed in relatively short periods, whereas the application of C.P. at 1 v has markedly increased specimen life. Cathodic protection is beneficial in extending life but failure eventually is likely caused by hydrogen.

6. Welded specimens have a markedly short life at 50% stress level with or without cathodic protection at 1 volt.

7. Metallurgical changes (e.g. 1 hour at 1500°F followed by re-aging) are decidedly beneficial. Duration at 1 volt is now* 216 days and still continuing.

8. Shot peening, also, by altering surface stress, has proven beneficial. Duration was 102 and 109 days with one still* on at 132 days at 1 volt and 50%.

9. There has been no opportunity yet to consider residual stresses on the welded areas on the foil itself, but these would be eliminated by the 1500°F heat treatment and alleviated by the shot peening.

10. The change in potential to 0.9 v while at 50% stress level has been of benefit for two specimens, but with one failure at 5 1/2 days, many more exposures are needed to establish a pattern, even 'though another lasted 97 days and the remaining one is still on at 97 days*.

11. Reduction of sustained stress level to 40% of ultimate has been beneficial (one at 50 days, 2 still on at over 190 days*).

* At November 30, 1966

(b) Corrosion Fatigue

I can make the same remarks with respect to these results too being only tentative. Some observations which may be made:

1. At the 48,000 psi mean stress level fairly consistent failures at 106,000 to 125,000 cycles were obtained (sea water, no C.P.).

2. Cathodic protection at 1 v gave improvement to 300,000 cycles and 5.66 million cycles with tests stopped because of leaks.

3. Cathodic protection at 1.2 v also appeared to be beneficial. Possibly the cycling rate is such that hydrogen might not exert its embrittling effect*. The two specimens went over 430,000 cycles (leaky cell) and over 8 million cycles with breakage outside the cell.

4. Another group stressed at high levels (62,000 psi mean stress) also showed a marked extension of life with 1.2 v C.P.

5. Embrittling by hydrogen from a "poisoned" acid electrolyte seems to be vastly different from that occurring at 1.2 v in sea water. Admittedly a single sample of each is hardly definitive but we hope to confirm these indications.

6. It is too early to say too much on the welded specimens but indications are that there is a markedly beneficial effect from one volt cathodic protection.

In general, cathodic protection at 1 volt (vs Ag/AgCl) level appears to be beneficial. While the corrosion fatigue specimens may be cycled at too rapid a rate to permit hydrogen embrittlement, the sustained tensile loading in the stress corrosion exposures certainly provides ample opportunity for embrittling. Our results strongly suggest that even here one volt is decidedly beneficial.

Conclusions

Much more confirmatory work is called for and will be carried out within limitations of staff and facilities at PNL.

* Brown, B. F., "Stress Corrosion Cracking and Corrosion Fatigue of High Strength Steels" in DMIC Report 210, 26-28 October 1964, published by Battelle Memorial Institute.

While initial results of the welded specimens at 50% stress level were most worrisome, subsequent results at 40% stress level are relatively optimistic. If found desirable, other means, e.g. heat treatment or shot peening, are available for markedly improving resistance of welded maraging steel to stress corrosion cracking.

Preliminary results show that cathodic protection is beneficial in corrosion fatigue. Cycling rate was such that hydrogen embrittlement might not be a factor.

PNL concludes that cathodic protection at approximately zinc potential is beneficial.

Acknowledgement

The material in this report includes the work of my associates J.A.H. Carson, LCDR K.W. Moore, R. Buckett and summer student D. Stephens.

TABLE 1

	Aging	Average Hardness RA	Load (% Ult*)	Cathodic Protection	Duration to Failure	Comments
Bar A (5 specimens)	900°F	72.6	83%	nil	75-118 days	
Bar A (5 specimens)	930°F	71.3	94%	nil	25-48 hours	Inadvertently set up at 94% because assumed uniform heat treatment.
Bar B (5 specimens)	900°F	73.2	80%		23 days (1 only)	Remainder removed to make way for tests to evaluate anomalous behaviour of Bar A.
Bar C (6 specimens)	930°F	72.6	83%	nil	19-40 days	
Bar D (2 specimens)	900°F	72.4	85%	nil	41 hrs, 57 hrs	
(2 specimens)	925°F	72.03	88%	nil	10.2 days 12.2 days	
(2 specimens)	950°F	71.2	95%	nil	11.1 days 16 days	
Bar E (3 specimens)	900°F	71.2	95%	nil	15 days, 2 at 17 days	
(3 specimens)	900°F	70.8	96%	1 V.	35.5 days** removed at 180 days (2 specimens)	(Actually 1.04 V. since day 70)
(3 specimens)	900°F	71.5	93%	1.2 V.	2 at 3 hrs, 1 at 33.5 days	Cathodic deposits may have lessened effective voltage at surface on long-lasting one.
Bar F (3 specimens)	900°F	72.2	85%	1.2 V.	2 at 16 hrs, 19 hrs.	
(3 specimens)	900°F	72.5	80%	1.2 V.	2 at 16 hrs, 17 hrs.	
(3 specimens)	900°F	72.3	75%	1.2 V.	3 at 48 hrs.	

* Ult = based on hardness and a few tensiles

** Stoppage in S.W. supply occurred at this time and probably resulted in higher potential than 1 V. Failure followed shortly after.

Table I (cont'd)	Aging Temp	Average Hardness RA	Load (% Ult*)	Cathodic Protection	Duration to Failure	Comments
Bar F (3 specimens)	900°F	72.3	70%	1.2 V.	1 at 69 hrs 1 at 91 hrs 1 at 112 hrs	
de Havilland (3 specimens) welded			50%	1 V.	3 days, 4 days one still unbroken at 268 days*	
Bar Ca (2 specimens) Cc	900°F	73.0	80%	1.2 V.	(a) 15 days (c) 13 days	
de Havilland (3 specimens) welded			50%	1 V.	3 still on at 216 days*	Re-heat-treated
de Havilland (3 specimens) welded			50%	1 V.	102 days, 109 days, and 1 still on at 132 days*	Shot-peened
de Havilland (3 specimens) welded			50%	0.9 V.	5½ days, 97 days and 1 still unbroken at 197 days*	
de Havilland (3 specimens) welded			40%	1 V.	50 days, 2 still unbroken at 190 days*	

Tensile Strengths

A5	212,000	(71.3 RA)	C6	259,000	(73.4 RA)
A10	253,000	(73.5 RA)	F7	254,000	(72.0 RA)
B6	247,000	(73.0 RA)	F10	251,000	(72.6 RA)

* As of November 30, 1966

Table I: Corrosion Fatigue

* Removed before failure due to leaking seal.

o Broke outside cell.

I Unwelded (a) 48,000 psi mean; 98,000 psi peak.

Test Conditions	Specimen Number	Hardness Rc	Mean Stress (KSI)	Stress Amp. KSI	Time (Min)	Speed (CPS)	Cycles to Failure
No Protection	A-1	46.7	49.6	48.3	124	15.4	114,500
	A-2	46.3	50.8	49.2	—	—	113,500
	A-3	47.6	51.2	48.2	116	15.2	106,400
	A-4	45.6	48.5	47.5	130	15.7	124,400
	A-5	46.4	49.7	48.1	120	15.0	108,400
	A-6	48.0	50.5	48.0	122	15.7	115,000
Cathodic Protection at 1.03 V. - Zinc	*A-7	46.9	51.0	48.5	310	16.2	303,600
	*A-8	47.8	50.0	48.5	347	16.3	340,700
	*A-9	48.1	51.6	50.4	6077	17.0	5,658,800
Cathodic Protection at 1.2 V.	*B-2	49.9	48.8	47.5	427	17	439,300
	oB-3	47.0	49.1	47.8	7400	18	8,139,800

(b) 62,500 psi mean; 125,000 psi peak.

No Protection	B-4	47.3	64	64	62	16.4	60,500
	B-5	47.1	63.5	63.5	58	16.2	56,300
	B-6	47.8	64	64	49	16.9	50,600
Cathodic Protection at 1.2 V.	oB-7	48.5	62.5	62	127	15.8	120,500
	oB-8	47.6	61.0	61	216	16.0	207,400
	B-9	47.3	60.0	60	1140	18.0	1,247,600

Table II (Cont'd)

Test Conditions	Specimen Number	Hardness Rc	Mean Stress (KSI)	Stress Amp. (KSI)	Time (Min)	Speed (CPS)	Cycles to Failure
Tested in Air	B-10	47.8	64	64	92	16	88,800
	B-11	48.2	63.5	63.5	200	16.8	213,200
Hydrogenated in H_2SO_4 at 2 Amps for 3¾ Hrs.	B-12	47.6	61	61	26	16.8	27,500
Tested at 1.2 V. after 1 week in Sea Water at 1.2 V.	B-13	47.9	62.5	62.5	1139	18.2	1,474,600
II Welded							
No Protection .07" Thickness	C-1	47.6	48.5	48.0	57	16.5	56,100
	C-2	48.6	49.2	48.7	120	16.4	118,100
	C-3	48.9	47.7	47.2	85	17.7	90,100
			(Nominal)	(Nominal)			
No Cathodic Protection 0.1" Thickness	F-1		48	48	82		86,400
	F-3		48	48	69		75,100
	F-4		48	48	105		114,200
	F-5		48	48	141		246,600
	F-8		48	48	92		97,100
Cathodic Protection 1 V. 0.1" Thickness	F-2		48	48	175		191,400
	F-6		48	48	305		325,800
	F-7		48	48	3480		3,925,600
	F-9		48	48	170		182,000

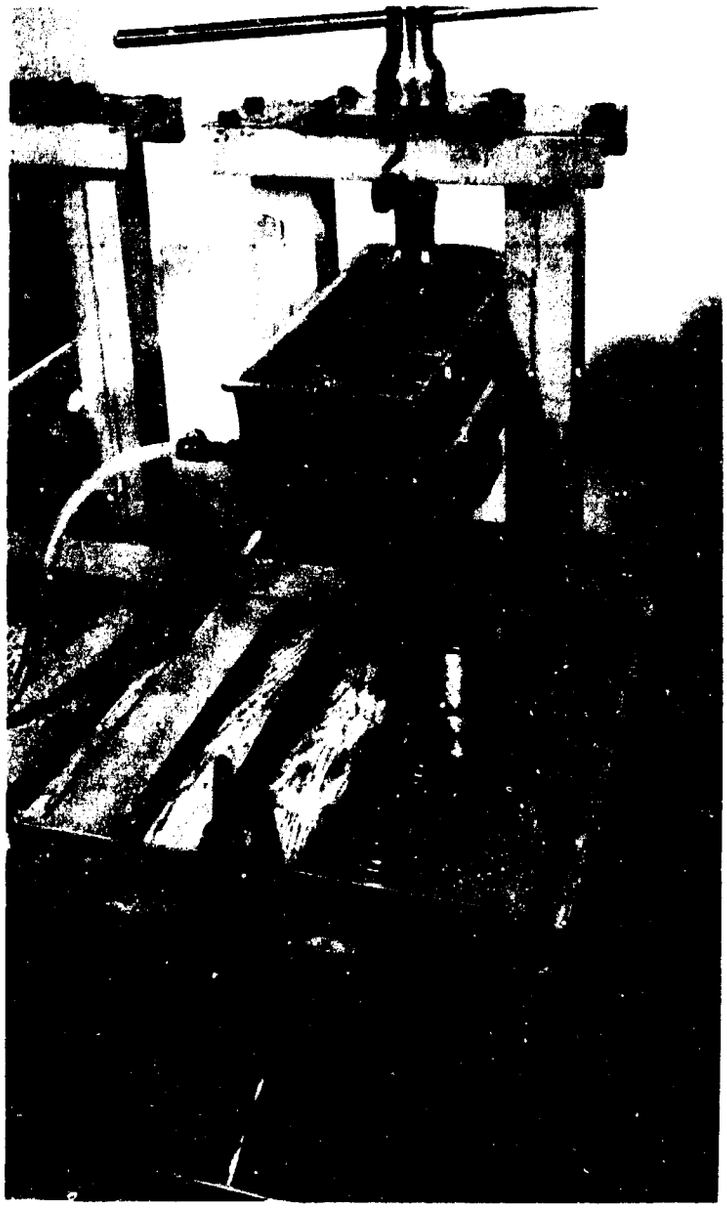

Figure 1

Photograph showing PNL-designed unit for stress corrosion exposure of maraging steel. The plastic tank in the unit permits the maintenance of a steady flow of sea water around the specimen.

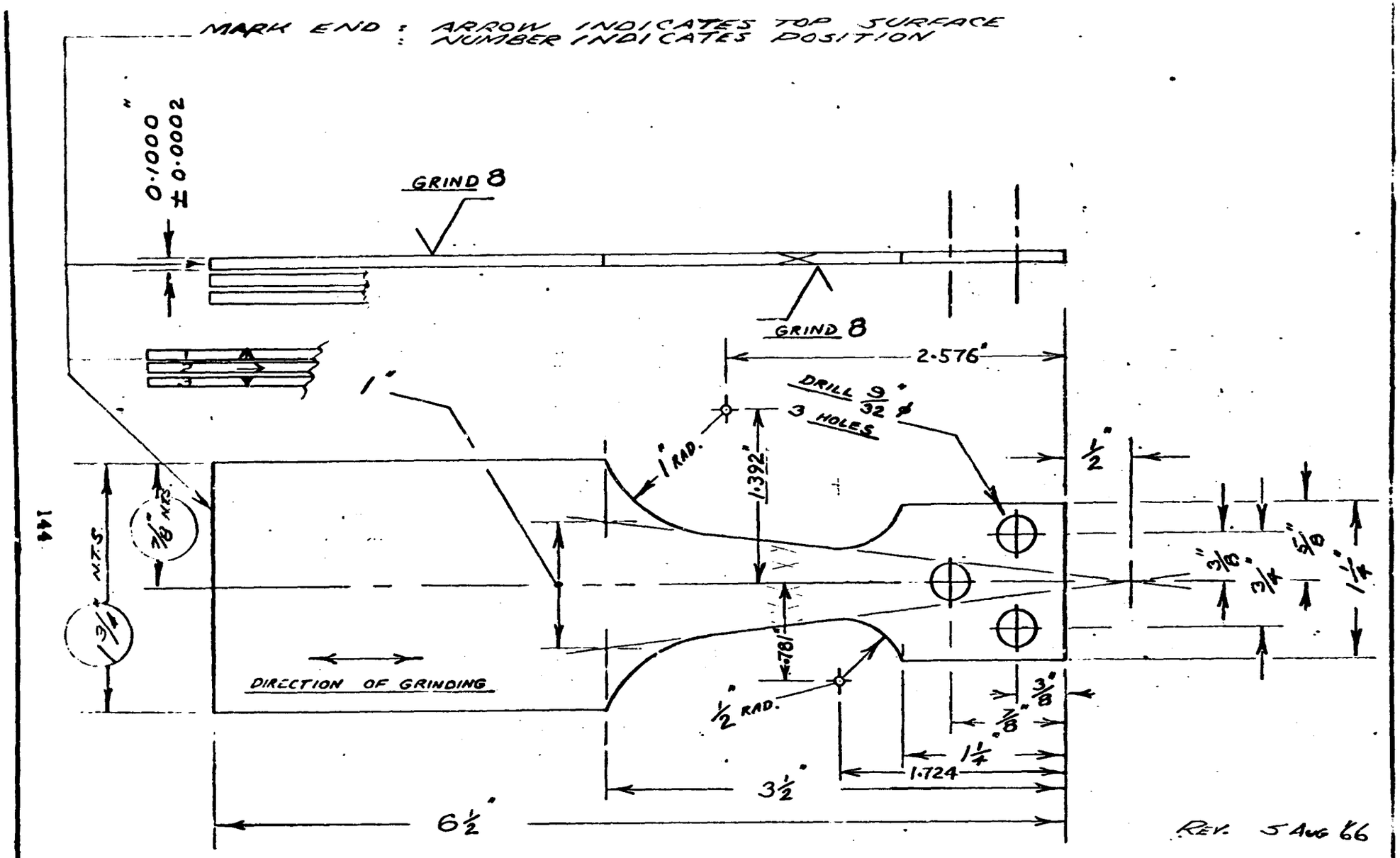

DATE: MAR. 24 / 65	FATIGUE TEST SPECIMEN	SCALE: FULL SIZE
DRAWN: G N.D	MARAGING STEEL	PNL: A-582-2.

Figure 2 - Detail of Corrosion Fatigue Specimens

CAVITATION EROSION FACILITIES AND DEVELOPMENTS AT THE U. S. NAVAL APPLIED SCIENCES LABORATORY

J. Z. Lichtman, D. H. Kallas and A. Rufolo

U. S. Naval Applied Sciences Laboratory

Brooklyn, New York

Introduction.

The erosive effects of cavitation have plagued ships and hydraulic systems for many years, in many ways. Probably the most common instances of cavitation attack on ships have been in the propellers, producing blade and hub erosion of the type shown in Figure 1. In ships' machinery, similar erosion occurs in turbine blades and in pump impellers. More recently, with development of high speed vessels such as hydrofoils, foil erosion of the type shown in Figure 2 has presented a problem. Developments in sonar systems, with their high power transducers, have introduced still another area of cavitation erosion on sonar domes, producing effects shown in Figure 3.

The cavitation phenomenon has been well explored, as to its causes and the mechanisms by which it produces damage. The explanations by Rayleigh (1) that pressure fluctuations produce vapor cavities and that, upon collapse, these cavities release violent hydrodynamic forces, has been the accepted basis for all later research of this phenomenon. A more precise insight into the more specific conditions which produce cavities and the mechanisms whereby damage occurs has been offered by Eisenberg (2) (3), by Naudé and Ellis (4) and by Godfrey (5), to name a few. The behavior of materials in cavitating environments has been reported by Rasmussen (6) (7), by Lichtman et. al. (8) and by others (9) (10). Theories have been presented on mechanisms which produce erosion and some correlations have been made between specific mechanical properties and the property of a material to resist erosion. In spite of this intense research, it is generally recognized that questions still remain unanswered relative to the mechanisms of cavitation erosion and the phenomenon of cavitation itself.

However, it has been necessary to satisfy engineering design requirements and, in order to do so, the development of data on cavitation erosion properties of materials has proceeded, as is often the case, ahead of scientific development. It is in this area of material development that the U. S. Naval Applied Science Laboratory (NASL) has played a modest but long-standing and persistent role. The result has been a large catalogue of data on erosion properties most of which has been published by Lichtman et. al. (8) (11) (12) and by Hydronautics, Inc. (9). To conduct these material studies, well-known investigational procedures were adopted for the design of various test devices which now comprise the Cavitation Laboratory at NASL. This paper describes these devices, some of the modifications which were made from time to time to meet needs of specific studies, and some material developments which evolved.

Materials subject to cavitation erosion may be broadly classified as those which are structural and those which provide a protective function for the structural material. Common examples of instances where the structure is exposed are in propellers, turbine blades, pump parts and pipe fittings. In other instances such as rudders, foils and sonar domes, the structure must be protected against corrosion and/or fouling, as well as erosion. In such instances the protective material may be a non-metallic coating, a metallic or non-metallic overlay, or a metallic cladding. NASL studies have included all of these categories and have extended to application techniques when it was recognized that this was an important contributor to material performance. To conduct these studies, NASL has established the four-unit laboratory which will be discussed in this paper.

Rotating Disk Apparatus.

Apparatus Description

The first unit established at NASL was a rotating disk apparatus similar to one used by Rasmussen (6) (7). Its design and operation has been described by Lichtman et. al. (8) (10) (11). It consists essentially of a cylindrical test chamber in which a 12 inch diameter by 1/8 inch thick disk is mounted on a shaft which is co-axial with the cylinder. The shaft is driven at speeds up to 3200 rpm with a 30 hp varidrive motor. Water fills and flows through the test chamber at an observed flow rate under controlled pressure and temperature. Figure 4 shows the essential details. The removed forward section in Figure 4 shows the radially positioned stilling vanes which are intended to minimize the rotational flow induced by the rotating disk. In operation, the location of the disk in the test chamber provides 5/8 inch clearance between the disk surfaces and the respective front and rear stilling vanes. Figure 5 shows a test disk, with 3/8 inch diameter hole which serves as a cavitation source, and a typical erosion pattern. Actually, test disks are prepared with multiple hole sources and test sites located at various radial distances to establish velocities up to 90 knots at 3200 rpm. Other features of the apparatus include a 280-gallon open stilling tank which serves as a means for controlling air content of the recirculating water; heat exchangers for controlling water temperature; and water flow controls for maintaining pre-set pressures in the test chamber.

Typical Rotating Disk Data

Most of the data on cavitation erosion resistance of materials collected at NASL over the last ten years has been acquired with the rotating disk apparatus These studies have been conducted on protective and structural materials, both metallic and non-metallic. The criteria for

evaluation have varied, data being reported in time required to penetrate a thickness of material; in amount of material eroded after a specific exposure; and in time rate of erosion under specific exposure. A qualitative judging system, applicable to all erosion test specimens, was also established, and based degree of erosion on an "order of merit" in which:

A - represented no visible damage

B - represented slight scuffing

C - represented slight erosion

D - represented extensive erosion

Characteristic erosion patterns are shown in the photographs, Figures 6 and 7, for elastomeric coatings and for several metals, respectively. Typical data for plastic coatings and elastomeric coatings are listed in Tables 1 and 2, respectively.

Venturi Nozzle Facility

Facility Description

The high speed nozzle facility was designed and installed to supplement the rotating disk apparatus for studying the performance of materials in hydrodynamic environments. An advantage of this second high speed fluid flow unit is its more readily identified fluid velocity relative to the test specimen, notwithstanding a degree of boundary layer drag. This unit consists of five - 3/4 inch ID nozzles mounted on an 8 inch pipe flange plate. The nozzle plate is bolted to an 8 inch manifold in a 6 inch line. The manifold in operation on a 6 inch pipe line is shown in Figure 8. A similar apparatus has been used by the International Nickel Company (13) (14) in studying the effects of high velocity fluid flow on corrosion and erosion rates of metal.

The test specimen is a 1 inch by 3 inch by 1/8 inch thick metal strip, mounted in slots in the nozzle and held in place by a retaining ring as shown in Figure 9. A typical specimen may include a 3/8 inch hole as the cavitation source located upstream from a recess which may hold the material to be evaluated. Other specimens are prepared by completely coating either or both sides of the test strip, with or without a cavitation source.

The facility is operated with sea water under 80 psi pressure which can be increased to 230 psi by a 125 hp booster pump. Water flow velocities up to 150 feet per second (90 knots) are monitored by a flowmeter installed in the 6 inch pipe line. Water temperatures vary seasonally from 45°F to 75°F. Pressure gages are located at the manifold and in the 6 inch line.

Typical Nozzle Test Data

Specimens are examined for degree of erosion or coating separation after various periods of exposure to water flow. Examples of specimens exposed to the nozzle test are shown in Figure 10.

Magnetostriction Apparatus

Apparatus Description

The magnetostriction apparatus is in the class of vibratory devices which generates the cavitation condition through a low-amplitude, high-frequency displacement of an immersed element. Unlike water tunnel and rotating disk devices, the magnetostriction apparatus operates with no water flow other than that developed adjacent to the driven element. The cavitation generated by the rapid fluctuations of pressure under the driver face is very similar to that generated at the face of a sonar transducer or at the water jacket side of an internal combustion engine.

The NASL magnetostriction apparatus consists essentially of two sets of transducer assemblies for operation at either 6.5 or 13.0 kilocycles per second; electronic driving and detecting equipment; cooling baths; and specimen plugs. The transducer assembly consists of a laminated nickel stack, a driving coil and a stainless steel mechanical transformer (horn). The driving equipment is an audio oscillator operated through a power transformer. The detecting equipment to measure displacement amplitude at the specimen end of the horn is a pick-up coil and a calibrated vacuum tube voltmeter. The use of an oscilloscope to determine wave-form of the pick-up coil voltage has been found helpful for detecting faulty drive or loose mechanical connections in the transducer system. The complete assembly is shown schematically in Figure 11, except that the diagram does not include the water jacket for cooling the transducer stack. During tests the specimen beaker is immersed in a thermostatically controlled bath for maintaining specific test temperatures. The mechanical transformers available for either transducer assembly are of the exponential and stepped horn types. A material under study is attached to a cylindrical plug which is screwed into the end of the horn before test.

In conducting an erosion study the cylindrical plug itself may be machined out of the material to be tested, or a specimen to be tested is attached to the face of a metallic plug. Coatings, overlay materials and some cladding metals are tested by adhering the test specimen to a plug machined from the intended substrate material. Plugs are 5/8 in. in diameter and 7/8 inch in length, including a 1/2 inch threaded length.

Measurements are made at 6.5 or 13.0 kilocycles per second, at double amplitudes of up to 3.0 mils at the specimen face, with the specimen immersed approximately 1/8 inch. Degree of erosion is usually determined by weighing the test plug before exposure and after various intervals of exposure to establish erosion rate.

Typical Magnetostriction Test Data

Typical erosion patterns are shown in Figure 12 for several coatings exposed for 2 hours with a 1.6 mil double amplitude at a 13 Kcps frequency. Tests were conducted in fresh water at 70°F. The low erosion resistant specimen No. 1 showed the characteristic erosion which is dominant at the center of the specimen, indicating greater intensity concentrations in this region. Perforations were noted at the centers of specimens No. 2, 3 and 4. Specimens Nos. 5 and 6 were slightly scuffed by the 2 hour exposure and would be considered good candidates for erosion protection applications, (craters in specimen No. 5 were in the coating prior to test).

Erosion of metal specimens are shown in Figure 13 for a representative range of erosion resistance characteristics. The concentration of erosion at the center region of the specimen was again noted. Figure 14 shows comparative erosion versus time data obtained for three metallic specimens tested by both the magnetostriction method and by the rotating disk method. These curves show the manner in which materials can be classified over a range of erosion characteristics. It is also noted that relative erosion intensities of the two devices might have some significance for materials with moderate erosion properties, as was noted for the Ti-6Al-4V. The differences in erosion intensities were less evident for very high (stellite) and for the very low (Ti-TIMET 35A) erosion resistant materials. The higher erosion intensity of the rotating disk device, evident in the Ti-6Al-4V curves of Figure 14, has been noted in the study of other materials.

High Sonic Pulse Facility

Facility Description

The high sonic pulse facility was constructed as a result of the sonar dome erosion problem mentioned earlier in the Introduction. The facility comprises a steel tank 12 feet long by 6 feet wide by 5 feet deep; a high power piezoelectric transducer; a specimen holder; electronic equipment for driving the transducer; meters for measuring transducer input; a conventional hydrophone; and accessory equipment for measuring hydrophone pick-up. The facility is shown in Figure 15 It has been used primarily for development of sonar dome coatings but can be used to study erosion

resistance characteristics of any material which might be intended for use in a cavitation environment of this type and intensity.

In operation, the panel to be tested is centrally located relative to the transducer and parallel to the transducer face at a distance of 1 inch, as shown in Figure 16. A pulse train generator operated through a power amplifier provides the sinusoidal pulse signal to the transducer at a sonar frequency. The signal is pulsed for a 4 second duration after each 26 second lapse interval. The signal is monitored, by a voltmeter and ammeter at the input to the transducer, to a level which produces the cavitation at the specimen surface shown in Figure 16. The transducer output is picked up by a conventional hydrophone and its wave shape is observed on an oscilloscope as an indication of the quality of the transducer operation. Test specimens coated on steel panels, are examined after periodic intervals of exposure to determine extent of erosion as judged by the area eroded and by the degree of penetration.

Typical Pulse Facility Data

This facility has been used exclusively to evaluate erosion resistance of candidate coatings for sonar dome application as protection against corrosion and fouling. Typical results obtained for a U. S. Navy vinyl paint and for a neoprene coating system are shown in Figures 17 and 18, respectively. These results show the effectiveness with which the method will distinguish between a conventional coating and one intended for use in a cavitating environment. Typical erosion resistances for various coatings, reported in terms of eroded area after a 23 hour exposure, are shown in Table 3, and indicate the range of this technique for evaluating this class of materials. It is noted that although the coating in Figure 17 was penetrated, probably well within the 23 hour exposure period, there was no erosion of the mild steel substrate panel. This would indicate a relatively lower erosion intensity than found in the rotating disk or magnetostriction methods which do produce considerable mild steel erosion in short exposure periods.

Comparison of Facilities

A comparison of the four NASL facilities is outlined in Table 4, showing pertinent details of the various units. The units may be broadly characterized as either high velocity fluid flow or high frequency vibratory types. It is also noted that a span of operating conditions is covered within the group. A consideration of cavitation intensities for the fluid flow types would establish the rotating disk as a higher intensity device than the venturi nozzle; and, in comparing vibratory types, the magnetostriction device would have much higher cavitation intensity than the high sonic pulse unit.

The selection of a method for a material evaluation is based on several considerations reflecting the intended purpose of the study. A study of a material intended for use in a highly turbulent fluid flow environment would be conducted in the rotating disk apparatus, while a sonar dome coating would be most accurately evaluated in the magnetostriction or high sonic pulse facilities. A study to evaluate effects of fluids on a material performance would be adequately and more conveniently conducted with the magnetostriction device. Finally, studies of hydrodynamic phenomena can be pursued more effectively with test devices which together embrace a degree of versatility, and such studies could provide the clues to mechanisms of failure in materials.

A comparison of material performance when evaluated by the various techniques, is outlined in Table 5, and shows a high degree of correlation among the test devices. Lapse in correlation noted for the neoprene No. 2 sheet could not be explained; however a lack of correlation for mild steel and titanium Ti-6Al-4V could reflect the differences in cavitation intensities of the respective facilities. In general, both the rotating disk and the magnetostriction devices have classified particular neoprene formulations as the most erosion resistant non-metallic materials, and stellite 6B as the most erosion resistant metallic material. It is interesting to note that these best metallic and non-metallic materials have similar cavitation erosion resistance characteristics. This similarity of performance for materials so widely different in mechanical properties is an indication of the complexity of the cavitation phenomenon, and provides a clue that energy absorption studies may hold the answers to erosion failure mechanisms.

Service Experience With Cavitation Erosion Protection

The screening of metallic and non-metallic erosion resistant materials has provided candidates for service applications. Table 6 lists some of the service applications made on propellers and hydrofoils, and their performance. Most of the service trials to date have had one common dominant failure - the failure to provide conclusive evidence of resistance to cavitation erosion as a result of premature coating or overlay separation. Service trials have served to demonstrate the need for high strength, water-resistant adhesives and for improved attachment techniques.

An example of service failure of a propeller blade coating is shown in Figure 19, where extensive removal of a solvent type neoprene coating occurred and frustrated any cavitation erosion resistance evaluation. Figure 20 shows another example of the separation failure of a similar coating from the nacelles and struts of the U. S. Navy Hydrofoil PC(H)1 after a relatively short period of foilborne operation. A later application of Stellite 6B, as protective overlay in cavitation vulnerable areas of the same hydrofoil, also separated from the struts and foils when the mechanical fasteners and adhesive bond failed.

It has become apparent that further large scale service trials must await development of improved adhesives and attachment techniques. Such a development effort is being vigorously pursued at NASL at present, using the facilities described in this paper. Recently applied "patches" of cured neoprene sheets on the aft foil of the PC(H)-1, using a newly development adhesive and an improved bonding technique, have remained in place after several flight tests.

Special Studies

The facilities of the Cavitation Laboratory at NASL have not been used exclusively for evaluating cavitation erosion resistance of materials. Several non-cavitation studies, some conducted by making equipment modifications, have been cited herein for general interest and to indicate the versatility which is available.

Adhesion

Recognizing the critical role of adhesives in attachment of protective coatings, dynamic tests of adhesives has become an important aspect of cavitation studies. Coatings and overlays have been adhered to disks of the rotating disk apparatus, without the usual cavitation sources, to determine the mechanical properties of adhesives in hydrodynamic environments. In some instances the overlay was mounted on the disks to determine the relative contribution of the design of the joint to its durability in environments generated by speeds of up to 100 knots. Results of such studies have contributed to the development of high strength adhesives, improved bonding techniques and more reliable joint designs.

Water Additives

Various polymeric water additives, which acted as modifiers of water flow characteristics, were studied in the rotating disk apparatus and in a magnetostriction facility (16). Cavitation erosion evaluations, made with and without additives, under similar operating conditions indicated the relative effect of the additives on erosion intensity of the test facility. Such additions have been considered for reducing erosion in closed circuit systems; for reducing drag in torpedo operations; and for reducing drag and erosion effects during hydrofoil take-off. The small quantity of fluid required in the magnetostriction apparatus is a particular advantage for investigating effects of liquids on cavitation erosion, permitting studies of the type conducted at the University of Michigan (17) to determine erosion of structural metals in liquid lithium.

"Spoiler" Materials

"Spoiler" are attached to the trailing edges of foils such as propellers to modify the wake characteristics (vortex shedding) of the foil, and thus eliminate "singing" of the foil. "Singing" is caused by vibration of the foil induced by the unmodified wake. The rotating disk apparatus was used (18) to develop the elastomeric materials which resisted tearing damage when exposed to the highly turbulent wake. The "spoiler" material studies were conducted by replacing the rotating disk with the 12 inch, centrally mounted rotating foil shown in Figure 21. Test materials were located at the trailing edges of the foils and simulated a proposed propeller attachment.

Concluding Summary

Review

It has been the objective of this technical presentation to provide a glimpse into the cavitation studies which have been conducted at the Naval Applied Science Laboratory over the last decade. We have shown how cavitation facilities, initially comprising only the rotating disk apparatus, were progressively augmented with installation of a magnetostriction device, a venturi nozzle installation and a high sonic pulse facility, to establish the integrated facility which we now call the "Cavitation Laboratory". A contribution of this Laboratory has been a massive catalogue of cavitation erosion resistance characteristics of hundreds of materials. Subsequent service applications of several of the most resistant of these materials for erosion protection provided further insight into material performance and demonstrated the existence of serious attachment problems which frustrated exploitation of the intended protective function. Consequently, a program on development of high strength adhesives and bonding techniques applicable in the field has evolved. The paper has discussed, briefly, some of the facility modifications which have permitted adhesive studies and other studies not directly related to cavitation erosion.

Future Prospects

It is anticipated that the Cavitation Laboratory will continue to play a role in the evaluation and development of erosion resistant coatings, overlays and structural materials. In addition, the flexibility and range available with the four facilities, existing as an integrated test establishment, will provide opportunity for more precise study of material performance in hydrodynamic environments, and a deeper study of the cavitation phenomenon. Studies will be made to identify hydrodynamic stresses and energy intensities for each facility, as an approach to an understanding of the mechanisms of erosion failure. The areas of future study may be summarized as follows:

a. Continued study of erosion characteristics of materials.

b Continued development of adhesives and refined bonding techniques.

c. Study of energy intensities in the test facilities

d. Correlation of material performance with cavitation theories.

e. Correlation of laboratory data with service data, related to erosion intensities and material performance.

BIBLIOGRAPHY

(1) Lord Rayleigh. On the Pressure Developed in a Liquid During the Collapse of a Spherical Cavity. Phil Mag (London) 34. 94-98. (1917)

(2) P. Eisenberg. Mechanisms of Cavitation. Section 12. Handbook of Fluid Dynamics. V. L. Streeter, Ed. New York. McGraw-Hill 1961

(3) P. Eisenberg, H. S. Preiser and A. Thiruvengadam. On the Mechanisms of Cavitation Damage and Methods of Protection. Society of Naval Architects and Marine Engineers Transaction. 73 (1965) 241-286

(4) C.F. Naude and A. T. Ellis. On the Mechanisms of Cavitation Damage of Non-Hemispherical Cavities Collapsing in Contact with a Solid Boundary Trans. ASME. J. Basic Eng. Dec. 1961. 648-656

(5) D. J. Godfrey. Cavitation Damage - A Review of Present Knowledge. Chemistry and Industry 23. 6 June 1959. 686-691

(6) R. E. H. Rasmussen. Experiments on Flow with Cavitation in Water Mixed with Air. Trans. Danish Academy of Tech. Sci. No. 1 1949

(7) R. E. H. Rasmussen. Some Experiments on Cavitation Erosion in Water Mixed with Air. Proc. National Phys. Lab. Symp. on Cavitation in Hydrodynamics. London. HMSO. 1956

(8) J. Z. Lichtman, D. H. Kallas, C. K. Chatten and E. P. Cochran, Jr. Cavitation Erosion of Structural Materials and Coatings. Corrosion. 17 (Oct 1961) pp 497t-505t

(9) Hydronautics, Inc. Technical Report 233-8. March 1965. Handbook of Cavitation Damage

(10) NASL. Project 9300-17. Final Report. 30 Sep 1964. Cavitation Damage Design Handbook. J. Z. Lichtman and E. R. Weingram. AD 460524

(11) D. H. Kallas, J. Z. Lichtman and C. K. Chatten. Cavitation Erosion Resistant Coatings. Procedings Seventh Joint Army-Navy-Air-Force Conference on Elastomers Research and Development. ONR-13 Vol. 2 pp 422-442. 1962

BIBLIOGRAPHY
(Continued)

(12) J. Z. Lichtman and E. R. Weingram. The Use of a Rotating Disk Apparatus in Determining Cavitation Erosion Resistance of Materials. Symposium on Cavitation Research Facilities and Techniques. New York. ASME 1964 pp 185-196

(13) Anon. Testing Materials for Hydrofoils. Bull of the Sea Horse Institute. May 1963 Vol. 4. No. 1 p. 1

(14) USNMEL. Report 72/64. The Corrosion of Metals as a Function of Sea-Water Velocity. J. L. Basil

(15) NASL Project 9300-41, Technical Memorandum #12 of 17 Jun 1966. Cavitation Erosion Resistance and Adhesion of Cured Sheet Elastomeric Coatings. J. Z. Lichtman

(16) NASL Lab. Project 9300-17, Technical Memorandum #5. 26 May 1964. Effect of Non-Newtonian Fluids on Cavitation Damage of Materials

(17) U. of Michigan. Dept. of Nuclear Engineering. Report 05031-5-T. May 1966. Ultrasonic-induced Cavitation Studies in Lithium at Elevated Temperatures. R. Garcia, F. G. Hammitt

(18) NASL Lab. Project 9300-41. Technical Memorandum #7. 2 March 1965. Development of Damage-Resistant Spoiler Materials for Singing Propellers. J. Z. Lichtman

FIGURES

FIGURES (Cont'd)

TABLES

TABLE 1

CAVITATION EROSION RESISTANCE OF PLASTIC COATINGS IN ROTATING DISK TESTS

Material	Coating Thickness mils	Time to Erode to Metal Substrates, hrs, at 150 fps	Order of Merit
Epoxy A	10	1	D
Epoxy B	60	1	D
Polyester-glass flake	15-30	1/4	D
Silicone resin	11	3/4	D
Nylon (flame-spray)	28	8	D
Nylon (fluidized bed)	24-27	18	C
Chlorinated polyether	40	1	D
Fluorocarbon (TFE)	60	5-1/3	D
Composite anti-corrosive and antifouling coating (vinyl)	7	1	D

TABLE 2

CAVITATION EROSION RESISTANCE OF ELASTOMERIC COATINGS IN ROTATING DISK TESTS

Material		Thickness, in. of Coating in Rotating Disk Cavitation Tests	Cavitation Test Exposure Period, hrs	Degree of Erosion at 150 fps After Exposure Period	Order of Merit
Neoprene solvent base, brush applied	A	0.030	24	scuffing	B
	B	0.025	17	scuffing	B
Neoprene, cured sheet, cold-bonded		0.062	14	none	A
Neoprene, in situ cured and bonded		0.060	10-1/2	none	A
Polyurethane, liquid	A	0.062	12	slight	C
	B	0.018	12	severe	D
	C	0.062	12	none	A
Polyurethane cured sheet, cold bonded	A	0.060	14	none	A
	B	0.062	12	severe	D
Polysulfide, liquid		0.062	12	severe	D
Polysiloxane, liquid		0.062	7	severe	D
Butyl, cured sheet, cold-bonded		0.060	2-1/4	severe	D
Butyl, in situ cured and bonded		0.060	12	severe	D
Cis-polybutadiene (98%) cured sheet, cold bonded		0.060	10	none	A
Polybutadiene (polysulfide modified) in situ cured and bonded		0.060	13	severe	D

TABLE 3

SONIC EROSION OF COATING MATERIALS

Panel No.	Material		Total Film Thickness (mils)	Total Number of Coats	Eroded Area After 23-Hr Exposure (sq. in.)	
	Base Coating	Antifouling Coating			Base Coating Removed	Antifouling Coating Removed
1	Vinyl	Vinyl	11.0	7	0.970	1.970
2	Chlorinated Rubber	None	10.0	5	1.202	-
3	Epoxy	Vinyl	14.0	6	0.960	1.850
4	Hypalon	Neoprene	21.5	9	0.018	0.088
5	Neoprene	Polyiso-butylene	28.0	23	0.000	0.185
6	Neoprene	None	22.0	21	0.000	-
7	Poly-urethane	None	18.0	5	0.000	-

TABLE 4

COMPARISON OF CHARACTERISTICS OF NASL CAVITATION EROSION FACILITIES

Characteristic	Facility			
	Rotating Disk	Venturi Nozzle	Magnetostriction	High Sonic Pulse
Water velocity and pressure	Independently controlled	Only velocity controlled	No velocity or pressure control	No velocity or pressure control
Water velocity relative to specimen - fps	60 to 150	150 (max)	No appreciable flow	No appreciable flow
Area occupied by facility	100 sq ft	200 sq ft	50 sq ft	1000 sq ft
Cavitation exposure	Continuous	Continuous	Continuous	Pulsed
Liquid medium	Fresh or sea water	Sea Water	Any	Fresh or sea water
Frequency of vibration	-	-	6.5 or 13 Kcps	Transducer Frequency
Pressure of liquid	0-30 psig	Not indentified	Atmospheric	Atmospheric
Temperature of liquid	65 to 80F	45 to 75F (seasonal)	70F	60 to 70F
Liquid capacity of apparatus	100 to 230 gal.	Open circuit only	400 cc	2500 gal

TABLE 5

CAVITATION RESISTANCE BY THE FOUR TEST METHODS

Material	Order of Merit			
	Rotating Disk Apparatus	Venturi Nozzle Facility	Magneto-striction Apparatus	High Sonic Pulse Facility
Neoprene (No. 1) - Sheet	A	-	A	-
Neoprene (No. 2) - Sheet	A	-	C	-
Neoprene (Solvent Base Coating)	B	-	B	B
Polyurethane (No. 1) Coating	D	-	D	-
Vinyl (NF-120, 121) Coating	D	D	-	D
Polyisobutylene (NF 134) Coating	D	-	-	D
Mild Steel	D	-	D	B
Titanium Ti-6Al-4V	C	-	B	-
Stellite 6B (Chrom-Cobalt)	A	-	A	-
Unalloyed Ti TIMET 35A	D	-	D	-

TABLE 6

SERVICE PERFORMANCE OF COATINGS AND OVERLAY MATERIALS

Application Site	Material Type	Material	Performance
Ships' Propellers	Elastomeric Coatings	Solvent Type Neoprene	Extension adhesion separation on suction and pressure faces occurred before erosion resistance could be identified. Some blistering of coating showed isolated adhesion failure (Figure 25).
		In Situ - Cured SBR	Adhesion separation (5%-75% of inlay area). Surface degradation. Only moderate erosion resistance because of inadequate cure in the field. Erosion correlated with rotating disk data.
		In Situ - Cured Neoprene	Adhesion separation (35% of inlay area). No erosion of adhered inlay.
Hydrofoils	Elastomeric Coatings	Solvent-Type Neoprene	Static immersion - blistering, peeling due to isolated low adhesive strength, and ply-to-ply low cohesive strength, related to method of application.
			Foil-borne operation - adhesion separation on aft foils, struts, nacelles. Erosion resistance could not be identified (Figure 26).
		Cured Sheet Neoprene (Epoxy) Adhesive, Vacuum Bonded and Contact Adhesive)	No separation after foil-borne operation. Applications in 1 sq ft patches on aft foil. No erosion damage.

TABLE 6
(CONTINUED)

Application Site	Material Type	Material	Performed
		Resinous Polyurethane	Satisfactory on struts and pressure faces of foils. Some erosion and adhesion separation on suction faces of foils.
	Plastic Coatings	Vinyl	Erosion after 20 minutes foil-borne operation, in isolated areas of nacelles, foils and struts.
	Metallic Overlays	Stellite 6B	Adhesion separation and failure of mechanical fasteners after foil-borne operation (Figure 27).

CAVITATION EROSION OF PROPELLER

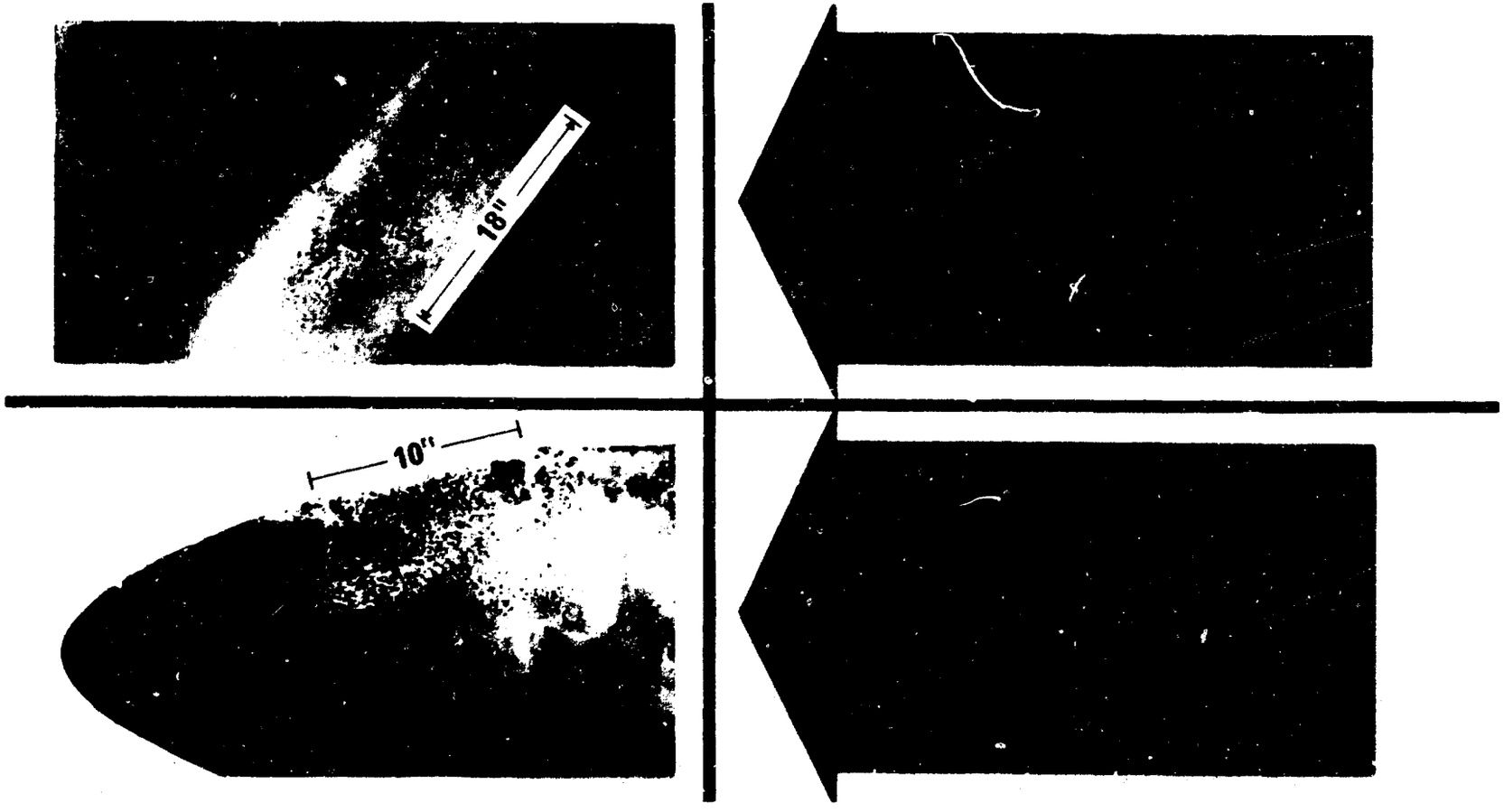

FIGURE 1 - CAVITATION EROSION OF PROPELLER

FIGURE 2 - EROSION OF VINYL COATINGS AFTER 20 MINUTES FLIGHT

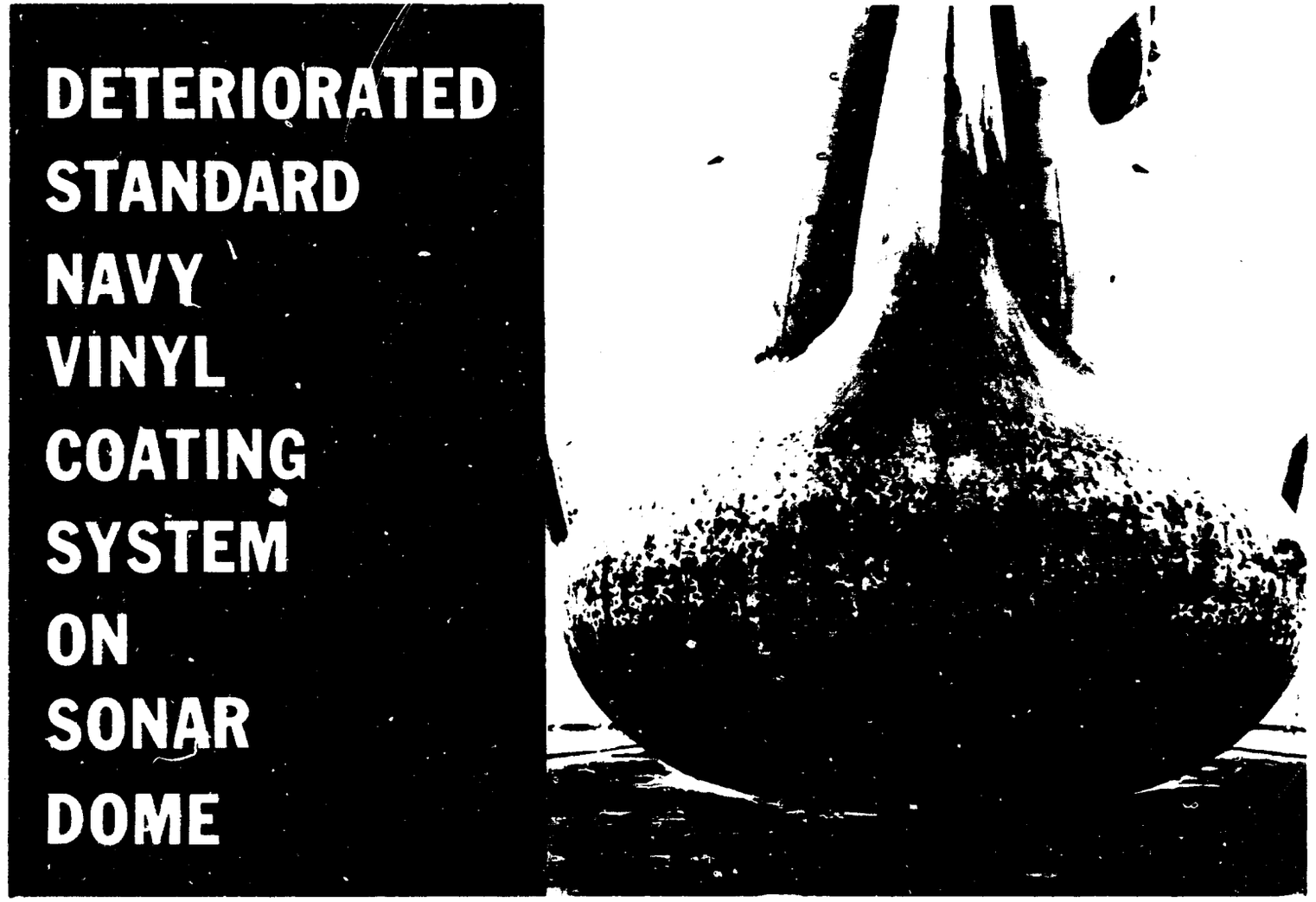

PHOTO L21305-1

FIGURE 3 - DETERIORATED STANDARD NAVY VINYL COATING SYSTEM SONAR DOME

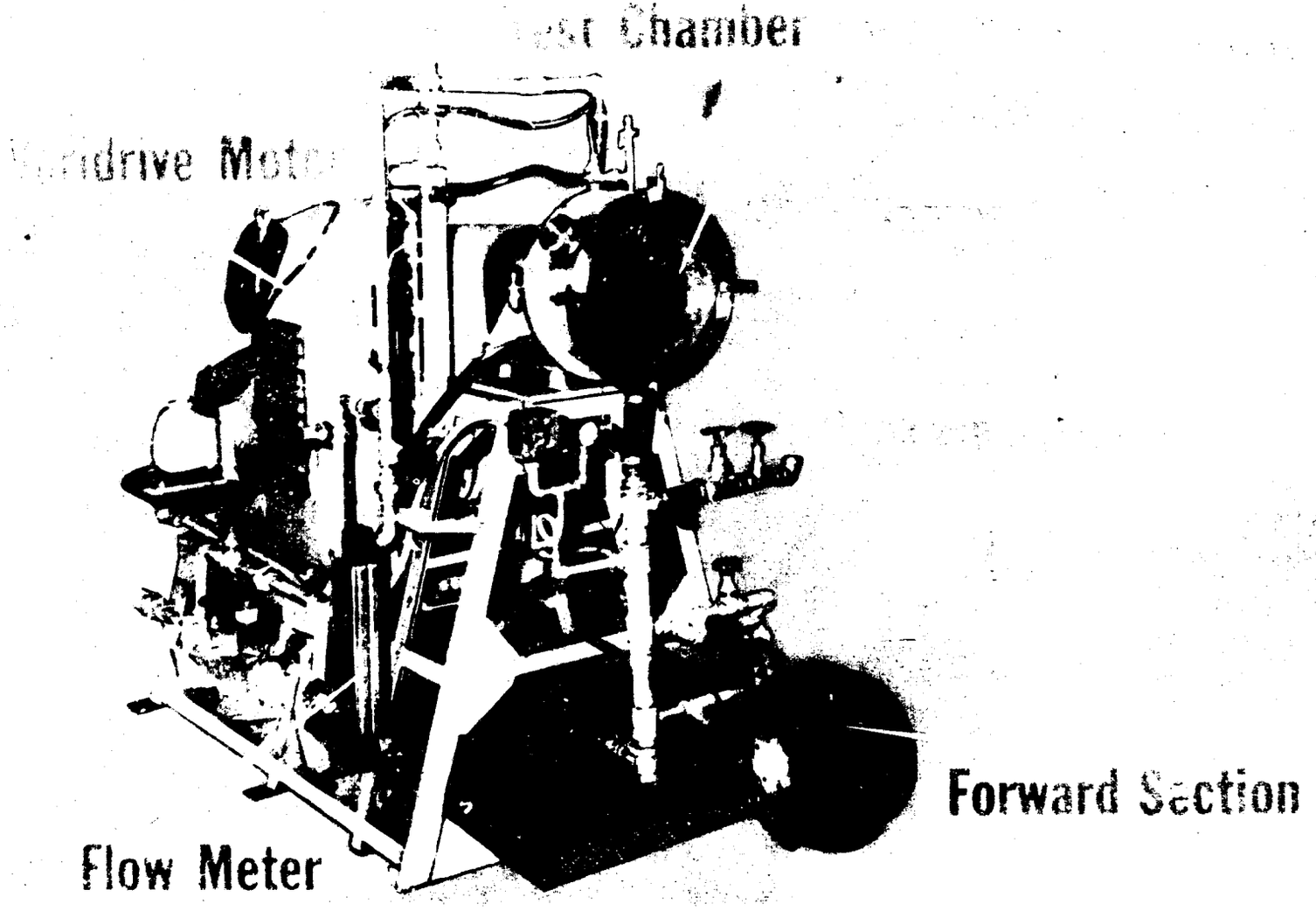

PHOTO L19930-70

FIGURE 4 - NASL ROTATING DISK CAVITATION EROSION FACILITY

TYPICAL EROSION DAMAGE OF ALLOY

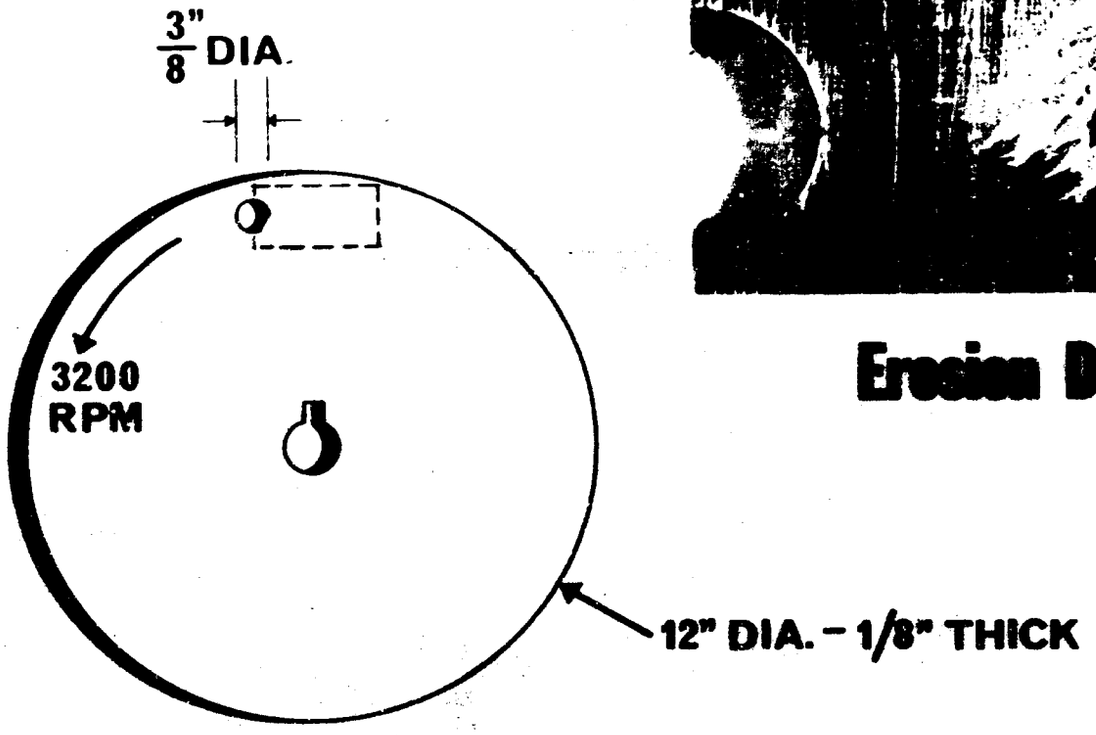

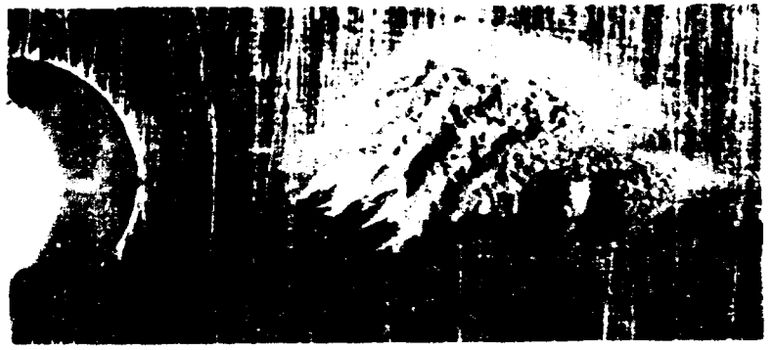

Erosion Damage

PHOTO L19930-69

FIGURE 5 - TYPICAL EROSION DAMAGE OF METAL IN ROTATING DISK APPARATUS AT 150 FPS.

Neoprene, solvent base, after 24 hrs.

Neoprene cured sheet, cold bonded, after 14 hrs.

Polyurethane, cured sheet, after 14 hrs.

Polysiloxane, liquid, after 7 hrs.

Butyl, in situ cured & bonded, after 12 hrs.

Styrene-butadiene copolymer, in situ cured & bonded, after 24 hrs.

PHOTO L20036-4

FIGURE 6 - CAVITATION EROSION OF ELASTOMERIC COATINGS IN ROTATING DISK APPARATUS AT 150 FPS.

EROSION OF METALS AFTER EXPOSURE IN ROTATING DISK APPARATUS

Stellite 6B, after 24 hrs.
0.03 mil/hr.

Inconel 718, after 12 hrs.
0.29 mil/hr.

Titanium 721, after 6 hrs.
0.61 mil/hr.

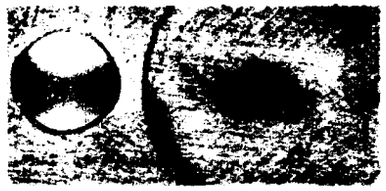

HY80 Steel, after 8 hrs.
0.90 mil/hr.

(Fresh Water)

PHOTO L21046-18A

FIGURE 7 - EROSION OF METALS IN ROTATING DISK APPARATUS AT 150 FPS.

PHOTO L19930-94

FIGURE 8 - HIGH SPEED EROSION TEST FACILITY (NOZZLE TYPE)

CAVITATION EROSION NOZZLE

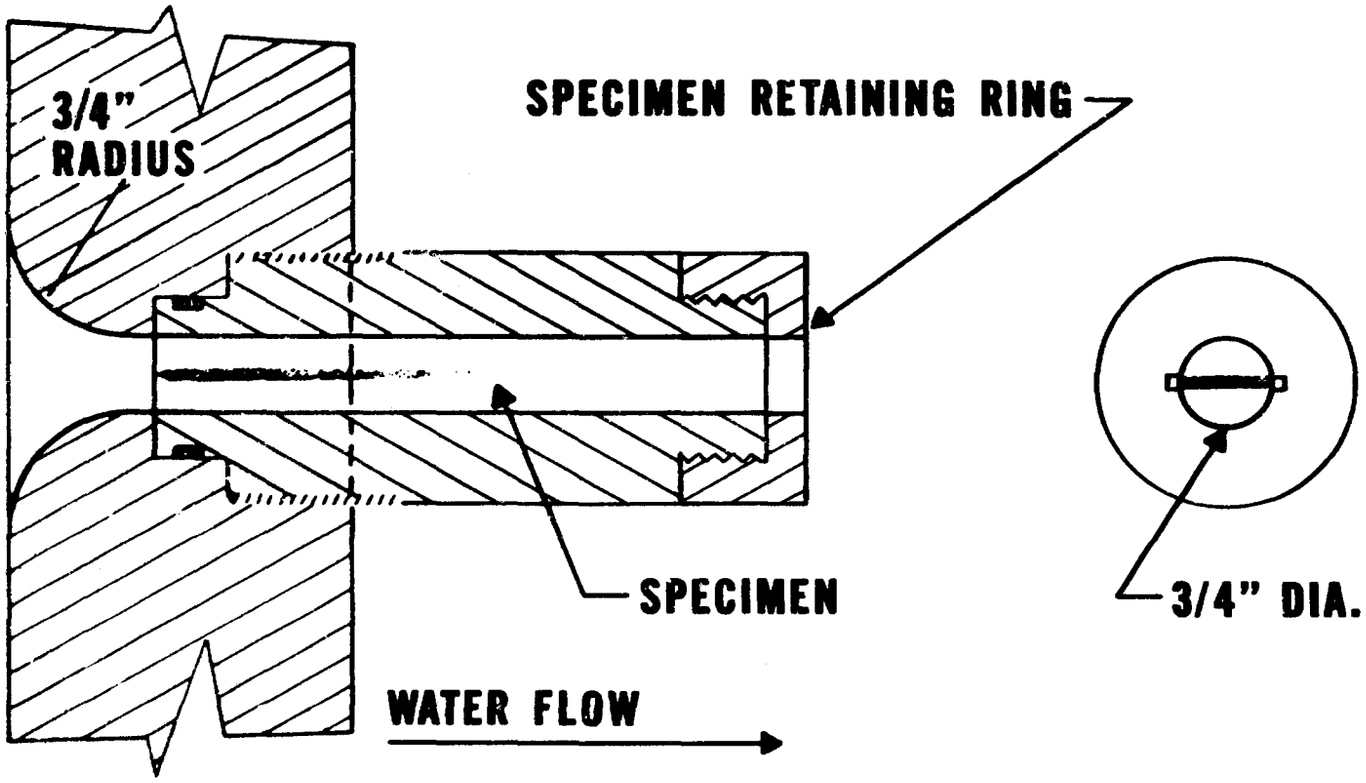

PHOTO L19760-20A

FIGURE 9 - CAVITATION EROSION NOZZLE

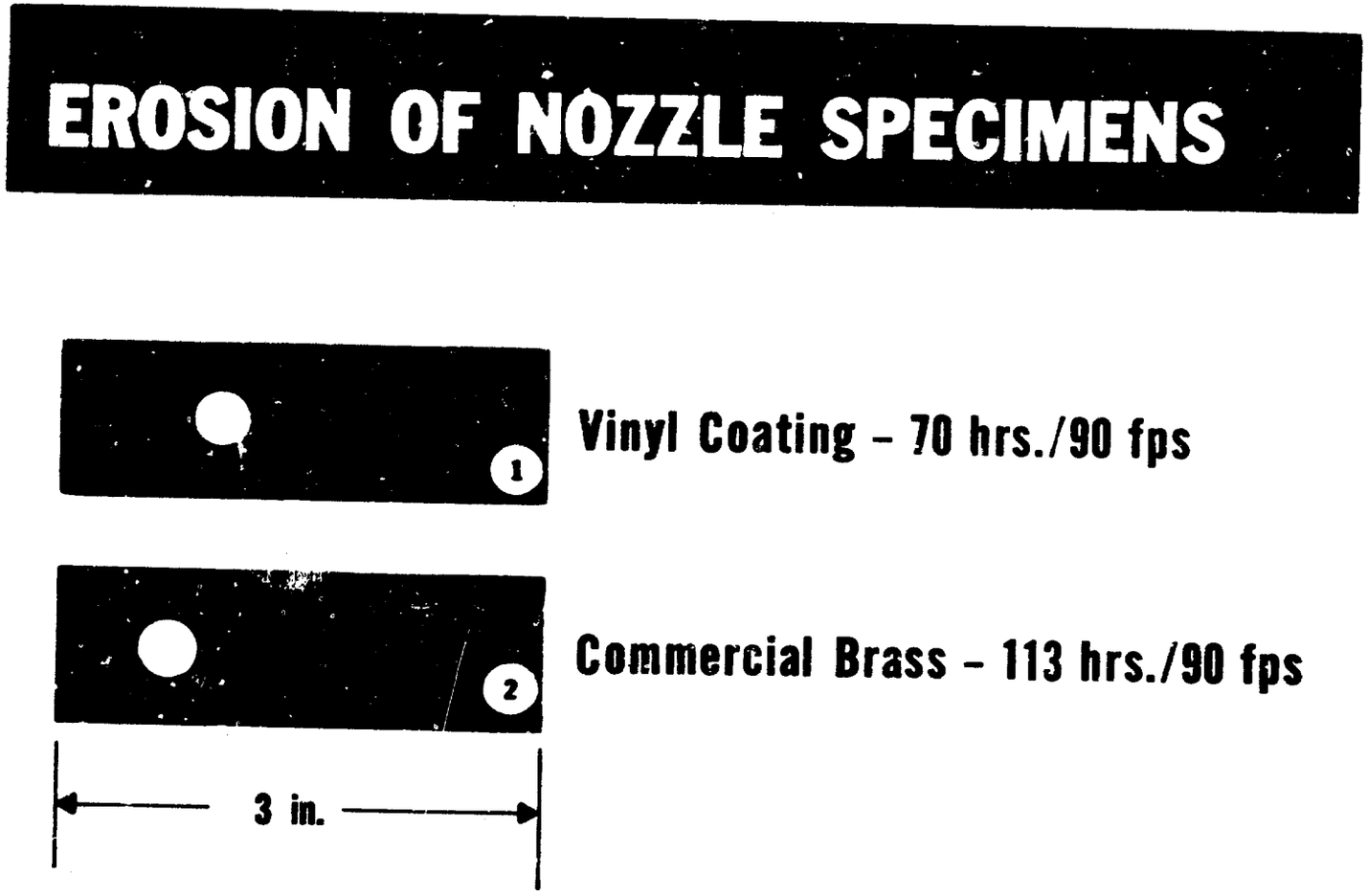

FIGURE 10 - EROSION OF NOZZLE SPECIMENS

PHOTO L21046-84

MAGNETOSTRICTION CAVITATION EROSION APPARATUS

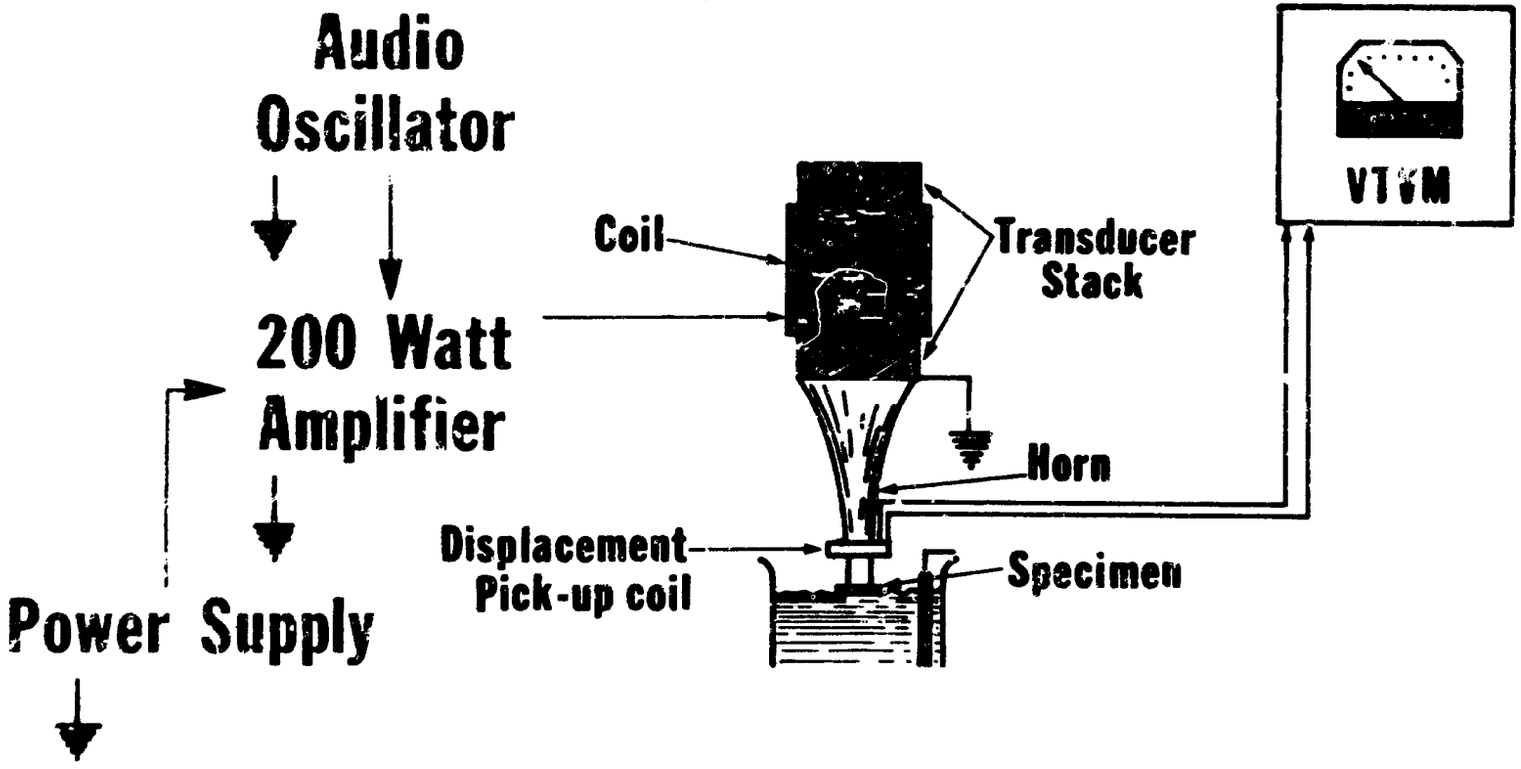

PHOTO L20030-85

FIGURE 11 - MAGNETOSTRICTION CAVITATION EROSION

EROSION OF COATED MAGNETOSTRICTION SPECIMENS
(0.625 inch diameter)

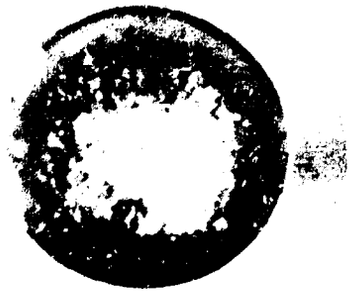

1. POLYURETHANE

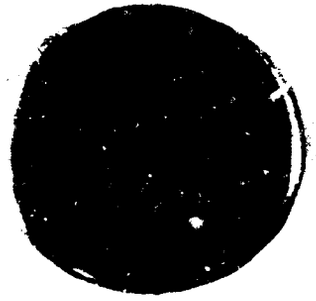

2. POLYURETHANE

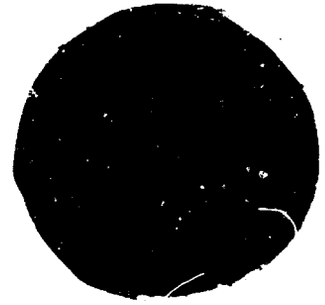

3. POLYURETHANE

4. NEOPRENE CURED SHEET

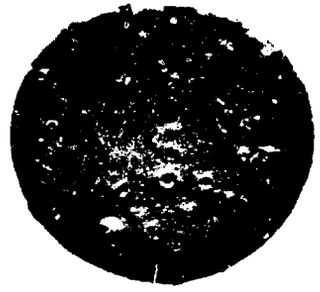

5. NEOPRENE SOLVENT BASE

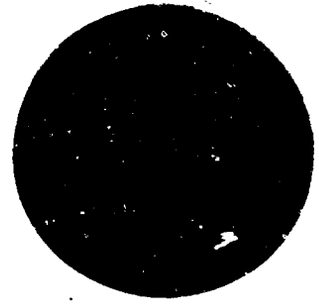

6. NEOPRENE CURED SHEET

PHOTO L21046-97

FIGURE 12 - EROSION OF COATED MAGNETOSTRICTION SPECIMENS

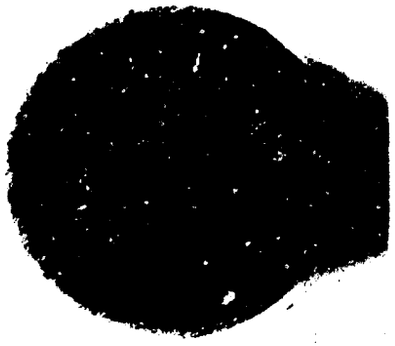

MILD STEEL

FRESH WATER 12 HR

13.1 KCPS, 2 MIL P-P AMPL

13.3 μI LOSS

NITINOL (60 NI/40TI)

FRESH WATER 8 HR

13.1 KCPS 2 MIL P-P AMPL

0.48 μI LOSS

STELLITE WELD DEPOSIT

SEA WATER 8 HR

13.1 KCPS 1.5 MIL P-P AMPL

0.13 μI LOSS

PHOTO L21185-48

FIGURE 13 - EROSION OF METALLIC MAGNETOSTRICTION SPECIMENS

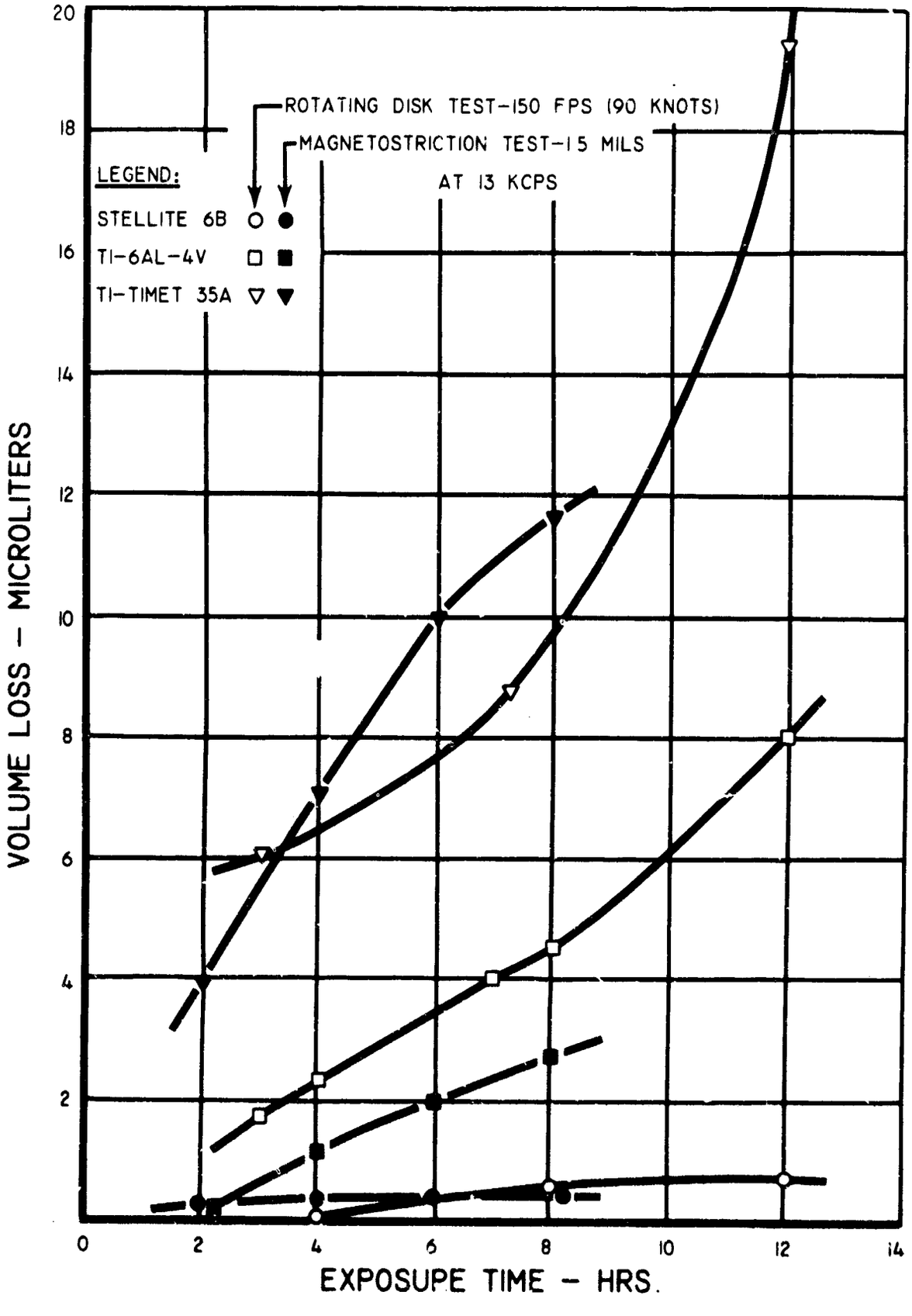

PHOTO L21185-44

FIGURE 14 - EROSION VS. TIME (METALS IN SLA GATEP)

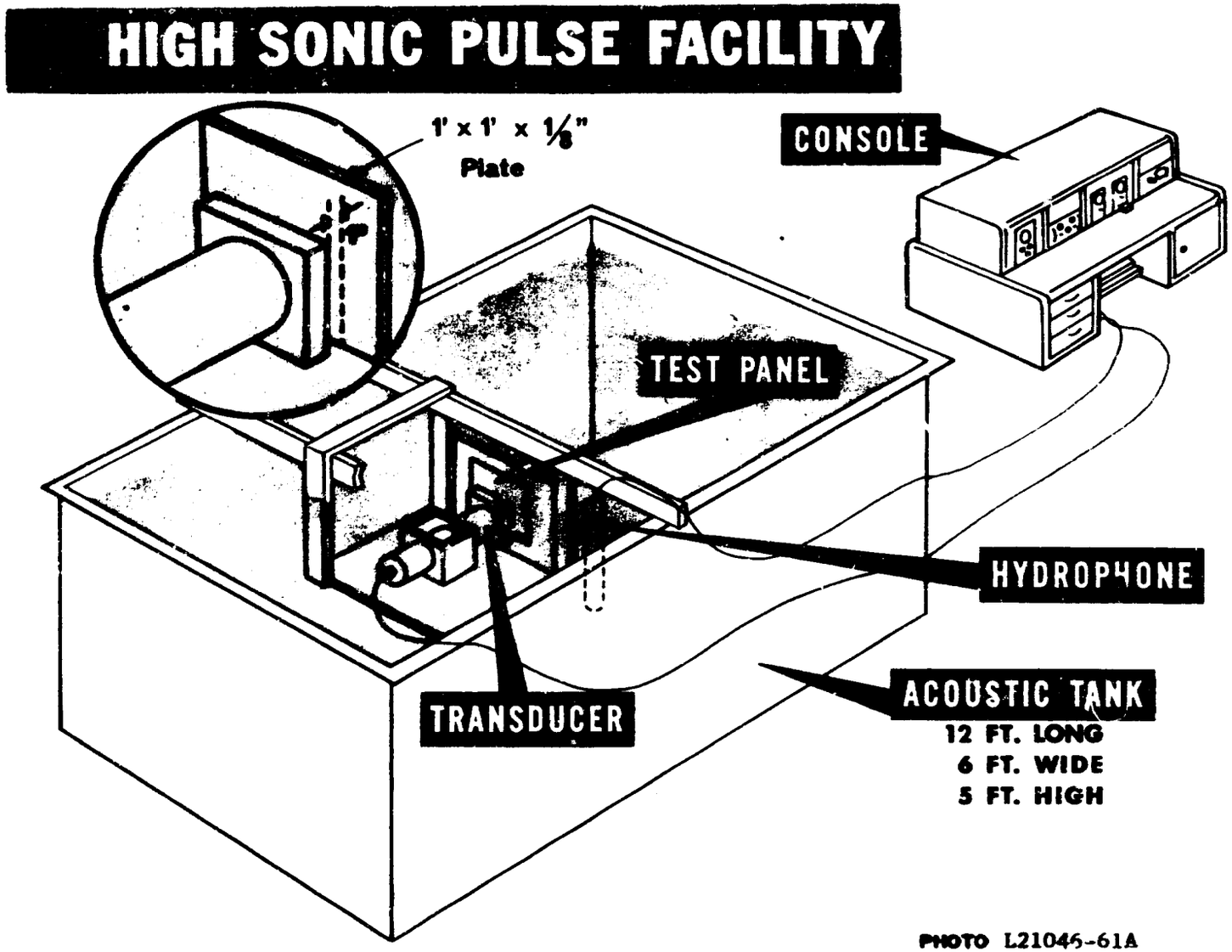

FIGURE 15 - HIGH SONIC PULSE FACILITY

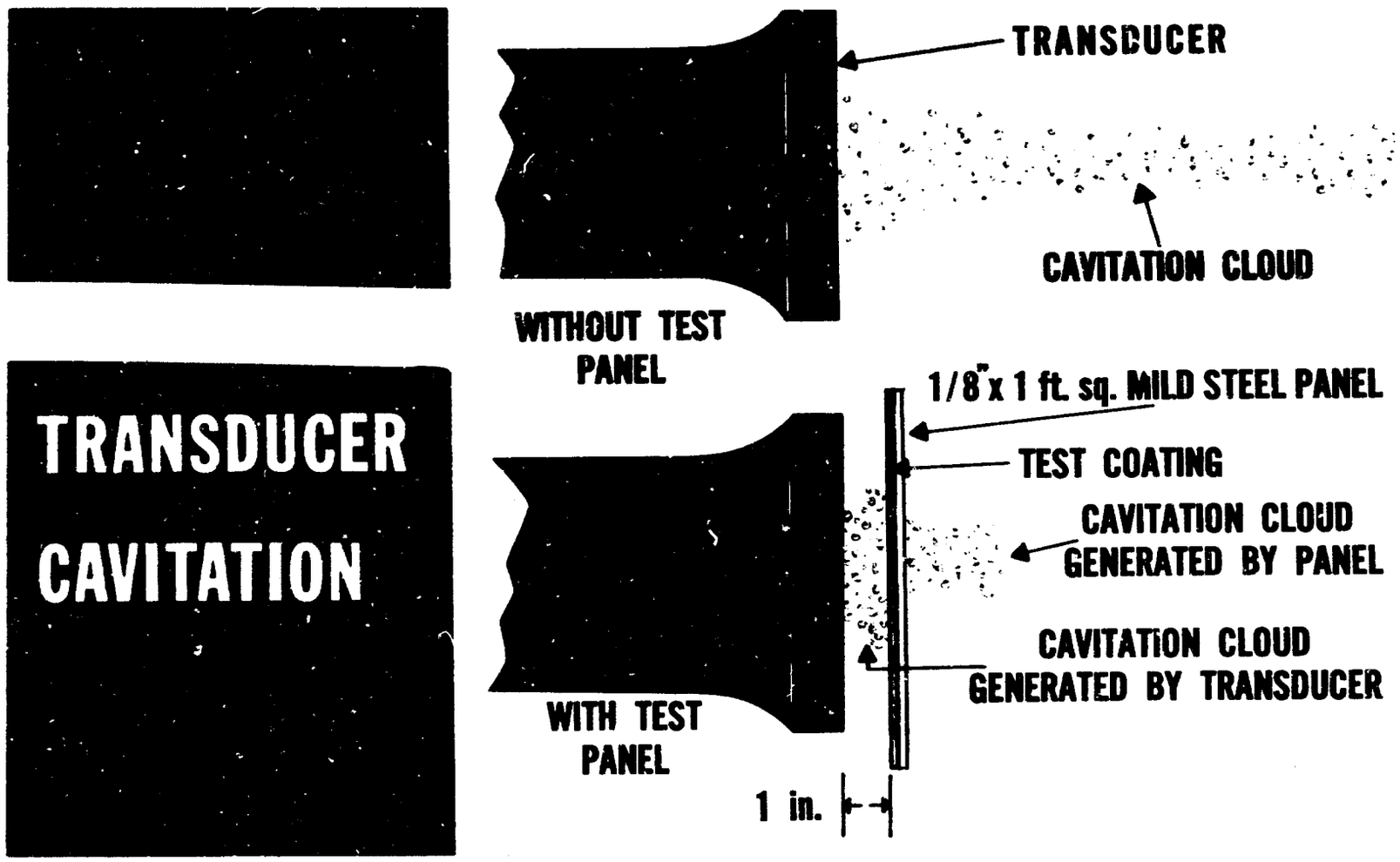

PHOTO L21046-91A

FIGURE 16 - HIGH SONIC PULSE TRANSDUCER CAVITATION

EFFECT OF HIGH SONIC PULSE FIELD ON SONAR DOME COATING

Standard Navy Vinyl Coating System

23 Hour Test Duration

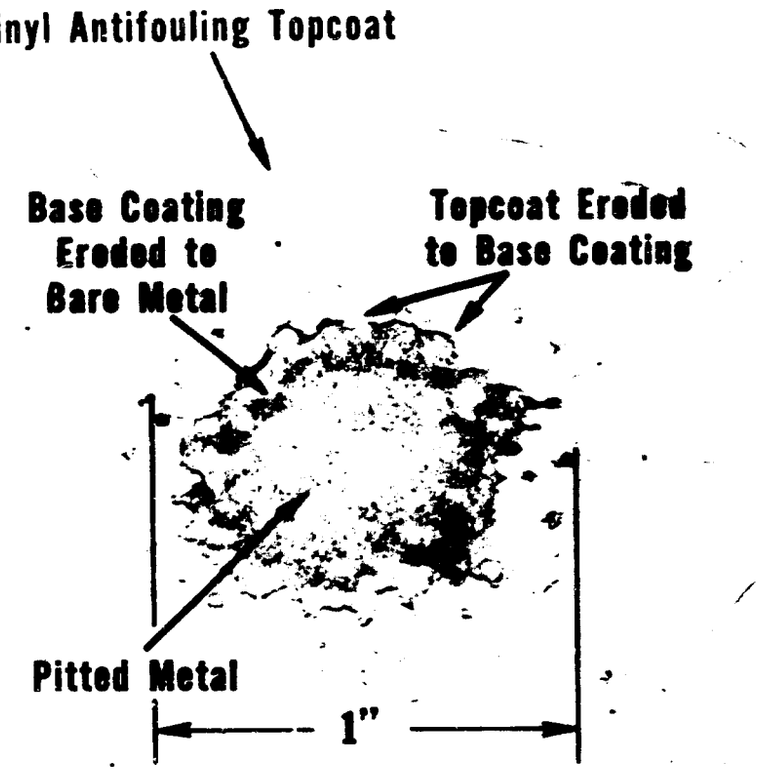

PHOTO L21046-63A

FIGURE 17 - EFFECT OF HIGH SONIC PULSE FIELD ON A SONAR DOME COATING (NAVY VINYL SYSTEM)

EFFECT OF HIGH SONIC PULSE FIELD ON SONAR DOME COATING

Neoprene, Solvent Base-Polyisobutylene Coating System

23 Hour Test Duration

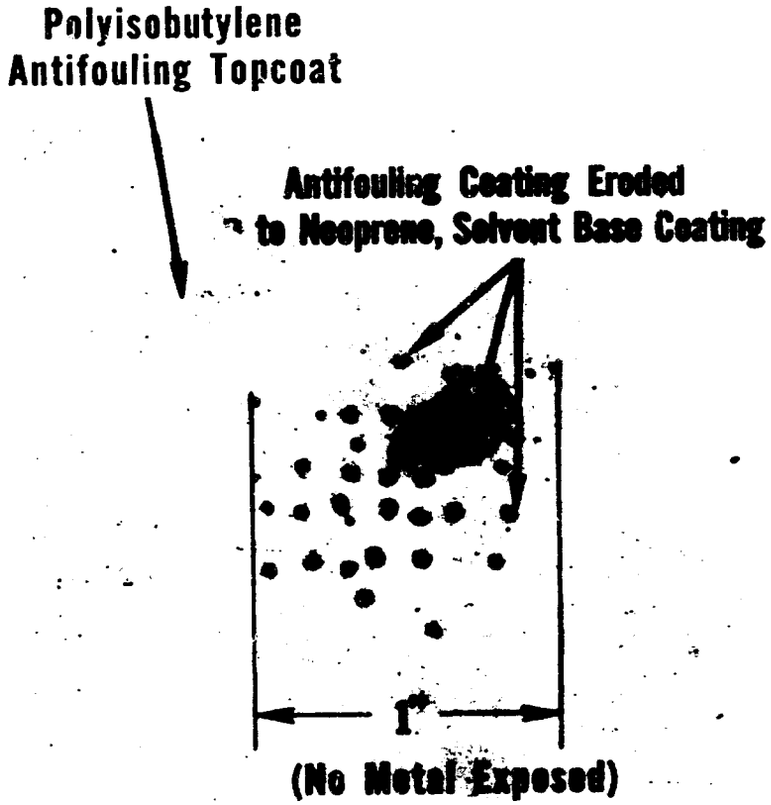

PHOTO 121049-621

FIGURE 18 - EFFECT OF HIGH SONIC PULSE FIELD ON A SONAR DOME COATING (NEOPRENE-POLYISOBUTYLENE SYSTEM)

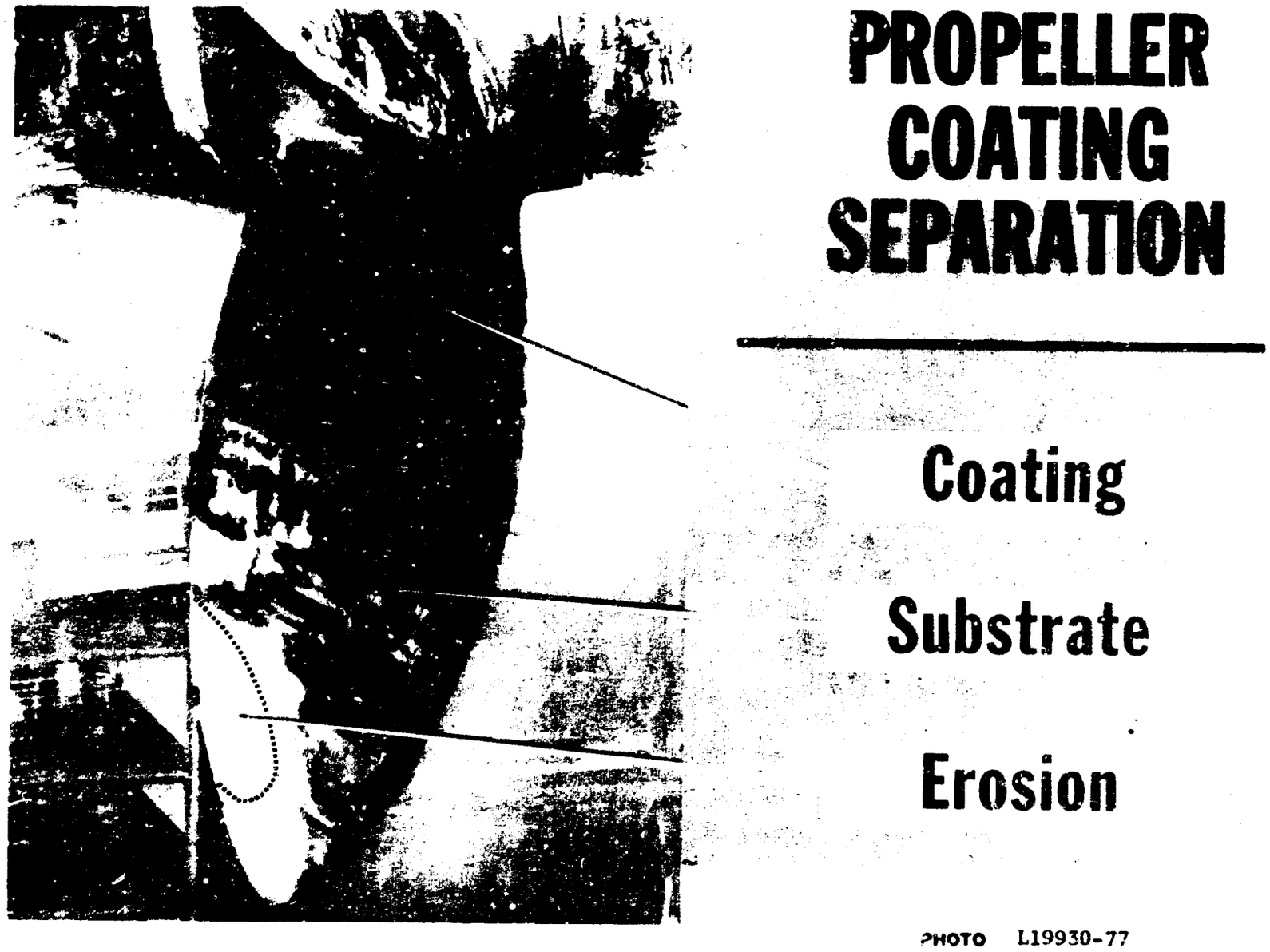

FIGURE 19 - SEPARATION OF NEOPRENE COATING FROM SHIP PROPELLER AFTER 81 DAY OPERATION

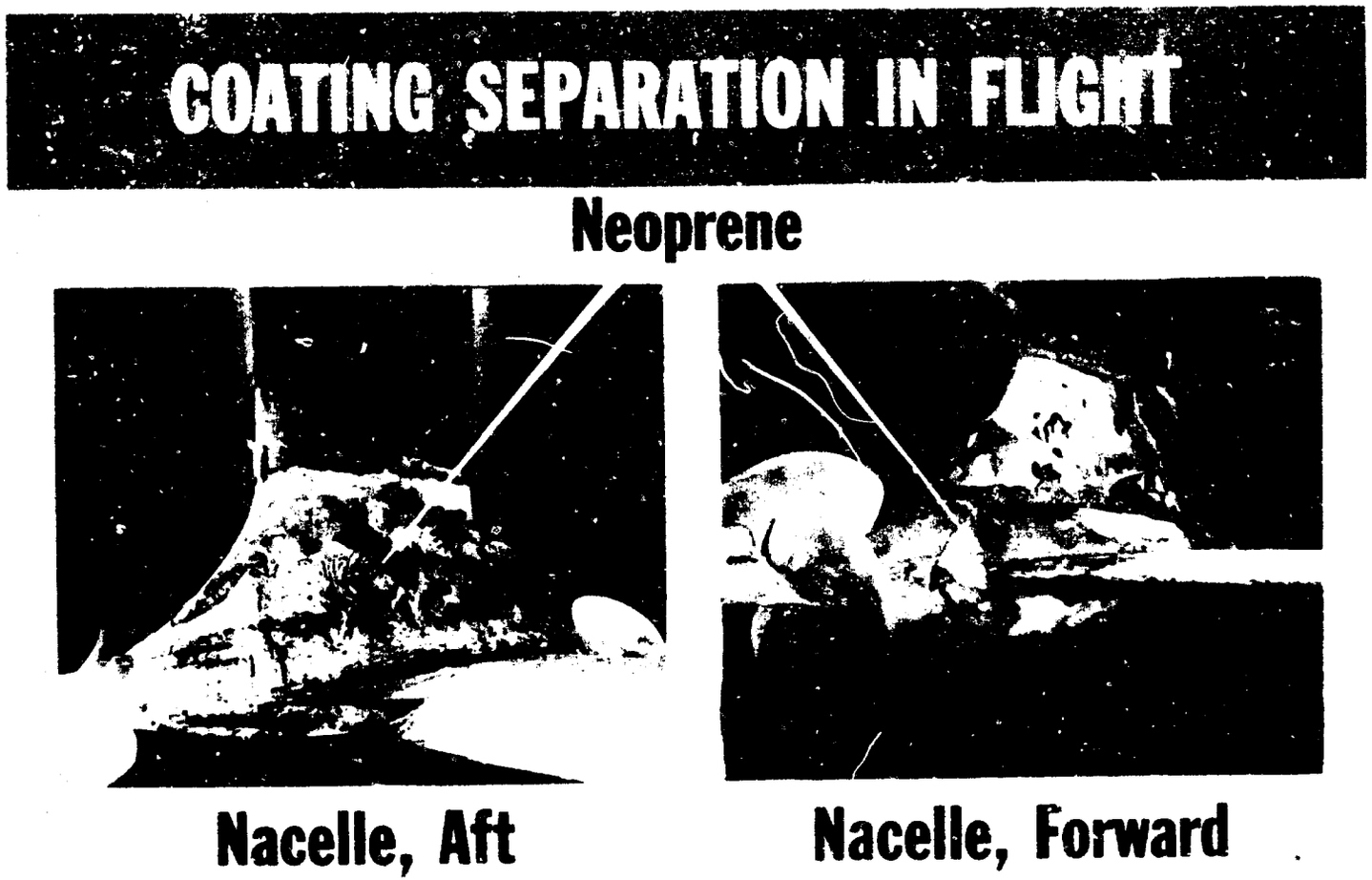

FIGURE 20 - SEPARATION OF NEOPRENE COATING FROM HYDROFOIL NACELLE AND STRUT STUB AFTER 2-1/2 HR. FLIGHT

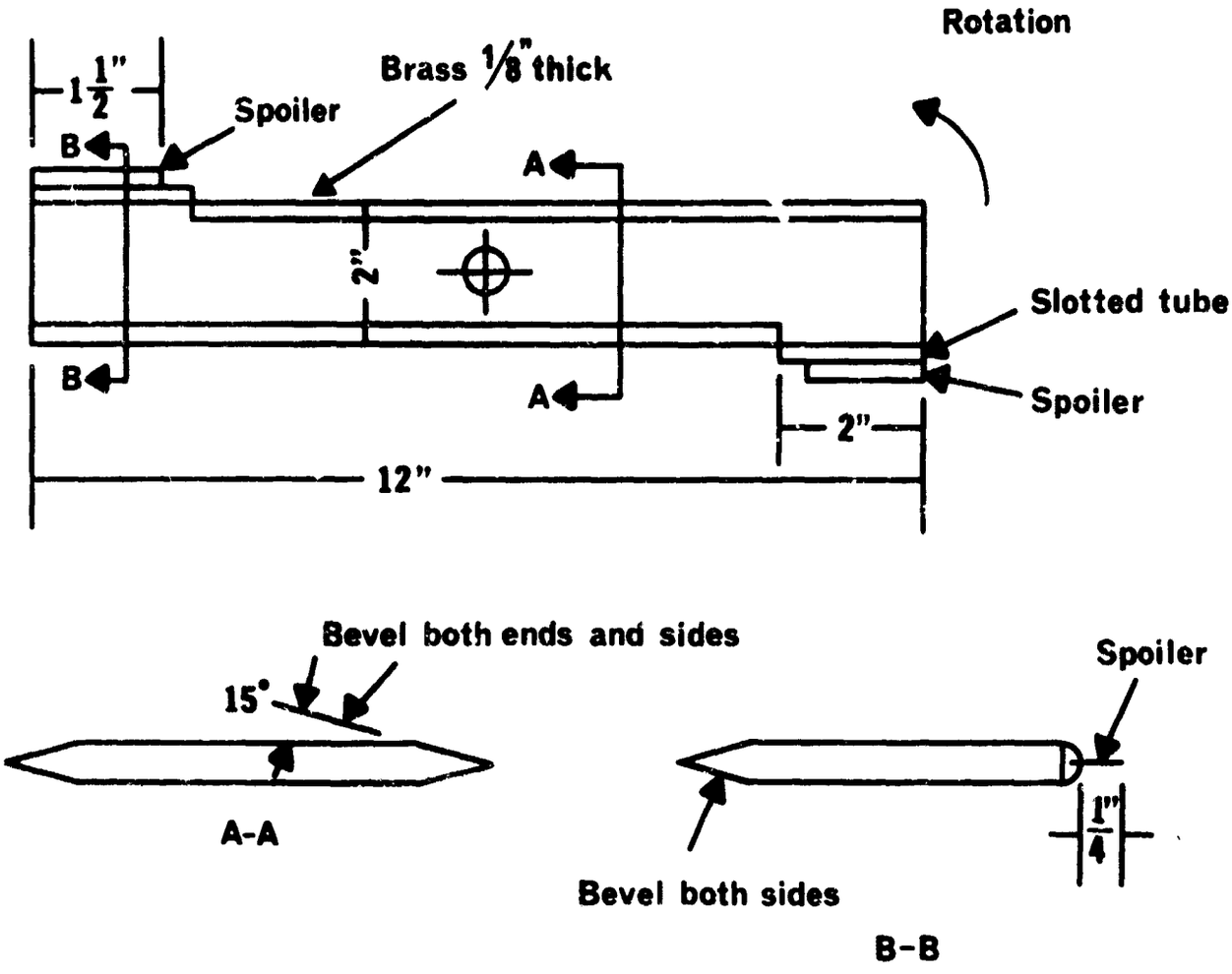

PHOTO L.21126

FIGURE 21 - SPOILER MATERIAL TEST FOIL

UNSOLVED PROBLEMS IN PREDICTING THE BEHAVIOR OF CONCRETE

Bryant Mather
U. S Army Engineer Waterway Experiment Station, Concrete Division
Jackson, Mississippi

Introduction

The discussions at this symposium have as their purpose the advancement of the art of correlating characteristics of materials with the performance of systems. The particular discussions at this session involve the effects of environment as these interact with material characteristics to affect performance. My title, "Unsolved Problems in Predicting the Behavior of Concrete," is one under which might be described any or all of the work that has been done and the knowledge that has been gained in the past 2000 years concerning the selection of concreting materials and mixtures that are intended to possess the characteristics needed to insure that the resulting concrete structures and structural elements will have the properties they need to insure that the systems in which they are incorporated will interact with the environments in which they are placed so as to insure that the systems will provide the service for which they were constructed to the satisfaction of those they were intended to serve. It would also be appropriate to describe all the projects and programs that all the workers on concrete research now have in progress or hope in the future to undertake in all the concrete research laboratories in the world. On the other hand, it seems pertinent to note that the failure of a system composed of concrete structural elements to give the desired service frequently results from its failure to have been built according to the principles that were intended to have been followed. Frontinus, in 97 A. D., after listing the material characteristics of concrete needed to provide proper performance of the aqueduct system of Rome, laid the blame on the workmen when he wrote, "All these the workmen know, but few observe." In the following sections of this paper I plan briefly to review what concrete is; to indicate how, because of its nature, it may manifest an infinite range in its properties; to suggest some aspects of the infinite range of environmental effects that any influence its performance; to examine some features of the state of knowledge of the consequences of the interaction of concrete properties with environmental conditions; and finally to propose that asking the proper questions regarding the extension of this knowledge is a delineation of the unsolved problems in predicting the behavior of concrete.

Concrete

Concrete is a construction material that is made by missing to a degree of homogeneity ingredients having an infinite variety of properties of widely varying significance, proportioned in accordance with a recipe selected according to

poorly defined rules. The ingredients are not uniform, either from place to place or batch to batch, or within a batch. Batches of the mixture are transported by one or more of a variety of methods, discharged into prepared forms of any desired size or shape, which may or may not have previously been provided with reinforcing steel or other items intended to be surrounded by the concrete, and compacted so as to more or less completely fill the form. Once the form is filled, the surface is normally struck off and finished. The mass then undergoes spontaneous chemical and physical changes described as setting, hardening, development of strength, and volume change. During the early stages of spontaneous activity of the mass, when these changes are taking place at the most rapid rates, there is normally some intentional external control of the immediate environment, referred to as "curing," intended to avoid what are regarded as "excessive" changes of temperature or moisture content. Once the mass has gone through its adolescence, which may be a period of from one to 21 days -- depending on the circumstances -- it is then pretty much on its own.

Concrete is a composite material consisting of two fundamental elements: aggregate and binder or matrix, a discontinuous phase that can be considered as inclusions in a continuous phase. The concrete with which I am familiar is that in which the binder includes a hydraulic cement, which is generally portland cement. Another well-known type of concrete is that in which the binder is a bituminous material. Such bituminous concretes have their major use in the construction of flexible pavements. For convenience, aggregates are considered in two size categories, designated respectively fine aggregate and coarse aggregate, the separation being made at the No. 4 (4760-micron)sieve. Fine aggregate is often spoken of as "sand," and natural sands are a principal kind of fine aggregate, but many other materials are also used, especially crushed stone, crushed slag, mine tailings, and various crushed sintered materials. The principal materials used as coarse aggregate are gravel, crushed stone, crushed slag, crushed gravel, and expanded clay, shale, slate, or slag. For most applications, the materials used as aggregates are required to be provided in specified ranges of particle-size distribution. It is advantageous to use as much aggregate as possible in each unit volume of concrete so as to reduce the volume of cement required, which reduces cost and reduces the tendency to volume change.

Hydraulic cements are materials that react with water to yield products having cohesiveness and continuity. The extent to which any given cement develops such properties in a given period of time depends on the ratio of the volume of cement to the volume of water with which it is mixed, the chemical activity of the cement, and the degree to which the environment accelerates or retards the progress of the reactions. In the case of portland cement, for example, when the ratio of water to cement exceeds about 20 U. S. gallons per 100 pounds of cement, or when the temperature of the mixture is held below about 11 F, or when the mixture contains more than traces of any of several sugars -- such as sucrose -- in solution in the mixing water, no significant development of cohesion or continuity will take place.

Properties of Concrete

Concrete has been and may at will be produced to possess, in its final stable mature state, any of an infinite range of properties. It may weigh anywhere from as little as 10 lb/cu ft to over 300 lb/cu ft. The exceedingly lightweight concretes are produced using air or some other gas as the major aggregate; the exceedingly heavyweight concretes are produced using pieces of metal as aggregate. Both of these extreme classes have their major uses in connection with nuclear applications; the former for blast shock mitigation; the latter for radiation shielding. Concrete may be produced that will set, harden, and develop ultimate unconfined compressive strengths ranging from a very few pounds per square inch to as much as 20,000 psi. The very low-strength concretes are usually produced from mixtures of high gas content and high water to cement ratios; the very high strength concretes require low water to cement ratios and aggregates that themselves have high strength. The rate of hardening may be varied within wide limits. A mixture may be produced that sets and hardens in a few seconds or minutes, usually as a result of the use of a chemical accelerator; or, by the use of appropriate amounts of a chemical retarder, the mixture may remain semifluid and remoldable for many hours or days; lesser degrees of acceleration and retardation are produced by changes in composition of the cement or by changes in the ambient temperature or both.

The foregoing comments concern properties that can be varied at will--controllable performance. More significant to most engineering uses of concrete are variations in properties that affect performance but that occur without having been intended or predicted.

One may encounter an apparently continuous volume of concrete in service of which a portion exhibits observably different behavior from an adjacent portion, thus indicating a nonuniformity either of properties of the concrete or of the environment. If it can be shown, or assumed with confidence, that the environment has been uniform, one seeks the explanation of the difference in behavior from a difference in properties of the concrete. However, before a meaningful assessment of significance of differences in concrete properties can be made, it is first necessary to develop a hypothesis concerning the kind of environmental interaction that produced the observed effects.

Environmental Effects

The environments in which concrete serves possess a wide variety of properties that interact with the properties of the concrete and result in behavior. Further, the properties of the environment interact with each other. For example, two major environmental influences are temperature and moisture, which together induce temperature change and moisture-content change in concrete. Temperature change in the environment, per se, within ranges where none of the constituents of the concrete undergo changes of phase or state, interacts with concrete to produce temperature change of the concrete that is manifested in behavior as volume change proportional to the coefficient of thermal expansion of the concrete. The

behavioral consequences of such volume change can be quite significant, depending on the requirements for volume stability of the structure or structural element, its restraint, its dimensions, the degree to which it has been provided with expansion and contraction joints, the degree to which cracking is significant to satisfactory rendering of the service expected of it, and so forth. However, the consequences of temperature change, per se, on behavior generally are less significant than those of temperature changes accompanied by moisture-content changes, since a reduction of environmental temperature to levels below the freezing point of water following a development of high-moisture content may cause destruction of the concrete as the water in its large permeable pore spaces undergoes the volume change accompanying the change of state to ice.

Other major properties of the environment include loading, abrasion and chemical attack.

Interactions Affecting Behavior

From the foregoing comments on the nature of concrete, the characteristics that it may possess, and the environmental effects that may influence its behavior, I believe that it is clear that the performance or behavior of a system in which concrete is used -- or the performance or behavior of the concrete in that system -- can be shown to be controlled in a manner illustrated by Fig. 1.

The kind of performance desired depends on the criteria of acceptability for the system. Surface defects, cracks, deflections, removal of surface layers, corners, or edges can be tolerated to much greater degrees in the service of some systems than others. No concrete is inert and unchanging. In the real world all substances alter with time and exposure. Thus the first step is to select criteria of acceptability of performance of the system, and hence for the concrete. A great deal of confusion and even bitterness that is encountered in many different confrontations, ranging from those of the home owner and the home builder to those of the Secretaries of Commerce and Transportation and the House Committee on Public Works could be avoided, or at least reduced, if these criteria were adequately defined and agreed upon before any system was created. Assuming that criteria of adequacy have been selected, it is then necessary, as Fig. 1 indicates, to consider the environmental effects under which these criteria must be achieved, to select the properties of the concrete that will, when it interacts with these environmental effects, give the desired performance, and thus to select the specification requirements for the work. The diagram suggests that specification requirements fall into three categories: properties of constituent materials, proportions thereof, and construction practices. In many cases it is preferable to specify concrete properties rather than materials, proportions, and practices, but it should be recognized that, when this is done, it merely transfers the responsibility to others to set appropriate requirements on these elements.

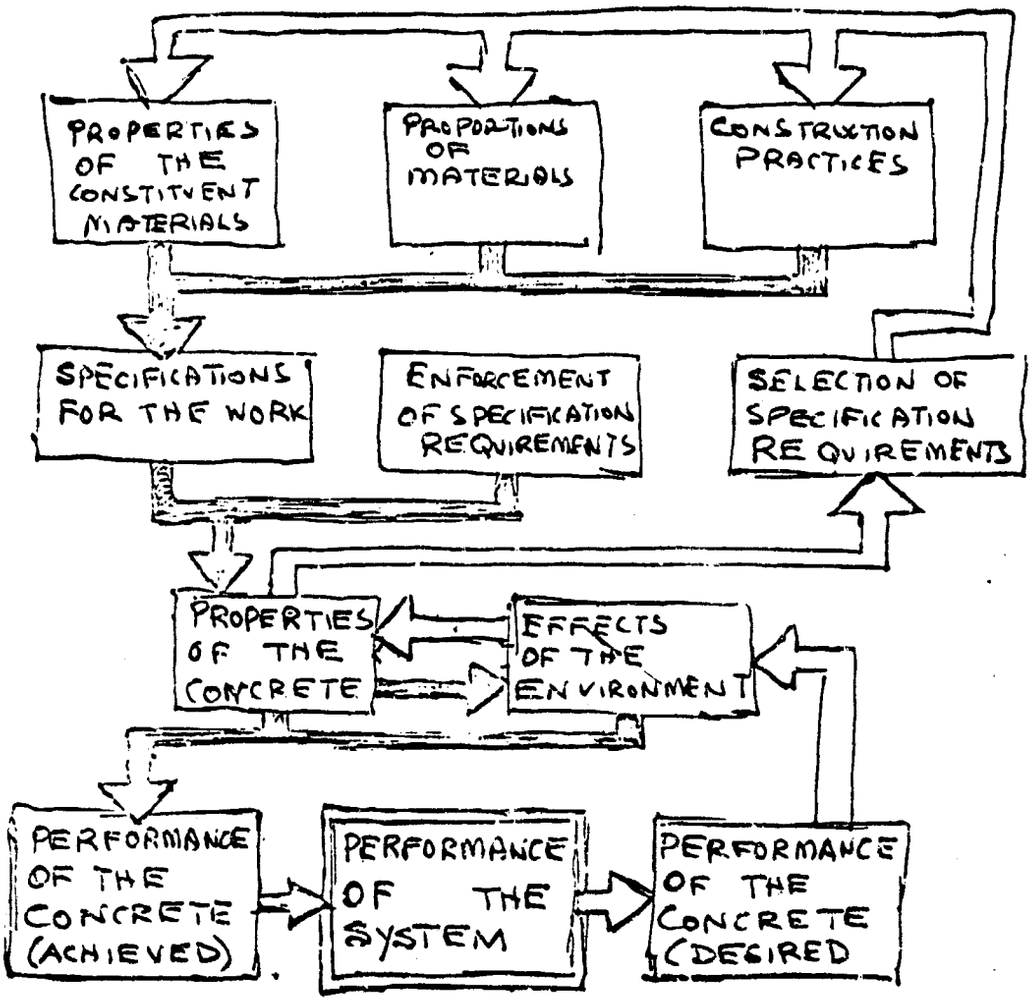
PROPERTIES OF THE CONSTITUENT MATERIALS
PROPORTIONS OF MATERIALS
CONSTRUCTION PRACTICES
SPECIFICATIONS FOR THE WORK
ENFORCEMENT OF SPECIFICATION REQUIREMENTS
SELECTION OF SPECIFICATION REQUIREMENTS
PROPERTIES OF THE CONCRETE
EFFECTS OF THE ENVIRONMENT
PERFORMANCE OF THE CONCRETE (ACHIEVED)
PERFORMANCE OF THE SYSTEM
PERFORMANCE OF THE CONCRETE (DESIRED

FIG 1

Let us consider a hypothetical example. For the past 30 years we have maintained an exposure station for concrete at the mean-tide level on the Atlantic Coast near Eastport, Maine. Specimens there are immersed in sea water twice a day as the tide rises above mean and are exposed to the air when the tide falls below mean. From periodic observation of changes and non-destructive tests for resonant frequency and compressional wave velocity, the changes in concrete properties are monitored as they are affected by this environment. Now suppose it were determined that a navigation lock were to be built on the St. Croix River near Calais, Maine, and the design called for a life of about 50 ft, a lock chamber about 100 ft deep, having gravity section walls founded on rock. Let us further assume that navigation through this lock would continue from April until November each year, that each winter when navigation had stopped, the lock would be pumped out, inspected, maintenance work would be done, and the lock would be rewatered the following April to be ready for resumption of traffic.

The first steps to be taken should be to develop quantitative data on the properties of concreting materials available within economic range, data on the performance of concrete made with these materials, data on the performance of concrete in similar service elsewhere, and data on the environmental effects that the concrete should withstand in service in the proposed system. The next phase of the study should be to develop concrete mixtures, to select construction practices, and to test concretes prepared according to these mixtures, using these practices to determine their relevant properties and to observe their behavior as they interact with the appropriate environmental influences in simulated service testing. Finally, specifications would be prepared and the system constructed.

The relatively unique feature of the environment that would need to be given greatest attention in this case is the evaluation of the effect upon the concrete of its exposure to the air from November to April each winter following the water soaking it received from April to November each year. When our studies at the exposure station near Eastport were begun, there was no combination of materials, mixture proportions, and construction practices that we knew how to specify that would produce concrete that could be used to make test specimens that could be placed thereon in November with any assurance that by April they would be other than in a state of complete disintegration. Soon we found that concretes made with some cements lasted longer than those made with others; concretes made with some aggregates lasted longer than those made with others; concretes made to some mixture proportions lasted longer than others, and so on; however, the major finding was that any concrete could be given the greatest improvement in frost resistance if it were mixed with a foaming agent that caused air voids to be disseminated through the binder so that the spacing of the bubbles was not greater than 0.008 in.

Thus, as we would select specifications requirements for the concrete to be used in this system, we would prepare requirements for the aggregate to limit the selection to materials having properties similar to those that gave

better service in actual use in the region and in the simulated service tests; we would impose similar requirements on the cements; we would require mixture proportions to be used that had done likewise, and we would require the incorporation of an air-entraining admixture shown to have the property of providing the desired level of entrained air in the paste.

Doing all these things will greatly improve the probability that the system will provide satisfactory performance. However, recent work has revealed that this would, in this case, not necessarily be sufficient, because concrete is a material that, when incorporated into the system of which it is to be a part, is a fluid mixture which only develops its significant properties over time after placement, and the rate at which these develop is itself a function of the interaction of the properties of the concrete and those of the environment. All the specimens that have been put on the test rack near Eastport were fabricated and cured elsewhere, in a different environment, and installed there in a relatively mature condition. After installation, no one of them has ever been exposed to temperatures below freezing for more than about six hours, since there are two tide cycles per day. The hypothetical lock is to be constructed in this environment, and the concrete is to be exposed to the winter air all winter. The significance of these factors becomes apparent only after some fundamental considerations.

The increase in volume undergone by water during its change of state from liquid to solid is about 9 percent. Water will not undergo this change at its normal freezing point if it is either under other than normal pressure, contains dissolved salts, or is present in pores of sufficiently small size. It is thus not possible to freeze all the water in any concrete, no matter how low the temperature may fall, and conversely, the lower the temperature -- and the longer the ambient temperature remains at a given low level -- the more of the water in a given concrete will freeze. Data now are available showing that at our exposure station near Eastport the ambient temperatures that are encountered and the duration of exposure of the concrete to them are such that substantially none of the water in any concrete that is much more than one foot from the surface of the concrete ever freezes. Similar data suggest that a very large specimen in the same environment, exposed at a location above high tide, might during a typical winter experience temperatures below 28 F to depths of as much as 6 ft below the surface.

Concrete is a permeable material. If a pore in concrete is more than 91% filled with water and the temperature of that water falls below its freezing point, part of the water will freeze and undergo an increase in volume. The remaining unfrozen water will be placed under hydrostatic pressure and will tend to move through the permeable pore space to regions of lower pressure or into other pores. If the thermal gradient, the cooling rate, the rate of frost penetration are low; the permeability high; the duration of exposure to freezing temperatures short, the concrete may experience no adverse effects, even if a substantial portion of its pores that are of a size large enough to contain freezable water are more than 91 percent filled, since the excess may be able to escape to other regions.

Another factor that influences the response of critically saturated concrete to freezing is the strength of the solid material. This influence is difficult to evaluate separately from other variables, since the processes by which concrete increases in strength are processes which concomitantly reduce the quantity of freezable water, reduce the fractional volume of pore space of sizes capable of containing freezable water, and reduce permeability. Thus, when it is observed that concrete becomes more frost resistant with increasing maturity, and increasing strength, it is difficult to assess the degree to which the increased frost resistance results from increased tensile strength of the material making up the walls of the pores that are critically saturated, from the decrease in fractional volume of such pores, or from the decrease in saturation. It has been shown, for example, that in the absence of an external source of water entering the concrete, a concrete should have the water content of its originally water-filled spaces reduced below critical saturation and thus become frost resistant upon achieving the degree of maturity indicated by the development of an unconfined compressive strength of 500 psi. Other studies have shown that, where there is an external source of water -- and perhaps other complicating environmental effects -- as at the surface of a pavement to which deicing chemicals are applied, otherwise good, properly air-entrained concrete will only achieve frost resistance when it has matured to the extent indicated by having achieved and confined compressive strength of 4500 psi.

To return to the hypothetical lock at Calais, Maine, it is the indication of very recent studies that concrete subjected during a period of seven or eight months to a hydrostatic head of about 50 ft and thereafter exposed for four or five months to severe winter air temperatures needs to have matured to the compressive streng h level of about 4000 psi if it is to be frost resistant, even if all other appropriate precautions are taken in the selection of materials, mixture proportions, and construction practices, including the provision in the binder of a satisfactory air-void system. In the absence of data such as those just mentioned, it is unlikely that specifications for a system in which structural loadings do not require strengths above, say, 2000 psi would insure the use of concrete mixtures that develop 4000-psi compressive strength prior to freezing of the concrete in the soaked condition.

Before leaving the discussion of interactions, I would like to point out that the sort of approach suggested in this discussion is being taken not only by workers concerned with the performance of concrete as a material but also by some of those concerned with the behavior of structural elements composed of concrete. Recently I received for review the final report of an extensive research project concerned with the time-dependent volume change of concrete due to sustained load. The report begins with the statement: "Concrete possesses many behavioral properties which are, as yet, not thoroughly understood or even completely defined. When used as a structural material, the problems associated with this lack of understanding have, to date, been solved by empirical methods..... The phenomenon of creep -- time dependent volume change due to load -- remains as a classic example ..... Extensive tests aimed at studying the time-dependent

deformation of loaded and unloaded concrete have continued since the first decade of this century.....numerous hypotheses have been presented which attempt to explain creep.....If one were to list all the parameters affecting creep of concrete, one needs list all the items associated with the manufacture and utilization of this material....In addition to the obvious interrelated effects of different mixture proportions, constituent materials, curing conditions, and stress conditions, are factors such as moisture exchange and variation, temperature change and variation, specimen size and shape, and admixtures. When one considers the complexity of concrete and its time-dependent structural and chemical non-homogeneity, the conclusion that any change in its composition or its environment will, as a consequence, affect its volume stability is inescapable. The parameters which are significant, though inseparable in actuality, will be dealt with under eleven general categories."

Further along in the report we find the conclusion that the primary influence of aggregate is in its restraining effect on the potential volume instability of the products of hydration of the cement. Variations in aggregate particle size and grading permit use of leaner mixtures. Different types of aggregate present varying degrees of restraint, which depend on their moduli of elasticity. The pore character of the aggregate indicates the amount of water than can be absorbed, the rate of absorption and drying.

After reviewing the effects of all 11 categories of paramenters, the report states: "The ideal prediction method would be one which would include all the possible variables...however this approach is not practical. Effects of variables such as mixing time and consolidation, for example, cannot be included, since the range of these factors is not known. Whether concrete may be considered an ideal composite hard material or an ideal composite soft material has been questioned. It has been shown that for concretes using normal weight aggregates the behavior is that of a composite soft material, that is, the compliances are added. The cement paste, on the other hand, can be considered a composite hard material."

Time-dependent volume change due to load is only one facet of concrete behavior and, indeed, often a minor facet. Our laboratory has conducted creep studies largely to provide a basis for more accurately estimating the stress in concrete structures from measurements of strain.

Unsolved Problems

In my introductory comment I proposed that the asking of the proper questions regarding the extension of knowledge of the consequences of the interaction of concrete properties with environmental conditions would delineate the unsolved problems in predicting the behavior of concrete. As is true of all aspects of the search for truth, the really difficult problem is asking the proper questions. Last year more than three billion tons of concrete were produced -- one ton for every living human being. Concrete, being ancient and ubiquitous, is assumed to be understood when actually we still do not understand the mechanisms by which it gains its strength, and we still do not have adequate theories to predict deformation

or failure. I believe we need to ask questions concurrently on a variety of levels, and we need to encourage workers trained in a wide range of disciplines to approach these questions. We need to ask why the constituents of cements react with water, how their atomic structure and its defects, dislocations, and substituents influence the rate and consequences of these reactions. We need to ask how the products of these reactions acquire their cohesiveness, continuity, strength, volume stability, and chemical resistance and what modifies these properties in what directions and to what degrees. We need to ask questions about all the kinds of rocks and minerals in the earth's crust that turn up as concrete aggregate constituents -- questions relevant to the contribution of the properties of these materials to the properties of concrete -- questions relevant to the interaction of the properties of these materials when incorporated as inclusions in a cementitious matrix with the properties of the environment in which the concrete serves. To date most of these questions have been approached by pure trial studies. One takes the cement one has and the aggregates one has and makes concrete according to the recipe one has; all of which one may have gotten from his grandfather. If he is a researcher, he may weigh the ingredients with greater care, and he may pay more concern to the "cleanness" of the ingredients than if he is a constructor of sidewalks. But the researcher, if he elects -- or is directed -- to investigate the interaction of concrete with temperature, or with neutrons, or with paper mill waste, will normally make concrete test specimens, will expose these to the existing influences or simulations thereof in the laboratory, and report, in due course, that recipe "A" yielded the most commendable behavior and recipe "N" the least commendable. Seldom will he learn why.

I suggest, therefore, that the unsolved problems are unsolved because we do not yet know why concrete behaves as it does.

In conclusion, I wish to explain briefly why I did not discuss the utility and application of the specific techniques of testing that are in use in the study of concrete. We have a battery of such tests ranging from the simple to the highly sophisticated and from the well known to the very poorly understood. However, these are used to measure properties of concrete not to predict behavior. The most widely employed nondestructive procedure is looking at concrete with the human eye, a technique about the employment of what a large book could, and should, be written. The most widely employed group of procedures that are described as "nondestructive tests" are those that do not measure strength but are believed to measure something related to strength that may be used to estimate strength. These include a variety of techniques for determining one or another resonant frequency of vibration; for determining the velocity of propagation of one or another type of mechanical disturbance, most frequently a compressional wave; and for determining the rebound of a hammer or pendulum. To the extent that these provide a basis for calculating approximate values for such mechanical properties as Young's modulus, or shear modulus, or Poisson's ratio, or coefficient of restitution, they are useful; what is lacking is an appreciation of the relation of these properties to most kinds of behavior. Other nondestructive procedures include radiography and the use of electrical or magnetic fields to

indicate the location of voids or inclusions such as reinforcing steel; the use of electrical resistance, electrical conductance, neutron attenuation, nuclear magnetic resonance, microwave attenuation or change in wave form, or other techniques to measure moisture content; the use of gamma radiation to measure density; the use of a wide variety of embedded sensors to measure stress, strain, moisture content, temperature, pore-water pressure, internal relative humidity, and such properties. Perhaps this is what I should have described here today. However, I have chosen rather to discuss what we might one day do with these bits of information rather than how we today obtain them.

THE CANTILEVER-BEAM STRESS-CORROSION CRACKING TEST
A NEW PHILOSOPHY IN CORROSION TESTING

M. H. Peterson
U. S. Naval Research Laboratory
Metallurgy Division
Washington, D. C.

Traditionally, susceptibility to stress-corrosion cracking (SCC) has been determined by exposing stressed specimens to a corrosive environment and observing the time-to-failure. Specimen geometry has varied widely from investigator to investigator as has the method of applying stress. Investigative methods range from cylindrical tensile specimens stressed in a tensile machine, through a variety of flat bend specimens constrained in two, three, or four point loading jigs, to U-bend specimens which have been deformed by bending around a mandrel. Most of the data in the literature was developed for smooth specimens with no stress raiser. There are, however, some data for notched cylindrical specimens stressed in tensile machines, but this is a relatively expensive method of developing such data. Almost without exception the criterion used to establish the severity of SCC has been the time-to-failure for the stressed specimen.

The traditional test methods have two major drawbacks. Because of the highly varied geometries and stress fields used, it has proved difficult or impossible to meaningfully compare the data reported by the various investigators. A second, and possibly more serious, drawback has been the widespread use of smooth specimens. Stress-corrosion cracking usually will not take place until a stress raiser has been formed, often as a corrosion pit. The time-to-failure is, therefore, more often a measure of the relative susceptibility to pitting than an index of the susceptibility of the alloy to SCC. For a metal such as titanium, which does not pit in the experimental environment, the use of smooth specimens will lead to the erroneous conclusion that an alloy is immune to stress corrosion.

The cantilever-beam precracked stress-corrosion test developed at the Naval Research Laboratory by B. F. Brown (1) does not suffer from these limitations, and, as will be shown, there are additional advantages in using this test method. The specimen used is shown in Fig. 1a. A bar specimen is center notched and then fatigued (usually by bending) until a fatigue crack is generated at the root of the notch. This fatigue crack acts as an extremely efficient stress raiser.

Susceptibility to SCC is determined by measuring first the moment required to fracture a precracked specimen in air, and then the moment required to fracture a similar specimen surrounded by the corrodent of interest. A relatively simple and inexpensive apparatus of the type shown in Fig. 2 is adequate for

these determinations. The size and design of the apparatus is dictated by the size of the specimen under study and the moment required for the dry break.

As SCC is a relatively slow process in some metals, it is convenient to be able to know whether the crack is growing without waiting for the specimen to break. One method of determining crack propagation is to monitor the deflection at the end of the cantilever beam with a dial micrometer. However, a simple extensometer of the type shown in Fig. 3 has proved to be more precise and less subject to extraneous deflections.

The main departure which distinguishes the cantilever-beam stress-corrosion test from traditional tests is not the use of the cantilever-beam specimen but the method used to reduce the data. By using the concept of stress intensity rather than the gross nominal stress, it is possible to apply fracture mechanics to SCC. An index of the susceptibility to SCC is obtained which is independent of the specimen geometry and, within limits, specimen size. The principal restriction on specimen size is that for each metal and each strength level there is a minimum specimen thickness which must be reached before the fracture mechanics equations are valid. Details of the geometric conditions which must be met may be found in reference 1.

Figure 1a shows the fracture mechanics equation developed by Kies (2) to describe the stress intensity (expressed in ksi $\sqrt{\text{in.}}$) at the root of a crack in a cantilever specimen. This equation was developed to describe the fracture toughness index, K_{Ic}, for a specimen broken dry. K_{Ic} is used to denote fracture toughness indices determined under carefully controlled conditions which are not fully met by the simple cantilever-beam experiments. For this reason, one will find in the literature the expression K_{Ix}, which denotes an estimate of the fracture toughness index under conditions less rigorous than prescribed by fracture mechanics for a highly accurate determination of K_{Ic}. K_{Iscc} is used to designate the stress intensity required to propagate stress-corrosion cracks.

To illustrate the method of estimating the stress intensity required to propagate a stress-corrosion crack, the data (shown in Fig. 4) from a paper by Brown and Beachem (3) will be used. In this instance a precise value of K_{Ic} was available to define the fracture toughness index of this AISI 4340 steel. A precracked specimen surrounded by corrodent was loaded at an initial stress intensity somewhat lower than that required for dry break and the time-to-fracture noted. As shown in Fig. 4, successively lower initial stress intensities were used until a stress intensity was reached which was insufficient to propagate the crack during the duration of the test. From these values one can estimate the minimum stress intensity required to propagate the stress-corrosion crack, i.e., K_{Iscc}. It should be noted that one cannot state with authority that a crack will never grow at a stress intensity lower than the observed K_{Iscc} since an extension of the time by one or two orders of magnitude might have resulted in crack growth. One can state with authority, however, than an initial stress

intensity higher than K_{Iscc} will cause crack growth by SCC. In this instance, the best estimate of K_{Iscc} is 12.7 ksi $\sqrt{in}$.

In addition to the cantilever specimens, Beachem and Brown (3) have used surface-cracked and center-cracked specimens to show the independence of K_{Iscc} from specimen geometry. Their surface-cracked specimen is shown in Fig. 1b with the associated equation developed by Irwin (4). The values of ϕ are elliptical functions of crack depth and length and may be obtained from Irwin's paper. The data from these experiments are shown in Fig. 5. The geometry and appropriate equation for K_I in a center-cracked specimen are shown in Fig. 1c. The values for the function $f\left(\frac{2a}{W}\right)$ may be obtained from the original paper by Paris (5). Figure 6 shows the data developed by Beachem and Brown for this specimen geometry. Crack growth in this specimen was so slow that a definite value of K_{Iscc} would not be determined. The curve asymptotically approached the lowest initial stress intensity studied, i.e., 14.2 ksi $\sqrt{in}$. K_{Iscc} must, therefore, be less than this value.

These data have shown that the K_{Iscc} obtained by using the equations for the cantilever specimen (Fig. 1a) and the surface-cracked specimen (Fig. 1b) are in very good agreement and are similar to the best estimate of K_{Iscc} available from the center-cracked specimen (Fig. 1c). One can, therefore, confidently use any of these specimen geometries, with corresponding equations to determine K_{Iscc}.

The surface-cracked specimen (Fig. 1b) is of particular interest because the limiting case for a crack of this type (a long shallow crack) is one of the most common types of flaws found under service conditions. For a long shallow crack, the complex equation of Fig. 1b reduces to

$$a = 0.21 \left(\frac{K_{Iscc}}{\sigma_{ys}} \right)^2 .$$

This relatively simple form can be used for estimating the critical flaw depth at which a stress-corrosion crack will begin to propagate through the metal.

The expanded formula has been used by Dahlberg (6) to predict the stress-corrosion behavior of a large titanium specimen with a surface crack of known geometry when stressed in a 3,000,000-pound tensile machine. Some idea of the massiveness of Dahlberg's plate specimen may be obtained from Fig. 7. The specimen dimensions were 1 in. x 6 in. x 24 in. The alloy for this study was Ti-7Al-2Cb-1Ta with a yield strength of 111,000 psi. In the cantilever-beam test this material was found to have a K_{Ix} (dry break index)

of 119 ksi $\sqrt{in.}$ and a K_{Iscc} of 31 ksi $\sqrt{in.}$. From these data it was predicted that the large surface-cracked specimen would fail at a gross stress of 50,000 psi by stress corrosion. When tested in a 3 1/2 percent NaCl solution, no crack growth was observed at a gross stress of 40,000 psi after 30 minutes. The gross stress was then increased to 50,000 psi. Crack growth began immediately and the specimen failed at 25 minutes.

Through the use of precracked cantilever-beam specimens, stress-corrosion data developed relatively rapidly and economically on small specimens can be used to accurately predict the behavior of much larger specimens and specimens of different geometry. In addition, the same data can be used to predict the critical-crack depth which will cause failure by SCC of any part of a structure stressed to the yield point of the material.

The precracked cantilever-beam SCC test is not a cure-all for all corrosion testing problems. It is, however, a simple and economical test for high strength materials of relatively low fracture toughness. When applied to materials of high fracture toughness, it becomes more difficult to meet the conditions required for valid application of the fracture mechanics equations: the specimens tend to become much larger and the apparatus to develop sufficient moment to break the specimens, more expensive. Data can be rapidly developed for titanium alloys and for some high strength steels in which stress-corrosion cracks propagate rapidly. The method is much more tedious for other steels, such as maraging steels in which the crack propagation rate is such that the specimen must be held several hundred hours at each moment value to determine whether crack growth will occur. The analysis of data for materials which are anisotropic with respect to fracture toughness, such as many aluminum alloys, is difficult, and the application of the method of these alloys may be limited to plates of sufficient thickness to provide specimens which may be broken in the TW or TR direction (7).

References

1. B. F. Brown, "A New Stress-Corrosion Cracking Test for High-Strength Alloys," Materials Research and Standards, Vol. 66, No. 3, (1966) p. 129.

2. J. A. Kies, et al., "Fracture Testing of Weldments," Fracture Toughness Testing and Its Applications, ASTM STP 381, American Society for Testing and Materials, (1965) pp. 328-353.

3. C. D. Beachem and B. F. Brown, "A Comparison of Three Pre-Cracked Specimens for Evaluating the Susceptibility of High-Strength Steel to Stress-Corrosion Cracking," presented at the ASTM Symposium on Stress-Corrosion Cracking, Atlantic City, New Jersey, June 26-July 2, 1966.

4. G. R. Irwin, "Relation of Crack Toughness Measurements to Practical Applications," Welding Journal Research Supplement, November 1962.

5. P. C. Paris and G. C. Sih, "Stress Analysis of Cracks," Fracture Toughness Testing and Its Applications, ASTM STP 381, American Society for Testing and Materials (1965) pp. 30-81.

6. E. P. Dahlberg, Private Communication.

7. ASTM Materials Research and Standards, Vol. 1, No. 5, May 1961.

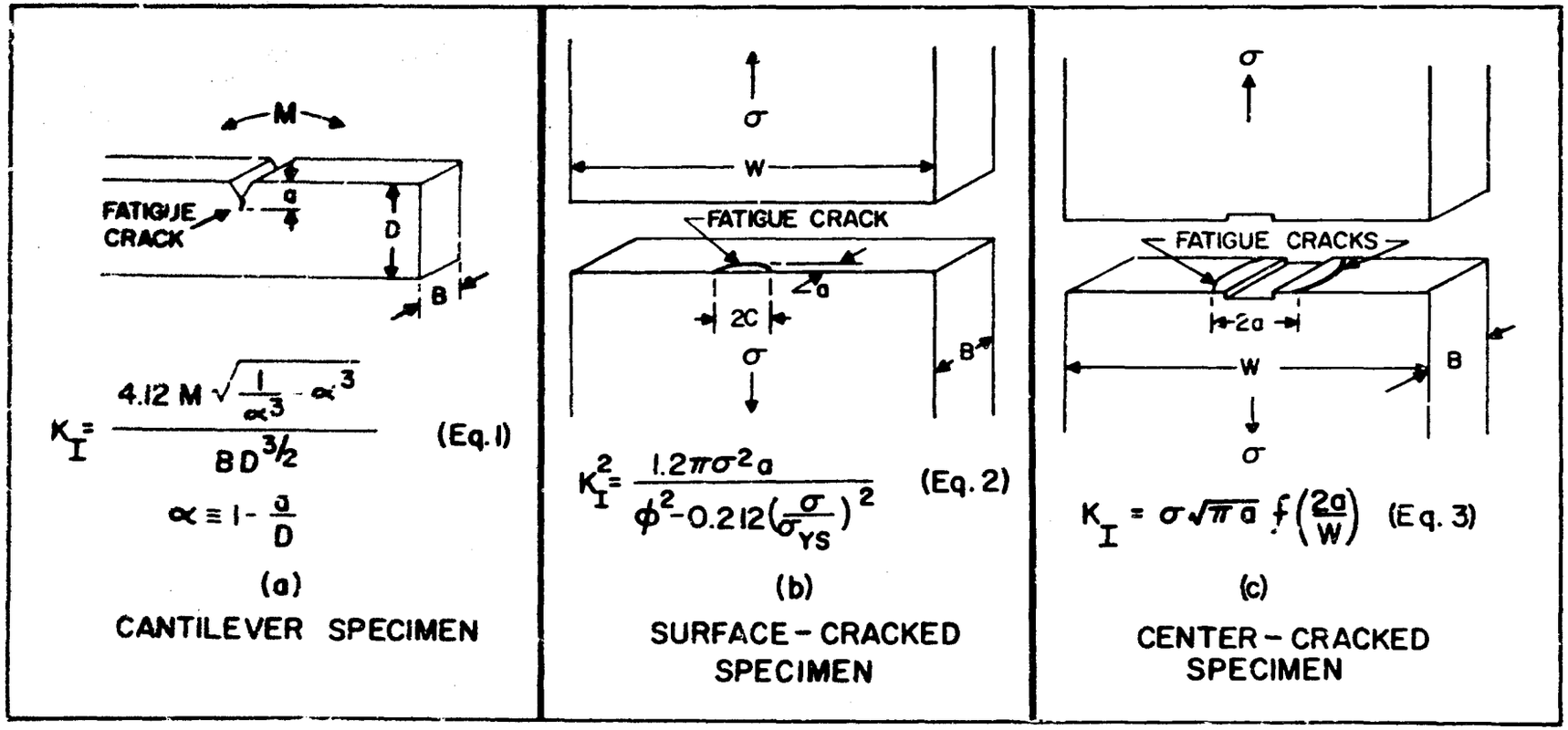

Fig. 1. Specimen dimension identification and equations. (a) Cantilever-beam specimen, (b) surface-cracked specimen, (c) center-cracked specimen.

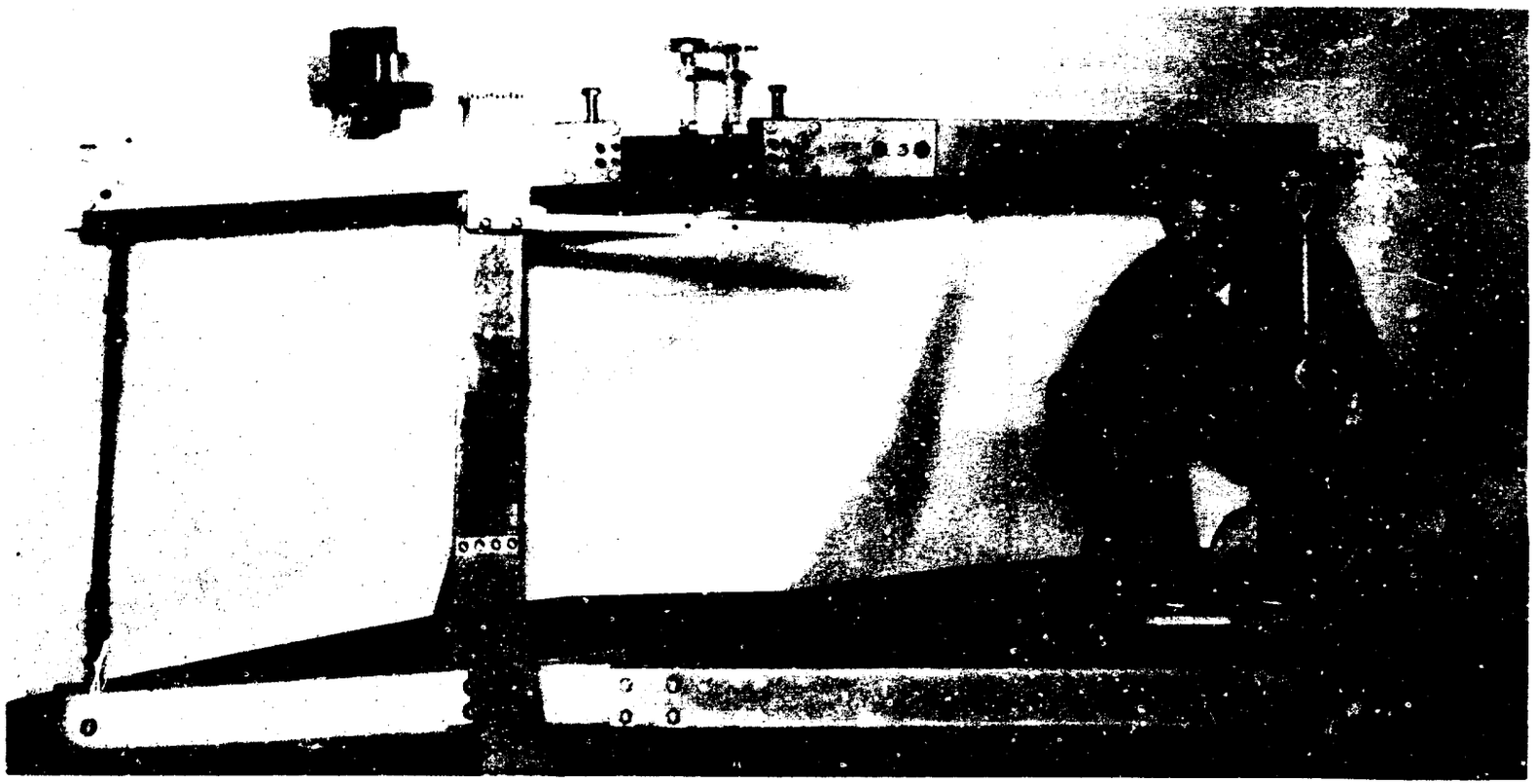

Fig. 2. Cantilever-beam stress-corrosion cracking test apparatus used by Brown (see reference 1).

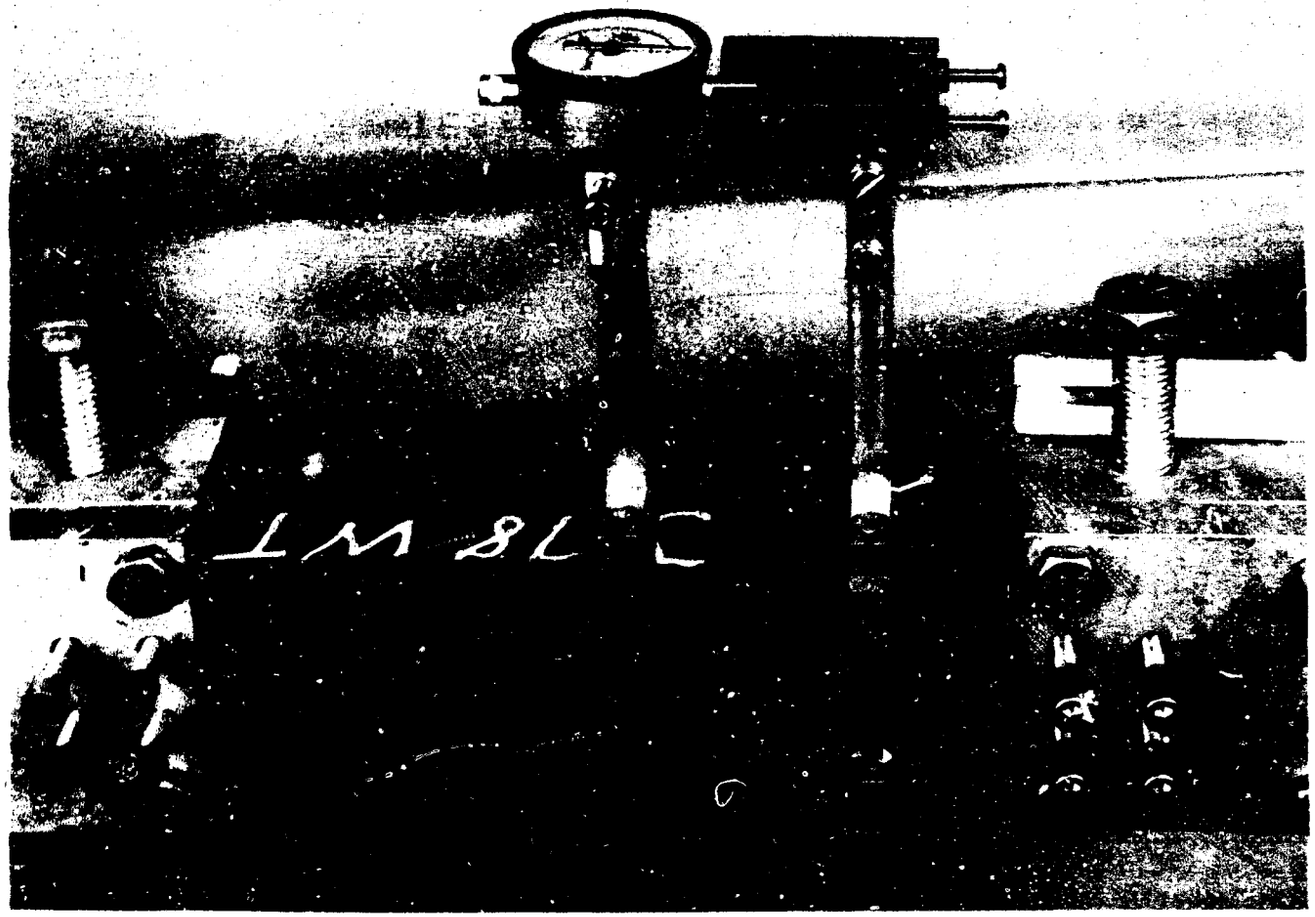

Fig. 3. Extensometer used to monitor crack growth in the cantilever-beam stress-corrosion cracking test method.

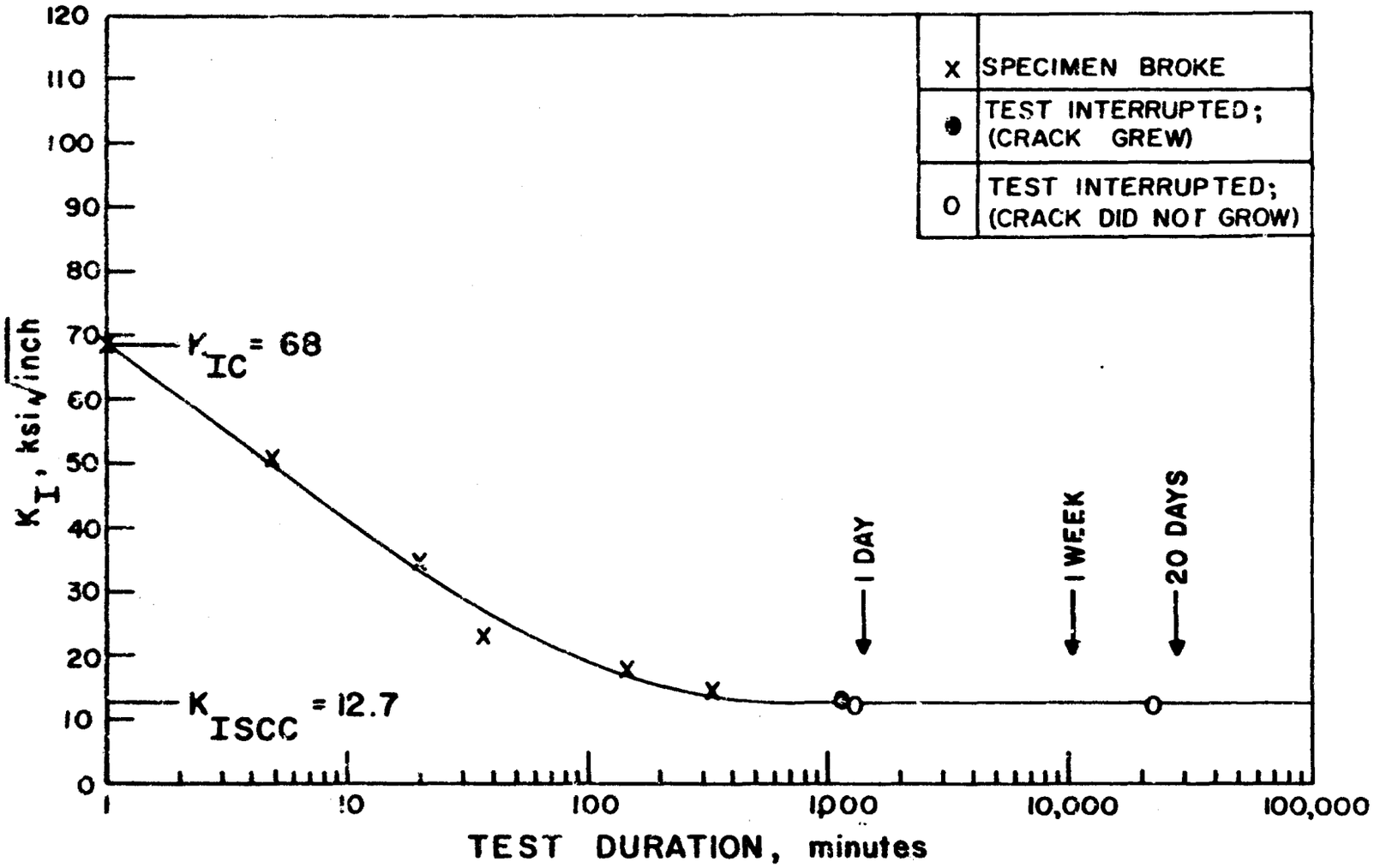

Fig. 4. Stress-corrosion cracking tests of AISI 4340 steel, using cantilev r-beam specimens in 3-1/2 percent NaCl solution.

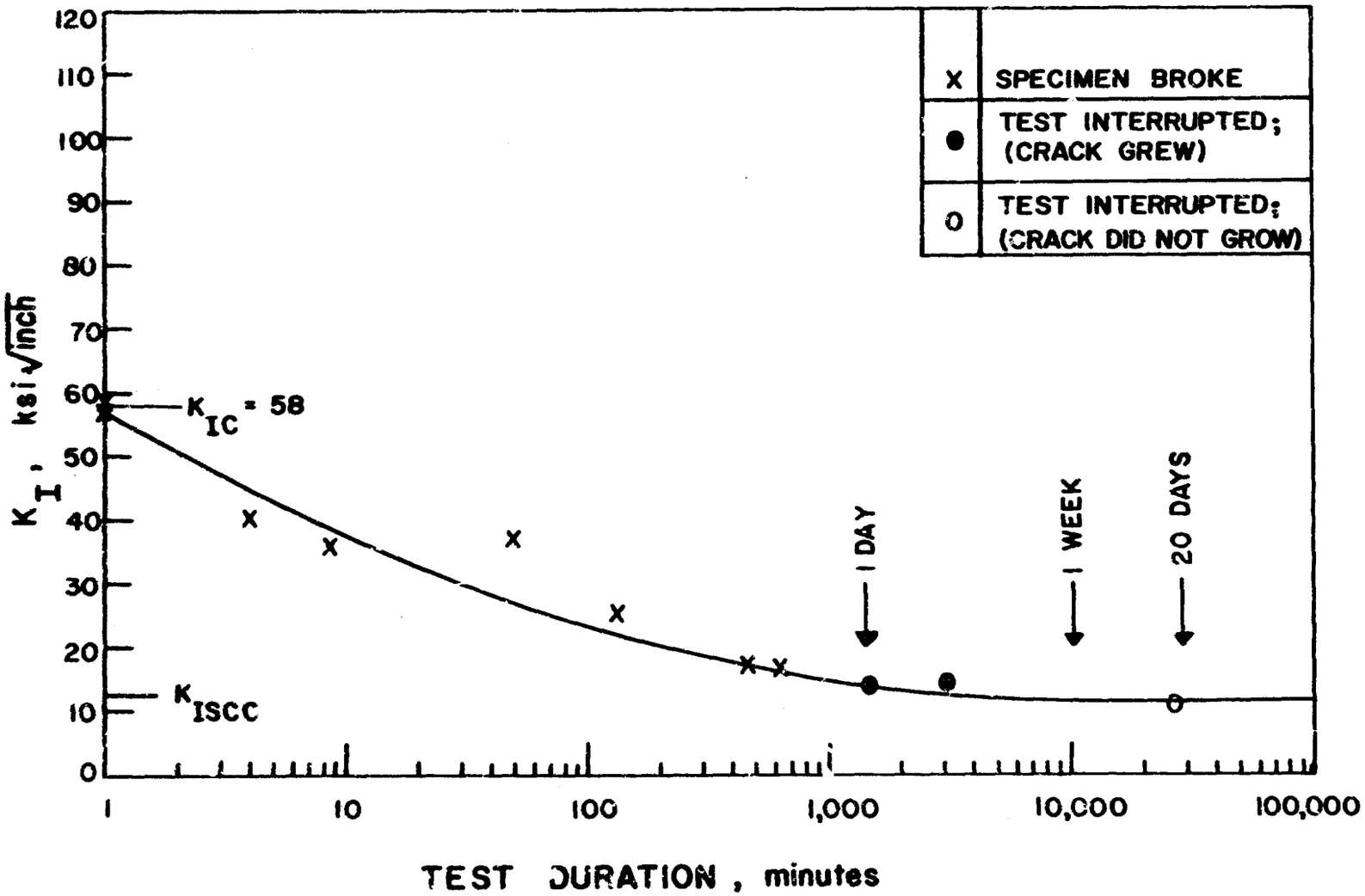

Fig. 5. Stress-corrosion cracking tests of AISI 4340 steel, using surface-cracked specimens in 3-1/2 percent NaCl solution.

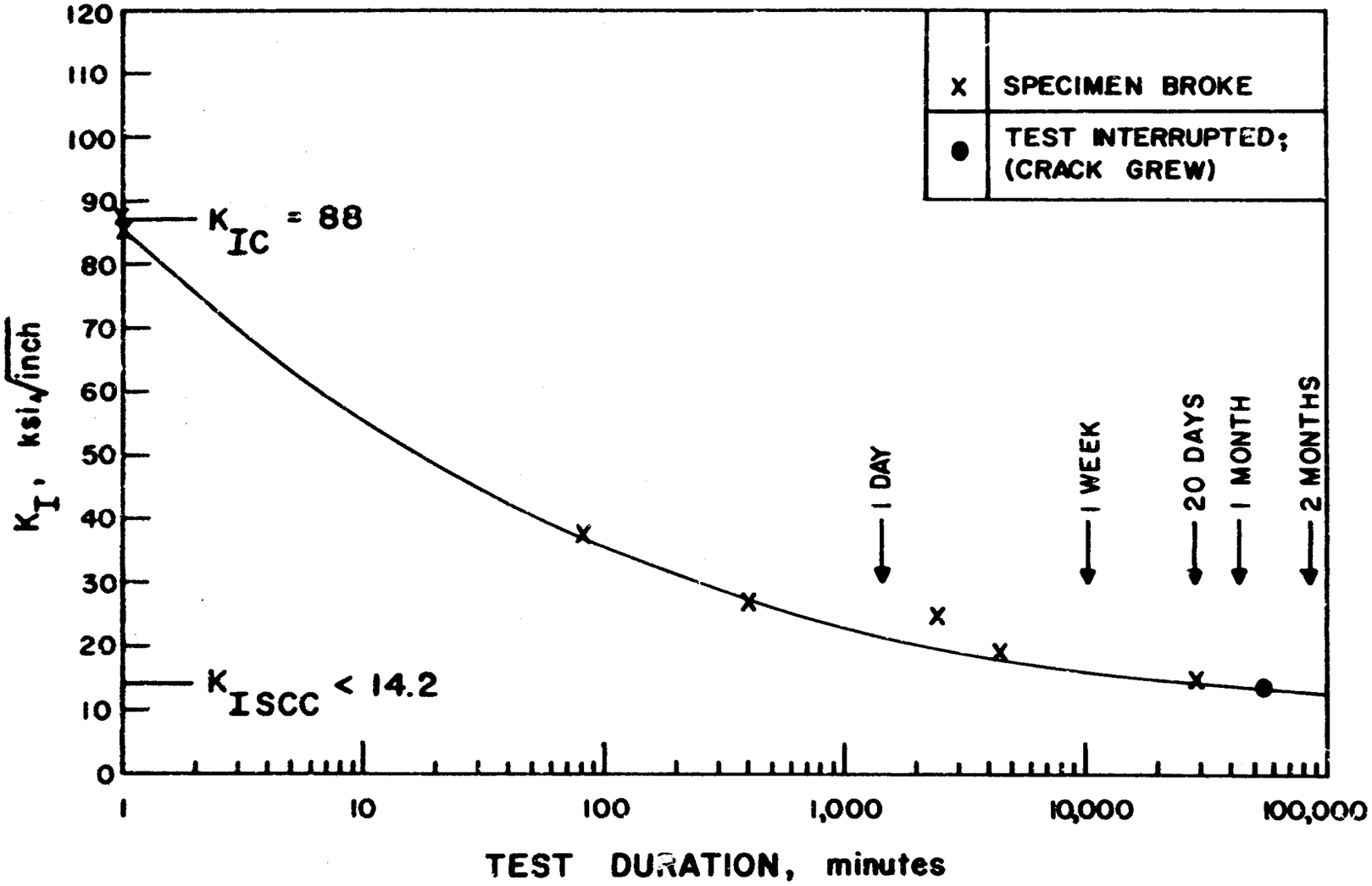

Fig. 6. Stress-corrosion cracking tests of AISI 4340 steel, using center-cracked specimens tested in 3-1/2 percent NaCl solution.

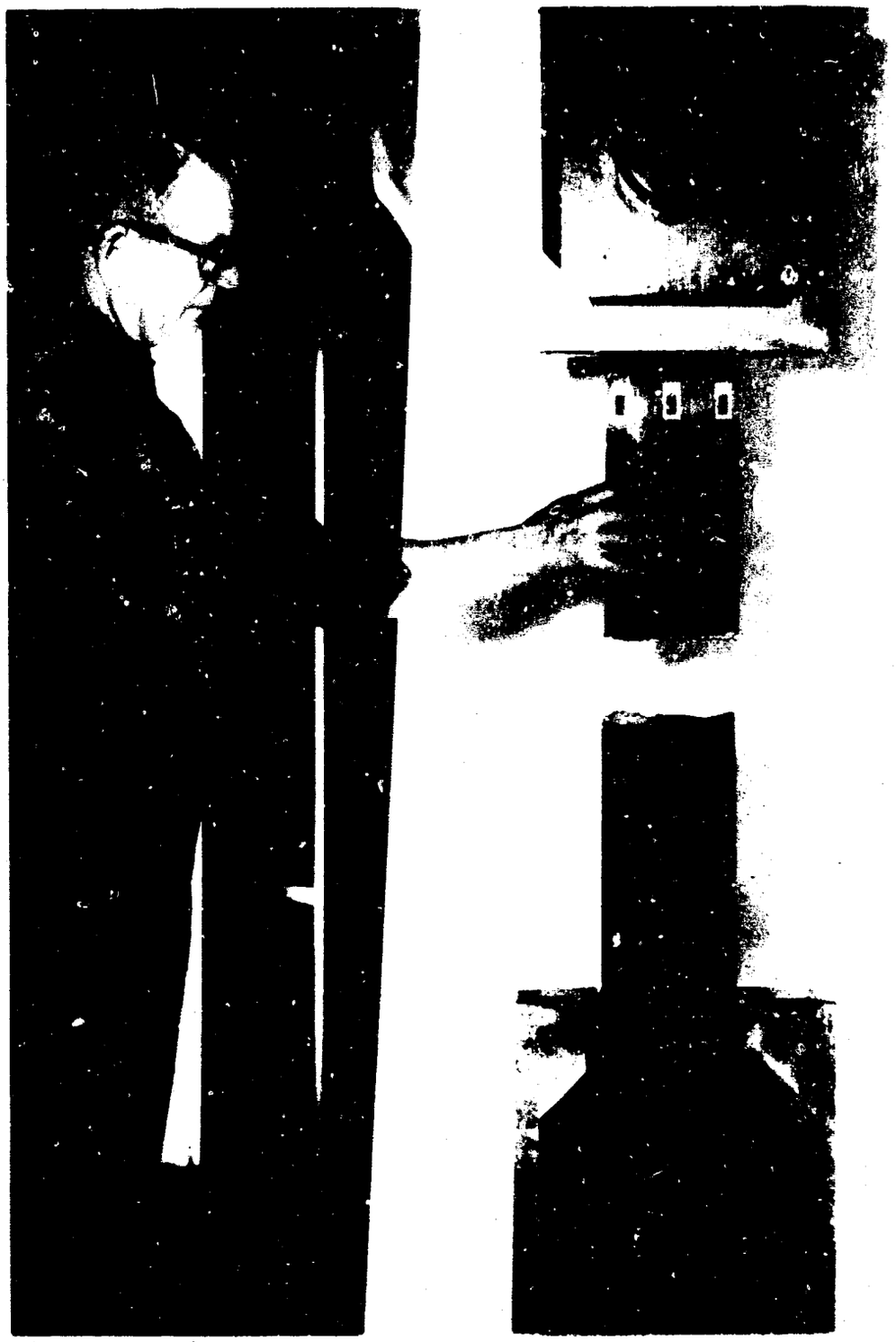

Fig. 7. The massive specimen used by Dahlberg (see reference 6) to predict the stress-corrosion behavior of a large Ti-7Al-2Cb-1Ta plate.

SOME FACTORS IN THE SELECTION AND CORRELATION OF NON-DESTRUCTIVE TESTING TECHNIQUES

D. Birchon

Admiralty Materials Laboratory, Holton Heath, U. K.

INTRODUCTION

Non-destructive testing has failed in its purpose when an unacceptable defect has escaped detection. With the wealth and sophistication of NDT techniques now available, the problem lies in choosing the most appropriate inspection techniques and establishing realistic rejection standards. The sensitivity of modern techniques is now so high that the majority of the "defects" which can be found are unlikely to affect systems performance. It is therefore considered that attempts to correlate NDT with behavior linked to failure patterns is more important and rewarding than attempting to correlate NDT with the mechanical properties of materials.

In the early days of NDT, when crack detection techniques were limited to "oil and chalk" and "wheel-tapping", the nature of the defects detected was obvious to all concerned. Components were often conservatively loaded and had a good reserve of ductility, so that appropriate action could be decided upon without too much confusion. By way of contrast, the application of modern NDT techniques has sometimes been plagued by a policy of perfection. This has arisen because some engineers have lacked the experience, judgement and hard technical knowledge required to dispute the findings of the black boxes, and it is sad to record that so many insignificant "defects" have been repaired at quite unnecessary expense. It is even more chastening to observe that in repairing some of these minor and unimportant flaws greater harm has been done to the structure than if the defects had been left alone.

The real purpose of modern NDT must therefore be to detect and evaluate all significant flaws and then to so interpret the data that unnecessary surgery is avoided.

A simple example of the kind of approach required is provided by consideration of a pressure vessel, having the usual array of nozzle connections, supporting brackets and other complicating features. (Lack of attention to the details of so-called "minor attachments" has often resulted in the initiation of failure in an otherwise satisfactory design, as pointed out by Biggs (1) and others) The essential problem is to determine the most likely causes of failure and then set up the most cost effective inspection technique. For the case of bursting, we can use fracture

toughness criteria (2) to calculate critical crack length, with encouraging precision for materials of limited ductility (3) (e.g., steels above some 150,000 p.s.i. proof stress). For more ductile materials there are other approaches (4,5) which enable the appropriate critical crack length to be determined, though possibly with less precision.

Enlightened NDT then demands:-

1. Identification of the areas in the structure in which such cracks are most likely to grow and in which their presence would be most dangerous.

2. Identification of the nature of built-in defects, which are liable to grow in service. Such "defects" may include non-metallic inclusions in the metal, cracks introduced by manufacturing processes such as forming or welding, etc.

3. Identification of the mechanisms by which sub-critical flaw growth may occur. This is most commonly by fatigue, but stress-corrosion cracking, hydrogen embrittlement and other processes may also be relevant.

The design must then be arranged so that access around critical areas determined as in (1) above (e.g., around nozzles, where tri-axial and thermally induced stresses may be at a maximum) is sufficient to ensure that defects can be detected before they have reached some fraction of the critical size. (This is really only an embellishment of the "leak before break" criterion). In order to allow a sensible margin for error, and crack growth between periodic inspections, it is necessary to work backwards from metallurgical considerations to ensure that the initial design permits adequate access to critical areas, and further, that operation of equipment between inspections, is limited in time to periods during which sub-critical flaw growth cannot conceivably reach critical dimensions. Consideration of this sort of argument can be made semi-respectable by the method outlined below.

THE LEO TECHNIQUE

This is simply a means of estimating the minimum permissible crack length which must be detectable in a particular component of structure. It is made up of three factors:-

1. The critical crack length which will cause failure, e.g., determined by calculation and verified by experience . . . = L

2. The maximum crack length which can be permitted to exist at the start of a period of operation . . = LE where "E" is a confidence factor based upon knowledge of the mechanism and rate of crack extension. Always less than unity, its value will increase with an increase in fracture toughness of the material and with increasing service experience of operating similar pieces of equipment. However, it is unlikely to exceed 0.5 except in very special circumstances, as when the structure is subjected to continuous surveillance.

3. The minimum crack length which must be detected during NDT inspection if failure is to be avoided during the next period of operation is then . . . = LEO where "O" is a measure of the operational efficiency of the NDT team and equipment. This factor is also less than unity, but may approach it closely given high grade NDT techniques, skilled operators, good access to critical areas and good comparison standards similar to the actual part under inspection. Such standards must provide defects above and below the LEO criterion, and, if spurious indications are possible (e.g., porosity in welds, a shortcoming sometimes of little significance (6) in terms of structural integrity) then samples containing such misleading flaws should also be available for comparison.

The determination of the first factor "L" is a matter for the engineer and metallurgist and considerable faith can now be put in the results and calculations of model experiments. The last factor "O" is in the hands of the designer and inspection authority and is relatively simple to control, though its numerical value is a matter for judgement. The second factor is the one involving the greatest area of ignorance at the present time, because so many different variables are involved and the mechanics of fracture propagation are currently imperfectly understood. This is an area in which we can learn a great deal from service failures, and the author and his colleagues are currently conducting a detailed analysis of service failures in the Royal Navy, using a fine filter of different parameters (principally metallurgical), making a distinction between the causes of initiation and those of propagation, since these are by no means always the same. The results of a preliminary sample analysis using only six broad classifications is shown in Fig. 1, together with the results obtained by Todd (7) for failures encountered in a fleet of fast passenger cargo liners. With the exception of brittle fracture, the trend is similar, and fatigue and corrosion are clearly the most important failure mechanisms.

This result is not unexpected, and in itself would not justify

the labour expended in its determination; it is only when some of the more subtle undertones are studied that guidance emerges on the determination of the value of "E". Some of the metallurgical aspects involved are discussed elsewhere (8). This paper is now six years old and therefore dated in parts. However, it draws attention to the means of determining the metallurgical Achilles heel in a design, and to avoid repeating some of the arguments it is reproduced as an appendix to this paper.

Two simple examples will serve to show how consideration of the metallurgical aspects can be used to predict sensitive areas requiring close study, the type of NDT technique required, and the LEO value, where appropriate.

Large high strength steel studs used to hold down the cylinder heads of a group of heavy marine diesel engines were found to be prone to failure. Metallurgical examination showed that these failures initiated as corrosion-fatigue, progressed by fatigue across most of the cross section of the studs and finally completed in tension when the remaining cross section was too small to carry the peak working load. In this case, remedial action was taken to eliminate the corrosion-fatigue initiation of failure, but meanwhile it was necessary to institute immediate and effective NDT examination of all studs in situ (about 400, each some 30" long and 3" diameter, in relatively inaccessible positions in the engine, with only the top of each stud in view).

The LEO technique may then be used as follows:-

L = 2 1/2" (determined from observations of the fracture surface of a large number of failures).

E = 1/2 (a relatively high value since crack growth rate was slow and the required safe life before new studs could be made and fitted was relatively short).

O = 1/2 (no higher value could be given, since it was intended that NDT should be conducted without removing the studs, and the integrity of the signals was therefore impaired by multiple echoes).

therefore LEO = 3/8"

By introducing an artificial crack into a stud (using a hacksaw) in the position of failure, the use of ultrasonics was proved to be able to detect any crack of depth more than 3/8", and this was therefore a valid technique for the inspection of studs in situ.

Another example concerned impeller blades in which relatively minor vibrations resulted in the slow development of corrosion fatigue fissures, the more prominent of which eventually accelerated as fatigue cracks, leading to increased vibration and rapid failure. In this case, "L" was found (from the examination of failures) to be about 1/16", "E" was conservatively rated as 1/4, and "C", due to the limited access and indifferent surface finish, was similarly rated at 1/4. LEO therefore became about 0.004", a dimension so low that effective NDT of the components could not be accomplished in situ. In both of these cases, the use of the LEO technique at the design stage would probably have resulted in the elimination of failures, due to correct anticipation of the mechanism of failure. Even without this benefit, it would have encouraged minor design modifications which would have made NDT examination more simple to conduct, more sensitive and more positive.

There are of course examples where the guidance of LEO is unnecessary. For example, during the drilling of holes in ultra high strength steels, a slightly blunt drill can result in the production of a very thin, cracked martensitic layer in the bore. Since such steels are inevitably highly stressed in service, the hole acts as a stress raiser, fatigue crack propagation is relatively rapid and critical crack length is relatively small, no bore cracks can be accepted. This means that the NDT inspection must be very sensitive and the best technique is probably a close-fitting eddy current plug probe, using moderately high frequencies (5-10 Kc/s)* to measure surface conductivity.

CURRENT AND FUTURE ROLE OF NON-DESTRUCTIVE TESTING

The methods now available are numerous and fully described elsewhere (9,10) and by other contributors to this Symposium. The range and sophistication of equipment is increasing rapidly, but it is the author's opinion that knowledge of the way in which certain techniques (particularly ultrasonics and eddy currents) actually work is lagging behind their application, and that this is a field in which considerable effort is justified in order to upgrade the value of observations and reduce the risk of expensive misinterpretation of spurious indications.

Non-destructive testing is currently well established in two fields:-

1. Examination of materials and components before and during construction.

2. Examination of completed equipment before service, and at intervals during service.

*The depth "p" at which the induced current falls to $\frac{1}{e}$ of the surface value is given by $p = 0.063 \sqrt{\frac{\rho}{\mu f}}$ inches

where ρ = resistivity (i.e., 10^9 x resistivity in ohm cm)

μ = permeability (unity for non-magnetic materials)

f = frequency

With our increasing knowledge of failure patterns, more onorous demands upon materials, and the increasing realisation that most structures have built-in defects and cracks anyway, it is suggested that we must now accept a logical extension of NDT to a third field, the continuous surveillance of critical areas of important structures in service. This is, after all, no more than is practised in so-called reliability engineering (11) in electronic equipment used for telecommunications and computers.

The need for continuous surveillance of structural integrity is particularly apparent in defence and space applications, and in these cases the problems of ensuring effective surveillance can be formidable. Personnel are usually already fully employed on their proper duties, and it is important that NDT monitoring should neither burden their time, encroach excessively upon space and weight, nor lower morale by making the operators too defect conscious. The use of the LEO approach assists in the formulation of a sensible policy, with correct allocation of priorities, in such problems. The need for such continuous surveillance increase as "L" decreases, and becomes mandatory when "E" is small and the structure is a critical one.

CONTINUOUS SURVEILLANCE TECHNIQUES

One of the most interesting developments in this field has been the introduction of fatigue sensors. These are basically foil strain gauges, which are bonded on to the structure in appropriate positions. The gauges are small (typically 1/4" square) and they are merely left in place like tiny postage stamps. A portable resistance meter is attached to the gauge when its resistance is to be measured, so that no permanent wiring installation is required. At present the gauge material is fully softened (commonly cupro-nickel or nickel-chromium) so that repeated changes in the strain in the surface to which it is attached result in accumulated plastic deformation within the foil material, which is manifested as an increase in resistivity.

The novel feature of the application of these gauges lies in the fact that for accumulated cyclic strains of the order required to cause fatigue failure in light alloys, the resistance change in the sensor is of the order of 10%. Thus, for a gauge having an initial resistance of 100 ohms, there will be a 10 ohm change at the time of fatigue failure of the panel or spar to which it is attached. This large change in resistance eliminates problems of contact resistance and the need for fixed lead wires, and it is only necessary to use a simple measuring instrument with a resolution of the order of 0.05 ohms.

However, there are certain limitations with current fatigue sensors.

1. The gauges must be calibrated on the full size test elements, since the cumulative fatigue damage laws are not sufficiently well known at present to enable known or predicted loading patterns to be properly correlated with the behavior of the fatigue sensor.

2. Strain gradients in the structure may be steep. Hence, if it were possible to use very small sensors, accurately aligned over the peak strain areas, high confidence could be expressed in their performance. But since we are usually unable to define the critical area with a precision of, say, ±0.025, it is necessary to use larger sensors, and these will then to some extent integrate the strain field beneath them.

3. It may not be possible to place the sensors as close to the critical area as we would like. Consider the simple case shown in Fig. 2. Here the important area may be the hole "A" in the spar and access difficulties from the attachment lug may mean that the sensor cannot be placed closer than the position shown, i.e., well away from the stress concentration effect of the hole and possibly also down the major strain gradient within the spar.

If we add these effects together we may find that a very promising 10% change in resistance is rapidly whittled down. For instance, item (1) may mean allowing for a 20% variation in the change in resistance, and item (2) may introduce a factor of 2, and item (3) may introduce a further factor of 2 or 3. The cumulative effect is therefore to reduce the anticipated resistance change at failure to around 2%.

Measurement of such a resistance change, using demountable equipment, is still feasible, but it is becoming more sensitive

to errors induced by temperature changes, and it will be very dependent upon protection from the atmosphere and good gauge bonding practice. If, now, we require to use a safety factor of 2, in order to detect weakened parts before actual failure has occurred, the resistance change is reduced to about 1%. Measuring the resistance of a number of sensors distributed over an aircraft or other structure at intervals of several months, to such a degree of precision, is clearly not a matter which can be regarded lightly.

This difficulty can sometimes be overcome by the use of mechanical strain magnifiers, which are merely additional pieces of metal attached across the high strain region, and of reduced cross section in the gauge area. These, however, introduce their own problems since it is necessary for the strain magnifiers to be bonded to the structure with a very high level of integrity. If this means drilling extra holes for fixing bolts, the proposal may well incur some disfavour. However, there might be a case for drilling a hole in some position such as "B" in Fig. 2, and fixing the fatigue sensor inside the bore, or around the circumference of such a hole, using a circular configuration.

Nevertheless, the use of electrical resistance fatigue sensors represents a valuable step forward, since the sensor is subjected to the actual loading regime experienced by the structure and correlation problems are immediately eased. Also, by using large numbers distributed over an aircraft or other structure, NDT during maintenance time can be focused upon the more highly loaded areas, thereby improving the efficiency of inspection without increasing the time required for non-destructive testing. A survey of the potentiality of a number of fatigue sensors has recently been made (12) and it is hoped that future developments in this field will provide first of all a greater signal for a given degree of accumulated plastic deformation, secondly, temperature coefficients of expansion matched closely to those of the structures upon which they are to be employed, and thirdly correlation of the change in electrical characteristics with load patterns.

To anticipate the need to monitor crack presence and extension rate in structures, we have considered various techniques suitable for continuous surveillance.

The requirements for such devices are:-

1. Unambiguous output signal.

2. Small size, rugged construction.

3. Absolute minimum of maintenance and operation.

4. Reliability at low cost.

5. Ease and speed of installation.

An obvious contender is the electric resistance strain gauge, which is small, and for which reliable portable read-out, recording or display equipment is available. If a crack is propagating in the vicinity of the strain gauge, two cases must be considered. Firstly, if the crack passes beneath the gauge, the indicated strain will rapidly increase by the amount reflecting the crack opening displacement. However, the limiting crack opening displacement beyond which fracture of the gauge will occur is small and also at rather lower maximum values of crack width, fracture of the gauge by fatigue may be expected in a relatively few cycles if the strain across the crack is varying. Therefore, in the case of a gauge going open-circuit, one can conclude that a crack has passed that position, so long as the integrity of the instrument is assured. The second case involves the crack passing nearby, in which event the pattern of strain change during operation will differ, with smaller strain excursion amplitudes than those previously observed. Again, the information can be considered unambiguous only if the integrity of bonding of the gauge is beyong reproach.

To evaluate the potentialities of this technique, foil strain gauges were attached with Eastman 910 adhesive across an artificial "crack" which could then be opened by known increments, using the caliper straining frame shown in Fig. 3. In all cases, two patterns of response were observed, a relatively low sensitivity to crack width up to some "break-away" point (probably corresponding to the displacement at which local elongation of the foil commences) followed by a much more sensitive regime until a gap width was reached at which excessive relaxation presaged imminent failure. The results are summarized in Table I.

Further consideration of the desirability of measuring crack opening displacement led to the development of the displacement transducer module shown in Figs. 4 and 5. This employs commercially available differential transformer transducers which require only a stabilized 6 volt D.C. supply to provide a voltage output directly proportional to the displacement of the core. Recorder modules of the type shown in Fig. 6 permit switched ranges of sensitivity of ±1, 2.5, 5, 10, and 50 thousandths of an inch to be selected, and the sensitivity of this equipment is of the order of 2×10^{-5}" with a maximum crack opening displacement capability of 0.1" which is greatly in excess of that of strain gauges. It is merely necessary to site the transducer across the path of an anticipated crack, for its

output to reflect the component of crack opening displacement parallel to the axis of the transducer module. The output can also be integrated, either on site, or by subsequent examination of stored data, to give information on the fatigue experience which has accumulated in the monitored region. For such purposes, a different form of recording equipment would be desirable.

Another technique which is being developed at the Admiralty Materials Laboratory is a transistorized eddy current crack detector of novel design. The circuitry employed (13) is unusual and arose from a close consideration of the physics of the behavior of a coil carrying an oscillating current, when placed close to a ferromagnetic material. A vector plot of impedance and phase angle shows that the response is approximately a circular arc, the centre of which is displaced from the orgin of the plot. By a balanced circuit design it has been found possible to measure the impedance of the coil from a reference position corresponding to the centre of the polar plot. The advantages of this technique, apart from the small size of the device and economy in components, is that the probe is relatively insensitive to the inductance of the material and its distance from the surface. In practice, it is possible to adjust the device so that gaps up to 0.05" between the probe face and the work introduce no significant deflection of the instrument, which is of considerable advantage in dealing with rough, painted or rusty surfaces. This instrument measures the surface conductivity of the material and is therefore sensitive only to cracks which break the surface within its field of influence, for which is gives a quantitative indication of crack length over the range shown, for a variety of geometries, as shown in Fig. 7. This particular device has been produced in two forms, one as a module and probe with remote indication and the other as a self-contained portable eddy current crack detector.

CONCLUSIONS

An attempt has been made to show the need for a very broad approach to be taken in the selection and employment of non-destructive testing techniques.

A method for estimating the validity of non-destructive testing for the detection of significant defects has been outlined, and the case for an extension of NDT to continuous surveillance of critical areas has been presented, together with a discussion of some methods which can be employed.

The author is indebted to his colleagues, notably Dr. R.H. Warren and Mr. D.E. Bromley, some of whose work has been described in this paper, which is published by permission of the Navy Department, Ministry of Defence. The views expressed are personal to the author.

TABLE I

Strain Gauge Response To Crack Opening Displacement

LENGTH OF FOIL GAUGE	INITIAL SENSITIVITY		SECONDARY SENSITIVITY	
	Minimum Detectable Gap*	Break-away Point	Minimum Detectable Gap*	Maximum Gap
1/2 inch	0.06×10^{-3}"	0.8×10^{-3}"	0.007×10^{-3}"	2.0×10^{-3}"
1/4 inch	0.04×10^{-3}"	$0.? \times 10^{-3}$"	0.006×10^{-3}"	1.5×10^{-3}"
1/32 inch	0.015×10^{-3}"	0.3×10^{-3}"	0.0008×10^{-3}"	0.8×10^{-3}"

* Assuming sensitivity of measurement of 1 in 10^5.

REFERENCES

1. Biggs, W.D., Brittle Fracture of Steel, MacDonald and Evans, 1960.

2. Irwin, G.R., and Wells, A.A. Metallurgical Reviews, London, Inst. Met., 1965, (10) 223.

3. ASTM Special Publication No. 381, June 1964.

4. Pellini, W.S., Goode, R.J., Puzak, P.P., Lange, E.A., and Huber, R.W., N.R.L. Report 6300, June 1965.

5. Nicholls, R.W., Irvine, W.H., Quirk, A., and Bevitt, E., U.K.A.E.A. Report TRG1004 (C) 1965.

6. Weck, R., Australian National Welding Convention, Melbourne, October 1965.

7. Todd, B., Jnl., West Scotland Iron & Steel Inst., 1964 - 5, (72), 42.

8. Birchon, D., Second Engineering Materials and Design Conference, London, November 1961.

9. Hinsley, J.F., Non-destructive Testing. MacDonald and Evans, 1959.

10. Mullins, L., Trans. Inst. Mar. Engrs., 1966 (78) 426.

11. L.N. St. James Bell Laboratories Record, May 1965, p. 163.

12. Horne, R.S., Air Force Flight Dynamics Laboratory Report AFFDL-TR-66-113, June 1966.

13. Bromley, D.E., Patent Application 46955/66.

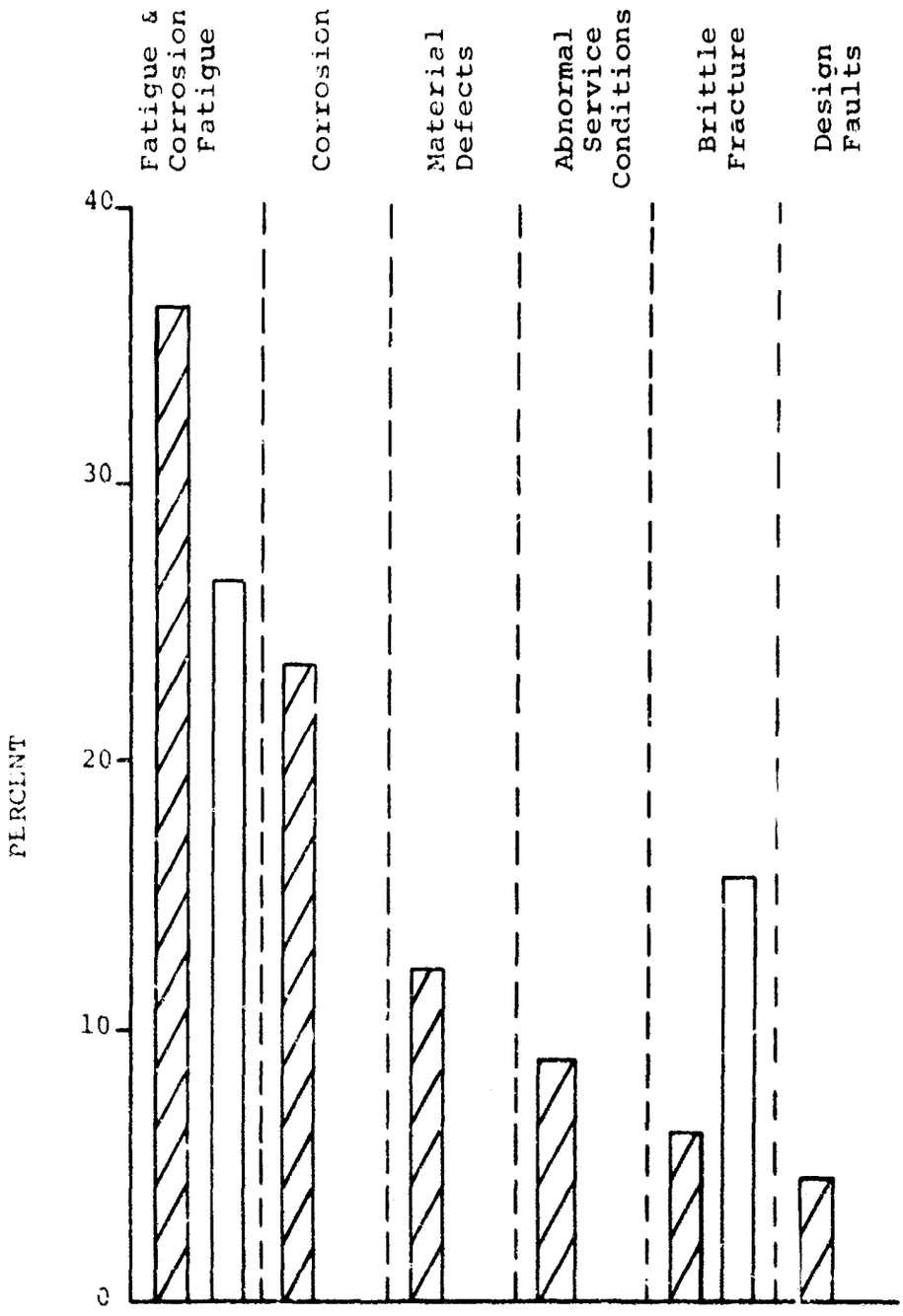

Fig. 1. Some causes of failure in marine engineering

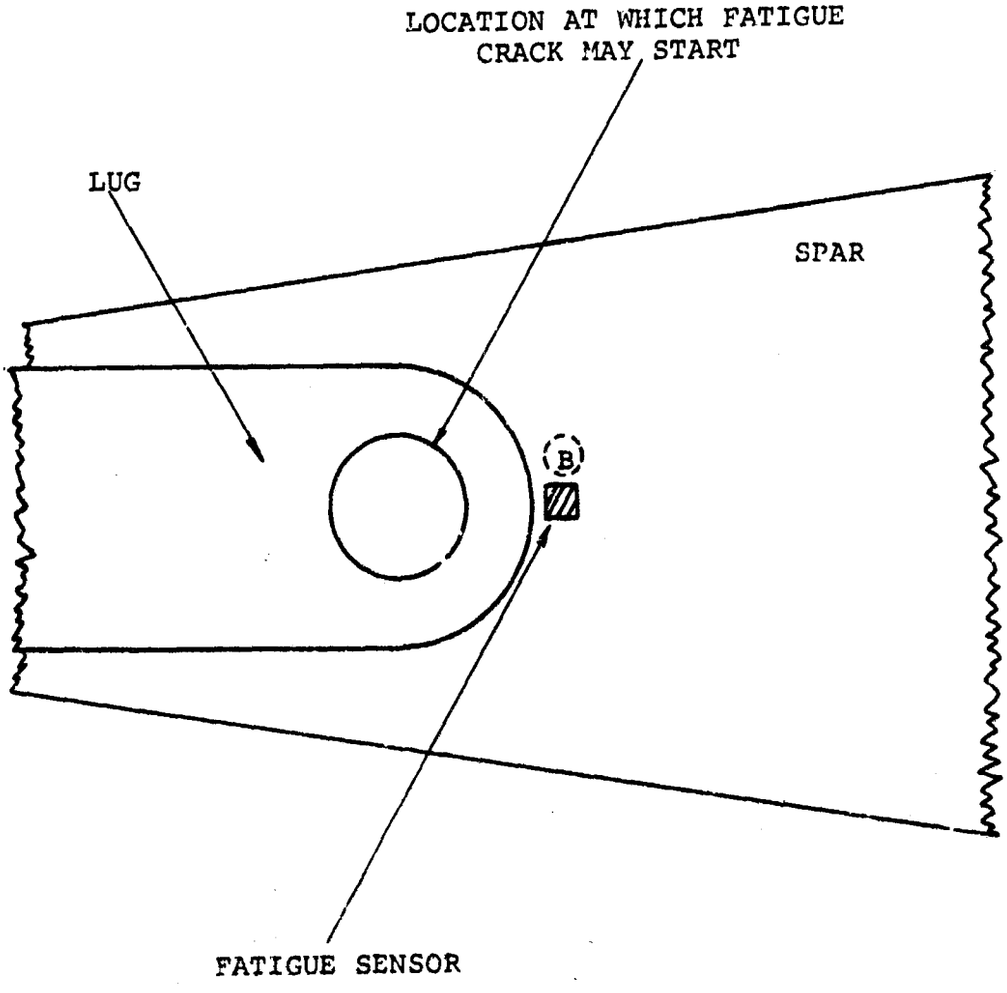

Fig. 2. Use of a Fatigue Sensor

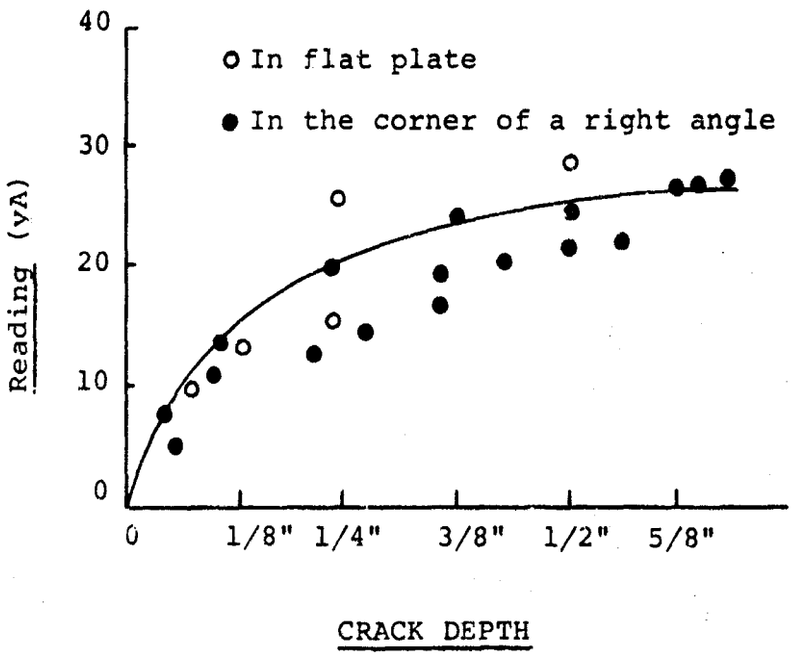

Fig. 7. Typical Response of Eddy Current Probe To Cracks of Varying Length

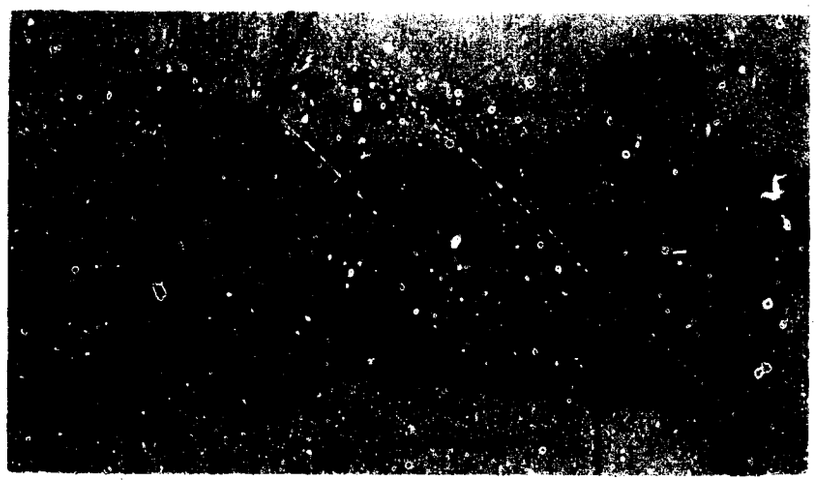

FIG. 3. CALIPER STRAINING FRAME WITH 1/32" GAUGE ATTACHED ACROSS ARTIFICIAL CRACK.

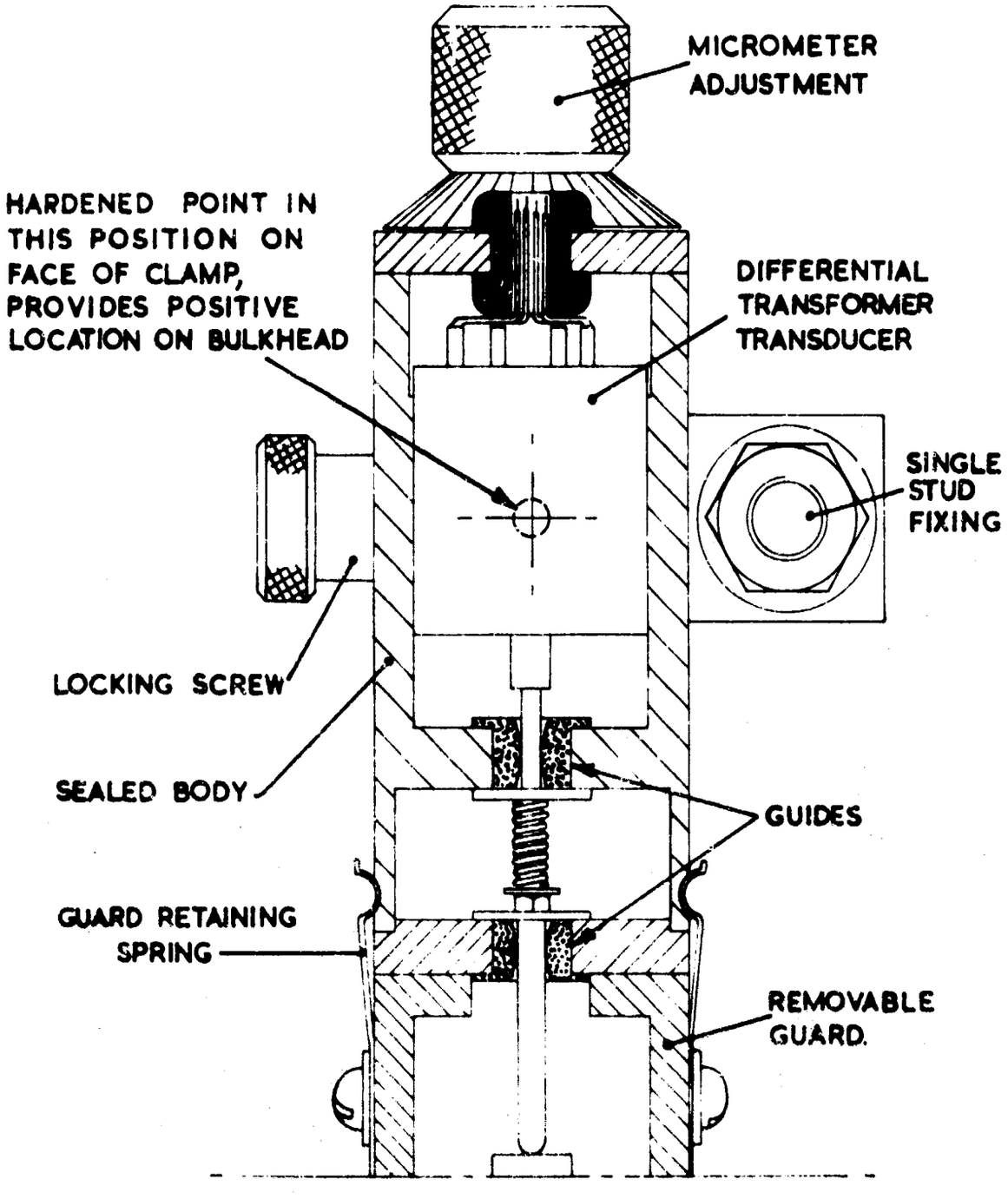

Fig. 4. LAYOUT OF TRANSDUCER MODULE

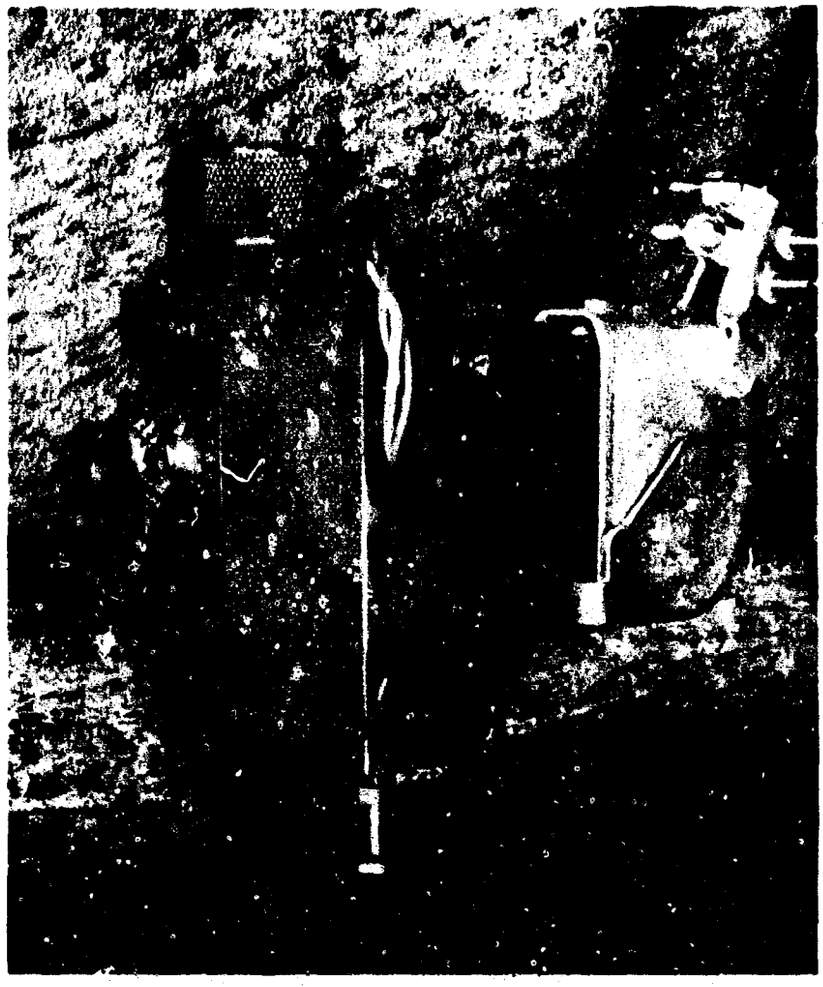

Fig. 5. INSTALLATION OF TRANSDUCER MODULE

Fig. 6. A GROUP OF SIX RECORDER MODULES